THE UNIVERSITY
of EDINBURGH

The effect of congruent gastro-intestinal pathogen infection on oral prion disease susceptibility

Alejandra Sánchez Quintero

A thesis submitted in partial fulfilment of the requirements of the University of Edinburgh for the degree of Doctor of Philosophy.

This programme of research was carried out at the Roslin Institute and the R(D)SVS, the University of Edinburgh

2017

Contents

Declaration

I declare that the work presented in this thesis is my own excepted were stated. All the experiments were designed in collaboration with my supervisors Professor Neil Mabbott, Dr. David Donaldson, Dr. Barry McColl. No part of this work has been, or will be submitted for any other degree, or will be submitted for any degree or professional qualification.

Alejandra Sánchez Quintero

October 2017

Abstract

Transmissible spongiform encephalopathies (TSEs) or prion diseases, are subacute neurodegenerative diseases that infect humans and animals. Many of these diseases are acquired by peripheral exposure (e.g. orally). After oral exposure prion replication within the Peyer's patches (PP) in the small intestine is necessary for the efficient spread of the disease to the brain. Within the intestine, bacteria and pathogenic microorganisms can affect the status of the gut associated lymphoid tissue (GALT). GALT consists of PP and isolated lymphoid follicles (ILF) that maintain homeostasis and protect from infections. Therefore, factors which modify GALT status, might dramatically affect oral prion disease pathogenesis by influencing the uptake of prions from the gut lumen or expanding their distribution within the host. Chronic intestinal helminth infections are common in animals and in man, and can cause significant pathology within the intestine. Little is known of the effects that intestinal helminth infections may have on oral prion diseases susceptibility. Therefore, in this study the influence that co-infection with *Heligmosomoides polygyrus* (a natural pathogen of the mouse small intestine) may have on oral prion disease pathogenesis and susceptibility was determined.

The studies consisted of groups of 4 (for *H. polygyrus* characterization and for early prion detection) and 8 (for *H. polygyrus*-prion co-infection to terminal stage) mice infected with *H. polygyrus* (orally) alone or subsequently infected with ME7 scrapie prions (orally) at different time-points after parasitic infection. The effects of the *H. polygyrus* infection alone, and on oral prion disease pathogenesis and susceptibility were then determined. Initially the characterization of *H. polygyrus* infection on the host intestine revealed that

this parasite caused significant pathology in the small intestine and affected the GALT microarchitecture. In the PP follicles, *H. polygyrus* infection increased the area of follicular dendritic cell expression, altered the positioning of mononuclear phagocytes and increased M cell density. *H. polygyrus* infection also reduced the number of ILF in both the small and large intestines. Additional studies in mice co-infected with a low dose of prions, revealed that these pathological changes affected the survival time and disease susceptibility. Data also show that the extent of the effects on prion disease pathogenesis and susceptibility were dependent on the stage of the helminth infection at which the mice were orally-exposed to prions.

Data demonstrate that co-infection with the gastrointestinal helminth *H. polygyrus* can influence oral prion disease pathogenesis and susceptibility. Helminth infections can significantly modify the microarchitecture of the gut and the GALT. Data presented suggest the pathological changes that pathogens such as small intestinal helminths cause, may also influence the uptake of prions from the gut lumen after oral exposure.

Lay summary

Transmissible spongiform encephalopathies, are neurodegenerative diseases that affect the nervous system of humans and animals. Many prion diseases are acquired orally through consumption of contaminated food. After consumption, the prions (responsible for the disease) first infect the immunological structures in the small intestine called Peyer's patches. In these structures the prions proliferate before they subsequently spread to the brain. Within the intestine, bacteria and other pathogenic microorganisms can adversely affect function of the Peyer's patches and the cells within them. Therefore, co-infection with these pathogenic microorganisms might dramatically affect the amount of prions acquired after oral ingestion which may also affect disease pathogenesis and susceptibility. Worm infections are common in animals and in man, and can adversely affect the intestine structure and function. Little is known of the effects that intestinal worm infections may have on oral prion disease pathogenesis and susceptibility. Therefore, in this study, the influence that a co-infection with an intestinal worm called *Heligmosomoides polygyrus* (specific of mouse small intestine) may have on oral prion disease was determined.

Initially the characterization of the effects of *H. polygyrus* infection on the intestine revealed that this parasite caused significant damage specifically in the small intestine breaking the epithelial barrier when the worms eat the intestinal villi. The infection also affected immune cell distribution within Peyer's patches. Experiments were then designed to determine whether the worm-induced changes to the gut microarchitecture might modify oral prion pathogenesis. Groups of mice were orally infected with *H. polygyrus* and subsequently orally infected with ME7 scrapie prions on different days after

worm infection. The effects of the *H. polygyrus* infection on oral prion disease pathogenesis and susceptibility were then determined. Data from these experiments showed that prion detection rate was significantly reduced 15 weeks post scrapie infection in Peyer's patches and mesenteric lymph nodes. And, although *H. polygyrus* infection did not affect the incubation period, the survival rate or the survival time of prion disease, it does increase the duration of the clinical signs. However, the changes in prion disease were dependent on the stage of the helminth infection at which the mice were orally-exposed to prions.

Data in this thesis suggests that the small intestine restricted helminth (*H. polygyrus*) causes significant changes to the gut. After oral exposure to prions, the initial accumulation of prions in Peyer's patches in the small intestine is essential for the efficient establishment of infection. However, the pathological disturbances to the small intestine and Peyer's patches caused by *H. polygyrus* infection had little influence on the early accumulation of prions in their subsequent spread to the brain.

Acknowledgements

First, I would like to thank the Mexican Council of Science and Technology (CONACYT; Reg. 298590) for funding my studies.

I would like to express my thanks to my supervisors **Professor Neil Mabbott, Dr. David Donaldson,** and **Dr. Barry McColl** for all their help, support and patience during my studies to accomplish this thesis.

I would like to thank **Professor Rick Maizels** (Institute of Infection, Immunity and Inflammation; College of Medical, Veterinary and Life Sciences; University of Glasgow) and **Elaine Robertson** (Institute of Immunology & Infection Research; University of Edinburgh) for providing the *H. polygyrus* larvae used in this thesis.

I would like to thank the BRF staff for all their help during this project: **Gordon Melville, Darren Smith** and in particular to **Rebecca Greenan** for her help, training and the weekly TSE scoring.

I would like to thank **Aileen Boyle** for the vacuolation scoring and **Pedro Picardo** for helping me and teaching me to interpret the brain pathology presented in this thesis.

I would like to express my thanks and gratitude to **Barry Bradford** for the training in the histopathology lab, for all the helpful discussions and laughs that helped me through the tough times.

I would like to express my gratitude to **Khalid Salamat** for his kindness sharing his knowledge with me. For having helped me to complement my knowledge and laboratory skills during the elaboration of this work; Thank you!

I would like to thank the friends I have made during my time in Edinburgh for their help and company in good and bad times; for listening, for the adventures, for the walks and the laughs, but above this, for supporting me**: Ciara Farren, Barbara Shih, Omar Alfituri, Kate Matters, Seb Cotton, Gabriela Peniche, Rocio Rojo, Carolina Peñaloza, Yenn Cortes**, and my flatmate **Adela Rabell**.

I would like to thank my family (Quintero's and Martinez') for all their support, specially to my aunts **Lourdes, Raquel, Ana** and **Cristian**; and my parents **Sandra L. Quintero** and **Jose L. Sánchez** who have supported me in all my decisions and for all the efforts they have made for their family.

Finally, a special thanks to my sisters **Annia** and **Ariadna** for growing up with me, for the laughs, for being my friends, my company and always stand there for me, even on the distance. Love you x

Abbreviations

BSE	Bovine spongiform encephalopathy
PrP^C	Cellular prion protein
CNS	Central nervous system
CCR2	C-C chemokine receptor type 2
CLEC9A	C-type lectin-like receptor
CWD	Chronic wasting disease
CFU	Colony forming unit
CSF1	Colony stimulation factor 1
cDC	Conventional dendritic cells
CJD	Creutzfeldt-Jakob disease
DC	Dendritic cells
DN cDC	Double negative conventional dendritic cells
EAE	Experimental autoimmune encephalomyelitis
FFI	Fatal familial insomnia
FAE	Follicle associated epithelium
FDC	Follicular dendritic cells
GFAP	Glial fibrillary acidic protein
GALT	Gut associated lymphoid tissues
ID	Infective dose
IgE	Immunoglobulin class E
IgG	Immunoglobulin class G
IHC	Immunohistochemistry
PrP^{Sc}	Infectious prion protein
IFN-γ	**I**nterferon gamma
IL-	Interleukin
i.c.	Intracerebral
Iba1	Ionized calcium binding adaptor molecule 1
ILF	Isolated lymphoid follicles

LysoMac	Monocyte-derived macrophage
LysoDC	Monocyte-derived DC
MHCII	Major histocompatibility complex II
MLN	Mesenteric lymph nodes
MNP	Mononuclear phagocytes
MUC2	Mucin 2
NSAID	Non-steroidal anti-inflammatory drugs
PET	Paraffin embedded tissue
PLP	Periodate-lysine-paraformaldehyde
PAS	Periodic acid Schiff
PP	Peyer's patches
pDC	Plasmacytoid dendritic cells
PrP^d	Prion disease-specific without PrP^{Sc} specific characteristics
PAR2	Protease receptors
RANKL	Receptor activator of nuclear factor kappa-B ligand
Tregs	Regulatory T cells
SIRPα	Signal regulatory protein α
SPL	Spleen
sCJD	Sporadic Creutzfeldt-Jakob disease
TNF	Tumor necrosis factor
IFN-1	Type 1 interferon
vCJD	Variant of Creutzfeldt-Jakob disease

Chapter 1. Introduction

1.1 Prion diseases

Prion diseases, are a group of progressive degenerative pathologies of the nervous system that can affect humans and animals [1]. The earliest recorded accounts of prion disease in animals date from the 18th century, when Spanish shepherds noticed an itchy/scraping behaviour in their sheep [2]. Later, this was described as a clinical sign of a prion disease pathology in the central nervous system (CNS) known today as scrapie. Prion diseases were first considered to be caused by infection with a slow-virus due to the very long disease incubation period [3]. With this theory in mind, many scientists tried unsuccessfully to inactivate the pathological scrapie agent in affected tissues either by using ionizing or UV irradiation, extreme temperatures and pressures, and other substances known to inactivate bacteria and virus [4-7]. This indicated that the infectious prion agent was extremely resistant, and resistance to ionizing and UV radiation hinted that the pathogenic agent may be able to replicate without the need of nucleic acid [8]. This raised the possibility that the infectious prion agent may be mostly, or entirely, comprised of protein [9-12]. But it was not until the 1980's that the term "prion" was used by Prusiner to describe the proteinaceous infectious particle which was responsible for the transmission of prion diseases [6]. Later on in that decade (1985), it was shown that the same protein was present in both infected and uninfected tissue, and that the uninfected material was linked to *PRNP* gene which encodes the cellular prion protein (PrP^C) [13, 14]. PrP^C was later also linked with prion disease development; as mice that lack PrP^C fail to develop prion diseases after infection [15].

Table 1.1 Prion diseases that affect human and animals

Human prion disease	Host	Aetiology
Sporadic CJD	Human	Spontaneous conversion of PrP^{C} to PrP^{Sc} [18, 19]
Familial/Genetic CJD	Human	*PRNP* gene mutation [20]
Iatrogenic CJD	Human	Accidental infection with prions of human origin via medical procedures [21]
variant of Creutzfeldt-Jakob disease (vCJD)	Human	Infection with BSE prions [22, 23]
Gerstmann-Sträussler syndrome (GSS)	Human	*PRNP* gene mutation [24]
Kuru	Human	Ritualistic cannibalism [25]
Fatal familial insomnia	Human	*PRNP* gene mutation (codon 178N and 129M) [26-28]
Animal prion disease		
Scrapie	small ruminants	Infectious [18]
Transmissible mink encephalopathy	mink	Infectious [18]
Chronic wasting disease	cervids	Infectious [18, 29]
Bovine spongiform encephalopathy (BSE)	cattle, exotic ungulates, wild and domestic cats	Infectious [18]
Feline spongiform encephalopathy	domestic cats	Infectious [30]

Infectious, sporadic and genetic forms of prion diseases have been described in humans and animals (Table 1.1). The acquired prion diseases include variant Creutzfeldt-Jakob disease (vCJD) and kuru in humans, and bovine spongiform encephalopathy (BSE), natural sheep scrapie, and chronic wasting disease (CWD) in cervids [1, 29, 31]. Past experience has shown that prion diseases can have a devastating impact on animal and public health.

Rates of prion diseases in humans are low and most are sporadic. Approximately only 1 person per million is affected annually with Creutzfeldt-Jakob disease (CJD) [32]. From those about 10% are genetic (familial) CJD, 2-5% are infectious and iatrogenic prion diseases [33], and the rest correspond to sporadic prion diseases.

However, the risk of human to human transmission remains due to the potential number of asymptomatic carriers [34, 35]. Data from the retrospective analysis of abnormal prion protein in human appendixes has estimated an overall prevalence of 493 per million people born between 1961 and 1985 in the UK [34]. In cattle, BSE was shown to have zoonotic potential, resulting in the occurrence of vCJD in the UK human population through consumption of BSE-contaminated food [36, 37]. The appearance of certain prion diseases such as BSE in domestic animals, can result in huge economic losses. For example, in the United States the identification of a single case of classical BSE in 2003 was estimated to have caused a $4.5 billion loss due to the barriers to beef exports and reduced domestic consumption [38]. In the United Kingdom, during the BSE epidemic 3 million cattle were estimated to be affected with the disease, with >180,000 diagnosed. This epidemic is estimated to have had public cost of more than £5 billion. Meanwhile, in the United States, natural sheep scrapie has an annual costs from $10-20 million

USD associated with the production and export losses, and the disposal of carcases [38].

1.2 Prion disease pathology

Prion disease pathologies within the CNS are characterized by neuronal cell loss, spongiform degeneration (vacuolation), gliosis, and in some cases amyloid plaque formation. Unfortunately, given that the brain is often the most affected organ, definitive diagnosis in humans can often only be determined by post-mortem histopathology. However, prion disease pathology can be clinically manifested in humans as dementia, muscle incoordination (gait abnormalities), tremors, visual and speech problems, dysphagia, and psychiatric disorders, among others [18, 39]. Since these manifestations are not pathognomonic of prion disease they can be easily misdiagnosed, especially during the early clinical stages. This may especially be the case for some patients with a genetic prion disease which do not have a known clinical history of prion disease. However, in these instances they may have a history of other neurological and psychiatric disorders [40].

The incubation period for prion disease vary: for scrapie in caprine it is 1 year while in ovine it is ~2 years; for BSE it is ~5 years; for kuru it is 15 years; and for iatrogenic CJD between 12-15 years [41]. A clinical diagnosis of probable prion disease can be made using complementary tests which include electroencephalograms, protein detection in cerebrospinal fluid and magnetic resonance imaging for sCJD; in the case of vCJD, neuropathological lesion profiles, genotype (codon 129 of the PRNP gene) and the confirmation of proteinase K-resistant prion protein are needed [42]. The detection of disease-specific prion protein in biopsy samples of lymphoid tissues such as tonsil or

appendix is also possible; but there are currently no treatments for these devastating diseases [34, 43].

1.3 Cellular prion protein (PrP^C)

The cellular prion protein, PrP^C, is expressed in many mammalian cells and tissues from the early embryogenesis stages [44]. Murine PrP^C is composed of 208 amino acids [45], and is a glycosylphosphatidylinositol-anchored glycoprotein that is normally attached to the lipid bilayer of the cell surface by its carboxyl-terminal domain (anchor) [46]. This domain consists of a long flexible amino-terminal tail, three α-helices and two-stranded anti-parallel β-sheets [47, 48]. One β-sheet is positioned towards the first α-helix while the second β-sheet links to the third α-helix [31, 49] (Figure 1.1). It has been suggested that there are some morphological differences in this protein domain between species. The link between the β-sheet and the third α-helix is considered to be rigid in cervids (elk and deer), but flexible in other species such as bovine and human [50].

The flexible N-terminal domain of PrP^C contains an octapeptide repeated region. This consists of a sequence of octameric amino-acid repeated five times [47], and is considered to have copper binding activity [51]. However, the precise function of each portion domain of the PrP^C protein are mostly uncertain.

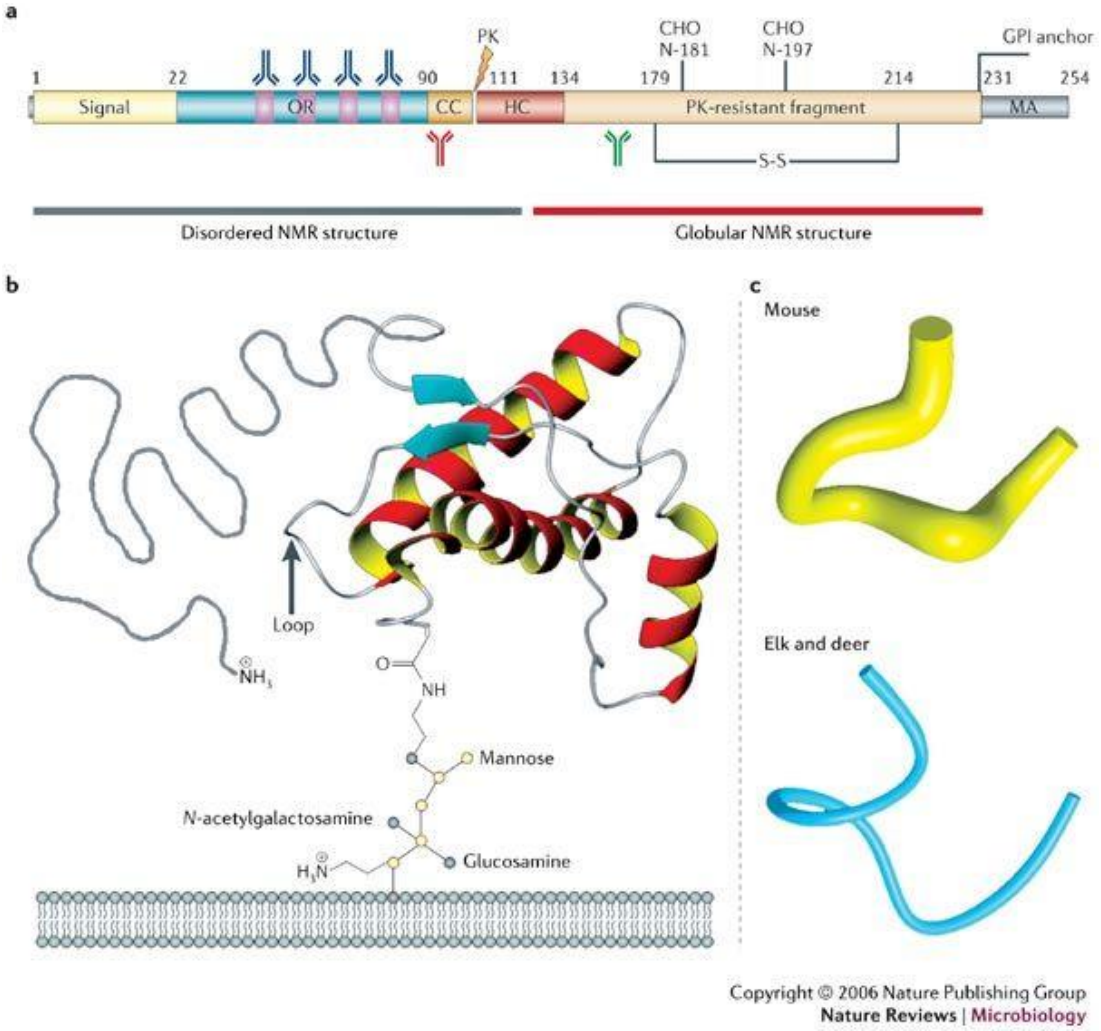

Figure 1.1 Cellular prion protein structure representation (taken from: Aguzzi A. and Heikenwalder M., Pathogenesis of prion diseases: current status and future outlook. Nature Reviews Microbiology, 2006.4:765-775). (A) Linear representation of the PrP^C (glycosyl phosphatidyl inositol (GPI)-linked glycoprotein) structure which shows the anchor domain to the membrane anchor region (MA) on the right and the N-Terminal domain on the left. It also highlights characteristics such as the hydrophobic core (HC in red) and proteinase K resistant fragment in the globular part of the structure. In the disordered structure, the charged cluster (CC), the octarepeat region (OR) that consist in a segment of five repeats of an octameric amino-acid sequence; and the secretory signal peptide at the extreme. High affinity epitopes recognised by POM2 (in blue), POM3 (in red) and POM5 (in green) monoclonal antibodies are also shown. (B) Bidimensional representation of the protein which in the base shows the glycosylphosphatidylinositol-anchored glycoprotein attached to the lipid bilayer of the cell (anchor), the three α-helices (yellow and red), and the N-terminal tail (in grey). (C) Suggested flexible (mouse, top) and rigid (elk and deer, bottom) morphological differences in this protein domain between species.

1.4 Expression and function of PrP^C

PrP^C has been reported to be expressed in mammals, turtles and amphibians [52, 53], suggesting that this protein is highly conserved in evolution. PrP^C is also expressed in a wide number of tissues implying that it may also have a variety of cellular functions. However, the evidence in this regard is not solid.

In the brain, it has been suggested that PrP^C is involved in synaptic transmission and plasticity [54, 55], memory formation [56, 57], calcium regulation [58, 59], circadian rhythm [60], neuroprotection [61, 62], and myelin maintenance [63] among others. Outside the brain, PrP^C is also expressed in the skin: in pilo-sebaceus units, keratinocytes, the non-keratinocyte epithelium of hair follicles, dermal axons and dermal lymphocytes [64]. In lymphoid tissues PrP^C is expressed on follicular dendritic cells (FDC) in the B cell follicles, and on most other immune cell types including lymphocytes, mononuclear phagocytes and mast cells [64-66]. PrP^C had also been identified in different cellular subsets in the post-gastric tract (gut wall), including enteroendocrine cells, villus myofibroblasts, and lamina propria lymphocytes [64]. It is also highly expressed in cells of the enteric nervous system, including enteric neurones, parasympathetic neurons of the oesophagus wall, myenteric neurons, the submucosal plexus and smooth muscle myofibrils [64]. Although a similar cellular distribution of PrP^C in the gastrointestinal tract has been suggested in different species, some differences exist. For example, PrP^{C+} cells in the epithelium of fundic and pyloric glands are mainly in the basal epithelium in the rat, while in the monkey and cow they are located in the middle area, but the three species consistently have lower PrP^{C+} cells in the colon than in other intestinal areas [67]. In the gut-associated lymphoid tissues (GALT), in lambs, the expression of PrP^C in lymphoid Peyer's patches was lower than the submucosa and muscularis [68]. In the intestine, it has been

suggested that the expression of PrP^C on enterocytes may be implicated in maintaining the integrity of cell-cell junctions (barrier property) [69-71]. While other studies suggest that PrP^C may also be implicated in the differentiation of on T and B cells, natural killer cells, platelets and monocytes where it is also expressed [66, 72-75].

1.5 Infectious prion protein (PrP^{Sc})

Infectious prion protein (PrP^{Sc}) is thought to be the main, if not only, molecule involved in the infectious pathogenesis of prion disorders. It has been suggested that PrP^C is essential substrate for the prion disease associated agent (PrP^{Sc})[15]. It is thought that the misfolding of PrP^C through a posttranslational process from α–helical to a high β–sheet, results in the generation of PrP^{Sc} [31]. Besides the infective characteristics of PrP^{Sc}, it is also differentiated from PrP^C by being insoluble in non-ionic detergents, showing only limited digestion by proteinase K (proteinase K resistant) and having the capacity to form aggregates [1, 31, 76-78].

1.6 Prion strains and host susceptibility.

Many different strains have been identified in humans and animals. Prion strains may differ in the biochemical properties of PrP^{Sc} which may impact in the disease pathology [79, 80]. This was first demonstrated with the infection of C57BL and VM mice with different prion strains; mice developed prion disease, but with differences in the incubation period, and the severity and distribution of the spongiform pathology within the CNS. Furthermore, these characteristics were retained and remained consistent in several subsequent passages in the mice [81, 82]. Later, the molecular diversity of the prion agent

was identified in scrapie-associated fibrils resulting in the isolation of the strains ME7 and 139A in mice, and 263K in hamster. ME7 and 139A differ from 263K in morphology, sedimentation rate, protein composition like posttranslational amino acid modification [83], and sensitivity to proteinase K [84]. Other strains and sub-strains, such as transmissible mink encephalopathy, were adapted in hamsters to the sub-strains hyper and drowsy. The hyper strain is characterized by the clinical signs of hyperexcitability and ataxia while drowsy strain produces lethargy [85]. Prion strain differences have also been identified in sheep [86, 87].

The prion protein is encoded by the gene *PRNP* [88, 89]. In humans, the *PRNP* gene locus is situated at chromosome position 20p 12-ter [89]. This single-copy gene spans 16 kb, comprises two exons and encodes a 253-amino acid protein by its larger exon (prion protein described in Section 1.3) [90-92]. The *PRNP* gene may have polymorphisms resulting in different alleles; mainly at codons 136, 154 and 171 [93]. The *PRNP* genotype may also influence host susceptibility to prion disease and the pathogenesis of the disease within the host. This means that prion strain characteristics may vary according the host *PRNP* genotype, even when the hosts are infected with the same prion strain [94]. Scrapie in sheep is an example of how these individual genetic characteristics determine host susceptibility: homozygous animals with ARR/ARR (representing the amino acid in codons 136, 154 and 171) are less susceptible to natural sheep scrapie, while animals with the VRQ/VRQ genotype are more susceptible in comparison with ARQ/ARQ wild type homozygous animals. Whereas heterozygous animals (ARR/VRQ) have longer incubation periods of scrapie disease [95].

Some prion diseases in humans are associated with genetic mutations in the *PRNP* gene. CJD and fatal familial insomnia (FFI**)** had been associated with

same genetic mutation (D178N) in the *PRNP* gene. However, they differ at another codon with a different amino acid located in the same position (codon 129): valine (CJD) or methionine (FFI) [96].

Although approximately 80 classical scrapie isolates (primary source of naturally acquired prion disease) have been described in Europe, the exact number of prion strains associated with distinct biological and biochemical phenotypes of prions is unknown [97, 98]. Strains characterization is based on characteristics such as: the time of clinical onset of the disease (incubation period), and the severity of the pathology [98-100]. Usually strains are characterized using transgenic mice with adapted mutation in the *PRNP* gene, as a mechanism to adapt the host to the prion strain in order to produce the disease. This process has limitations such as the cost to produce and maintain the mice line. However, three sheep strains (ME7, 87A, and 87V) had been well characterized in inbred mice [101, 102]. Similar studies in mice have also pointed to the possibility of a different strain of BSE responsible for human infection (zoonotic strain) [103, 104]. However, the exact strain responsible for the human disease zoonosis remains unknown.

1.7 Routes of prion transmission

Data suggest that acquired prion isolates may be horizontally transmitted between host species by a range of different exposure routes. For example, it has been suggested that some prion isolates can be excreted through urine (experimentally in mouse [105], deer (CWD) [106], and naturally in vCJD in humans [107]), saliva (sheep and deer [108]), colostrum (sheep), milk (sheep), placenta and faeces (sheep and cervids) [109-117]. Therefore, these secretions either by contaminating the environment (bedding/pasture) or feed may

provide means of oral prion transmission. Studies also indicate that certain prions, such as BSE may also be vertically transmitted from an infected mother to developing foetus of mice expressing bovine PrP (boTg) when mated close to the onset of the clinical disease [118]. In humans, vCJD is considered to have been acquired through the oral consumption of BSE contaminated food. This disease (vCJD) could have also been accidentally spread to other humans through transfusion of blood or blood products from a vCJD infected donors [119]. Studies that used protein misfolding amplification (PMCA) technique had successfully detected PrP^{Sc} in whole-blood and in its individual fractions (plasma and white cells) from patients affected with vCJD [120, 121]. Other examples of accidental iatrogenic transmission of prion disease (CJD) in humans have been associated with patients that received corneal transplant (cases were either associated with sCJD or unspecified CJD due patient death) [122], and with the use of contaminated surgical instruments (this was not proven) [123].

1.8 Cells involved in the spread of prions from the gut lumen to the CNS

Many acquired prion diseases are mainly considered to be orally acquired, most-likely through the consumption of prion contaminated food or pasture. Many studies, mostly in experimental animals (especially mice and hamsters) have been undertaken to determine the interactions of prions with the host after oral exposure, and to determine how prions establish infection in the brain after infecting the intestine. By understanding this process, it may be possible to create novel mechanisms to block the spread of prions from the gut to the brain, and by doing so, block oral prion disease transmission. The

sections below describe our current understanding of how orally-acquired prions establish host infection.

1.8.1 M cells

After oral ingestion, prions first transit through the epithelium which overlies gut associated lymphoid tissues (GALT) in the small intestine. Although GALT are distributed along the entire intestine, evidence suggest that the small intestine GALT are the essential sites for prion acquisition from the intestinal lumen [124], as in the specific absence of Peyer's patches (PP), gastrointestinal infection with prions was blocked [125]. GALT refers to the lymphoid organs such as PP and isolated lymphoid follicles (ILF) which are distributed throughout the small and large intestines [126, 127]. GALT contains B cell follicles with a germinal centre and are covered by a specialised follicle associated epithelium (FAE) [128]. The FAE predominantly contains M cells, goblet cells and enterocytes. M cells are a unique subset of epithelial cells which function to constitutively sample the intestinal luminal contents to enable the mucosal immune system to mount an effective immune response to gut pathogens or their toxins [129]. M cell differentiation is regulated by stimulation from the cytokine RANKL which is produced by stromal cells in the sub-epithelial dome region of the GALT beneath the FAE [130, 131]. Many pathogens including reovirus, polio virus, and *Mycobacterium avium subsp. paratuberculosis* can use M cells to enter mucosal tissues and establish host infection [129, 132-134]. Furthermore, it has been suggested that for some pathogens such as *Yersinia enterocolitica*, M cells are essential intestinal entrance sites [135, 136]. In the absence of M cells, prion disease pathology is blocked [135]. Conversely, when M cells are increased, so is the susceptibility

of mice to oral prion infection [137]. However, other potential routes of prion entrance into the GALT cannot be excluded. Enterocytes are found along the intestine and are involved in the uptake of nutrients and macromolecules from the gut lumen via endocytosis [138]. A potential role for enterocytes in the uptake of prions from the gut lumen has been suggested [139, 140]. However, if this was a major route for prions to establish infection after oral exposure, one would not expect the prion disease pathogenesis to be blocked in the specific absence of M cells**.**

1.8.2 Mononuclear phagocytes

Mononuclear phagocytes are originated in the bone marrow [141, 142]; these cells evolve from pluripotent stem cells that undergo different progenitor stages: from granulocyte/macrophage colony-forming unit (CFU) to macrophage-CFU to monoblast to pro-monocyte [143]. At these stage, a specific differentiation begins to osteoclast progenitors (in the bone) or monocytes [143]. This differentiation is in response to the colony-stimulation factor 1(CSF1) [143]. Monocytes are released in the circulatory system to different body tissues.

Monocytes differentiate into varied cell types. Over many years, it was considered that bone marrow monocytes differentiate into bone marrow macrophages in response of CSF1 [142, 143]; depending on grow factors, cytokines and inflammation into dendritic cells (DC); tissue resident macrophages (e.g. microglial cells or Langerhans cells) [144]; alternatively activated macrophages (M2) in response to allergic conditions, parasitic infections and tissue repairing process; and inflammatory macrophages (M1) at infection and injury sites [143]. However, nowadays there is evidence that

adult tissue macrophages can have an embryonic origin [145-147]; but whether the functionality of different-origin macrophages is interchangeable or specific remains unclear [145].

The relationship between macrophages and DC has been matter of debate. However, the importance of DC relies on their property to be antigen-presenting myeloid dendritic cells and the ability to activate naïve T cells [142]. While the importance of macrophages is their phagocytic function to clear apoptotic or dying cells, as well as their ability to regulate functions and differentiation of neighbour cells [142]. The possible origin of the controversy between macrophages and DC may be natural ageing process. For example, yolk-sac-derived macrophages have a characteristic $CX3CR1^{hi}F4/80^{hi}CD11b^{lo}$ expression pattern during embryogenesis [147-149]; but at adult stage, as many resident tissue macrophages originated during embryogenesis alter these cell-surface markers expression [145, 148]. These reduces the ability to precisely track macrophage populations.

In the intestine the interaction of mononuclear phagocytes (DC and macrophage) with M cells is necessary for antigen presentation to immune effector cells [150]. Antigen presentation by the mononuclear phagocytes, is key to induce a mucosal immune response [151]. However, the role of each phagocyte subpopulation in infection has remained unknown due the lack of definitive phenotype markers for each subset. Up to date, there is an overlap in several surface markers between macrophages and DC (e.g., CD11c, CD11b, SIRPα, and the major histocompatibility complex class II (MHCII)) [150, 152].

In PP, conventional DC (cDC) precursors derive in two subsets: cDC1 and cDC2. These were first identified through the expression of either CD8α (cDC1) or CD11b (cDC2) in addition to CD11c and MHCII [153, 154]. Nowadays, there are more specific markers for these subsets. For cDC1, XCR1

and Clec9a [155-160] and for cDC2, SIRPα. This cDC2 marker is more widely distributed than CD11b, but is also shared with macrophages [161]. A third DC subset has also been suggested. The double negative cDC (DN cDC) neither expresses CD11b nor CD8α [162, 163]. However, it had also been suggested that this subset (DN cDC) is a different stages of the cDC2 subset [164]. All these types of DC are present in PP domes [162, 165].

The identification of the macrophages in the PP has not been conclusive due to the lack of expression of classic macrophage markers (F4/80 (EMR1), sialoadhesin (Siglec1/CD169), Mannose Macrophage Receptor (MMR/CD206), or Fc Gamma Receptor I (FcGRI/CD64)) [166], and the overlap of CD11c, CD11b, MHCII, and SIRPα (surface markers), between macrophages and DC [152]. This led to confusion about location and functions of both dome phagocyte populations.

Nevertheless, it is possible to distinguish dome cDC from monocyte-derived cells (dome macrophages (LysoMac) and the monocyte-derived DC (LysoDC)) [164, 166, 167]. Dome monocyte-derived cells express CD11c, CD11b, SIRPα, BST2, CX_3CR1, MerTK, and lysozyme [166, 168]. Specifically, $CD11c^+$ LysoMac are large long-lived cells, dependant on the growth factor M-CSF for their development [166], express CD4, and low levels of MHCII. Furthermore, according on the expression of the phosphatidylserine receptor TIM-4, there had been described two main subsets of LysoMac [166]. All these contrast with LysoDC, which are short-lived DC, express high levels of MHCII, no CD4, and are strongly dependent on CCR2 (chemokine receptor that allows monocyte egress from the bone marrow) [166]. Upon stimulation with the TLR7 agonist R848, LysoDC secrete IL-6 and TNF but no IL-10 [166].

Other type of DC in the PP are the plasmacytoid DC (pDC). These are a specialized subset of DC which sense viral and bacterial pathogens and release high levels of type I interferon (IFN-I) in response to infection [169]. pDC are also implicated in the pro-inflammatory activation of effector T cells, cytotoxic T cells, and conventional DC [169]. Like monocyte-derived cells express higher levels of BST2 and lower levels of CD11c and SIRPα than LysoDC and LysoMac [164, 166]. PP pDC are also distinguished from monocyte-derived cells, thanks to their B220 expression. PP pDC differentiate from the pDC in other tissues by their inability to secrete abundant type I IFN in response to the TLR9 agonist CpG [170], their reduced expression of the mucosal migratory receptor CCR9, and the reduction of the specific transcriptional regulator of the pDC lineage E2-2 [171]. Like other pDC, PP pDC are derived from the same precursor and induced by Flt3L [171]. The recruitment of PP pDC requires type I IFN/STAT1 signalling. This conditional signalling could be the factor that favour the production of inflammatory cytokines IL-6, IL-23, and tumor necrosis factor (TNF) instead of type I IFN [171].

In the lower part of the PP dome, phagocytes are mainly composed of $CD11c^{+}CD11b^{+}$ cells [162, 164, 168]. Although they were thought to be cDC2, these $CD11c^{+}CD11b^{+}$ cells also express CX_3CR1 and lysozyme and belong to the monocyte-derived family of phagocytes (LysoDC and LysoMac) [164]. They represent two-third of subepithelial phagocytes. This contrast with the subepithelial dome cell population, which contains few cDC, mainly DN cDC2 ($JAM\text{-}A^{-}CCR7^{-}CD11b^{-}SIRP\alpha^{+}$ cDC) [164]. However, both subepithelial LysoDC and DN cDC2 can penetrate the FAE and interact with M cells, meanwhile LysoMac remain mainly located in the lower part of the PP [164]. Their different anatomical localization within PP suggests a regional specialization of macrophage functions [166].

1.8.2.1 Mononuclear phagocytes role in prion disease

Antigens that cross the FAE through M cells are subsequently deposited in the basolateral pocket of the M cell which contains mononuclear phagocytes [172, 173]. After prions cross the epithelial barrier, they are similarly released into the basolateral pockets of M cells, in the sub-epithelial dome of the PP. There, the prions are taken up by mononuclear phagocytes where they may be either phagocytosed and destroyed by macrophages or conveyed to the follicular dendritic cells (FDC) within the B cell follicles by DC.

Bone-marrow-derived DC have the capacity to acquire antigens directly from the gut lumen through dendrites that can penetrate the epithelium [174], or indirectly acquire them after their transcytosis across the gut epithelium by goblet cells [175] or M cells [176]. The antigens acquired by DC are commonly processed into short peptides for display on the cell surface in association with MHCII. These peptides are then presented to T lymphocytes to initiate a specific immune response to the antigen [177]. Consistent with this role, *in vitro* studies suggest that some DC can also degrade prions[178]. However, some DC are able to retain antigens in their native states and deliver them to B cells [179]. In the absence of $CD11c^+$ DC prion neuroinvasion is impaired or delayed [180]. These absence of $CD11c^+$ cells was tested in using CD11c-diptheria toxin receptor transgenic mice where $CD11c^+$ cells were specifically depleted in the GALT, and after prion infection with ME7 and 139A scrapie, early prion accumulation was block in GALT, and the susceptibility to prion disease was reduced [180]. However, this study make reference to migratory $CD11c^+$ DC and as previously mentioned, this is not a specific marker of DC.

Outside the PP, in the intestine, macrophages tend to be positioned closer to the lamina propria epithelium than DC [181], possibly to enable them to uptake intestinal luminal antigens. These cells can also extend processes through the epithelial layer to trap antigens [182]. Besides the lamina propria, they are also situated in the serosa and muscularis layers of the intestine where they interact with the enteric nervous system [183, 184]. In the PP, prion accumulation has also been identified within macrophages of hamsters after oral prion infection [185]. Prion degradation by macrophages had been proved to reduce prion disease susceptibility after intraperitoneal inoculation of C57BL mice with a bovine cell line Bo120 of macrophages infected with scrapie brain homogenate [186]. Prion degradation had also been tested in $CD11c^{+}$ myeloid dendritic cells in vitro [178]. This suggests that mononuclear phagocytes can clear the prions from the host by phagocytosing and destroying them.

1.8.3 FDC in prion disease

Follicular dendritic cells (FDC) are a subset of heterogeneous and non-migratory stromal cells which reside within the B cell follicles and germinal centres of secondary lymphoid organs (e.g. lymph nodes, spleen, PP, ILF, tonsils and appendix) [187-191]. FDC characteristically trap and retain antigens as complement-opsonized complexes on their surface for long periods [191, 192]. After prions are acquired by mononuclear phagocytes, they are delivered to FDC where they replicate upon their surfaces before neuroinvasion [125, 193]. Prions are similarly acquired by FDC as complement-opsonized complexes [191, 194-197]. In the absence of complement C3 component or C1q, scrapie infection is delayed [197].

Prion replication on FDC within lymphoid organs had been suggested necessary for prion neuroinvasion [125]. However, data suggest that FDC are as important as their location. The small intestine PP are the essential sites for prion entrance and replication [139][198]. After prions accumulate in the PP, they then disseminate to and accumulate within FDC in the mesenteric lymph nodes (MLN) that drains the gut. Stimulation via tumor necrosis factor receptor 1 (TNFR1) through TNF and lymphotoxin (LT) α; and stimulation via LTβ receptor by LTα/β heterotrimers is necessary for the development of secondary lymphoid organs [199-203]. Activation of LTβ receptor is also necessary for maturation and maintenance of FDC [204]. Therefore, for prions to accumulate in MLN, TNF and LT are required to have optimal developed FDC. In the absence of lymphotoxin, prion accumulation is ablated in spleen and MLN, but in the absence of TNFR, prion infection was still detected in MLN but not in spleen [204]. Nonetheless, prion accumulation in the spleen does not impact prion disease development after oral exposure. In splenectomised mice, the percentage of survival and the incidence to prion disease remain the same as in control groups [205].

1.9 Prion neuroinvasion occurs via the peripheral nervous system

Prion neuroinvasion is considered to occur via infection of the peripheral nerves within the lymphoid tissues [139, 206]. The prions then spread along these nerves to the CNS where they ultimately cause neurodegeneration and death of the host [207]. This is based on the detection of prion disease-specific PrP upon the plasma membranes of enteric neurones in the myenteric plexus on day 21 post oral prion infection in mice [208]. Also in hamsters PrP^{Sc} has been detected half-way through the incubation period within enteric ganglia

and the vagus nerve in accordance with a similar temporal sequence of prion spread to the CNS [206]. Furthermore, in mice with hyper innervated lymphoid organs the disease incubation period after peripheral prion infection was significantly reduced [207]. In contrast, the incubation period is significantly extended in mice that underwent sympathectomy (extraction or destruction of the sympathetic nerves) prior to prion infection [207]. How the prions initially establish infection within peripheral nerves after replication upon FDC is not known, but the distance between FDC and peripheral nerves has been shown to influence the rate of prion neuroinvasion [209]. Here DC have been proposed to play a role as it has been suggested that DC are able to transmit prion infection directly to the nervous system [210]. However, studies in this regard are not conclusive as mononuclear phagocytes and B cells were unable to transmit the disease to peripheral nervous system in the absence of FDC in a different study [211].

1.10 Factors which may influence prion disease pathogenesis and susceptibility.

Along the life of humans and animals, individuals experience many different health conditions. The origin of these could be infectious, genetic, accidental, autoimmune, idiopathic as well as the natural process of ageing. As described below, the effects of these processes on the key cells and tissues mentioned above may also influence prion disease pathogenesis and susceptibility.

1.10.1 Ageing

Over the time, physical, psychological, and even social alterations are accumulated. This process is known as ageing [212-214]. During ageing, M cell maturation and density in the FAE of PP is reduced and therefore the ability to transcytose particulate antigens into PP is similarly reduced [215]. In sheep, cattle and humans, it has been reported that age affects PP development, as the weight of PP in cattle and the number of PP in humans decreases over time [216].

In the MLN of mice, FDC activity significantly decreases with age, as well as their ability to retain immune complexes [217, 218]. However, the ability of macrophages in the lymph nodes to uptake immune complex is not impeded with age [218]. In the spleen, the FDC are also affected in aged mice. Aged murine FDC have been reported to be atrophic, and like those in aged MLNs, lose their ability to efficiently trap and retain immune complex [218].

In the spleen, there are also changes on the marginal zone, where the distribution of macrophages and B cells is adversely affected. The disorganized marginal zone may affect its ability to clear antigens from the blood stream and deliver immune complexes to FDC in the B cell follicles [219-221].

Each of these ageing-related structural and morphological changes may significantly influence susceptibility to peripherally acquired prion diseases. For example, in aged mice, prion deposition in lymphoid tissue was reduced [222]. Effects on M cells and PP size similarly may reduce the uptake of prions from the gut lumen, and help explain the reduced susceptibility of aged animals, humans and mice to oral prion infections.

1.10.2 Differences between vCJD and sCJD

Although the ageing process may negatively affect prion disease due the cellular changes described above, other factors such as the type of disease may influence prion disease pathogenesis and susceptibility. In humans, two prion diseases: variant and sporadic CJD behave different. Positive cases of vCJD have almost exclusively been observed in people with a mean age of 29 years old. In these individuals the mean duration of disease was 13 months and, although rapid progressive dementia is rare in this disease, psychiatric symptoms at the onset of the disease as well as sensory symptoms (pain, paraesthesia (tingling sensation) and dysesthesia (unpleasant sensation felt when touched) are common [223]. Contrary, sCJD cases predominantly occur in older people (median 67 years old) with the mean duration of the illness around 4 months. While the rapid progressive dementia is common in sCJD, the psychiatry and sensory disorders are rare [223]. vCJD is also differentiated from other human prion diseases by the formation of amyloid plaques [224].

1.10.3 Inflammation

In the intestine, inflammation can occur following infection, with treatments such as non-steroidal anti-inflammatory drugs (NSAID) [225], infection with pathogens or parasites (e.g. *Ascaris lumbricoides*) [226] and certain autoimmune diseases (e.g. intestinal bowel diseases) [227]. Although NSAID (e.g. aspirin, diclofenac or ibuprofen) are commonly used, they are associated with gastrointestinal mucosal injury. NSAID inhibit the synthesis of prostanoids which derivate from the arachidonic acid by cyclo-oxigenase (COX) isoenzymes [228, 229]. There are two isoforms of COX; NSAID aim to inhibit COX2 which induces inflammation. Unfortunately, NSAID do not have

specific target and also affect COX1, which is present in endothelial cells, gastrointestinal epithelium and platelets [229]. Inhibition of COX1 reduces prostaglandin secretion which have a cytoprotective effect of the gastric mucosa [230]. The gastroenteritis associated with NSAID, led to erosions and ulcers of the gastrointestinal tract [231]. As with NSAID, intestinal inflammation may affect the integrity of the cellular epithelial junctions in the lining of intestine, resulting in increased gut permeability that may compromise intestinal epithelial barrier function [232, 233]. Damage to this barrier may potentially enhance the entrance of intestinal luminal pathogens into the host, including prions. The immune response to chronic inflammation may induce the formation of granulomas. As granulomas can express PrP^{C}, experiments show that the they can also act as additional sites of prion replication in prion infected animals [234]. Also, the formation of FDC-containing ectopic lymphoid tissues in chronically-inflamed kidneys, pancreas and livers, have also been shown to be potential sites of prion accumulation in affected hosts [235]. In a similar response, it had been shown the neo-formation of ILF under inflammatory conditions [236, 237].

The occurrence of autoimmune diseases may also have an impact on the pathogenesis of some prion diseases. In a study of C57BL/6J mice infected with 1% scrapie brain homogenate and experimental autoimmune encephalomyelitis (EAE; characterized by the inflammation of the CNS), prion disease survival time was reduced. The presence of EAE did not influence the abundance of PrP^{Sc} in the spleen or brain. Instead, this reduction was considered to be due to enhanced demyelination, immune cell infiltrates, gliosis, and PrP^{Sc} deposition in the spinal cord [238].

1.10.4 Pathogen co-infection

The inflammation and pathology that other pathogens may also cause to host cells and tissues may also modify prion disease pathogenesis and susceptibility. For example, clinical prion disease is exacerbated in mice co-infected with adenovirus and prions [239]. However, whereas co-infection of NIH3T3-22L fibroblast with murine friend leukemia virus (retrovirus) can enhance accumulation of scrapie strain 22L prions *in vitro*, viral co-infection had no effect on prion disease pathogenesis *in vivo* [240]. Analysis of a natural co-infection model in sheep, showed that although Visna-maedi virus did not affect the risk of natural sheep scrapie transmission, the inflammation it caused in the host did favour the accumulation of prions in organs such as lung or inflamed mammary gland [241]. Studies in mice have also suggested that the inflammation caused in the cecum and colon by infection with the pathogenic bacterium *Salmonella typhimurium* (M556) increased the risk of prion disease in mouse model [242]. However, co-infection of mice with a natural helminth pathogen parasite that specifically infects the caecum of the large intestine (*Trichuris muris*), did not influence prion disease pathogenesis or susceptibility [198].

1.11 *Heligmosomoides polygyrus*: a model helminth pathogen with infection restricted to the murine small intestine

1.11.1 *Heligmosomoides polygyrus*

H. polygyrus is a nematode (round worm) of the Strongylida order and Trichostrongylina suborder [243]. It is a natural small intestinal helminth parasite of mice. However, the intensity and length of the infection depends on the mouse strain affected. Susceptible mouse strains such as CBA, C3H, SL, A/J, C57BL/6, and C57BL/10 can host chronic *H. polygyrus* infections which may last 20 weeks or more [244, 245]. Other parasites such as *Haemonchus contortus* and *Teladorsagia circumcincta* (ruminant parasites) or *Ancylostoma duodenale* and *Necator americanus* (human hookworm parasites) have close genetic similarities with *H. polygyrus*. These similarities make *H. polygyrus* an excellent comparative model to study the mechanisms used by these parasites to cause chronic infections [243, 246, 247].

1.11.2 *H. polygyrus* life cycle

H. polygyrus has a direct life cycle with the mouse as definitive host [245, 246]. The larval stage 3 (L3) is the infective form when orally acquired. Within 24 hours of oral exposure, the larvae reach the small intestine submucosa. There, they undergo two moult developmental stages before emerging into the small intestine lumen as adult worms on or around day 8. The adult worms then establish infection in the lumen. There, they coil around the villi to avoid being expelled and feed on epithelial cells. *H. polygyrus* adult worms reside in the duodenum and jejunum where the height of the villi is longer when compared to other intestinal regions, allowing the parasite to wrap their highly coiled

bodies around them [243, 248, 249] (Figure 1.2). While in lumen, the worms also mate and begin to produce eggs from around day 10 of infection. The eggs are then excreted from the host in the faeces. Outside the mouse, the eggs hatch the first larval stage (L1) which undergoes two moults to become a larval stage L3. The life cycle starts again [248, 250].

During its life cycle within the host *H. polygyrus* causes significant damage to the epithelium of the small intestine: both while the parasite transits in and out of the submucosa; and also as it feeds on it. Therefore, the disruption of the epithelium at those moments (days 1 and from day 8) may potentially increase the susceptibility of the host to another orally-acquired pathogen infection such as prions.

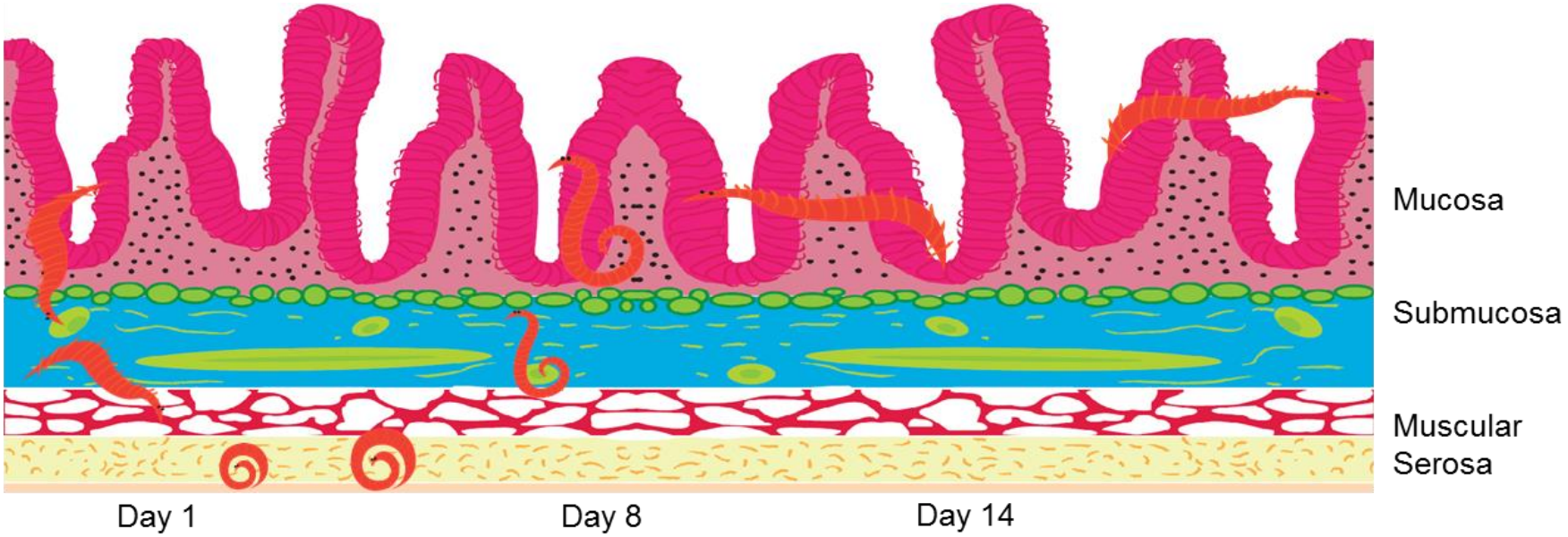

Figure 1.2 Location of *H. polygyrus* from larval to adult stages during infection in the mouse small intestine. L3 is the infective stage which is acquired orally by the mice. Within the first 24 hours (day 1), the larvae reach the small intestine submucosa. There, it undergoes two moult development-stages in 7 days and the adult worms emerge into the lumen around day 8. In the lumen, adult worms coil around the villi where they feed on epithelial cells, mate and produce eggs (about day 10). These are excreted in faeces and follow an external development until L3 to complete the cycle.

1.11.3 Pathological changes to the intestine caused by *H. polygyrus*

H. polygyrus infection causes direct damage to the small intestinal tissue by the attachment of the parasite to the villi, the feeding process and the migration of the larvae in and out of the subepithelial layers. During infection, there are also multiple cellular changes as a consequence of the host immune response to the infection [245, 251-253].

The enteropathological changes caused by *H. polygyrus* infection induce the modification of the villi:cript ratio, cellular reactions in mononuclear phagocytes, Paneth cells, goblet cells, enteritis and granuloma formation [245, 254-256]. As a consequence of the infection other organs such as spleen or mesenteric lymph nodes can be also affected. A particular response of the host immune system is the formation of granulomas. These are developed as a consequence of *H. polygyrus* infection in the sites of larval tissue encystment. They are considered to be an immune response to immobilize and trap external bodies, parasites and bacteria and as a response to chronic inflammation [256-259]. These nodules consist of specialized macrophages surrounded by fibroblasts and lymphocytes.

1.11.4 Effect of *H. polygyrus* infection on goblet cells

As part of the host innate responses to *H. polygyrus* infection, there is an increased mucus secretion into the intestinal lumen. To increase mucus production goblet cells proliferate (hyperplasia) [260]. A main component of the mucus is mucin 2 (MUC2) [261]. This mucin had been correlated with the expulsion of other pathogenic worms such as *T. muris* and *Nippostrongylus brasiliensis* [262, 263]. Although there is currently no evidence of MUC2 role in the expulsion of *H. polygyrus*, these studies suggest that it is plausible MUC2

may a similar role in the expulsion of many gastrointestinal parasites. Goblet cells also secrete the antimicrobial peptide RELMβ into the gut lumen [264]. This protein can inhibit the ability of the *H. polygyrus* to feed and therefore reduce the worm burden and their fecundity [265].

1.11.5 Effect of *H. polygyrus* infection on intestinal peristalsis

Peristalsis is the movement of muscle by contractions. In the intestine, this acts to facilitate the movement of the intestinal contents through the gastrointestinal tract. This mechanism can be modified by the host in response to intestinal infections to enhance the excretion of the intestinal contents. It has been reported that in mice, guinea pigs, and rats, activation of the protease receptors (PAR2) stimulates the enteric nerves to trigger intestinal contractions [266-268]. In *H. polygyrus* infection IL-4 has been shown to stimulate hyper-contractibility of the intestinal smooth muscle [269]. Although the activation of PAR2 in *H. polygyrus* infection is dependent on IL-4, in *Trichinella spiralis* infection, the activation of PAR1, which can also induce smooth muscle hypercontraction, was dependant on IL-13 but not IL-4 [269, 270]. These data demonstrate that although this response is considered to be an innate host response to pathogen infection, it can also be activated by the adaptive immune response through secretion of Th2 cytokines.

1.11.6 Predominant Th2 response to *H. polygyrus* infection

The immune protection against *H. polygyrus* is mainly Th2 dependent [271, 272]. This refers to the adaptive immune response by $CD4^+$T cells which differentiate into T helper cells (Th1, Th2, Th17 and regulatory T cells (Tregs)) [273]. Th2 cells have been closely related with the host immune response to

external parasites. It is considered that dendritic cells can prime Th2 response [274]. Th2 activation results in the production of Th2 cytokines (IL-4, IL-5, IL-13 and IL-25) [273]. However, Th2 cells can also regulate IgE production by B cells [275]. Immune complexes with IgE can also activate innate immune response, such as basophils and mast cells. The innate immune response is also activated during *H. polygyrus* infection. Th2 cytokines are responsible for the alternative activation of macrophages [276-278]. Macrophages can be activated through pattern-recognition-receptor of microbial stimuli, by complement receptors (immune response), by IFN-γ stimuli (classical activation), and by IL-4 and 13 (alternative activation) [279]. Macrophages may be mediators of smooth muscle hypercontraction in helminth infections [280] and are involved in tissue remodelling and debris clearance [272, 281].

1.11.7 Effect of *H. polygyrus* infection on mast cells

Intestinal mast cell activation by Th2 cells results in their degranulation and the release of inflammatory mediators that can increase vascular permeability and smooth muscle contractions [282]. In *H. polygyrus* infection, mast cell activation (mastocytosis) is also evident and can be induced by the Th2 cytokine, IL-9 [272]. The induction of mastocytosis during *H. polygyrus* infection has been associated with the suppression of worm fecundity [283, 284]. Although mastocytosis has been related to epithelial barrier dysfunction, this may also help eliminate parasites such as *H. polygyrus* from the host. The increased secretion of intestinal fluids due to increased gut permeability is considered to increased worm expulsion [285-287].

1.11.8 Effect of *H. polygyrus* infection on B cells

During *H. polygyrus* infection, the activities of B cells in the MLN are also altered by the Th2 response to the infection [288, 289]. This results in the production of parasite-specific antibodies of the IgG and IgE isotypes [290]. However, IgE does not have a protective role in *H. polygyrus* infection [291], but IgG produced by pregnant mothers can protect their neonatal offspring from infection [292].

All the above immune mechanisms triggered by *H. polygyrus* infection are aimed at clearing the parasite from the host. However, effects on the host such as the epithelial barrier dysfunction, the formation of granulomas, the B cell activation in the mesenteric lymph nodes, the goblet cell hyperplasia and even the hyper-stimulation of the smooth muscle may influence the establishment of a secondary infection. For example, epithelial damage may increase the ability of another pathogen to infect host tissues, whereas increased gut motility may enhance the expulsion of the pathogen from the host.

1.11.9 Excretory-secretory products of *H. polygyrus*

Excretory-secretory products are parasite secretions which include digestive, urinary contents and many other substances, some which may have immunomodulatory effects on the host. Although the immune response to primary *H. polygyrus* infection is predominantly Th2 polarized and accompanied by regulatory T cell activation, it fails to achieve a fast expulsion of the parasite in almost all mouse strains [250, 254, 293]. Many of the immunomodulatory effects of *H. polygyrus* are likely to be the result of the action of its excretory-secretory products on the host, which can modulate or impede DC function, induce Tregs and suppress Th2 response [294-298]. Over

200 proteins have been identified in excretory-secretory extracts from *H. polygyrus* including macrophage migration inhibition factor and acetylcholinesterase [299, 300].

Given the potent immunoregulatory properties of *H. polygyrus* excretory-secretory products, it is plausible that they may also influence host susceptibility to a secondly pathogen infection, by modulating the immune response to the pathogen.

1.11.10 *H. polygyrus* infection induces the formation of granulomas

Granulomas are formed in host tissues as part of the host's immune response to persistent antigen stimuli. These can be induced by bacteria, parasites or external bodies which stimulate chronic inflammation [301-305]. In the intestine, chronic inflammatory autoimmune disease can also cause granulomas [306, 307]. There are different classifications of granulomas according their origin or morphology [305, 308]. According to their morphology, granulomas can be divided into epithelioid, foreign body, suppurative and necrotizing [309]. Generally, granulomas contain $CD4^+$ T cells, $CD11c^+$ dendritic cells and macrophages [253, 310]. Specifically, in *H. polygyrus* infection the granulomas form as a consequence of the Th2-polarized immune response [253, 281, 310]. Their development begins when *H. polygyrus* larva reach the submucosa. Here, $CD11b^+$ macrophages cells then attach to the larvae and attempt to trap it [311]. The granulomas also contain Th2 cells and a large number of alternatively activated macrophages [253, 310]. However, the function of these structures in *H. polygyrus* infection is not known.

Studies have shown granulomas can harbor infectious prions even in the absence of FDC [234]. These data suggest that during a chronic infection with

H. polygyrus, the induction and formation of granulomas may provide additional sites for prion accumulation within the gut.

1.12 Project aims

The aim of this thesis is to determine the effects of co-infection with *H. polygyrus* on oral prion disease susceptibility and duration. Previous studies have shown that the uptake and replication of prions within the small intestinal GALT, especially the PP, is essential for their efficient transmission to the CNS where they ultimately cause neurodegeneration [124, 139]. After prions are orally acquired they first cross the gut epithelium by M cells in the small intestine GALT [124, 125, 135]. Then, in the sub-epithelial dome region of the GALT, the prions are then phagocytosed and destroyed by macrophages or transported by DC to the FDC in the B cell follicles [129, 139, 191, 312]. The FDC in the GALT are the first sites of prion replication in the intestine [191, 194-197]. Prions may also replicate in chronic inflamed tissues in presence or absence, such as in granulomas, of FDC [110, 234, 313]. After the prions replicate upon the FDC in PP, they also disseminate inside the host, to other secondary lymphoid organs before they spread to the CNS (neuroinvasion) [125, 193, 314, 315]. Helminth infections are common in humans and animals. A widely used laboratory model to study small intestinal parasitic infections is *H. polygyrus*. Its infection in mice has been well characterized and numerous studies have described its pathological effects on the intestinal epithelium, goblet cell hyperplasia, mastocytosis, hypercontractibility of the smooth muscle, activation of macrophages and granuloma formation. Furthermore, *H. polygyrus* in mice is restricted to the duodenum in the small intestine. *H. polygyrus* can also modulate host immunity through the activation of its

excretory-secretory products. This raises the hypothesis that the effects of *H. polygyrus* on the gut and GALT specifically in the small intestine may significantly influence oral prion disease pathogenesis and susceptibility. However, the effects of *H. polygyrus* on the microarchitecture of the GALT have not been studied in significant detail. Therefore, given the importance of the small intestinal GALT in prion pathogenesis, Chapter 3 will assess the effect of *H. polygyrus* infection on the microarchitecture of the GALT. Data from this chapter will be used to identify the key times after *H. polygyrus* infection with distinct pathological characteristics in the gut and GALT. These data will be used in Chapter 4 to identify the times after *H. polygyrus* infection in which mice will be co-infected with prions. Chapter 4 will therefore test the hypothesis that congruent infection with a small intestine-dwelling gastrointestinal pathogen may significantly influence disease pathogenesis and susceptibility to an orally-acquired prion infection.

Chapter 2. Materials and methods

2.1 Mice strains and housing

Female six to twelve weeks old C57BL/6J mice (Charles River Laboratories International, Inc. Margate, UK.) were maintained in the small animal facility unit under SPF conditions at The Roslin Institute. Mice were provided with food and water ad libitum unless otherwise stated.

All the studies were approved by the Institute's Ethical Review Committee and performed under project licence and regulations of UK Animals Scientific Procedures Act. 1986.

2.2 Parasitic infection with *H. polygyrus*.

H. polygyrus (L3, infective stage) were kindly provided by Professor Rick Maizels (Institute of Infection, Immunity and Inflammation; College of Medical, Veterinary and Life Sciences; University of Glasgow) and stored in sterile water at 4°C until use.

H. polygyrus (L3) were administered to mice by oral gavage in water (~200 L3 / 0.2 ml). The parasitic infection was confirmed by the presence of worm eggs in the faeces. To count the number of eggs, two or three faecal pellets per mouse were collected and weighed. Faecal pellets were mixed with 1 ml sterile water until dissolved and left to rest for 5 min, mixed again and passed through a tea strainer. The faecal suspension was centrifuged for 5 min at 100*g* at room temperature and the supernatant discarded. The pellet was re-suspended in 1 ml of flotation fluid (saturated sodium chloride (Thermo Fisher Scientific; Waltham, MA USA) / 50% w/v glucose (Scientific Laboratory Supplies Limited; Nottingham, UK.) in water), rested for 3 min and the eggs

were counted using a McMaster chamber and viewed using a Leica Mz-8 stereoscopic microscope (Leica Microsystems (UK) Ltd., Milton Keynes, UK).

2.3 ME7 prion infection

Brain homogenates in sterile saline solution were prepared from mice with clinical signs of ME7 scrapie infection.

For oral exposure, mice were fed individual food pellets doused with 50 μl of a 1% dilution of scrapie brain homogenate prepared from mice terminally-affected with ME7 scrapie prions containing approximately 3.3 log10 i.c. ID_{50} units. For infection, mice were temporarily caged individually in bedding and food free cages with water *ad libitum*. One single pellet with the prion dose was placed in the cage. The mice were returned to their original cages once the pellet was observed to be completely ingested.

All mice infected with prions were closely monitored and scored weekly from day 210 after oral exposure until the clinical signs of disease appeared or the animal's wellbeing was considered to be compromised. Clinical condition was assessed by the development of clinical signs of prion disease which include: loss of weight, staring coat, blinking eyes, hunched position, straight tail, wet genitals, gait problems, ataxia and a general decrease of awareness.

2.4 Periodic acid Schiff (PAS) staining

Snap frozen samples of intestine, Peyer's patches (PP) and mesenteric lymph nodes (MLN) were stored at -20°C until mounted in OCT for sectioning at 6 μm on a Leica CM1900 cryostat, sections mounted in Menzel-Gläser Superfrost Plus slides, and after drying overnight at room temperature they

were stored at -20°C until future use. For staining, slides were warmed up for 30 min at room temperature before fixing them in acetone (Sigma-Aldrich Company Ltd.; Dorset, UK) for 10 min after which they were air dried for 15 min. Staining was achieved using the PAS stain kit (mucin stain) from Abcam (Cambridge, UK) according to manufacturer instructions. Briefly, slides were immersed in periodic acid solution (5 min), Schiff's solution (15 min), haematoxylin (modified Mayer's) (3 min), bluing reagent (30 sec), and light green solution (2 min) with rinses of distilled water between each step. Slides were then dehydrated in a Leica Auto Stainer XL. They were washed in water twice (3 min each), Scott's tap water (2 min), wash in water (2 min), ethanol 70% (30 sec), ethanol 95% (30 sec), ethanol 95% (30 sec), ethanol 99% (1 min), ethanol 99% (1 min), ethanol/xylene (1 min), xylene (1 min), xylene (1 min), xylene (1 min). Finally, slides were mounted with ClearVue Mountant XYL (Thermo Fisher Scientific). Sections were viewed using a Nikon brightfield compound upright microscope (Nikon; Surrey, UK.). For the analysis, the number of goblet cells in 4 villi per mouse were counted. Data are presented as the number of cells adjusted to epithelial surface length.

2.5 Immunohistochemistry (IHC)

2.5.1 Whole mount immunostaining of isolated lymphoid follicles (ILF)

Three different areas of the gut were sampled (duodenum, ileum, and colon). Fresh samples of intestine (~2 cm) were used for whole mount immunohistochemistry. For this purpose, sections of intestine were collected and maintained in PBS at 4°C. Gut contents were gently squeezed out, and the tissues opened up and pinned down with lumen side up in a 35 mm petri dish filled with paraffin wax (Thermo fisher Scientific)/10% Mineral oil (Thermo

fisher scientific). Individual petri dishes were used per mouse; each contained the 3 sampled sections. The intestinal epithelium was gently washed with PBS to remove any remaining contents and mucus. Prior to use, the intestinal pieces were washed again 3 times (3 min each) with PBS on a shaker at 90 rpm.

The intestinal epithelium was then removed by incubation in HBSS (Thermo fisher scientific)/5 mM EDTA (Thermo Fisher Scientific) for 15 min at 37°C. Tissues were then fixed in 10% formal saline (CellPath Ltd.; Wales, UK) for 1 hr at 4°C. After fixation, the intestinal pieces were washed on the shaker as before using TBS-Triton (TBS (0.05M Tris pH7.6 (Sigma-Aldrich Company Ltd.) / 0.15 M NaCl (Thermo Fisher Scientific)) /0.5% Triton x100 (Sigma-Aldrich Company Ltd.) and then blocked with 2.5% normal goat serum (Jackson ImmunoResearch Laboratories Inc., West Grove, PA, USA) for 30 min at room temperature. To detect follicular dendritic cells (FDC), tissues were then stained overnight at 4°C with 2 ml of 0.5 μg/ml anti-mouse CD35 monoclonal antibody (clone 8C12, BD Biosciences; Ca, USA) in TBS-Triton.

The samples were then washed as before with TBS-Triton, and subsequently stained with 2 ml of 4 μg/ml of Alexa Fluor 594 goat anti-rat IgG (Thermo Fisher Scientific) in TBS-Triton for 2 hr on a shaker at 40 rpm in the dark. To detect B cells, the samples were washed in TBS-Triton and consequently stained with 2 ml of 2 μg/ml Alexa Fluor 488 conjugated rat anti-mouse CD45R (B220) monoclonal antibody (Thermo Fisher Scientific) for 3 hr on a shaker at 40 rpm. The intestinal pieces were washed again (three times) with TBS-Triton, and then mounted on a Menzel-Gläser Superfrost Plus slide with Dako fluorescence mounting medium.

Images were taken using a Zeiss inverted confocal microscope LSM 710 (Zeiss). The total number and area of each ILF per sample was calculated manually using Zen Blue software (Zeiss). One piece of intestine per small

intestine area (duodenum, ileum and colon) per mouse was examined. Calculations were adjusted to the area size.

2.5.2 Whole mount immunostaining for M cells

Fresh PP samples (approximately 1 cm long) were treated as mentioned in section 2.5.1 to remove the intestinal contents and mucus. Proximal and distal PP were placed in a petri dish. These were fixed with BD Cytofix/Cytoperm™ (BD Bioscience) for 1hr at 4°C followed by 3 washes of 3 min in PBS in a shaker at 90 rpm. Then, PBS-BSA-SAP (PBS / 0.5% BSA (Sigma-Aldrich Company Ltd.) / 0.1% Saponin (Sigma-Aldrich Company Ltd.)) was added for 30 min to block the fixation. The PBS-BSA-SAP was removed, and to detect M cells, the tissues were stained with 2 ml of 2.5 μg/ml anti-Gp2 monoclonal antibody (MBL International; Woburn, MA, USA.) in PBS-BSA-SAP and incubated overnight at 4°C.

The PP were then washed with PBS, and 2 ml of 2.5 μg/ml of Alexa Flour 488 conjugated goat anti-rat IgG (Thermo Fisher Scientific) in PBS-BSA-SAP was added and incubated for 2 hr at 40 rpm on a shaker. The PP were then washed with PBS and 2 ml of 5 μg/ml rhodamine conjugated Ulex Europaeus Agglutinin I (UEA-1, Vector laboratories Inc. Burlingame, CA, USA) in PBS-BSA-SAP was added to detect goblet cells (UEA-1+ GP2-) and incubated for 30 min. Tissues were washed again, and actin was detected using 2 ml of 10 μg/ml Alexa Fluor® 647 conjugated phalloidin (Thermo Fisher Scientific) for 2 hr before a brief wash in PBS prior mounting with Dako fluorescent mounting media on cavity slides (15 mm diameter x 0.6 mm depth; Thermo fisher scientific)

Sections were imaged using a Zeiss LSM5 Pascal (Zeiss) upright microscope and the analysis was performed using Zen Black software (Zeiss). Z-Stack images (20 Slices) of 2 PP follicles per mouse were collected to determine the area of the PP and the number of M cells and goblet cells. The thickness of imaged area ranged from 25.14 to 65.35 μm for duodenum and from 50.29 to 90.52 μm for ileum.

2.5.3 Detection of cellular markers by IHC on frozen tissues

Immunofluorescence was used to detect a number of different cell markers on PP and intestine samples. The antibodies used are presented in Tables 2.5.1 and 2.5.2. Sections were prepared as previously described in section 2.4. Prior to use, slides were washed 3 times for 5 min with TBS-BSA (0.05 M Tris pH7.6 / .15 M NaCl / 0.2% (w/v) BSA) before adding 150 μl of 5% blocking serum (normal goat serum). After 20 min incubation, the first primary antibody (Table 2.5.1) at the appropriate concentration was added and incubated overnight at 4^0C.

Slides were then washed 3 times in TBS-BSA as mentioned above. Afterwards, 150 μl of secondary antibody (Table 2.5.2) at the appropriate concentration in TBS-BSA was added and incubated for 1 hr before another series of washes in TBS-BSA. Consequently, when required, 150 μl of conjugated primary antibody (Table 2.5.1) in TBS-BSA at the appropriate concentration was added and incubated for 2 hrs at room temperature followed by washes in TBS-BSA. Washes were followed by another with PBS before counterstaining with 300 μl of 2.9 μM DAPI (Thermo Fisher Scientific) in PBS for 3 min. After a brief wash in PBS the sections were mounted in Dako fluorescent mounting media.

Slides were visualized in a Zeiss LSM 710 Confocal Microscope. Images were captured using Zen Black software.

Table 2.5.1 Primary antibodies used for IHC

Target/Antigen	Clone	Specie/isotype	Cell target	Source
GP2	2F11-C3	mouse/IgG2a	M cells	MBL International
CD45 (B220)	RA3-6B2	rat/IgM	B cells	Thermo Fisher Scientific / BD Biosciences
CD11b	M1/70	rat/ IgG2b	DC, MΦ	BioLegend (London, UK)
CD11c	N418	hamster/IgG	DC	BD Biosciences/ BioLegend
CD68	FA-11	rat/ IgG2a	Tissue MΦ	AbD Serotec (Kidlington, UK)/BioLegend
CD21/35	7G6	rat/ IgG2b	FDC	BD Bioscience
Synaptophysin 1	polyclonal	rabbit	Synaptic vesicles	Synaptic systems (Goettingen, Germany)
PrP	1B3	rabbit	Prion protein	[316]
Iba-1	polyclonal	rabbit	Microglia	Wako Chemicals GmbH (Neuss, Germany)
GFAP	polyclonal	rabbit	Astrocyte	Dako

Table 2.5.2 Secondary antibodies used for IHC

Antibody	Source
Alexa Fluor 488 goat anti rat IgG (H+L)	Thermo Fisher Scientific
Alexa Fluor 594 goat anti rat IgG (H+L)	Thermo Fisher Scientific
Alexa Fluor 647 Goat Anti rabbit IgG (H+L)	Thermo Fisher Scientific
Goat anti rat biotin	Jackson ImmunoResearch Laboratories Inc.
Goat anti rabbit IgG (H+L) biotin	Jackson ImmunoResearch Laboratories Inc.

2.5.4 IHC of paraffin embedded tissues

Paraffin embedded tissues (spleen, MLN, and PP) were used to detect CD21/35 and PrP^d. Tissues for paraffin embedding were fixed overnight in 2% periodate-lysine-paraformaldehyde (PLP) in phosphate buffer or for at least 24 hrs in 10% formal saline. PLP fixed tissue samples were processed in a tissue processor (Leica ASP 300s; Leica microsystems) using the following program: 70% ethanol (30 min, 37° C), 90% ethanol (30 min, 37° C), 90% ethanol (30 min, 37° C), absolute ethanol (35 min, 37° C), absolute ethanol (35 min, 37° C), absolute ethanol (30 min, 37° C), xylene (30 min, 37° C), xylene (20 min, 37° C), xylene (20 min, 37° C), paraffin wax (10 min, 62° C), paraffin wax (15 min, 62° C) and paraffin wax (15 min, 62° C); all this under 35 kPa (g) pressure/vacuum cycle.

Tissues fixed in formal saline were prepared using the following program: 70% ethanol (40 min, 37° C), 90% ethanol (40 min, 37° C), 90% ethanol (40 min, 37° C), absolute ethanol (40 min, 37° C), absolute ethanol (40 min, 37° C), absolute ethanol (30 min, 37° C), xylene (30 min, 37° C), xylene (30 min, 37° C),

xylene (30 min, 37° C), paraffin wax (25 min, 62° C), paraffin wax (25 min, 62° C) and paraffin wax (25 min, 62° C); under 35 kPa (g) pressure/vacuum cycle.

After paraffin embedding, 6 μm sections were cut using a microtome, mounted on glass slides (Menzel-Gläser Superfrost Plus) and dried overnight at 50°C and stored until use. For IHC, slides were dewaxed in Leica Auto Stainer XL (Leica microsystems) using the following program: xylene (5 min), xylene (5 min), xylene (5 min), ethanol 99% (3 min), ethanol 99% (3 min), ethanol 95% (2 min) and washed in water (5 min). Then, the slides were autoclaved at 121° C for 15 min either in Target Retrieval Solution (Dako) for CD21/35 or in distilled water for PrP^d immunostaining. Afterwards, the slides were cooled for 10 min in cold running water. For detection of PrP^d, the sections were subsequently immersed in 98% formic acid for 10 min and then washed for 5 min in running tap water. Slides were then immersed for 10 min in a 0.6% solution of hydrogen peroxide in methanol. Then, they were washed 5 min in PBS-BSA buffer (0.1% BSA / PBS). Sections were then blocked for 20 min in 5% normal goat serum before overnight incubation at 4°C with appropriate primary antibodies (Table 2.5.1). Then slides were washed in PBS-BSA 3 times (5 min each), and the secondary antibodies (Table 2.5.2) were added and incubated for 1 hr at room temperature. Slides were washed in PBS-BSA, and ABC kit vectastain PK-6100 standard solution (Vector Laboratories Inc.) was added according to manufacturer instructions. After slides washed in PBS-BSA, immunostaining was revealed by either 3, 3'-diaminobenzidine (DAB; Sigma-Aldrich Company Ltd.) or Vector nova red peroxidase substrate kit (Vector Laboratories Inc.). Then slides were washed in running water and counterstained with haematoxylin and dehydrated in a Leica Auto Stainer XL using the following program: wash in water (5 min), haematoxylin (30 sec), wash in water (3 min), wash in water (3 min), Scott's tap water (2 min), wash

in water (2 min), ethanol 70% (30 sec), ethanol 95% (30 sec), ethanol 95% (30 sec), ethanol 99% (1 min), ethanol 99% (1 min), ethanol/xylene (1 min), xylene (1 min), xylene (1 min), xylene (1 min). Finally, slides were mounted with ClearVue Mountant XYL.

Slides were visualized in a Nikon brightfield compound upright microscope using Zen Blue software for imaging.

2.5.5 IHC analysis of brain tissues

Brains were fixed in 10% formal saline. Paraffin-tissue embedding and cutting was undertaken by the Easter Bush Pathology Department (The Royal (Dick) School of Veterinary Studies, the University of Edinburgh).

Slides were dewaxed as mentioned in section 2.5.4. Slides were immunostained to detect PrP^{d} and glial fibrillary acidic protein (GFAP) by the protocol mentioned in section 2.5.4. For ionized calcium binding adaptor molecule 1 (Iba1) immunostaining, slides were first microwaved in citrate buffer solution (pH 6 of 0.29% tri-sodium citrate (BDH Laboratory Supplies; Dorset, UK)/0.05% Tween 20 (Amresco; Solon, Ohio, USA) in distilled water) for 10 min. Additional buffer was added throughout the process to ensure the tissue was completely immersed. Slides were then cooled in running tap water for 10 min.

All the slides were then pre-treated for 10 min in a 0.6% solution of hydrogen peroxide in methanol before being immunostained as described in the protocol in section 2.5.4.

Slides were visualized with a Nikon optic microscope using Zen Blue software.

2.5.6 Paraffin embedded tissue (PET) blot IHC detection of PrP^{Sc}.

PLP-fixed, paraffin embedded tissue sections prepared and cut as mentioned in Section 2.5.4 were mounted on 0.45 μm nitrocellulose membrane (Bio-Rad Laboratories, Inc. Germany) [317] and dried overnight at 50°C, and stored until use. The sections were dewaxed (Xylene (5 min), Xylene (5 min), Xylene/Isopropan-2 ol (5 min), 100% Isopropan-2 ol (5 min), 95% Isopropan-2 ol (5 min), 70% Isopropan-2 ol (5 min), 50% Isopropan-2 ol (5 min), distilled water (5 min) and TBST (0.01 M Tris pH 7.8 (Sigma-Aldrich Company Ltd.) / 0.1 M NaCl / 0.05% Tween-20) (5 min), TBST (5 min)). Sections were then cut out to fit in a 24 well plate with TBST and then, the TBST was replaced with a solution of 0.4% proteinase K (PK; Sigma-Aldrich Company Ltd.) in 0.01 M Tris pH 7.8 / 0.1 M NaCl / 1% Brij (Sigma-Aldrich Company Ltd.) in water for overnight incubation at 55°C.

After, the PK was removed, the membranes were washed 3 times in TBST (5 min each). Afterwards, the sections were incubated in guanidine isothiocyanate solution (0.01 M Tris- pH 7.8 / 35.46% guanidine isothiocyanate (BD Biosciences)) for 10 min, followed by another 3 washes with TBST. Next, a 2% casein (disodium maleate / Western blocking reagent, Roche Diagnostics GmbH; Mannheim, Germany) in TBST solution was added and incubated for 30 min. Sections were then immunostained with 1B3 anti PrP antiserum (Table 2.5.1) for 2 hr at room temperature. The membranes were then washed and subsequently incubated for 1 hr with goat anti-rabbit alkaline phosphate (Jackson ImmunoResearch Laboratories Inc.) in 2% casein/TBST solution. Then, the membranes were washed 3 times, and subsequently incubated in sodium-tris-magnesium (NTM) solution (0.8 M Tris pH9 (Sigma-Aldrich Company Ltd.) / 0.99 M NaCl / 0.48% $MgCl_2$ (Thermo Fisher Scientific)) for 10 min. The NTM was removed and immunostaining revealed on the membranes

by alkaline phosphatase substrate (Sigma Fast™ BCIP®/NBT, Sigma-Aldrich Company Ltd.). The reaction was stopped using 0.02 M EDTA solution (5 min). Finally, the membranes were washed with distilled water and dried overnight before analysis and storage.

Membranes were visualized using a Zeiss StereoLumar V12 Fluorescent Stereomicroscope with Zen Blue software.

2.6 Image analysis of fluorescently stained sections

The magnitude of immunostaining in specific tissue regions was determined using ImageJ software. Sets of images were taken under the same microscope settings. PP were mostly imaged under 10x objective in order to have the full view of the follicle and for the intestinal epithelium.

Thresholds were established for each set of images before the color analysis. The thresholds were established using the Image J macro for multiple colour backgrounds (Appendix 7.1). To do so, a straight line was draw. This line should cross all the intensities of each colour in each channel. With the line placed in the image, the macro was run. This displayed one graph per channel in which the intensity of the pixels that the line cross were shown. Using these graphs, the minimal threshold was determined and the background colour avoided for further analysis.

Image analysis for colour quantification was determined using the Image J macro for multiple colour analysis (Appendix 7.2). First, the macro was modified using the previous established thresholds. Then, the image was open in Image J and color/channel order was corrected (if needed) to match the macro (Ch1=red, Ch2=green, Ch3=blue). After selecting the area of interest using freehand or polygon selection, the macro was run. The result was a list

of numbers from 1 to 7 and their values. Each number represent a color; 0=black, 1=red, 2=green, 3=yellow, 4=blue, 5=magenta, 6=cyan, 7=white. The value corresponds to the number of pixels. Considering that 0 is the lack of colour, primary colours (red, green and blue) are absolute, and secondary colours are co-localized staining (yellow=red + green; magenta=red + blue; cyan=blue + green; and white=red + green + blue), it was possible to determine the number of pixels of determined intensity in certain area.

2.7 Brain pathology assessment

Formalin-fixed brains were coronal cut in five different anatomical sections (cranial to caudal: septum, hippocampus, superior colliculus, cerebellum and medulla) and embedded in paraffin for sectioning at 6 μm. The assessment of the brain histopathology was blinded.

2.7.1 Assessment of prion- specific spongiform encephalopathy in brain tissue.

The magnitude of the spongiform pathology (vacuolation) was assessed, in 9 different grey matter regions and 3 distinct white matter regions of the brain as described [94]. Sections were stained with H&E and the magnitude of vacuolation was determined using a scale of 0-5 index (0 represents no vacuolation and 5 represents dense vacuolation) in the nine grey matter areas (G1=medulla, G2=cerebellum, G3=superior colliculus, G4=hypothalamus, G5=thalamus, G6=hippocampus, G7=septum, G8=retro-splenial cortex, G9=cingulate and motor cortex) and a scale of 0-3 index for the 3 white matter areas (W1=cerebellum, W2=tegmentum, W3=basal cerebral peduncle or pyramidal tract).

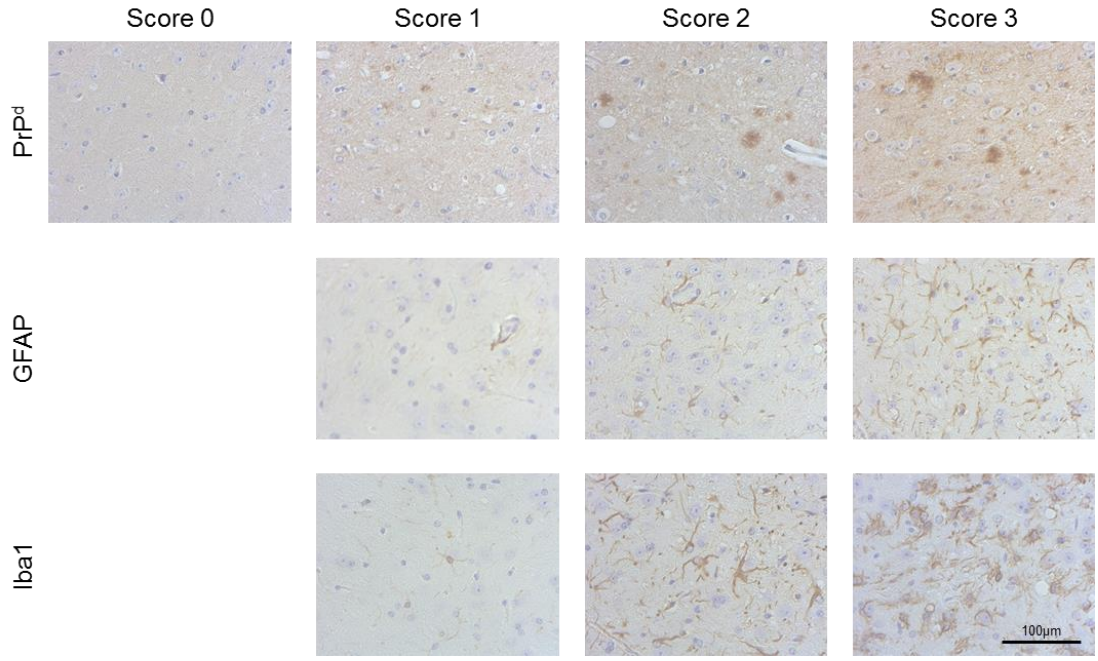

Figure 2.1. Brain pathology scoring system for PrP^d, GFAP and Iba1.

The magnitude of PrP^d deposition, astrocyte and microglia reactivity was determined using a scale of 0-3. Sections of brain from C57BL/6 mice infected with scrapie (ME7) were stained with 1B3, anti-GFAP or anti-iba1 to detect PrP^d, astrocytes and microglia respectively. The scoring system assigns a value of 0 where no staining is detected and 3 where dense staining is detected. A score of 0 was not assigned to anti-GFAP and anti-iba1 stained sections as astrocytes and microglia are normally found in the areas scored. Representative images are shown.

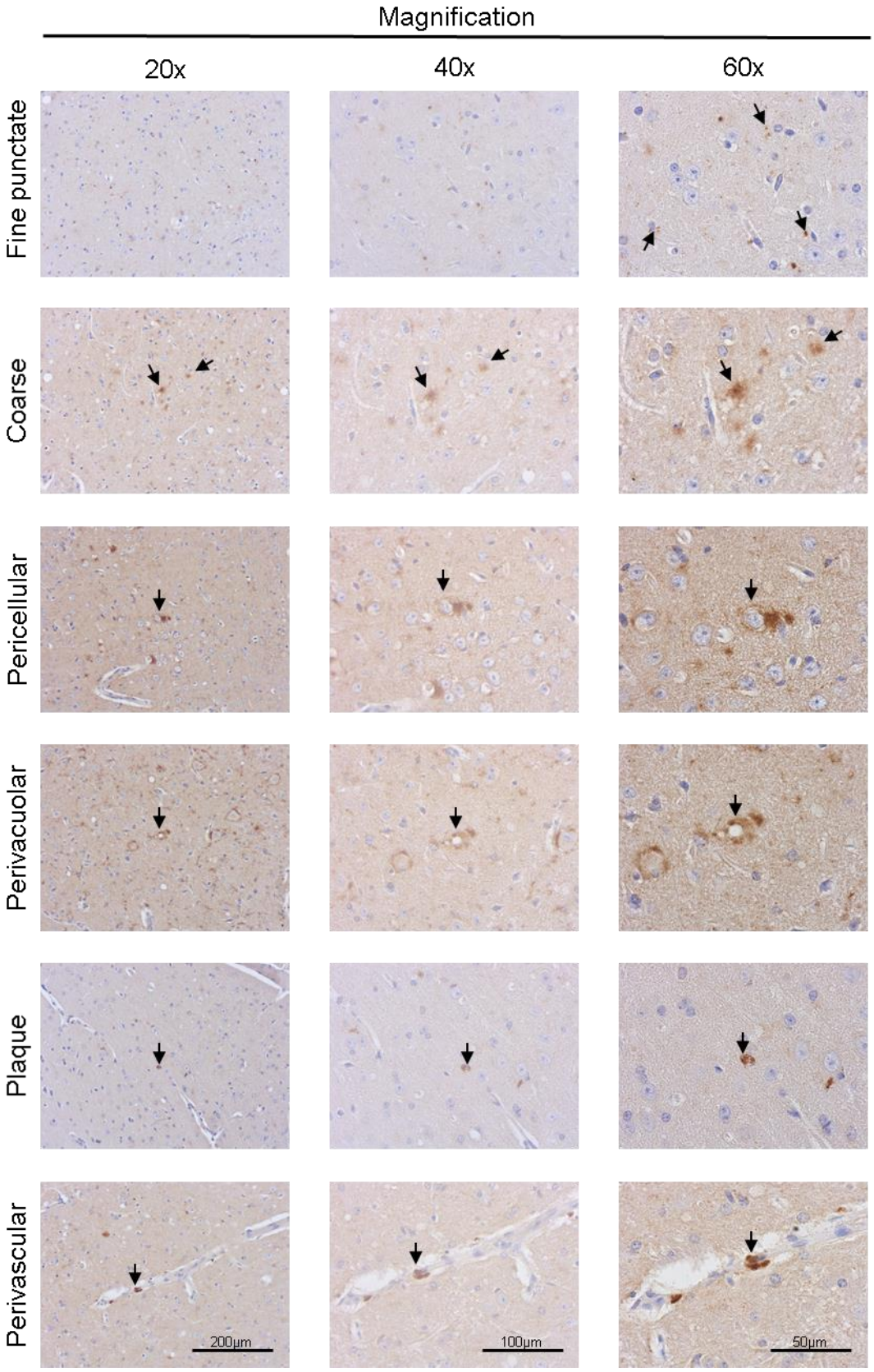
Magnification
20x
40x
60x
Fine punctate
Coarse
Pericellular
Perivacuolar
Plaque
Perivascular
200µm
100µm
50µm

Figure 2.2. Types of PrP^{Sc} deposition in C57BL/6 mice infected with scrapie (ME7).

Each raw show a representative image at different magnification (column) of different types of PrP^{Sc} deposition in brain sections of C57BL/6 mice infected with scrapie (ME7). Deposition types were classified as fine punctate deposits, coarse, pericellular, perivacuolar, plaque, and perivascular deposition.

2.7.2 Assessment of PrP^d deposition in brain tissue.

The magnitude of the presence and the magnitude of PrP^d deposition was assessed in 7 different grey matter regions of the brain. Sections were stained as described in section 2.5.5 and the magnitude of PrP was determined using a scale of 0-3 index (0 represents no PrP^d detected and 3 represents dense deposition detected) (Figure2.1). The grey matter areas analysed were G2=cerebellum, G4=hypothalamus, G5=thalamus, G6=hippocampus, G7=septum, G8=retro-splenial cortex, G9=cingulate and motor cortex). Within each area, the type of PrP^{Sc} deposition was determined and classified as: no PrP^d detected; fine punctate deposits; coarse deposition; and other forms of deposits (plaque, perivascular, perivacuolar and pericellular) (Figure 2.2).

2.7.3 Assessment of astrocyte reactivity in brain tissue.

The magnitude of astrocyte reactivity was assessed in 6 different grey matter regions by GFAP expression. Sections were stained as described in section 2.5.5 and the magnitude of GFAP was determined using a scale of 1-3 index (1 represents normal expression of GFAP detected and 3 represents dense GFAP expression detected) (Figure 2.1). The grey matter areas analysed were G4=hypothalamus, G5=thalamus, G6=hippocampus, G7=septum, G8=retro-splenial cortex, G9=cingulate and motor cortex.

2.7.4 Assessment of microglia reactivity in brain tissue.

The magnitude of microglia reactivity was assessed in 7 different grey matter regions by Iba1 expression. Sections were stained as described in section 2.5.5 and the magnitude of Iba1 expression was determined using a scale of 1-3 index (1 represents normal expression of Iba1 detected, and 3 represents dense Iba1 expression detected) (Figure 2.1). The grey matter areas analysed were G2=cerebellum, G4=hypothalamus, G5=thalamus, G6=hippocampus, G7=septum, G8=retro-splenial cortex, G9=cingulate and motor cortex.

2.8 Statistical analysis

Statistical analysis was performed using GraphPad Prism 7 () and Microsoft Excel. Data are presented as median of individuals. Differences between groups were determined by one way analysis of variance (ANOVA), followed by Dunnett post-hoc test to compare each group with the control group. P values of <0.05 were accepted as significant.

Chapter 3. Effect of *H. polygyrus* infection on the gut microarchitecture and the gut associated lymphoid tissues (GALT)

3.1 Abstract

H. polygyrus is a natural murine helminth that specifically infects the small intestine and is a useful comparative model for helminth infections in humans and livestock. Although the host immune response to *H. polygyrus* infection has been well characterized, the influence of the parasite on the microarchitecture of the intestine and the gut associated lymphoid tissues (GALT) has not been described. GALT consist of Peyer's patches (PP) and isolated lymphoid follicles (ILF). These tissues help to protect from infections and maintain the homeostasis of the intestine. These functions may be enhanced or compromised by *H. polygyrus* infection or the actions of its excretory products. This chapter shows that *H. polygyrus* infection increases the size of follicular dendritic cells (FDC) in PP follicles. *H. polygyrus* infection also altered the positioning of mononuclear phagocytes within PP and reduced the number of ILF in both the small and large intestines. These data demonstrate that *H. polygyrus* infection significantly alters the microarchitecture of the GALT. *H. polygyrus* infection also induces the formation of granulomas (lymphoid cell aggregates surrounded by fibroblasts formed as an inflammatory response) in the gut wall. These granulomas could be characterized into different developmental stages and were first detected from day 8 post infection.

Data presented in this chapter confirmed that *H. polygyrus* infection was specific to the small intestine and identified significant effects on FDC, mononuclear phagocytes, and M cells which are also known to have an active role in prion disease pathogenesis. Since granulomas are also important sites of prion accumulation, their induction during *H. polygyrus* infection may also serve as a prion accumulation site. These data will be used to inform the design

of the studies of the subsequent chapter which will determine the effects of congruent infection with *H. polygyrus* and prion diseases.

3.2 Introduction

H. polygyrus is a natural mouse small intestine restricted helminth parasite and has been widely used as a comparative model to study human (*Ancylostoma duodenale, Necator americanus)* and livestock (*Haemonchus contortus, Teladorsagia circumcincta)* helminths, due its similar phylogenetic origin [247]. Although *H. polygyrus* has been well characterized, little is known of the possible implications of parasitic co-infections on the pathogenesis of infectious prion diseases.

Within the intestine, luminal antigens are taken up into the gut associated lymphoid tissues (GALT) via the specialised follicle associated epithelium (FAE) [318, 319]. In the FAE of GALT (Peyer's patches (PP) and isolated lymphoid follicles (ILF)) reside M cells which sample intestinal contents [129, 320]. Dendritic cells may also be able to perform this function by extending their dendrites into the gut lumen and directly sampling the contents [173, 321, 322]. Smaller antigens can also cross the gut epithelium via goblet cells and enterocytes [139, 175, 323]. Once the antigens are taken up from the intestinal lumen by any of these cells, they are subsequently acquired by macrophages or dendritic cells [208, 323, 324].

During nematode infections (including *H. polygyrus*), the host develops enteritis (small intestine inflammation) [254], goblet cells hyperplasia [260], mastocytosis [283], and epithelial damage. These inflammatory processes can affect the permeability of the intestine by weakening the tight junctions between the epithelial cells [254, 325, 326]. These alterations to the gut could potentially enhance the uptake of other pathogens during the parasitic infection. Increased antigen uptake had been reported in Crohn's disease

affected ileum with low grade inflammation [327, 328]. However, the effect of *H. polygyrus* on antigen uptake has not been studied.

The aim of this chapter, therefore, is to characterize the effects of *H. polygyrus* infection on GALT and gut microarchitecture. These data will then be used in the subsequent chapter to study their potential effects on oral prion disease pathogenesis and susceptibility.

3.3 Results

3.3.1 Confirmation of *H. polygyrus* infection

C57BL/6J female mice (90 days old) were orally infected with 200 L3 by gavage. To confirm the infection, individual faecal samples were analysed to determine the number of eggs/g of faeces using the McMaster technique. Figure 3.1 shows fecal egg burden on days 11, 18, 25 and 32 post infection. The maximum egg production was reached on day 18 with a mean of 1522 eggs/g of faeces. These data confirmed that *H. polygyrus* had established a chronic infection which lasted at least 32 days.

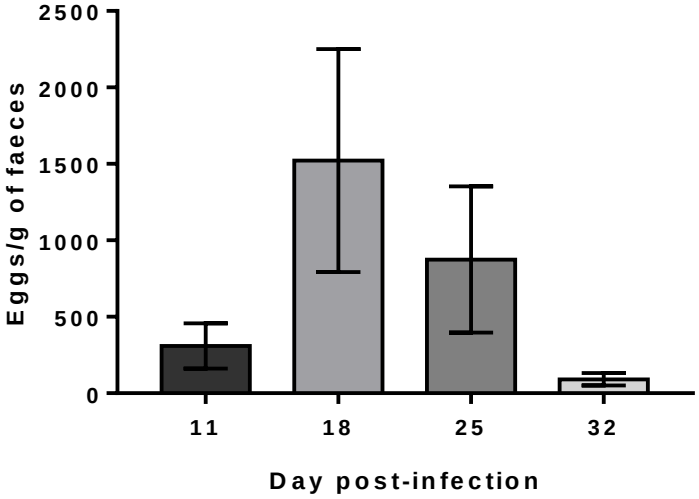

Figure. 3.1 Mean faecal egg burden following infection of C57Bl/6 mice with *H. polygyrus*. Groups of 4 female C57Bl/6J mice were orally infected with 200 L3 larvae, and the number of eggs in faeces was determined at intervals afterwards. Each bar represents mean ± SD number of egg/g of faeces from 4 individual samples.

3.3.2 Effect of *H. polygyrus* on villi microarchitecture

The intestinal epithelium consists of a permeable mono-cellular layer that act as a barrier in contact with the exterior, and it has been suggested that a dysfunction of this can predispose to other disease [329, 330]. To determine the effect of *H. polygyrus* infection on villus microarchitecture, groups of mice infected with *H. polygyrus* were culled at different times (days 1, 3, 8, 14, 21, and 35) post infection and tissues were collected for analysis. Snap frozen sections of duodenum, ileum and colon were H&E stained. Figure 3.2 shows that damage to the epithelium and the presence of worms were evident in the duodenum from day 8 onwards; in the ileum there were no evident changes until day 14 when there was an apparent increase of goblet cells. In the colon, no changes were observed.

Next, the effect of *H. polygyrus* on villus length, width, and perimeter were determined. Usually, 8 to 12 duodenal villi and 8 to 14 ileal villi were analysed per mouse for each characteristic. To determine villus width, each villus width was measured at the base (from crypt to crypt), at the middle of the villus length and at the top; and the mean of these measurements determined. Figure 3.3A, shows the effects of *H. polygyrus* infection on duodenal villi. This analysis showed that although *H. polygyrus* infection did not alter villus length or perimeter, there was a significant increase in villus width ($p \leq 0.011$) on days 8 and 14 post infection. In contrary, assessment of the villi in the ileum did not reveal any significant difference in villus width (Figure 3.3B). However, there were significant differences in villus length ($p=0.035$) and perimeter ($p=0.019$) at day 1 post infection. No effect of *H. polygyrus* infection on the histopathology of the colon was observed (Figure 3.3C).

These data confirm that changes to the villi caused by *H. polygyrus* infection are restricted to the small intestine. The changes predominantly consist of damage to the epithelium, an increase in villus width in the duodenum; and an acute reduction of the villus length and perimeter in the ileum.

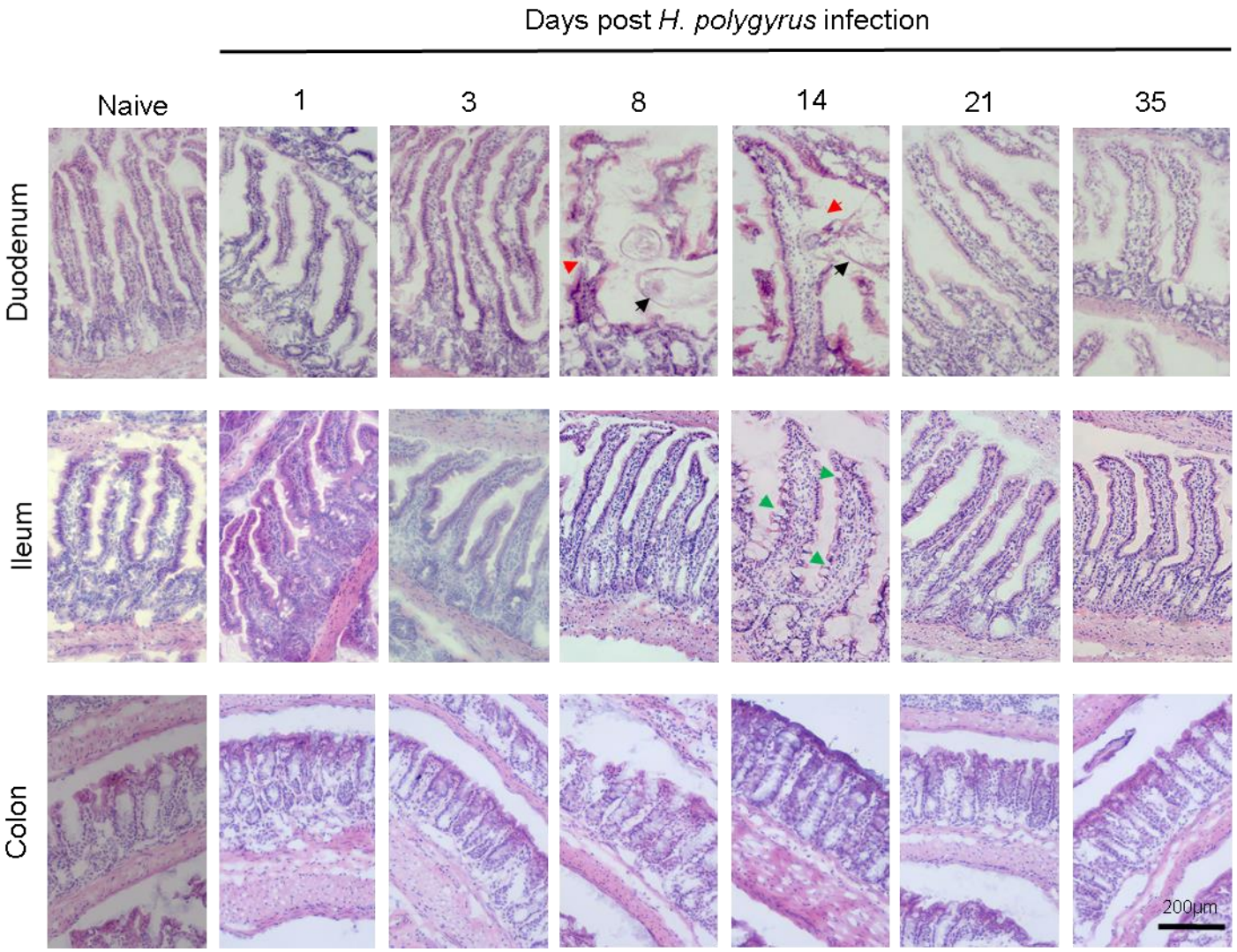
Days post H. polygyrus infection
Naive
1
3
8
14
21
35
Duodenum
Ileum
Colon
200μm

Figure 3.2 Effect of oral *H. polygyrus* infection on the gut epithelium. Groups of 4 female C57Bl/6J mice were orally infected with 200 L3 larvae, and the duodenum, ileum and colon collected at intervals afterwards and H&E stained tissue sections analysed by microscopy. In the duodenum, damage of the epithelium (red arrows), and the presence of worms (black arrows) were visible on days 8 and 14 post infection. In ileum, on day 14, unstained spaces apparently correspond to goblet cells (green arrows).

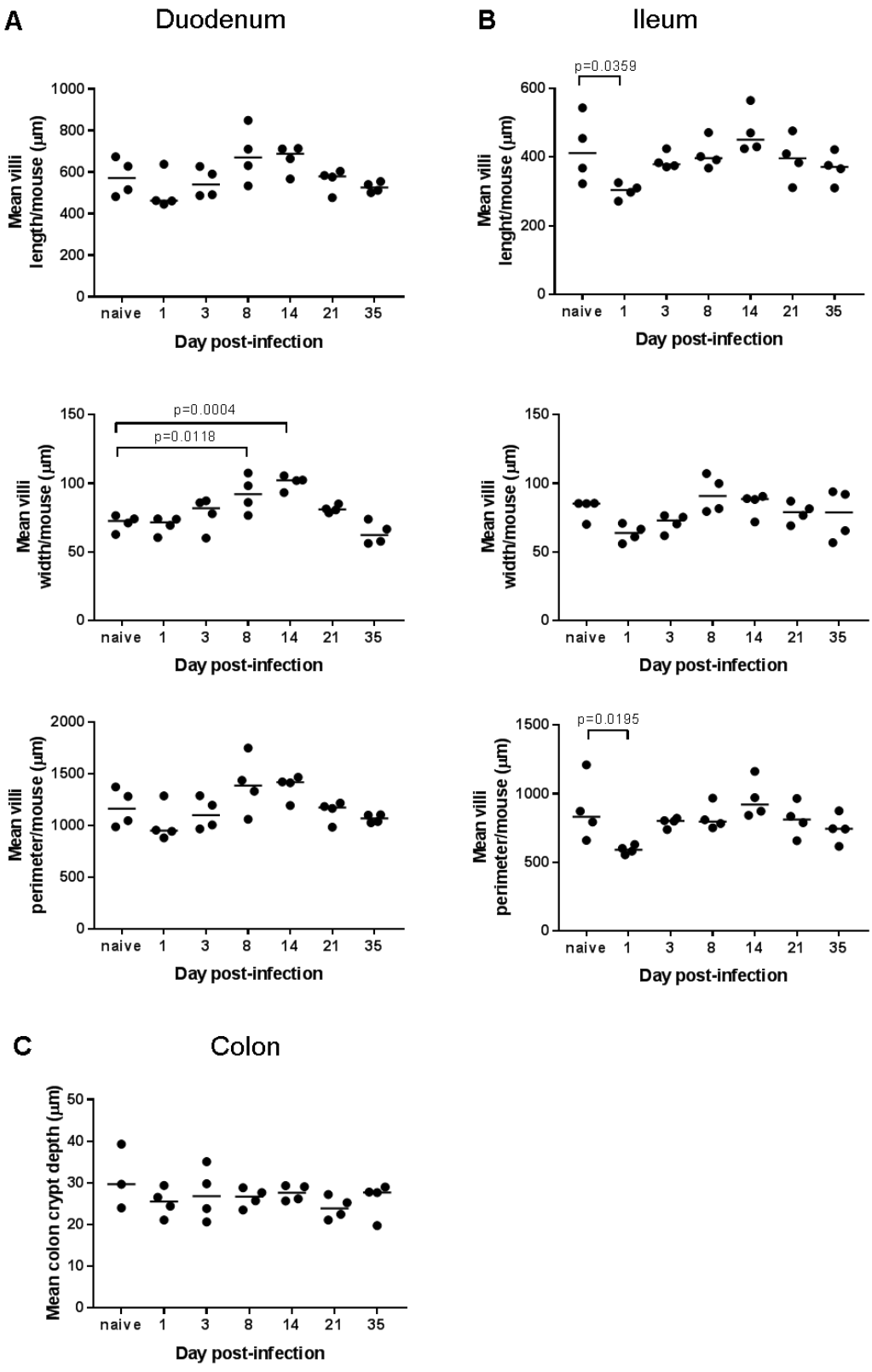
A
Duodenum
B
Ileum
Mean villi length/mouse (µm)
Mean villi lenght/mouse (µm)
p=0.0359
Mean villi width/mouse (µm)
p=0.0004
p=0.0118
Mean villi perimeter/mouse (µm)
p=0.0195
C
Colon
Mean colon crypt depth (µm)
naive 1 3 8 14 21 35
Day post-infection

Figure 3.3 Effect of oral *H. polygyrus* infection on the morphology of the gut epithelium. Groups of female C57Bl/6 mice were orally infected with 200 L3 larvae, and the duodenum, ileum and colon collected at intervals afterwards and H&E stained tissue sections analysed by microscopy. Villus length, width and perimeter were determined in (A) the duodenum, and (B) the ileum. Data show mean ± SD for 4 mice/group. 8-12 villi/mouse were measured in the duodenum, and 8-14 villi/mouse were measured in the ileum. (C) Crypt depth was compared in the colon in 3 distinct regions in 3-4 mice/group. Significant differences to the naïve group were compared by ANOVA, followed by Dunnett's multiple comparison test.

3.3.3 Effect of *H. polygyrus* on goblet cells

To determine the effect of *H. polygyrus* infection on goblet cells, sections of duodenum were stained with Periodic acid–Schiff (PAS). Figure 3.4A shows the abundance of goblet cells (magenta) at different days post *H. polygyrus* infection. Goblet cell hyperplasia was clearly evident on day 14 post infection. Quantitative analysis of goblet cells density in the gut epithelium revealed a statistically significant increase in the number of goblet cells ($p \leq 0.023$) in duodenum on days 14 and 21 post *H. polygyrus* infection (Figure 3.4B).

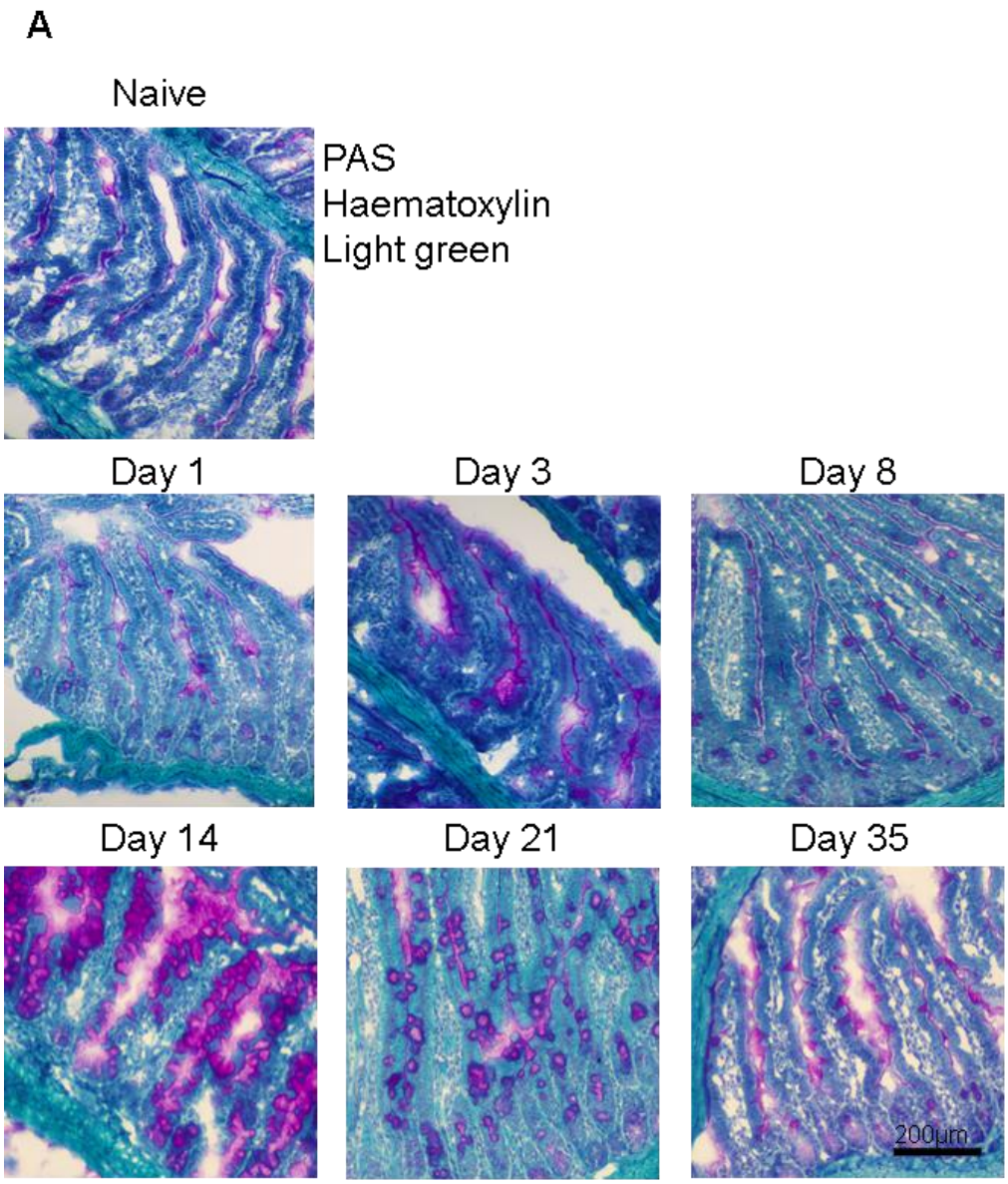
A
Naive
PAS
Haematoxylin
Light green
Day 1
Day 3
Day 8
Day 14
Day 21
Day 35
200µm
B
p=0.0238
p=0.0001
Mean number of goblet cells/100µm of duodenum epithelial surface / mouse
0
1
2
3
4
naive
1
3
8
14
21
35
Day post-infection

Figure 3.4 Effect of oral *H. polygyrus* infection on goblet cell density in the duodenum. Groups of female C57Bl/6 mice were orally infected with 200 L3 larvae, and the duodenum collected at intervals afterwards and PAS stained to detect goblet cells. (A) Images show the abundance of PAS+ goblet cells (magenta) in representative samples from the duodenum at each time point. Sections were counterstained with haematoxylin (blue) to detect cell nuclei. (B) Morphometric analysis of goblet cell density in the villous epithelium in the duodenum. Data were obtained from four villi/mouse and show mean ± SD for 4 mice/group. Significant differences to the naïve group were compared by ANOVA, followed by Dunnett's multiple comparison test.

3.3.4 Effect of *H. polygyrus* on mononuclear phagocytes in the lamina propria of the small intestine.

Mononuclear phagocytes in the lamina propria of the small intestine (duodenum and ileum) were also analysed by immunohistochemistry (IHC) at different time-points post *H. polygyrus* infection. The markers used to detect the mononuclear phagocytes were CD11c, CD68, and CD11b (Figures 3.5A and 3.6A). A statistically significant increase in the level of $CD11b^+$ staining ($p=0.0068$) in the lamina propria of the duodenum was observed at day 21 post infection (Figure 3.5B). Levels of $CD68^+$ and $CD11c^+$ staining (Figure 3.5B) were unchanged. A similar trend was also observed in the ileum (Figure 3.6B). $CD11b^+$ staining was significantly increased on day 21 ($p=0.0469$), whereas $CD11c^+$ and $CD68^+$ staining appeared unchanged. Nonetheless, it is important to notice that the significant increase of $CD11b^+$ staining in the ileum is caused by the high staining levels in only one of the four mice studied. However, these data show that *H. polygyrus* significantly influenced $CD11b^+$ expression in the lamina propria of the small intestine.

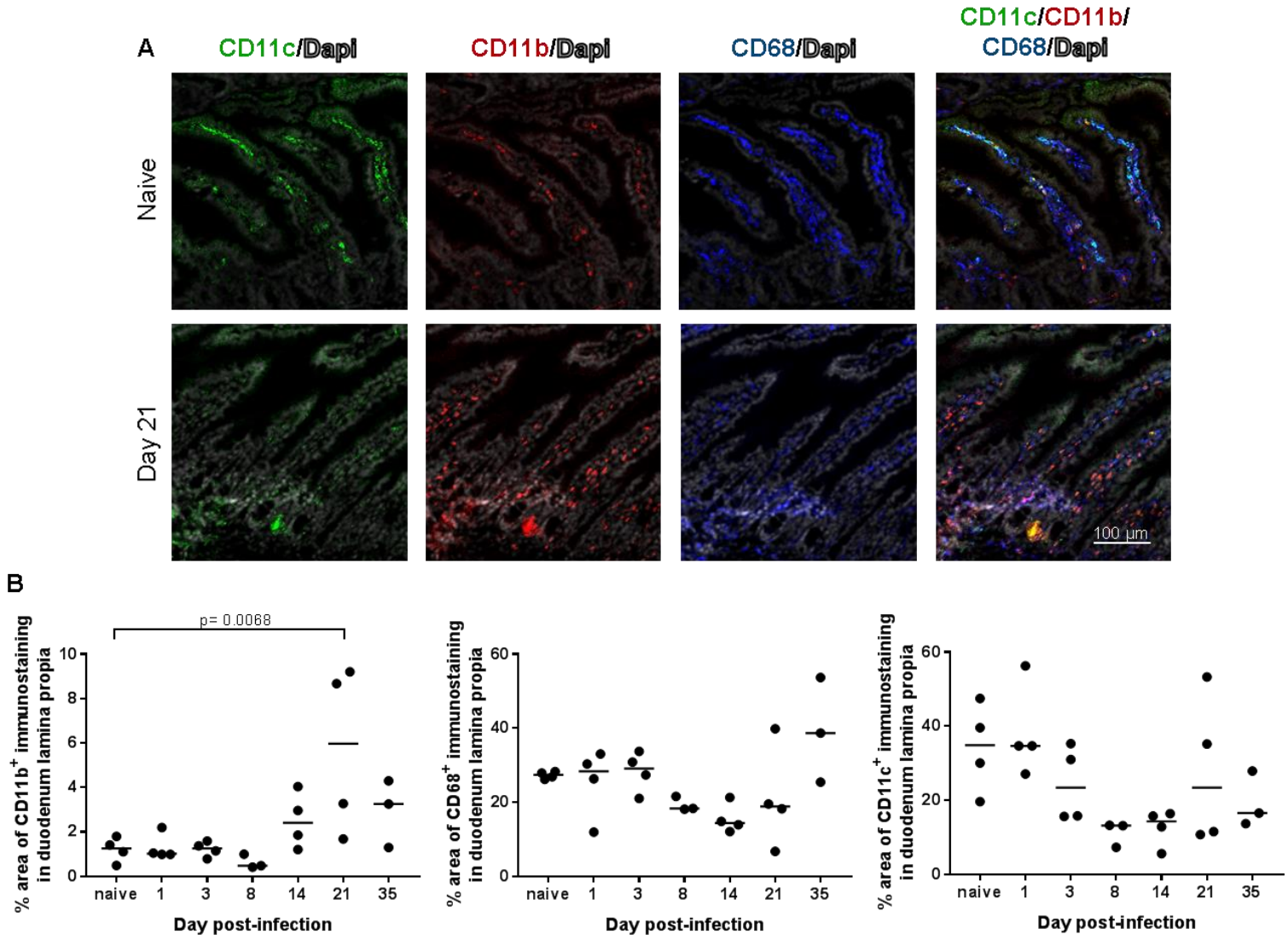
A
CD11c/DapI
CD11b/DapI
CD68/DapI
CD11c/CD11b/
CD68/DapI
Naive
Day 21
100 µm
B
p= 0.0068
% area of CD11b+ immunostaining in duodenum lamina propia
% area of CD68+ immunostaining in duodenum lamina propia
% area of CD11c+ immunostaining in duodenum lamina propia
naive
1
3
8
14
21
35
Day post-infection

Figure 3.5 Effect of oral *H. polygyrus* infection on the distribution of mononuclear phagocytes in the lamina propria of the duodenum. Groups of female C57Bl/6 mice were orally infected with 200 L3 larvae, and the duodenum collected at intervals afterwards. (A) Sections were immunostained to detect $CD11c^+$ (green), $CD68^+$ (blue), $CD11b^+$ (red) mononuclear phagocytes, and counterstained with DAPI (white) to detect cell nuclei. (B) Morphometric analysis of the % area $CD11c^+$, $CD68^+$ or $CD11b^+$ immunostaining in the lamina propria. Each point represents the data from individual mice (3-4 mice/group). Horizontal bar represents the median of the group. Significant differences to the naïve group were compared by ANOVA, followed by Dunnett's multiple comparison test.

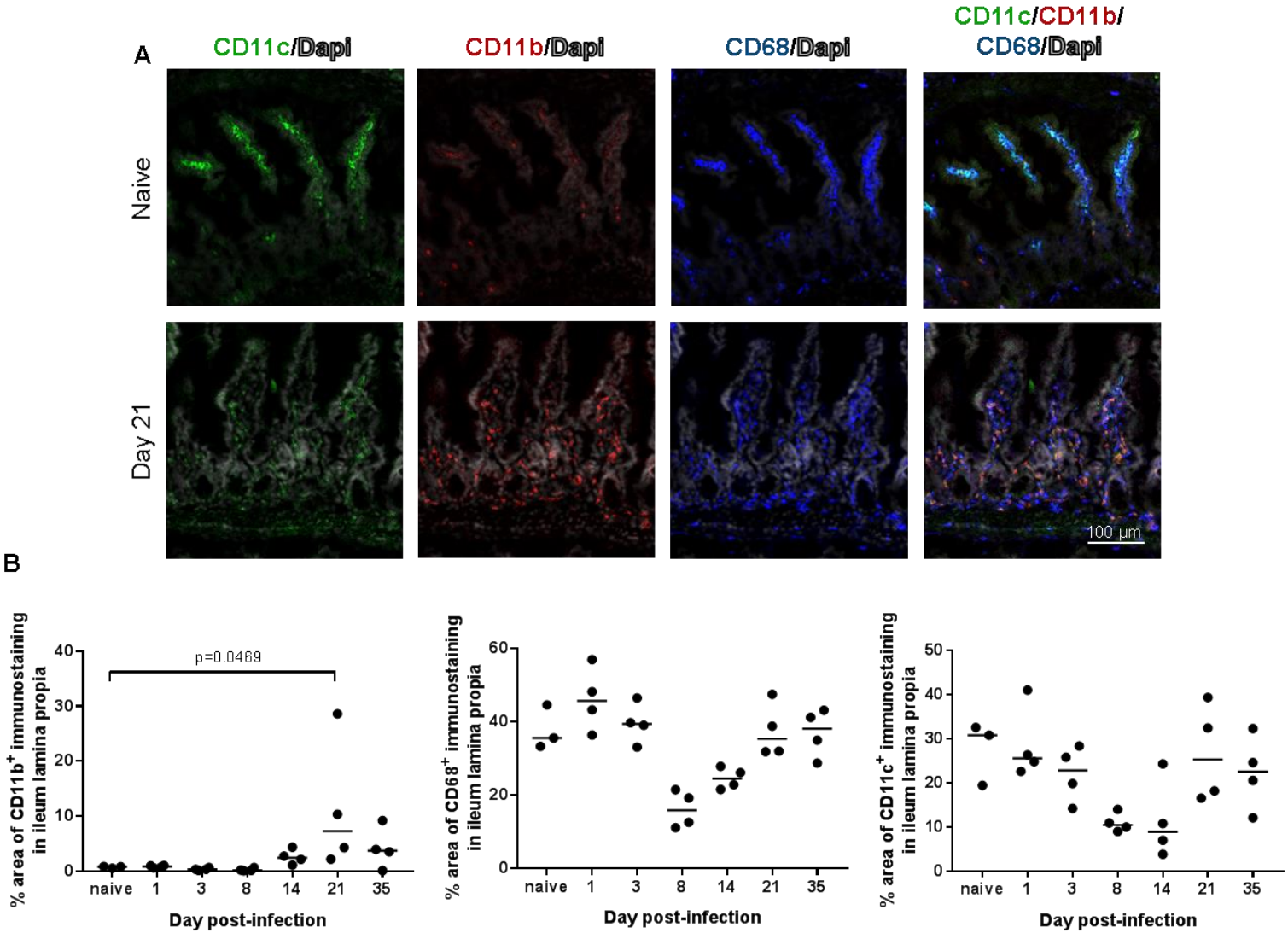
A
CD11c/Dapi
CD11b/Dapi
CD68/Dapi
CD11c/CD11b/
CD68/Dapi
Naive
Day 21
100 µm
B
% area of CD11b+ immunostaining in ileum lamina propia
p=0.0469
naive 1 3 8 14 21 35
Day post-infection
% area of CD68+ immunostaining in ileum lamina propia
naive 1 3 8 14 21 35
Day post-infection
% area of CD11c+ immunostaining in ileum lamina propia
naive 1 3 8 14 21 35
Day post-infection

Figure 3.6 Effect of oral *H. polygyrus* infection on the distribution of mononuclear phagocytes in the lamina propria of the ileum. Groups of female C57Bl/6 mice were orally infected with 200 L3 larvae, and the ileum collected at intervals afterwards. (A) Sections were immunostained to detect $CD11c^+$ (green), $CD68^+$ (blue), $CD11b^+$ (red) mononuclear phagocytes, and counterstained with DAPI (white) to detect cell nuclei. (B) Morphometric analysis of the % area $CD11c^+$, $CD68^+$ or $CD11b^+$ immunostaining in the lamina propria. Each point represents the data from individual mice (3-4 mice/group). Horizontal bar represents the median of the group. Significant differences to the naïve group were compared by ANOVA, followed by Dunnett's multiple comparison test.

3.3.5 Effect of *H. polygyrus* infection on enteric nerves

Studies suggest that the spread of oral prion infection to the central nervous system is through enteric nerves [206, 331, 332] and thus the effect of *H. polygyrus* infection on enteric nerves was determined. To identify the presence of nerves, sections of small intestine were stained with anti-synaptophysin-1 to detect synaptic vesicles (Figure 3.7A). Levels of synaptophysin-1 staining were unchanged at any of the time-points after *H. polygyrus* infection (when compared to the naive group (Figure 3.7B). As PrP^{Sc} needs PrP^{C} as substrate, the level of PrP^{C} on enteric nerves was determined in a parallel set of duodenal sections. Representative images from each time-point post infection are presented in Figure 3.8A. PrP^{C} staining levels were also unchanged when compared to the naive group (Figure 3.8B). Together, these data suggest there was no significant effect of *H. polygyrus* infection on enteric nerve status in the lamina propria.

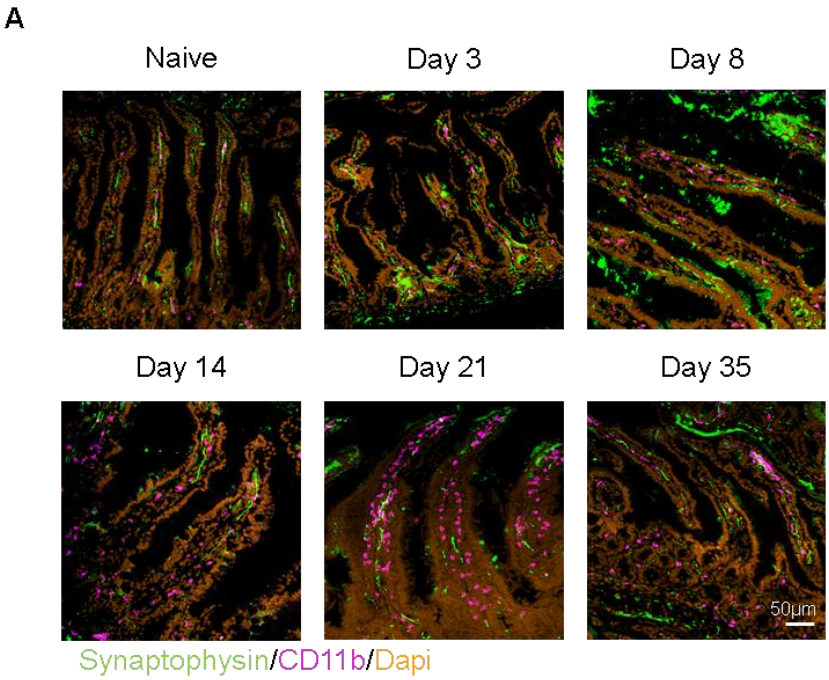
A
Naive
Day 3
Day 8
Day 14
Day 21
Day 35
50µm
Synaptophysin/CD11b/Dapi

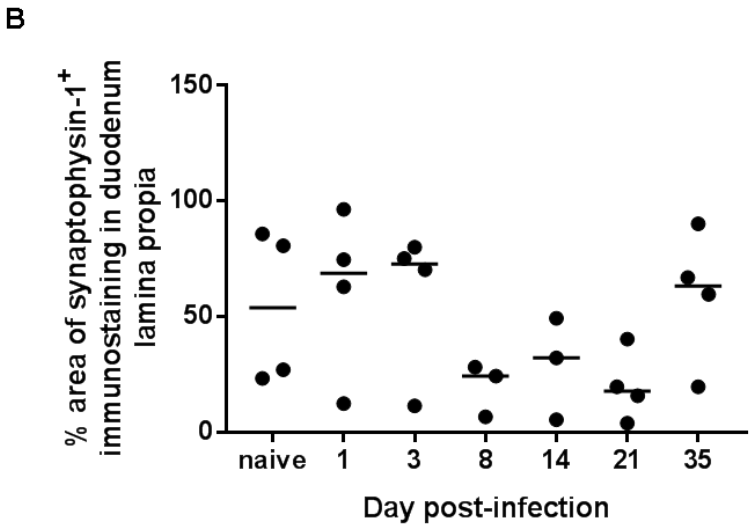
B
% area of synaptophysin-1+ immunostaining in duodenum lamina propia
150
100
50
0
naive
1
3
8
14
21
35
Day post-infection

Figure 3.7 Effect of oral *H. polygyrus* infection on the distribution of synaptophysin-1 expressing enteric nerves in the lamina propria of the duodenum. Groups of female C57Bl/6 mice were orally infected with 200 L3 larvae, and the duodenum collected at intervals afterwards. (A) Sections were immunostained to detect synaptophysin-1 (green), CD11b (red) and counterstained with DAPI (orange) to detect cell nuclei. Non-specific staining localized out of the lamina propria (e.g. Day 8) was not considered for analysis. (B) Morphometric analysis of the % area synaptophysin-1^+ immunostaining in the lamina propria. Each point represents the data from individual mice (3-4 mice/group). Horizontal bar represents the median of the group. Significant differences to the naïve group were compared by ANOVA, followed by Dunnett's multiple comparison test.

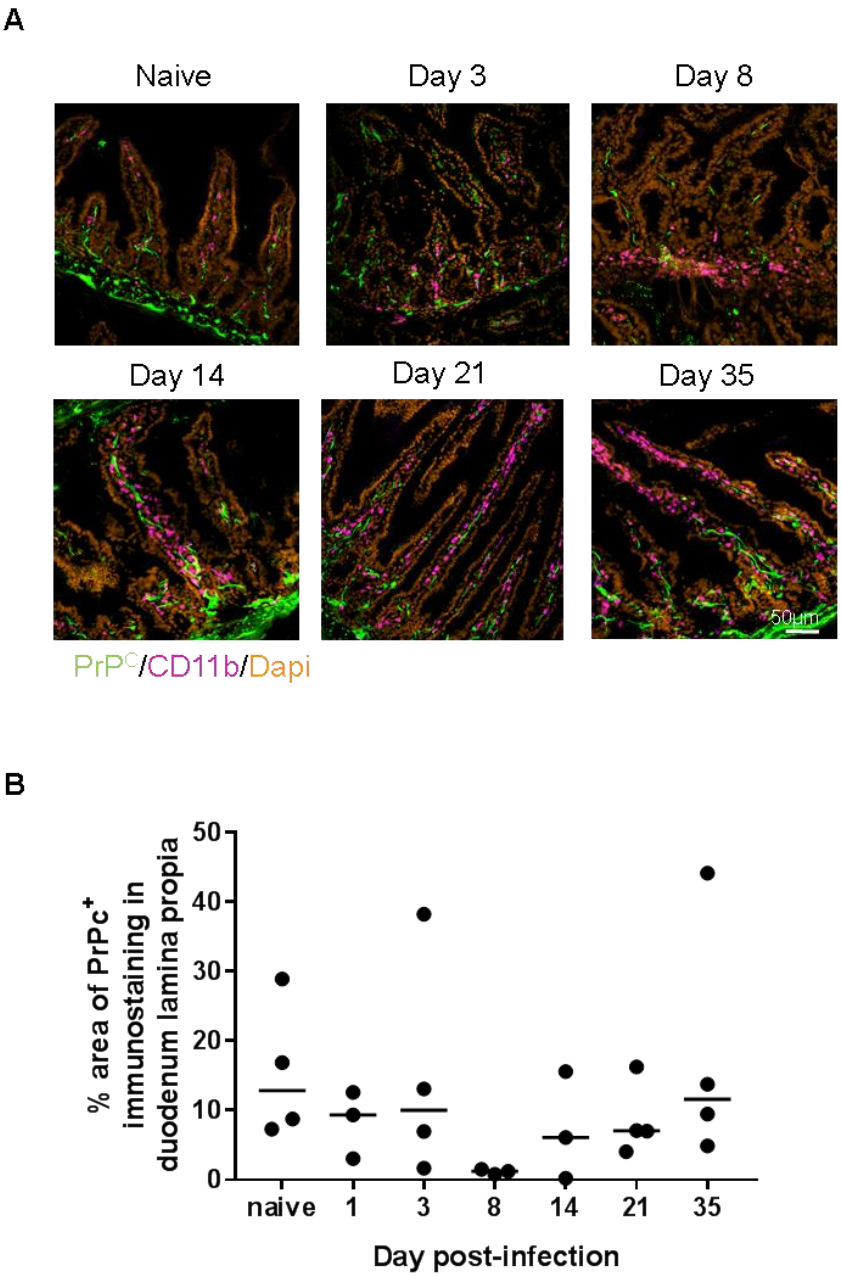

Figure 3.8 Effect of oral *H. polygyrus* infection on the distribution of PrP^C expressing enteric nerves in the lamina propria of the duodenum. Groups of female C57Bl/6 mice were orally infected with 200 L3 larvae, and the duodenum collected at intervals afterwards. (A) Sections were immunostained to detect PrP^C (green), CD11b (red) and counterstained with DAPI (orange) to detect cell nuclei. (B) Morphometric analysis of the % area PrP^{C+} immunostaining in the lamina propria. Each point represents the data from individual mice (3-4 mice/group). Horizontal bar represents the median of the group. Significant differences to the naïve group were compared by ANOVA, followed by Dunnett's multiple comparison test.

3.3.6 Effect of *H. polygyrus* infection on the number and size of ILF

ILF are dynamic lymphoid structures similar to the Peyer patches that may uptake and replicate prions [333-335]. In order to determine if ILF density or size was altered during *H. polygyrus* infection, pieces of duodenum, ileum and colon were whole-mounted immunostained with B220 antibody to detect the B cell clusters (ILF) at different times post *H. polygyrus* infection (Figure 3.9A to 3.11A). The density and the area of ILF were calculated in each sample. In the duodenum (Figure 3.9A), there was a statistically significant reduction in the number of ILF ($p=0.038$) on day 14 post *H. polygyrus* infection (Figure 3.9B). In the ileum (Figure 3.10A) no statistically significant effects of *H. polygyrus* infection on either the number (Figure 3.10B) or size (Figure 3.10C) of the ILF were detected. Meanwhile, in the colon (Figure 3.11A), there was a statistically significant reduction in the number of ILF ($p=0.018$) on day 14 post *H. polygyrus* infection (Figure 3.11B), but the size of the ILF was not altered (Figure 3.11C). Therefore, these data show that *H. polygyrus* infection significantly reduced the number of ILF on the duodenum and colon on day 14 post-infection.

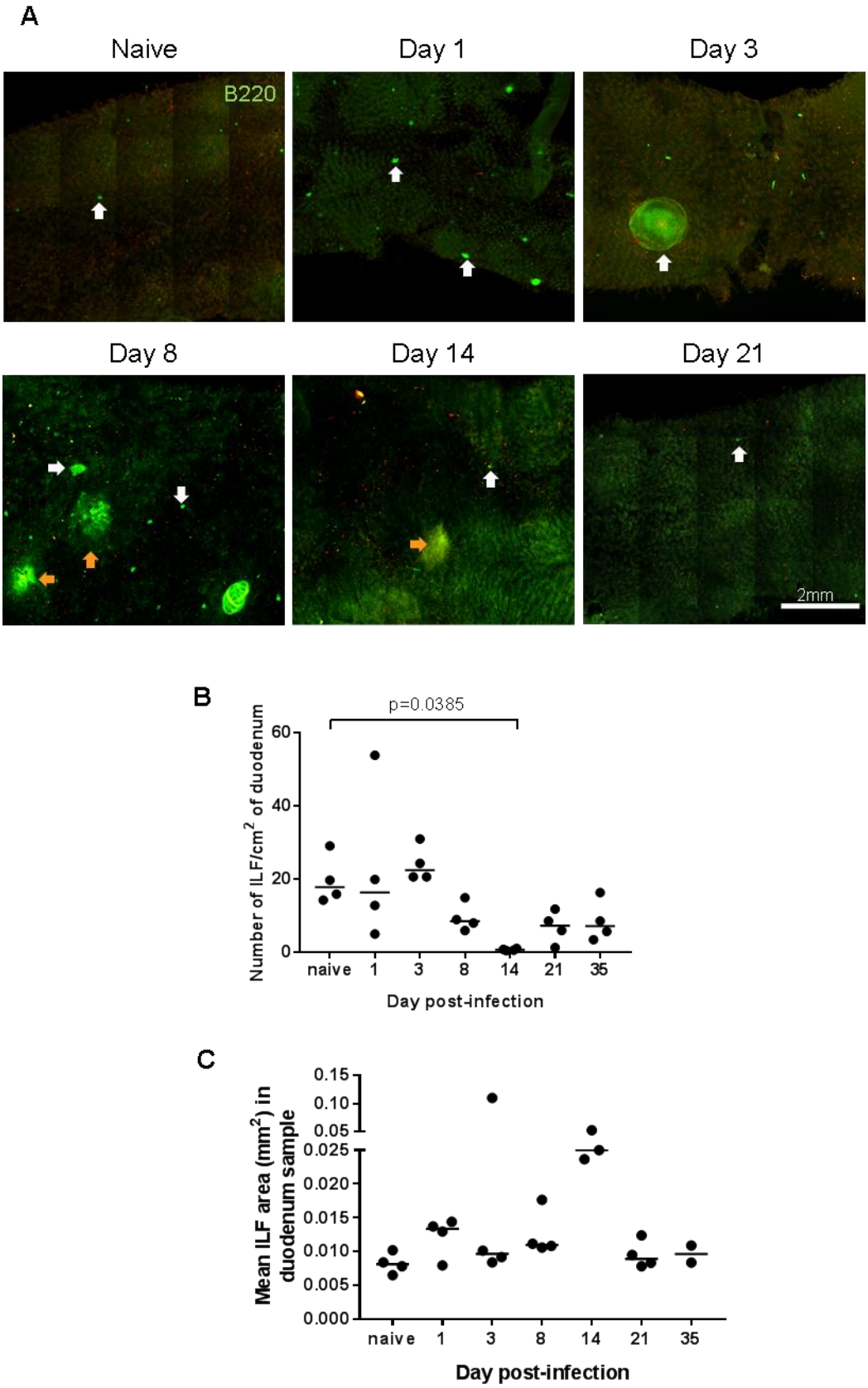
A
Naive
Day 1
Day 3
B220
Day 8
Day 14
Day 21
2mm
B
p=0.0385
Number of ILF/cm2 of duodenum
60
40
20
0
naive
1
3
8
14
21
35
Day post-infection
C
Mean ILF area (mm2) in duodenum sample
0.15
0.10
0.05
0.025
0.020
0.015
0.010
0.005
0.000
naive
1
3
8
14
21
35
Day post-infection

Figure 3.9 Effect of oral *H. polygyrus* infection on the density of isolated lymphoid follicles (ILF) in the duodenum. Groups of female C57Bl/6 mice were orally infected with 200 L3 larvae, and the duodenum collected at intervals afterwards. (A) 2 cm portions of duodenum were whole-mount immunostained using B220 to detect B cell clusters (ILF) (white arrows, green). Orange arrows show sites of *H. polygyrus* damage to epithelium. Morphometric analysis of the (B) number of ILF and (C) the mean ILF area in each sample. Each point represents data from individual mice (4 mice/group). Horizontal bar represents the median of the group. Significant differences to the naïve group were compared by ANOVA, followed by Dunnett's multiple comparison test.

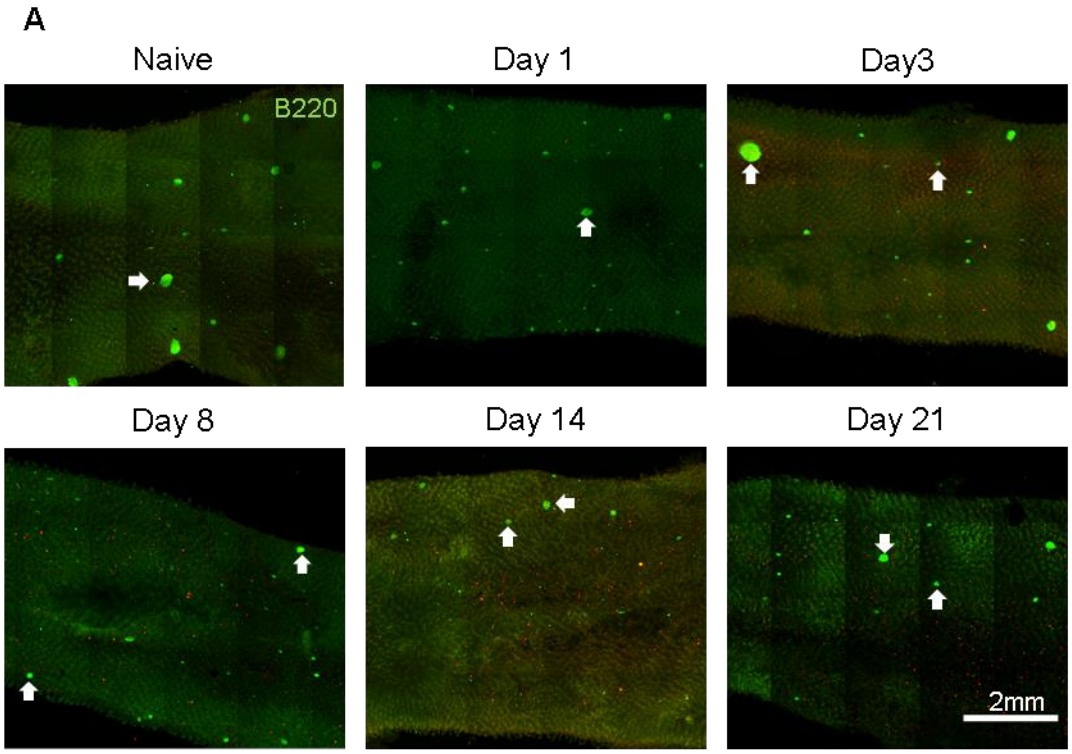
A
Naive
Day 1
Day3
B220
Day 8
Day 14
Day 21
2mm

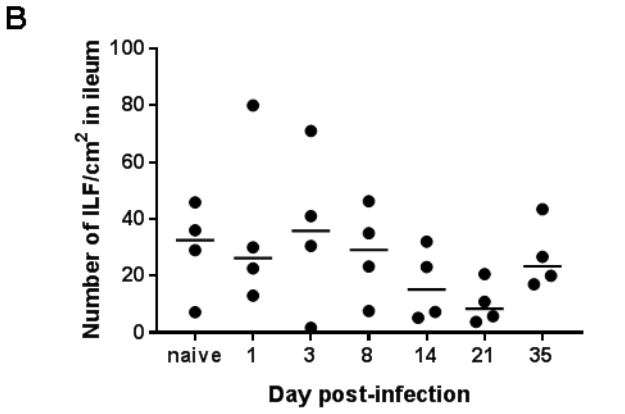
B
Number of ILF/cm2 in ileum
100
80
60
40
20
0
naive
1
3
8
14
21
35
Day post-infection

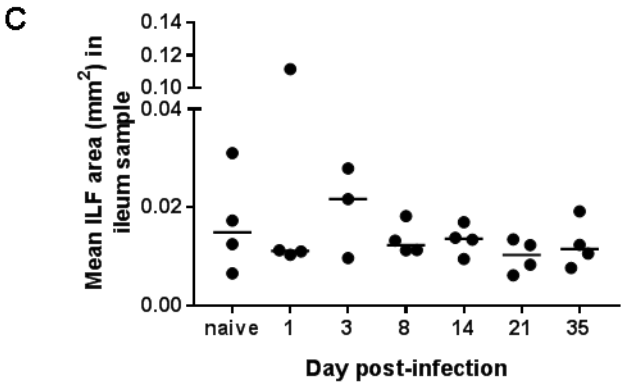
C
Mean ILF area (mm2) in ileum sample
0.14
0.12
0.10
0.04
0.02
0.00
naive
1
3
8
14
21
35
Day post-infection

Figure 3.10 Effect of oral *H. polygyrus* infection on the density of isolated lymphoid follicles (ILF) in the ileum. Groups of female C57Bl/6 mice were orally infected with 200 L3 larvae, and the ileum collected at intervals afterwards. (A) 2 cm portions of ileum were whole-mount immunostained using B220 to detect B cell clusters (ILF) (white arrows, green). Morphometric analysis of the (B) number of ILF and (C) the mean ILF area in each sample. Each point represents data from individual mice (4 mice/group). Horizontal bar represents the median of the group. Significant differences to the naïve group were compared by ANOVA, followed by Dunnett's multiple comparison test.

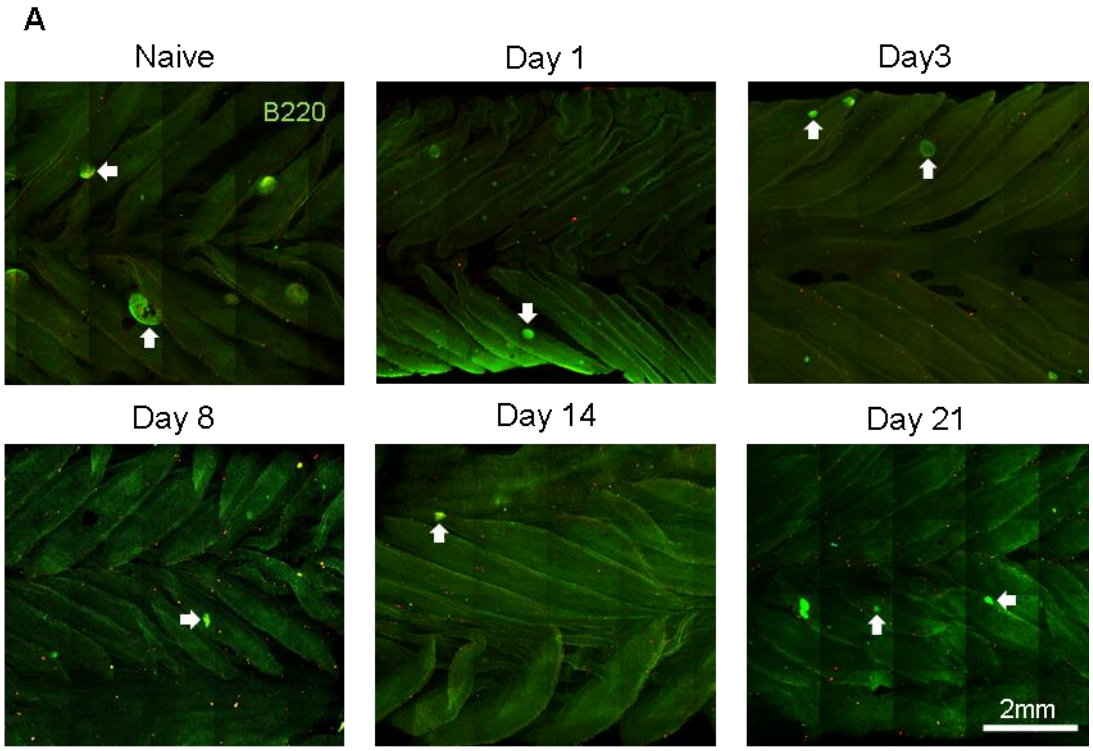
A
Naive
Day 1
Day3
B220
Day 8
Day 14
Day 21
2mm

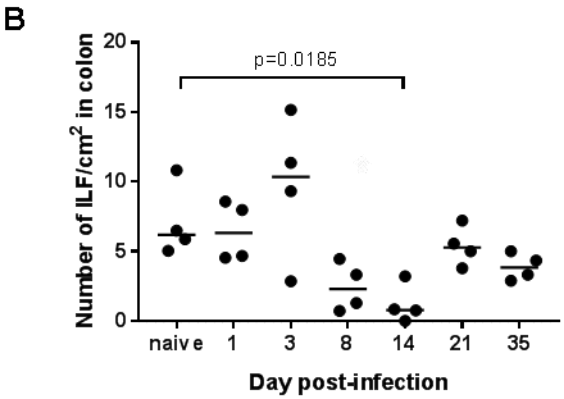
B
p=0.0185
Number of ILF/cm2 in colon
20
15
10
5
0
naive
1
3
8
14
21
35
Day post-infection

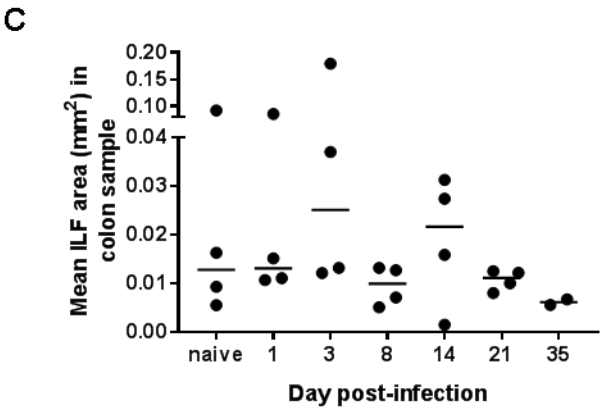
C
Mean ILF area (mm2) in colon sample
0.20
0.15
0.10
0.04
0.03
0.02
0.01
0.00
naive
1
3
8
14
21
35
Day post-infection

Figure 3.11 Effect of oral *H. polygyrus* infection on the density of isolated lymphoid follicles (ILF) in the colon. Groups of female C57Bl/6 mice were orally infected with 200 L3 larvae, and the colon collected at intervals afterwards. (A) 2 cm portions of colon were whole-mount immunostained using B220 to detect B cell clusters (ILF) (white arrows, green). Morphometric analysis of the (B) number of ILF and (C) the mean ILF area in each sample. Each point represents data from individual mice (4 mice/group). Horizontal bar represents the median of the group. Significant differences to the naïve group were compared by ANOVA, followed by Dunnett's multiple comparison test.

3.3.7 Influence of *H. polygyrus* infection on the FAE overlying the Peyer's patches.

M cells which sample luminal antigens such as prions or bacteria are present in the FAE of the Peyer's patches [336-338]. Goblet cells are also present, and it has been suggested that these can also act as antigen entrance sites [175, 323]. To assess the effect of *H. polygyrus* infection on the PP microarchitecture, at each time-point, one duodenal and one ileal PP were whole mounted immunostained to detect M cells ($GP2^+$cells; green) and goblet cells ($GP2^-$UEA-1^+ cells; red) (Figures 3.12A & 3.13A). From each image, the area of each FAE was measured as well as the number of M cells and goblet cells within them. No statistically significant effect of *H. polygyrus* infection on the area of the FAE in duodenum (Figure 3.12B) or ileum (Figure 3.13B) was detected. However, in the duodenum, M cell density was statistically significantly increased ($p=0.0003$) on day 35 post *H. polygyrus* infection (Figure 3.12C). In the ileum, *H. polygyrus* infection had no statistically significant effect on M cell density (Figure 3.13C). The density of goblet cells was also statistically significantly increased on days 14, 21 and 35 in the duodenum (Figure 3.12D; $p\leq0.0026$), and on days 21 and 35 (Figure 3.13D; $p\leq0.039$) in ileum. These data demonstarte that *H. polygyrus* infection significantly increased the density of M cells and goblet cells in the FAE of PP.

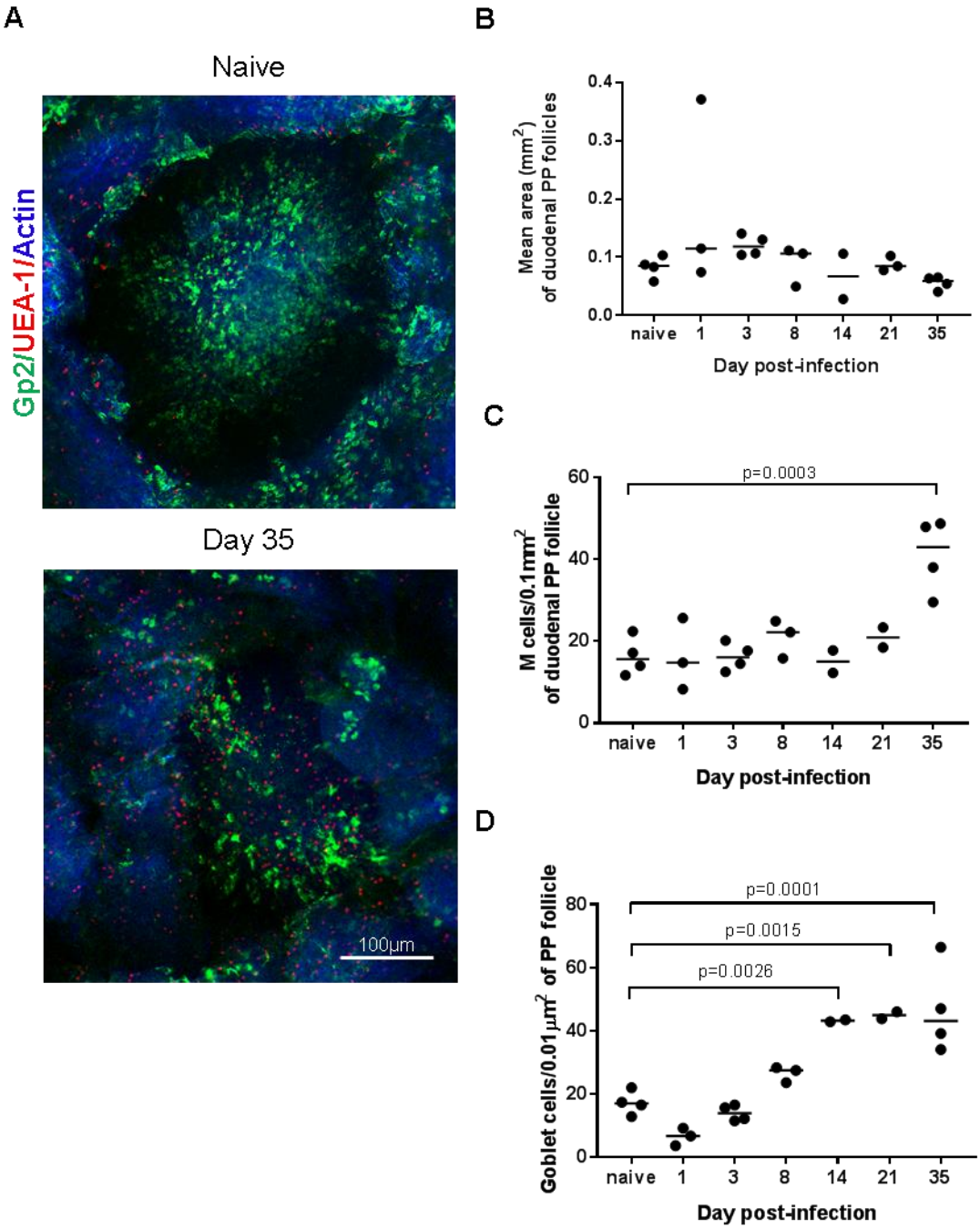
A
Naive
Gp2/UEA-1/Actin
Day 35
100µm
B
Mean area (mm2) of duodenal PP follicles
0.4
0.3
0.2
0.1
0.0
naive 1 3 8 14 21 35
Day post-infection
C
M cells/0.1mm2 of duodenal PP follicle
p=0.0003
60
40
20
0
naive 1 3 8 14 21 35
Day post-infection
D
Goblet cells/0.01µm2 of PP follicle
p=0.0001
p=0.0015
p=0.0026
80
60
40
20
0
naive 1 3 8 14 21 35
Day post-infection

Figure 3.12 Effect of oral *H. polygyrus* infection on the density of M cells and goblet cells in the follicle-associated epithelia (FAE) overlying the Peyer's patches (PP) in the duodenum. Groups of female C57Bl/6 mice were orally infected with 200 L3 larvae, and the duodenum collected at intervals afterwards. (A) PP were whole-mount immunostained to detect M cells (Gp2+ cells, green) and goblet cell (UEA-1+ cells, red). Tissues were counterstained to detect F-actin (blue). Morphometric analysis of the (B) mean FAE size in each PP, (C) M cell (Gp2+UEA-1- cells) density, and (D) goblet cell density (Gp2-UEA-1+ cells). Each point represents mean data from two FAE from 2-4 mice/group. Horizontal bar represents the median of the group. Significant differences to the naïve group were compared by ANOVA, followed by Dunnett's multiple comparison test.

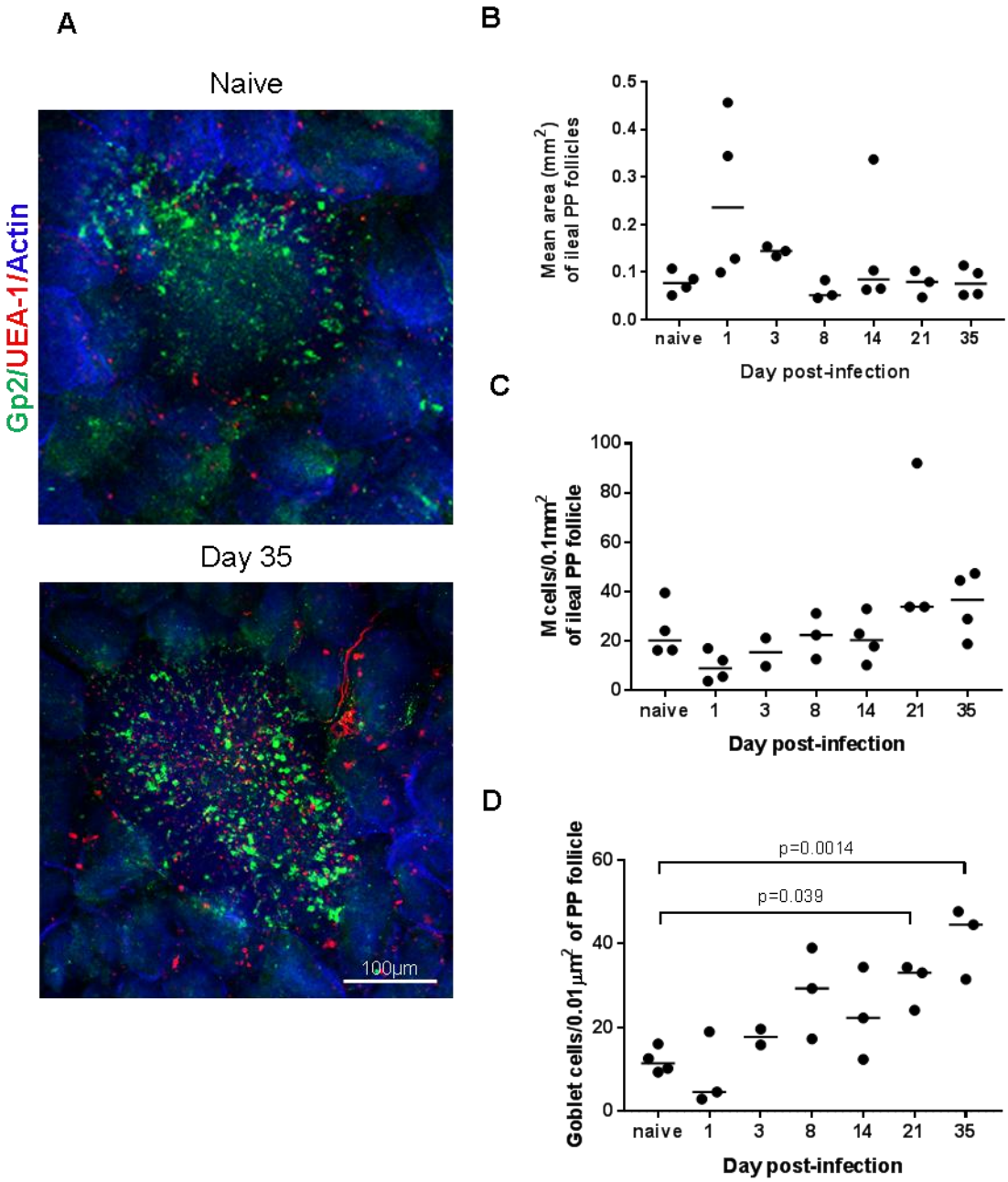
A
Naive
Gp2/UEA-1/Actin
Day 35
100µm
B
Mean area (mm2) of ileal PP follicles
0.5
0.4
0.3
0.2
0.1
0.0
naive 1 3 8 14 21 35
Day post-infection
C
M cells/0.1mm2 of ileal PP follicle
100
80
60
40
20
0
naive 1 3 8 14 21 35
Day post-infection
D
Goblet cells/0.01 µm2 of PP follicle
p=0.0014
p=0.039
60
40
20
0
naive 1 3 8 14 21 35
Day post-infection

Figure 3.13 Effect of oral *H. polygyrus* infection on the density of M cells and goblet cells in the follicle-associated epithelia (FAE) overlying the Peyer's patches (PP) in the ileum. Groups of female C57Bl/6 mice were orally infected with 200 L3 larvae, and the ileum collected at intervals afterwards. (A) PP were whole-mount immunostained to detect M cells (Gp2+ cells, green) and goblet cell (UEA-1-binding cells, red). Tissues were counterstained to detect F-actin (blue). Morphometric analysis of the (B) mean FAE size in each PP, (C) M cell (Gp2+UEA-1- cells) density, and (D) goblet cell density (Gp2-UEA-1+ cells). Each point represents mean data from two FAE from 2-4 mice/group. Horizontal bar represents the median of the group. Significant differences to the naïve group were compared by ANOVA, followed by Dunnett's multiple comparison test.

3.3.8 Effect of *H. polygyrus* infection on mononuclear phagocytes in the Peyer's patches.

Mononuclear phagocytes (macrophages and dendritic cells) have the ability to sample the lumininal content [321, 339], and in the absence of $CD11c^+$ cells oral prion infection is impaired [180], suggesting a necessary role in oral prion infection. To determine if this cells are affected by *H. polygyrus* infection, PP sections were immunostained to detect $CD11c^+$ and $CD68^+$ mononuclear phagocytes (Figure 3.14). An increased abundance of $CD11c^+$ and $CD68^+$ mononuclear phagocytes was observed on day 8 post infection in the PP of duodenum and ileum (Figure 3.14).

PP areas were next divided into three distinct regions: dome (from crypt to crypt), middle and base (Figure 3.15A). In the duodenum no statistically significant differences in the overall abundance of these cells was observed (Figure 3.15 All). However, detailed analysis of the different regions of the duodenal PP, showed that after *H. polygyrus* infection, the expression of CD68 was statistically significantly increased in the base of the PP folicles (Figure 3.15B) on day 1 and 14 post infection ($p \leq 0.046$) when compared to naive mice. The distribution of CD11c expression in duodenal PP was unchanged. In the ileum, no statistically significant changes in the expression of $CD11c^+$ or $CD68^+$ cells were detected (Figure 3.16). These data show that although *H. polygyrus* infection do not significantly affect the abundance of $CD11c^+$ and $CD68^+$ mononuclear phagocytes in the PP follicle, $CD68^+$ cells concentrated in the base of the duodenal PP follicles on day 1 and 14 post H. polygyrus infection.

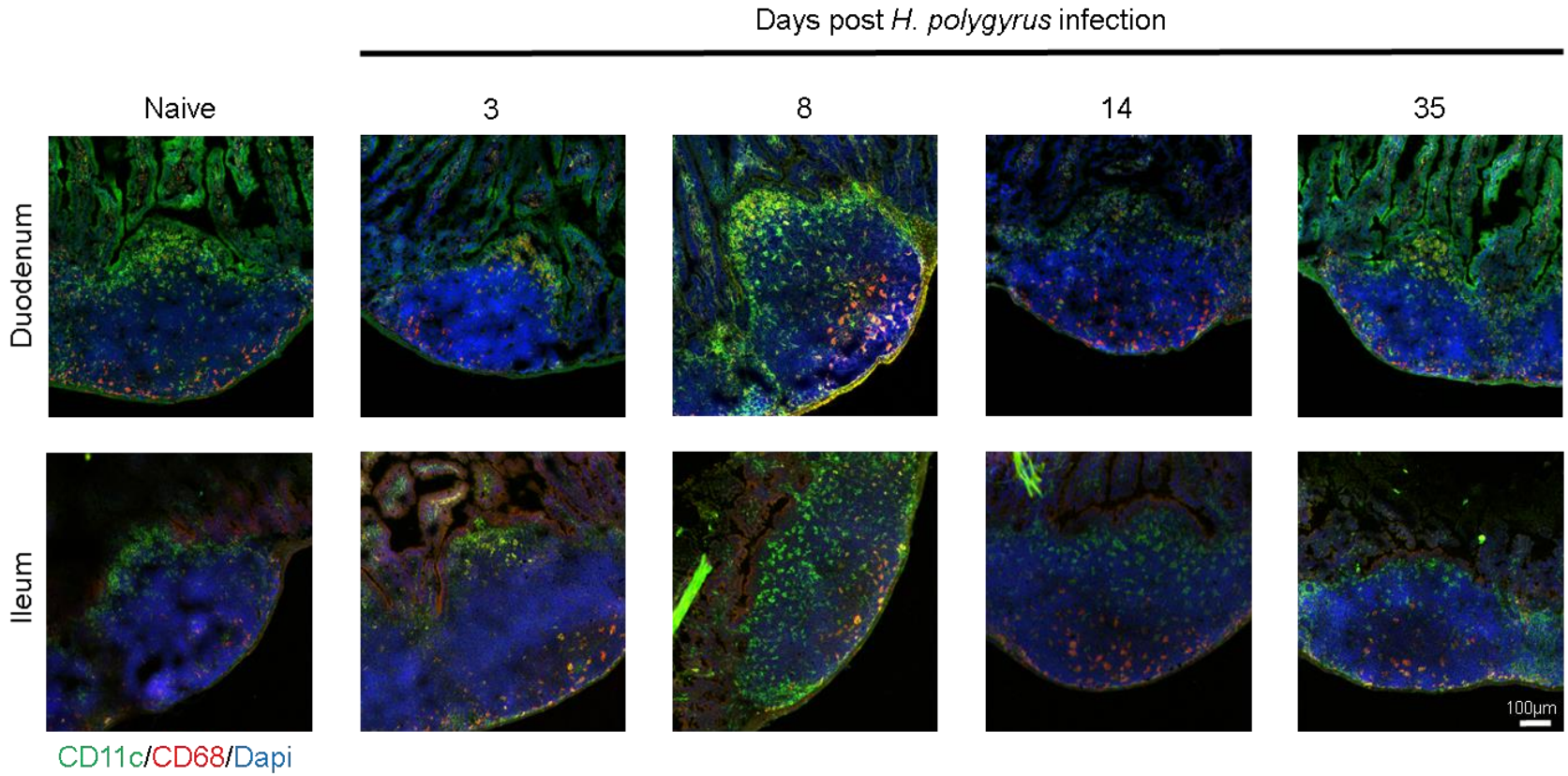

Figure 3.14 Effect of oral *H. polygyrus* infection on mononuclear phagocytes in the Peyer's patches of the duodenum and ileum. Groups of female C57Bl/6 mice were orally infected with 200 L3 larvae, and Peyer's patches collected at intervals afterwards. Sections were immunostained to detect $CD11c^+$ (green), $CD68^+$ (red), and counterstained with DAPI (blue) to detect cell nuclei. Upper panels, duodenal PP; lower panels, ileal PP. Images are representative of one mice/group

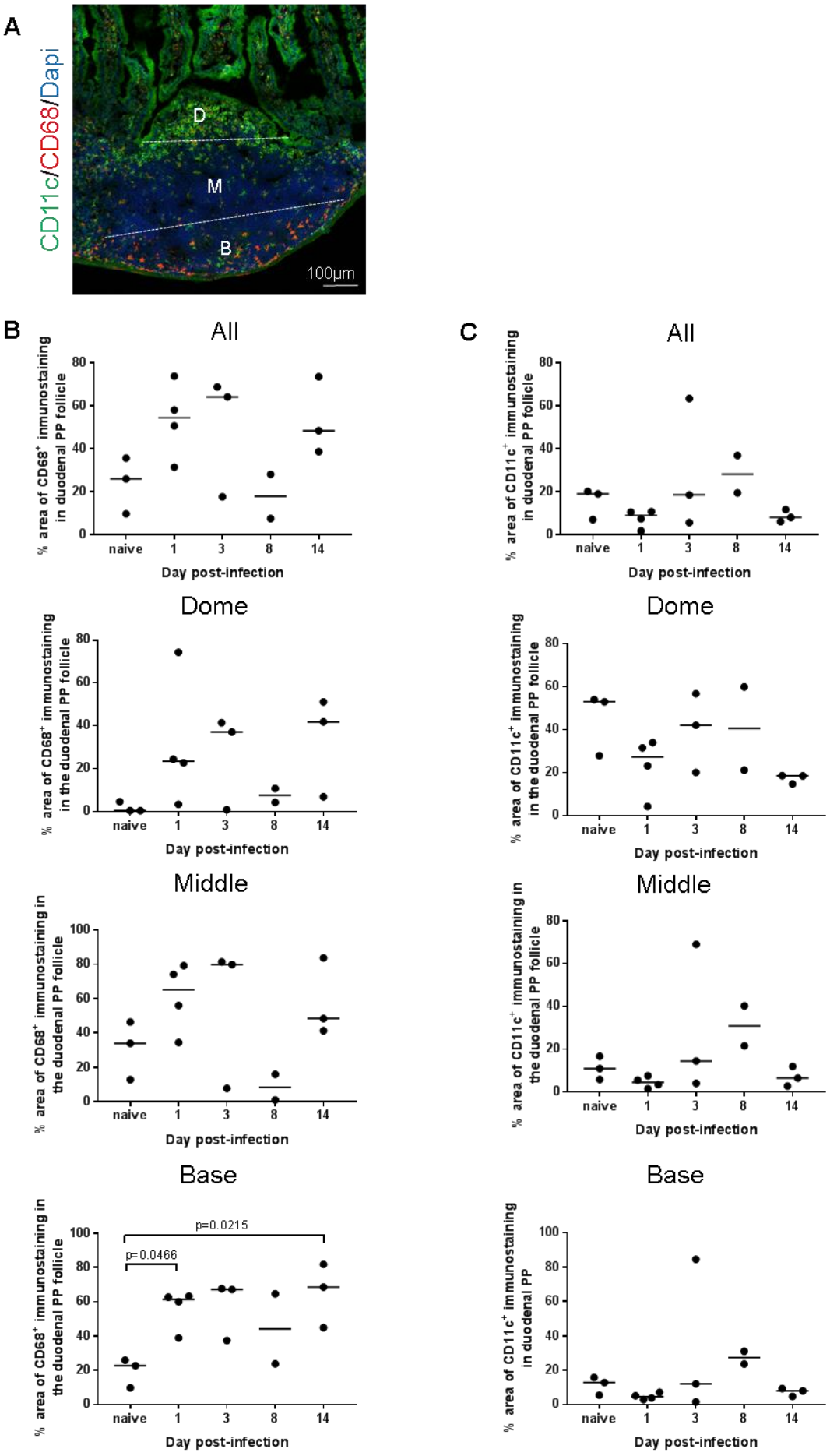
A
CD11c/CD68/Dapi
D
M
B
100µm
B
All
% area of CD68+ immunostaining in duodenal PP follicle
Day post-infection
Dome
% area of CD68+ immunostaining in the duodenal PP follicle
Middle
% area of CD68+ immunostaining in the duodenal PP follicle
Base
% area of CD68+ immunostaining in the duodenal PP follicle
p=0.0215
p=0.0466
C
All
% area of CD11c+ immunostaining in duodenal PP follicle
Dome
% area of CD11c+ immunostaining in the duodenal PP follicle
Middle
% area of CD11c+ immunostaining in the duodenal PP follicle
Base
% area of CD11c+ immunostaining in duodenal PP
naive
1
3
8
14

Figure 3.15 Effect of oral *H. polygyrus* infection on the distribution of mononuclear phagocytes in the Peyer's patches (PP) of the duodenum. Groups of female C57Bl/6 mice were orally infected with 200 L3 larvae, and the duodenal PP collected at intervals afterwards. (A) Representative PP immunostained to detect $CD11c^+$ (green), $CD68^+$ (red), and counterstained with DAPI (blue) to detect cell nuclei. D, dome region; M, middle region; B, base region. (B) Morphometric analysis of the % area $CD68^+$ immunostaining in each PP region. (C) Morphometric analysis of the % area $CD11c^+$ immunostaining in each PP region. Each point represents the data from one PP follicle from each mouse/group. Horizontal bar represents the median of the group. Significant differences to the naïve group were compared by ANOVA, followed by Dunnett's multiple comparison test.

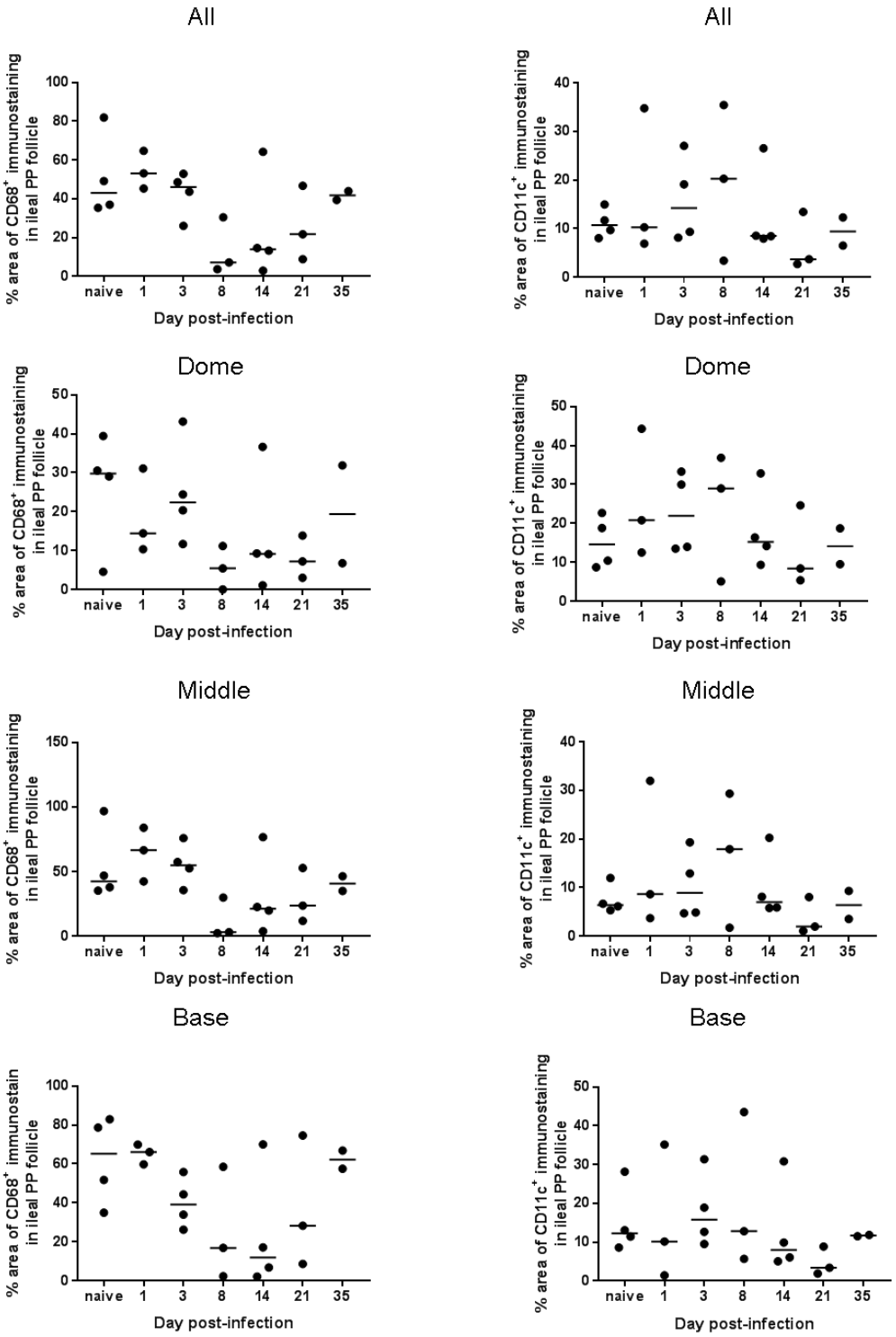
All
% area of CD68+ immunostaining in ileal PP follicle
naive 1 3 8 14 21 35
Day post-infection
All
% area of CD11c+ immunostaining in ileal PP follicle
naive 1 3 8 14 21 35
Day post-infection
Dome
% area of CD68+ immunostaining in ileal PP follicle
naive 1 3 8 14 21 35
Day post-infection
Dome
% area of CD11c+ immunostaining in ileal PP follicle
naive 1 3 8 14 21 35
Day post-infection
Middle
% area of CD68+ immunostaining in ileal PP follicle
naive 1 3 8 14 21 35
Day post-infection
Middle
% area of CD11c+ immunostaining in ileal PP follicle
naive 1 3 8 14 21 35
Day post-infection
Base
% area of CD68+ immunostain in ileal PP follicle
naive 1 3 8 14 21 35
Day post-infection
Base
% area of CD11c+ immunostaining in ileal PP follicle
naive 1 3 8 14 21 35
Day post-infection

Figure 3.16 Effect of oral *H. polygyrus* infection on the distribution of mononuclear phagocytes in the Peyer's patches (PP) of the ileum. Groups of female C57Bl/6 mice were orally infected with 200 L3 larvae, and the ileal PP collected at intervals afterwards. (Left-hand panels) Morphometric analysis of the % area $CD68^+$ immunostaining in each PP region (see Figure. 3.15). (Right-hand panels) Morphometric analysis of the % area $CD11c^+$ immunostaining in each PP region. Each point represents the data from one PP follicle from each mouse/group. Horizontal bar represents the median of the group. Significant differences to the naïve group were compared by ANOVA, followed by Dunnett's multiple comparison test.

3.3.9 Effect of *H. polygyrus* infection on FDC within the Peyer's patches.

Follicular dendritic cells are prion replication sites [197, 204, 340, 341]. Within the GALT, these cells are located in the germinal centre of the PP. To determine the effect of *H. polygyrus* infection on FDC, duodenal and ileal PP were also immunostained to detect FDC ($CD35^+$ cells), PrP^C and B cells ($B220^+$ cells) at different times post *H. polygyrus* infection (Figures 3.17A & 3.18A). Analysis of the duodenal PP follicles showed that *H. polygyrus* infection increased the area of $CD35^+$ staining with statistical significance ($p \leq 0.0198$) on days 8 and 14 (Figure 3.17B). However, within the the FDC area the levels of $CD35^+$ or PrP^{c+} staining were unchanged (Figure 3.17C). Parallel analysis of ileal PP sections (Figure 3.18A), showed no statistically significant effect on the area of $CD35^+$ staining (Figure 3.18B) or in $CD35^+$ stained area (Figure 3.18C). These demonstrate that *H. polygyrus* infection significantly increases the size of the FDC networks in duodenal PP.

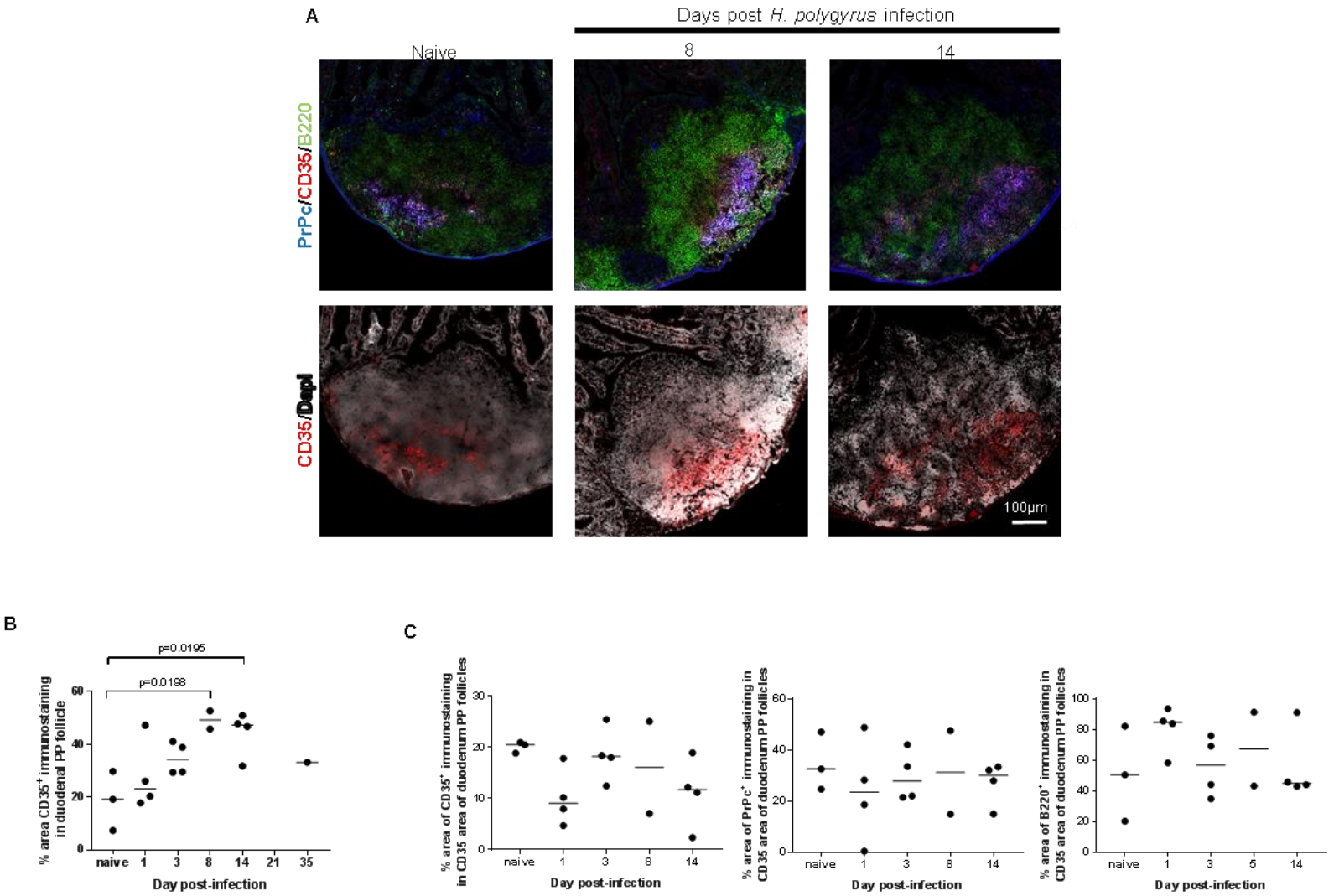
A
Days post H. polygyrus infection
Naive
8
14
PrPc/CD35/B220
CD35/Dapi
100µm
B
p=0.0195
p=0.0198
% area CD35+ immunostaining in duodenal PP follicle
naive 1 3 8 14 21 35
Day post-infection
C
% area of CD35+ immunostaining in CD35 area of duodenum PP follicles
% area of PrPc+ immunostaining in CD35 area of duodenum PP follicles
% area of B220+ immunostaining in CD35 area of duodenum PP follicles
naive 1 3 8 14
naive 1 3 5 14
Day post-infection

Figure. 3.17 Effect of oral *H. polygyrus* infection on follicular dendritic cell (FDC) status in the Peyer's patches (PP) of the duodenum. Groups of female C57Bl/6 mice were orally infected with 200 L3 larvae, and the duodenal PP collected at intervals afterwards. (A) Sections were immunostained to detect PrP^{C}-expressing (blue) FDC ($CD35^{+}$ cells; red) in the B cell follicles ($B220^{+}$ cells, green). Representative images are shown on the top row. Below, same sample/images show immunostaing to detect FDC and DAPI (white). B) Morphometric analysis of the % area $CD35^{+}$ immunostaining (FDC size) within the B cell follicles of each PP. (C) Morphometric analysis of the % area $CD35^{+}$ immunostaining (upper panel), % area PrP^{C+} immunostaining (middle panel), and % area $B220^{+}$ immunostaining (lower panel) in each PP. Each point represents mean data from one PP follicle from each mouse/group. Horizontal bar represents the median of the group. Significant differences to the naïve group were compared by ANOVA, followed by Dunnett's multiple comparison test.

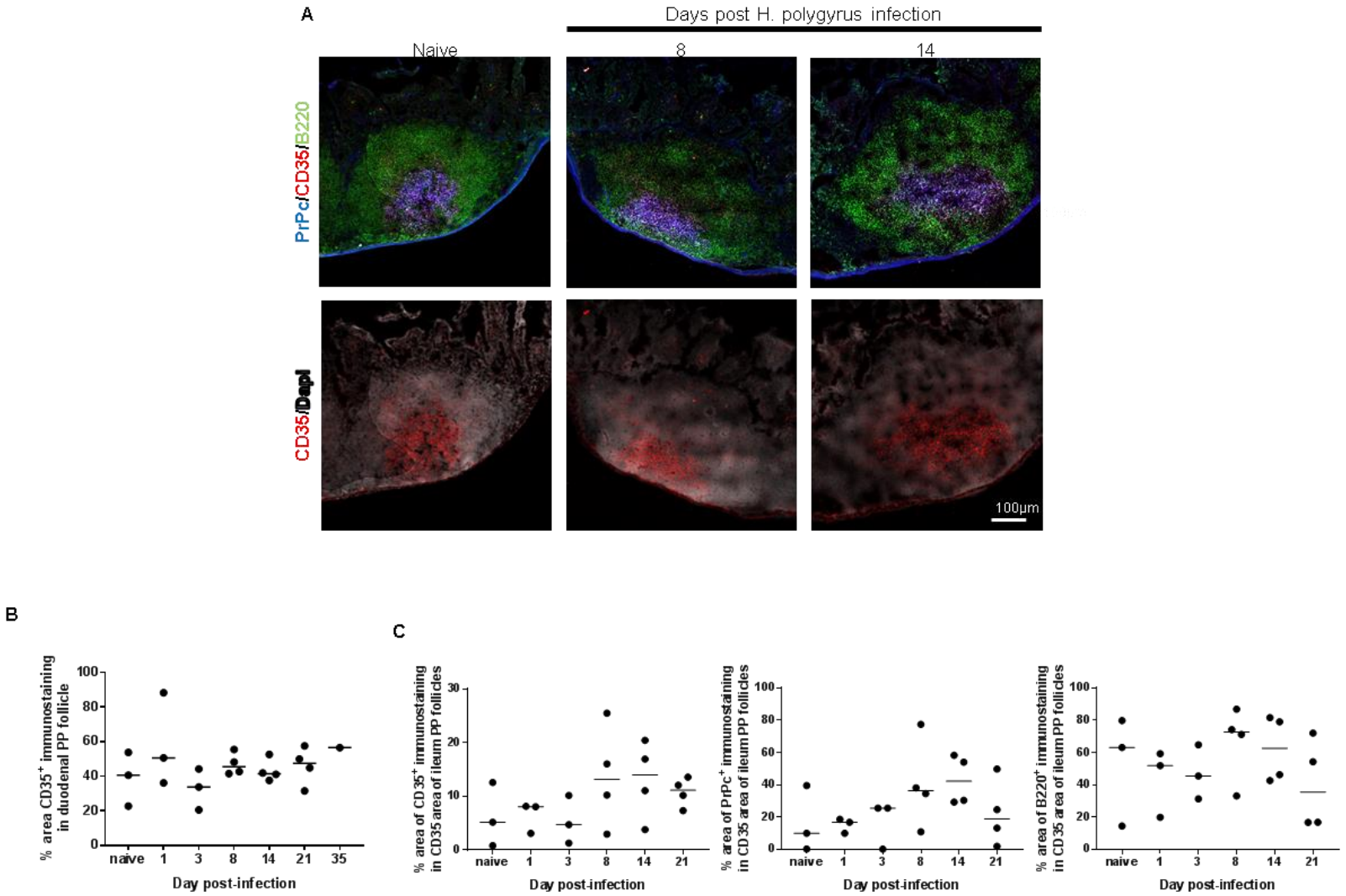
A
Days post H. polygyrus infection
Naive
8
14
PrPc/CD35/B220
CD35/DapI
100µm
B
% area CD35+ immunostaining in duodenal PP follicle
naive 1 3 8 14 21 35
Day post-infection
C
% area of CD35+ immunostaining in CD35 area of ileum PP follicles
% area of PrPc+ immunostaining in CD35 area of ileum PP follicles
% area of B220+ immunostaining in CD35 area of ileum PP follicles
naive 1 3 8 14 21
Day post-infection

Figure. 3.18 Effect of oral *H. polygyrus* infection on follicular dendritic cell (FDC) status in the Peyer's patches (PP) of the ileum. Groups of female C57Bl/6 mice were orally infected with 200 L3 larvae, and the ileal PP collected at intervals afterwards. (A) Sections were immunostained to detect PrP^{C}-expressing (blue) FDC ($CD35^{+}$ cells; red) in the B cell follicles ($B220^{+}$ cells, green). Representative images are shown on the top row. Below, same sample/images show immunostaing to detect FDC and DAPI (white). B) Morphometric analysis of the % area $CD35^{+}$ immunostaining (FDC size) within the B cell follicles of each PP. (C) Morphometric analysis of the % area $CD35^{+}$ immunostaining (upper panel), % area PrP^{C+} immunostaining (middle panel), and % area $B220^{+}$ immunostaining (lower panel) in each PP. Each point represents mean data from one PP follicle from each mouse/group. Horizontal bar represents the median of the group. Significant differences to the naïve group were compared by ANOVA, followed by Dunnett's multiple comparison test.

3.3.10 Assesment of the granulomas caused by *H. polygyrus* infection.

Granulomas are host inflammatory derived structures which can form around non degradable persistent antigen [308]. It has been implied that granulomas can act as prion replication sites, even in the absence of FDC [234]. In this study, the granulomas that formed during *H. polygyrus* infection were found at different developmental stages even in the same animal. Using H&E staining, it was evident that *H. polygyrus* cysts were visible from day 3 post infection. Next, the granulomas formed during *H. polygyrus* infection were clasified into 5 types (G1-G5) according to their developmental stage (Figure 3.19A). These structures begin as a cyst, which contains the worm in what could correspond to a moult stage (G1). The G2 stage was characterized by disperse eosinophilic agregation. Then, the agregation consolididates into a more compact rounded structure which begins to develop the characteristic features of a granuloma, such as a fibrous capsule (G3). This develops into G4 stage, a carefully organized structure with a compact nucleus predominantly compromising macrophages surounded by a mixed collagen-fibroblast capsule. At this stage, a granuloma can either rupture, expelling all its content or remain. After the granuloma ruptures, the tissue repairs and remodels itself (G5). Using this classification, it was possible to characterize the presence of these different developmental stages of the granulomas at different times post *H. polygyrus* infection. During the early *H. polygyrus* infection, there was a predominant presence of the G1 and G2 stages, whereas at the later times, the G5 stage prevailed (Figure 3.19B).

Complementary IHC analysis of the granulomas, demonstrated an abundance of $CD11b^{+}$ macrophages within them, surrounded by a dense network of nerves positive for PrP^{C} and synaptophysin-1 (Figure 3.20). The presence of

PrP^{C+} expressing nerves in these granulomas, suggests that they may be potential sites of prion accumulation in prion affected individuals.

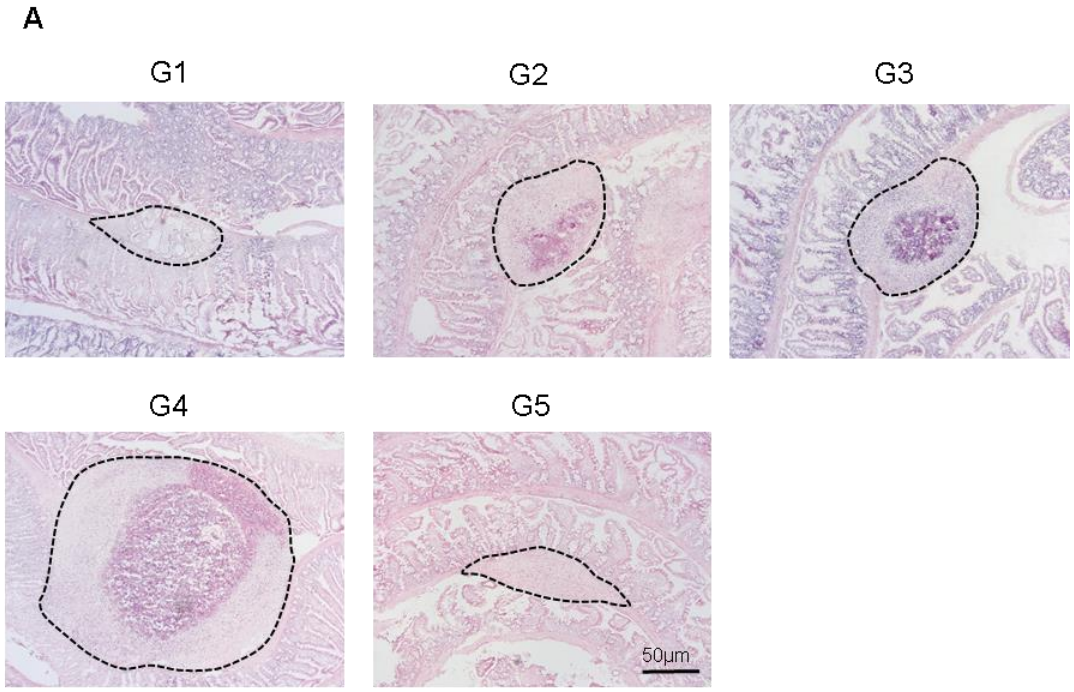

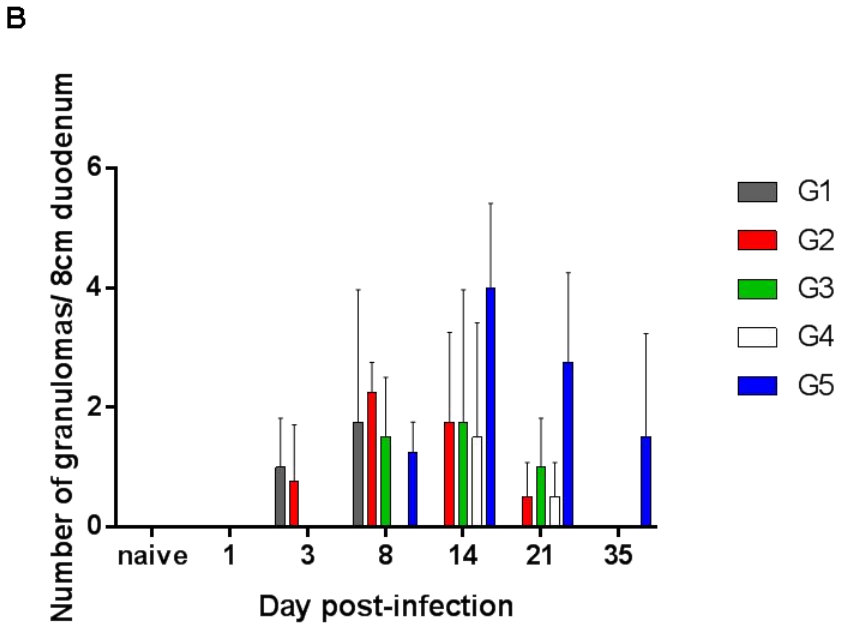

Figure 3.19 Oral *H. polygyrus* infection induces the formation of granulomas in the wall of the duodenum. Groups of female C57Bl/6 mice were orally infected with 200 L3 larvae, and the duodenum collected at intervals afterwards. (A) Representative H&E stained sections of intestines from infected mice. Granulomas were classified into five distinct stages: G1 - formation of the cyst or larvae moult stage; G2 - dispersed eosinophilic agregation around the cyst site; G3 - consolidation of the agregate into a more compact and rounded structure which begins to develop the typical characteristics of a granuloma such as the presence of a fibrous capsule; G4 - fully organized granuloma structure with a compact nucleus predominantly containig macrophages, by a mixed collagen-fibroblast capsule and G5 - tissue repair and remodelling after rupture of the granuloma. (B) 8 cm of duodenum was analysed and the number of each type of granuloma at intervals after *H. polygyrus* infection was determined. Each bar represents mean ± SD number of granulomas of each type in two tissue samples from 4 mice/group.

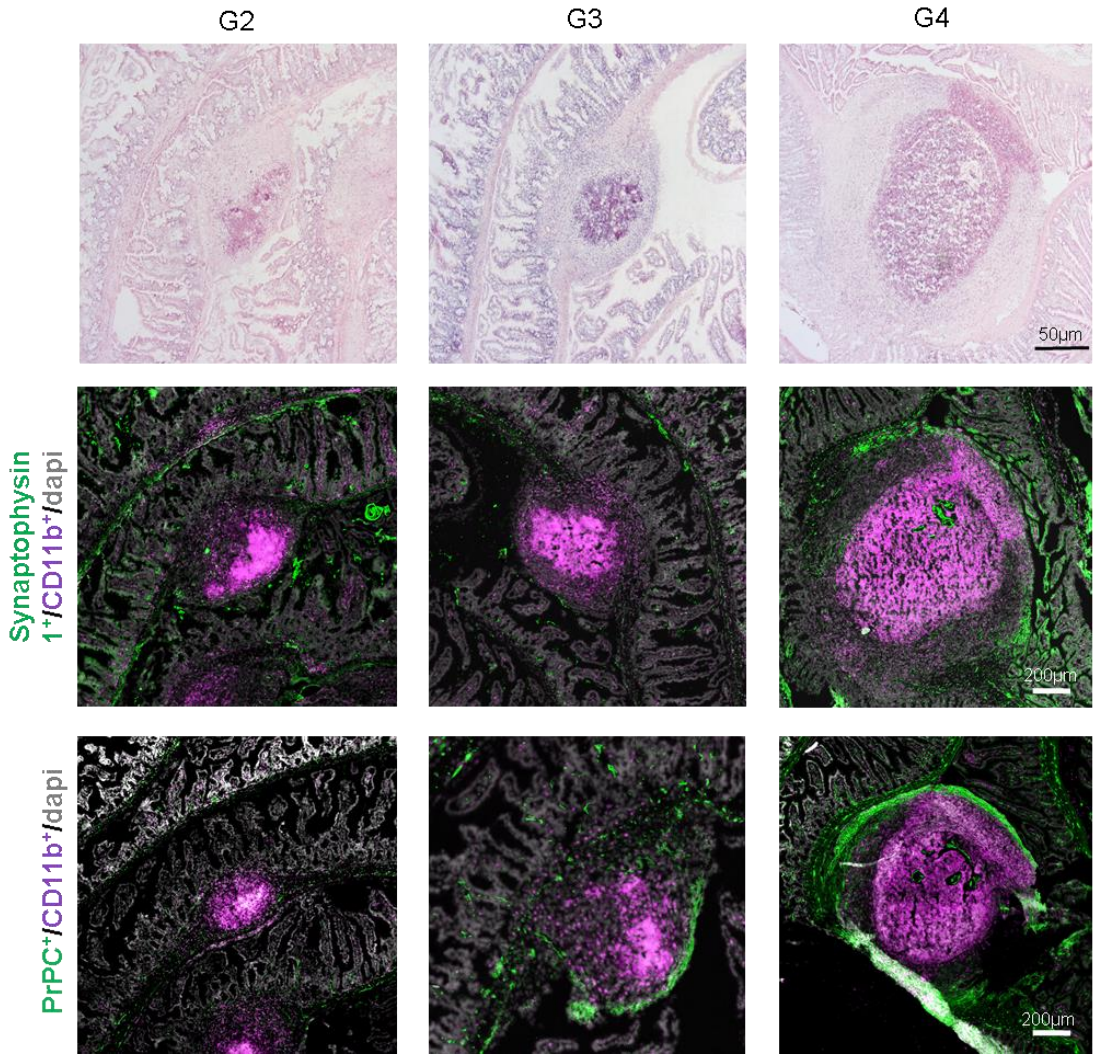

Figure 3.20 The granulomas induced in the wall of the duodenum after oral *H. polygyrus* infection contain mononuclear phagocytes and are surrounded by synaptophysin-1 and PrP^C expressing enteric nerves. Groups of female C57Bl/6 mice were orally infected with 200 L3 larvae, and the duodenum collected at intervals afterwards. (Upper row) Representative H&E stained sections of G2, G3 and G4 granulomas in the intestines from infected mice. (Middle row) Sections were immunostained to detect synaptophysin-1-expressing enteric nerves (green), $CD11b^+$ mononuclear phagocytes (pink) and cell nuclei (grey/white). (Lower row) Sections were immunostained to detect PrP^C-expressing enteric nerves (green), $CD11b^+$ mononuclear phagocytes (pink) and cell nuclei (grey/white).

3.4 Discussion

In this chapter, the effect of *H. polygyrus* infection on the gut and GALT microarchitecture was determined. This analysis showed that the worm infection was restricted to the small intestine. *H. polygyrus* infection adversely affected the intestinal villi (epithelial disruption, goblet cells hyperplasia and increased $CD11b^+$ staining in the lamina propria), and reduced the number of ILF in duodenum and colon. In PP, *H. polygyrus* infection increased the number of M cells, altered the positioning of $CD68^+$ mononuclear phagocytes, and increased the area of $CD35^+$ expressing FDC. *H. polygyrus* infection also caused the formation of granulomas surrounded by a dense membrane containing synaptophysin-1 and PrP^C expressing nerves. Previous studies suggest that the small intestine is the main site of prion acquisition [198]. It has also been shown that M cells and enterocytes in the FAE of PP transport prions [135, 139, 198]. Goblet cells can also transport molecules smaller than 70 kD [342] and the minimal prion infection unit is thought to be between 50-150 kD [343-345], suggesting that goblet cells may be able to transport prions. Therefore, since these cells can play an important role in prion neuroinvasion, it is plausible that the effects of *H. polygyrus* on the gut and GALT microarchitecture may significantly affect the uptake of orally acquired prions.

H. polygyrus infection increased M cell and goblet cell density in the FAE of PP. Although increased number of M cells has also been reported as a consequence of bacterial infection such as *Salmonella* or *Streptococcus* [346], the effects on M cells occurred as an acute response within the first few days post bacterial infection. This contrasts with the findings in this study where M cell density was increased at later times. M cell density has been correlated with prion disease susceptibility [347]; and prion disease is ablated in the absence of M cells [135]. FDC are esential sites for prion replication and play a key role

in prion disease pathogenesis [204, 348]. In the germinal centres of the PP follicles, the size of FDC ($CD35^+$) was also significantly increased on day 8 and 14 post *H. polygyrus* infection, suggesting increased activation of these cells. However, from data presented it was uncertain whether this was due to an increased number of FDC, increased FDC size, or whether FDC activity/function was altered.

H. polygyrus infection altered the positioning of $CD68^+$ mononuclear phagocyte in PP. Given that there has been a dabate regarding the type and origin of the mononuclear phagocytes, and regarding the wide expresion of CD11c, in this study CD68 was used as a marker for monocytes/macrophages and CD11c as a DC marker. The importance of these cells rely on their capacity to sample antigens from the intestinal lumen (when located in the dome), present antigens to FDC in germinal centre and degrade antigens. As expected both markers were expresed. In naïve mice $CD11c^+$ staining was mainly located in the PP dome; contary although $CD68^+$ staining was located in the oposite side, in the base of PP, there was also some colocalized staining. The increased CD68 staining (indicative of macrophages) with statistical significance in the base of duodenal PP during *H. polygyrus* infection and the particular effect observed on day 8 post *H. polygyrus* infection on mononuclear phagocytes, suggests changes in the positioning of the mononuclear phagocytes in the PP. However, these may also be result of an increased influx of the number of these cells, an alteration to their activation status, or an increase expresion of CD68. Further experiments are clearly necessary to resolve this issue. An increased abundance of macrophages at the time of oral prion infection, potentially lead to increased phagocytosis and destruction of the prions, reducing disease susceptibility. Also, changes in the abundance of mononuclear phagocytes in

the dome could influence the amount of antigen sampling and therefore, the suceptibility to an infection.

As expected, the hyperplasia of goblet cells in PP and villi ratify findings of other studies which found a goblet cell hyperplasia between days 6-14 post infection [254, 265]. Although an increased number of goblet cells is an innate response against enteric and worm infections as a defence mechanism [265, 349], it had been suggested that the goblet cell hyperplasia cause during *H. polygyrus* infection is also a T cell dependent event [260]. However, independently of the goblet cell hyperplasia origin, goblet cell function is associated with an increase of mucus which had been associated with parasitic infection clearance [264] as well as the increase contractility of the smooth muscle present during the infection [269, 350]. Therefore, these factors can either reduce the possibilities of antigen uptake during *H. polygyrus* infection due the faster intestinal transit or increase those probabilities. The latter may be possible, because in the PP, the intestinal mucus is not attached to the FAE [351]. Therefore, the mucus can be cleared constantly from PP with the increased intestinal peristalsis during infection [351]. This may leave the FAE exposed to other antigens such as prions; in which case, the time that prions take to cross the FAE would be an important factor to consider. Also, as the goblet cells may be antigen entrance sites, their increase population may increase the probabilities that prions get through the FAE from the gut lumen.

The reduction of ILF (B cell follicles) in the duodenum and colon coincides with the reported increased number of B cells in the mesenteric lymph nodes (MLN) after *H. polygyrus* infection [352]. It is possible that migration of B cells from the intestine to the MLN in response to *H. polygyrus* infection is responsible for the effect on ILF. Similar to the proposed redistribution of the systemic T and B lymphocytes to the MLN during *H. polygyrus* infection [353].

In the small intestinal villi, mononuclear phagocytes expression was determined using CD11c, CD68 and CD11b markers. All are normally detected in the lamina propria as showed in naïve mice. In this study, although statistical analysis did not show significant differences in CD11c and CD68 expression in the lamina propria, the increased abundance of $CD11b^+$ expression was statistically significant in duodenum and ileum. Although in the ileum only one out of four mice had this reaction, in the duodenum half of them did. A similar increase in $CD11b^+F4/80^+$ cells has been observed in the peritoneal cavity following *H. polygyrus* infection [256]. However, the $CD11b^+F4/80^+$ cell accumulation is suggested to occur within 7 days post *H. polygyrus* infection [256]. This contrasts with the findings in this study where lamina propria $CD11b^+$ cells were not significantly increased until day 21 post infection. As there were no significant changes in CD11c or CD68, specific changes in CD11b expression may be related with the mechanism to trap the parasite and the granuloma formation. CD11b complement receptor is expressed by *H. polygyrus* larvae, and this may mediate macrophages ($CD11b^+$) adherence to *H. polygyrus* larvae as a trapping mechanism [311]. Also, in other infections (B*rucella melitensis* and *Mycobacterium bovis*) $CD11b^+$ cells are main components of granulomas [354, 355]. Therefore, the increased expression of this marker in the lamina propria on day 21 post *H. polygyrus* may suggest a relation with the granulomas formed during *H. polygyrus* infection. The major number of granulomas (G2-G4) were detected on days 14 and 21 post infection. Given that by day 21 the number of granulomas seems to be reduced, it is possible that the increase of $CD11b^+$ mononuclear phagocytes may be related with tissue repairing and clearance of granuloma debris.

Atrophy of the intestinal villi and hypertrophy of the crypts have also been observed during *H. polygyrus* infection [251, 260]. These changes were evident

in the duodenum on days 8 and 14 post infection and are most likely associated with an inflammatory process caused by the adult parasite as it bursts out of the submucosa and begins feeding on the gut epithelium. Enteritis is observed between days 6 and 15 post *H. polygyrus* infection when calculated using a score system which considers the extension of the epithelial damage, edema, villus length, crypt depth and inflammatory cell infiltrates [254, 356]. As mentioned before, the inflammatory process can affect the permeability of the intestine by weakening the tight junctions between the epithelial cells [254, 325, 326] and therefore, be a potential site of prion entry.

Data in this chapter show that *H. polygyrus* infection has a significant effect on the gut microarchitecture of the gut and GALT. These changes may influence the efficiency of the uptake of antigens sampled from the gut lumen. Taking all these data into consideration, days 1, 8 and 14 of *H. polygyrus* infection may represent interesting time-points that may influence the uptake of second pathogens such as orally acquired prions. On day 1 post *H. polygyrus* infection the infecting larvae invade the epithelium and reach the serosa layer for its implantation. On day 8 post infection, the adult worms emerge from the intestinal wall and establish infection in the lumen where they cause epithelial disruption and changes to the villus morphology. At this time, $CD68^{+}$ mononuclear phagocyte positioning within the PP was altered, FDC size was increased, and granulomas were evident in the gut wall. On day 14 post infection, the integrity of the duodenal epithelium was disrupted, there was an increased number of goblet cells, a reduction in the number of ILF in duodenum, and the increased FDC size remained, as well as granulomas.

Since the integrity of the intestinal epithelium and mononuclear phagocytes are important for the efficient uptake of prions from the gut lumen, and FDC and granulomas can be sites of prion replication, these suggest that *H.*

polygyrus infection may have a significant influence in prion disease. Therefore, on the next chapter, the effects of co-infection with *H. polygyrus* on prion disease pathogenesis and susceptibility will be determined.

Chapter 4. Effect of *H. polygyrus* infection on orally acquired prion disease

4.1 Abstract

Data in the previous chapter showed that *H. polygyrus* caused significant pathology only in the small intestine and the gut associated lymphoid tissues (GALT) within it. Since early prion accumulation within Peyer's patches (PP) in the small intestine is essential for the efficient transmission of disease to the brain, in this chapter the effects of *H. polygyrus* infection on oral prion disease pathogenesis were determined. Groups of mice were first orally infected with *H. polygyrus* and either on the same day (day 0) or on days 1, 8 or 14 post infection, the mice were subsequently orally co-infected with ME7 scrapie prions. The effect of *H. polygyrus* co-infection on the early accumulation of prions upon follicular dendritic cells (FDC) in the PP, mesenteric lymph nodes (MLN), and spleen was then determined, as well the subsequent effects on prion disease susceptibility and duration. The results showed that co-infection with *H. polygyrus* had a significant influence on the early accumulation of prions upon FDC in the MLN. However, co-infection with *H. polygyrus* had only modest effects on oral prion disease susceptibility and disease duration. Although the histopathological signs of prion disease in the brain were similar in all groups whether they were co-infected with *H. polygyrus* or not; in certain brain regions the magnitude of the spongiform pathology and PrP^{Sc} accumulation was modestly but significantly reduced in the mice co-infected with prions and *H. polygyrus* on the same day. Therefore, although data in Chapter 3 showed that oral infection with *H. polygyrus* causes significant pathological disturbances in the small intestine, data presented in this chapter showed that co-infection with *H. polygyrus* had only a modest influence on oral prion disease pathogenesis and susceptibility.

4.2 Introduction

Chapter 3 determined the effects of oral *H. polygyrus* infection on the microarchitecture of the gut associated lymphoid tissues (GALT) and the small and large intestines. Data from those studies confirmed that *H. polygyrus* infection and the effects that it caused on the gut and GALT microarchitecture were restricted to the small intestine. As described in the previous chapter, the main effects caused by *H. polygyrus* infection that were observed on the intestine included enteritis, disturbances to villous morphology, epithelial damage, increased abundance of $CD11b^+$ mononuclear phagocytes in the lamina propria, and increased goblet cell density in the gut epithelium. *H. polygyrus* infection also caused a reduction in the number of isolated lymphoid follicles (ILF) in duodenum and colon, and in the Peyer's patches (PP) modified the abundance of CD68 expression by mononuclear phagocytes, increased the size of the FDC in the B cell follicles and increased the density of M cells in the follicle-associated epithelium (FAE). *H. polygyrus* infection also induced the formation of granulomas in the gut wall, which were surrounded by a dense network of PrP^C-expressing enteric nerves.

After oral exposure many prion isolates initially accumulate and replicate upon PrP^C-expressing follicular dendritic cells (FDC) within the GALT in the small intestine, such as the PP [357, 358]. This initial replication of prions upon FDC in the PP is essential for the efficient spread of disease to the central nervous system (CNS) [340, 359, 360]. The prions are first considered to be transported across the gut epithelium by M cells, enterocytes or dendritic cells [321, 361, 362] in the FAE which covers the PP [361, 363, 364, 365]. Data show that the prions are subsequently acquired by $CD11c^+$ mononuclear phagocytes (conventional dendritic cells (DC)) which deliver them to the FDC within the B-cell follicles of the PP [179, 211, 312, 366].

Inflammation and pathogen infection can significantly affect prion disease pathogenesis, for example by enhancing the uptake of prions from the site of infection, or by providing additional sites of prion accumulation within host tissues [234, 238, 313, 367]. Data also show that M cell density in the gut epithelium can significantly influence oral prion disease susceptibility [333]. Increased M cell-density at the time of oral exposure significantly increased the uptake of prions from intestine into PP, shortening survival times and increasing disease susceptibility [137]. Since M cells, $CD11c^{+}$ mononuclear phagocytes and FDC each play important role in the uptake of prions from the gut lumen, and their subsequent propagation to and replication within PP, the effects of *H. polygyrus* infection on these cells in the small intestine may also have a significant effect on oral prion disease pathogenesis and susceptibility. Therefore, the aim of the experiments described in this chapter was to test the hypothesis that co-infection with a small intestine-restricted pathogen such as *H. polygyrus* may significantly influence oral prion disease pathogenesis and susceptibility.

4.3 Results

4.3.1 Co-infection with *H. polygyrus* and ME7 scrapie prions

Since oral exposure to a limiting dose of ME7 scrapie prions typically yields a disease incidence of 100% in wild-type (control) mice, its use here would enable the effects of *H. polygyrus* co-infection on survival time and prion disease susceptibility to be determined. C57BL/6J female mice (90 days old) were orally infected with 200 L3 infective larvae by gavage. Then, on different days post *H. polygyrus* infection (days 0, 1, 8 and 14) groups of mice were subsequently orally infected with a limiting dose consistent of 50 μl of 1% dilution of scrapie brain homogenate prepared from mice terminally-affected with ME7 scrapie prions containing approximately 3.3 log10 i.c. ID_{50} units. A parallel group of mice were orally infected with prions alone as a control.

H. polygyrus infection was confirmed in 5 mice/group by calculating the number of eggs/g of faeces using the McMaster technique as described in Section 2.2. This analysis was performed at weeks 2, 3, and 4 post *H. polygyrus* infection, and then at monthly intervals for the remainder of the experiment (either until the mice developed terminal clinical prion disease, or when the study was terminated at 504 days post prion infection). This analysis confirmed that *H. polygyrus* infection for each group was successful.

The mean faecal egg burdens for each mouse group co-infected with prions at different weeks (Figure 4.1) had some differences in comparison with the egg burden presented in chapter 3 (Figure 3.1). Mice infected with *H. polygyrus* alone had a maximum mean egg production of 1522 eggs/g of faeces at day 18 post infection. Similarly, mice co-infected with prions and *H. polygyrus* on the same day (day 0) had a similar trend. However, mice infected with prions at

day one after *H. polygyrus* infection had a reduced egg burden; and mice infected with prions at day 8 post *H. polygyrus* infection had their maximum egg burden at later time (day 21). Responsiveness to *H. polygyrus* infection is dependent on the mouse strain. C57BL/6 mice are considered to be intermediate responders to *H. polygyrus*; it takes them from 8 to 20 weeks to clear worm burden [245]. Similarly, when mice were co-infected with prions on day 8 and 14 post *H. polygyrus* infection, the worm eggs were detected in the faeces until 16-20 weeks (23±25 eggs/g of faeces) after parasite exposure. In contrast, in mice that were co-infected with prions on the same day (day 0) or on day 1 after *H. polygyrus* infection, eggs were detectable in the faeces for up to 4 weeks (17±19 eggs/g of faeces) after oral exposure. Subsequent monthly analyses showed that after these times the eggs were undetectable in the faeces of mice from all groups, suggesting that the parasite infections had been cleared by the host.

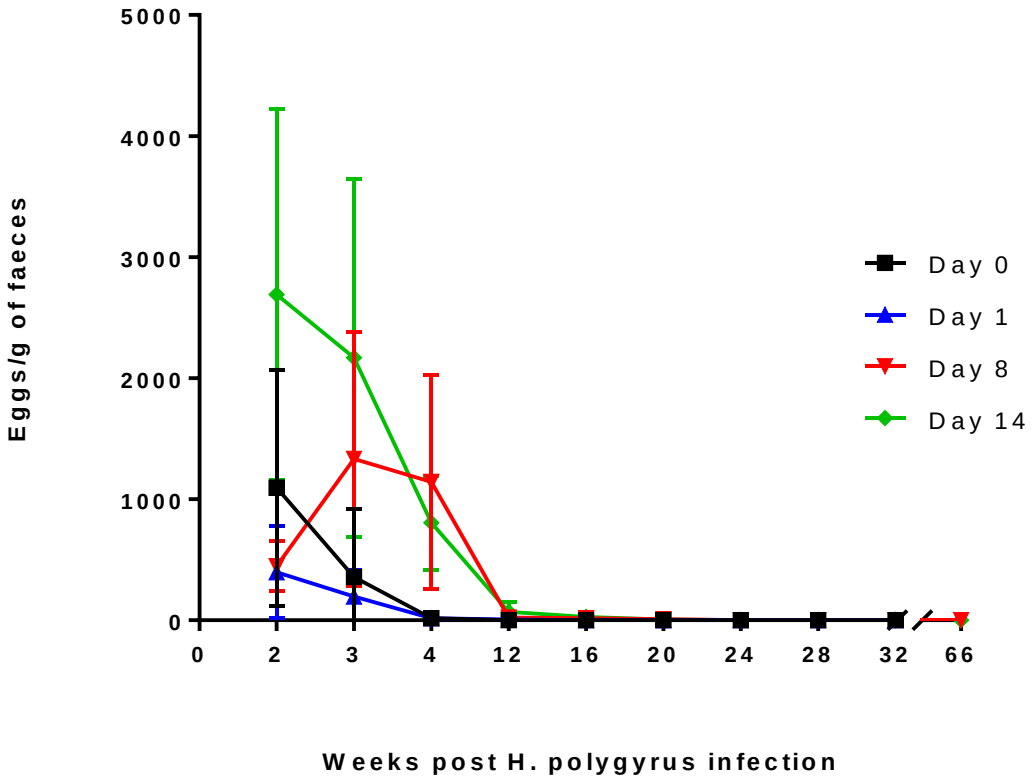

Figure 4.1 Mean faecal egg burden following infection with *H. polygyrus*. Female C57Bl/6 mice were orally infected with 200 L3 larvae, and then on days 0, 1, 8 or 14, the mice were subsequently orally infected with ME7 scrapie prions. The number of eggs in faeces was determined at intervals afterwards. Each point represents mean ± SD number of egg/g of faeces from 5 individual mice/group.

4.3.2 Effect of *H. polygyrus* infection on the early accumulation of prions in the PP.

Within weeks after oral exposure, high levels of ME7 scrapie prions first accumulate upon FDC before they establish infection in the nervous system [204, 340, 348, 360]. The effects of *H. polygyrus* on the early accumulation of prions within the PP was therefore determined. Mice orally infected with *H. polygyrus* and prions as described above were culled at 5, 10 and 15 weeks after prion infection (4 mice/group) and the influence of *H. polygyrus* infection on prion accumulation within the PP was determined (Figure 4.2).

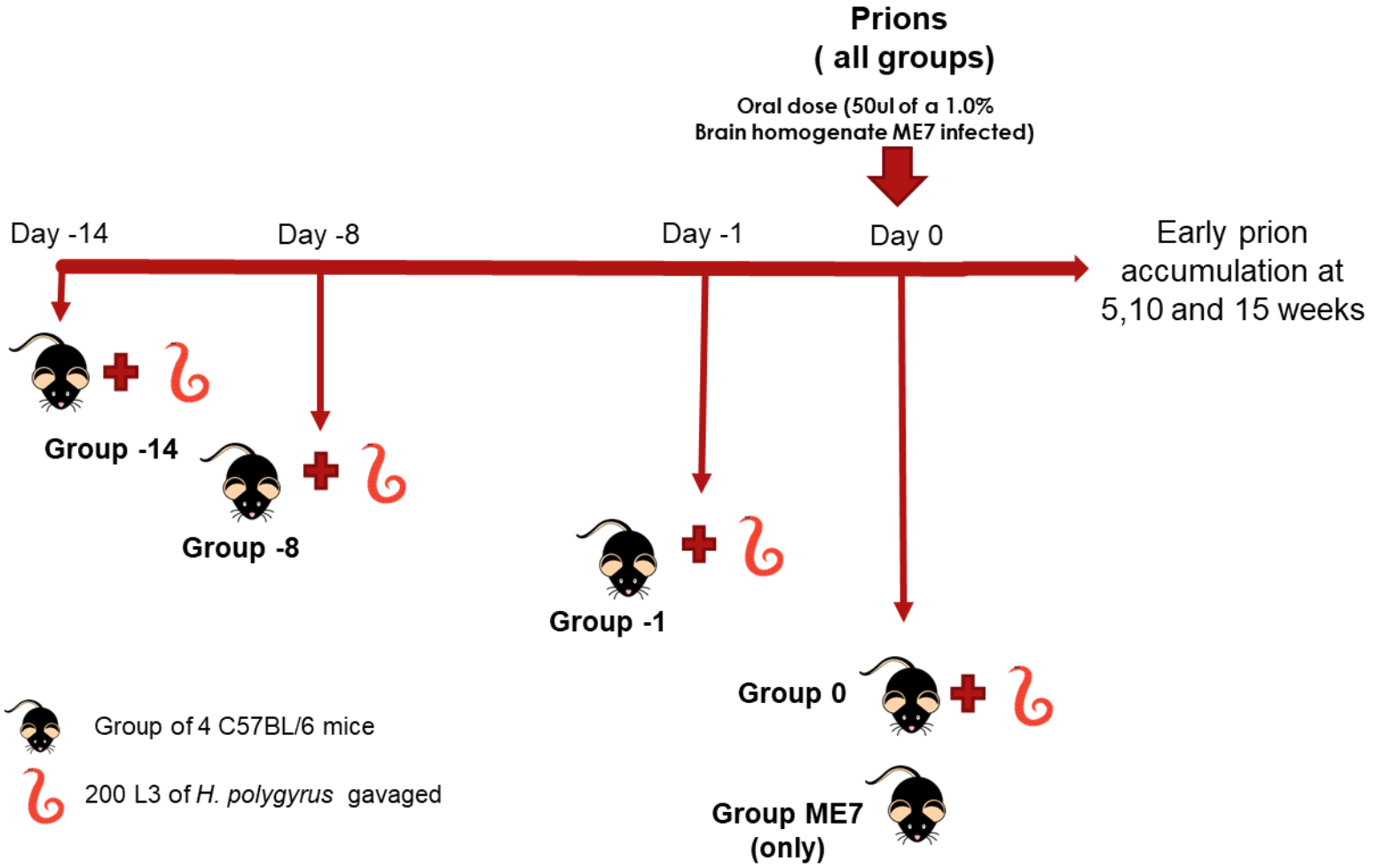
Prions
(all groups)
Oral dose (50ul of a 1.0%
Brain homogenate ME7 infected)
Day -14
Day -8
Day -1
Day 0
Early prion
accumulation at
5,10 and 15 weeks
Group -14
Group -8
Group -1
Group 0
Group ME7
(only)
Group of 4 C57BL/6 mice
200 L3 of H. polygyrus gavaged

Figure 4.2 Experimental design for early prion detection at 5, 10 and 15 weeks in *H. polygyrus* co-infected mice. Groups of 4 female C57BL/6 mice were orally infected with 200 *H. polygyrus* L3, and on days 0, 1, 8 or 14 the mice were subsequently orally infected with a limiting dose of ME7 scrapie prions. Also, a control group was infected with prions alone. Tissues (PP, spleen and MLN) were harvested at 5, 10 and 15 weeks post prion infection to detect early prion accumulation.

First, serial sections of PP were cut and immunostained to detect CD21/35-expressing FDC and the prion disease-specific (PrP^{d}) abnormal PrP accumulations [368]. PrP^{d} refers to prion disease-associated abnormal PrP detected by IHC in affected tissues. Paraffin-embedded tissue (PET) blot analysis (Section 2.5.6) was used to confirm that any PrP^{d} accumulations were prion disease-specific, proteinase K-resistant PrP^{Sc} (Figure 4.3A).

The incidence of PrP^{Sc+} FDC networks in tissues from each mouse/group was then determined. First, the number of FDC networks ($CD21/35^{+}$) was determined in each mouse sample; then, each FDC network was compared in the serial sections stained to detect PrP^{d} and PrP^{Sc}. If the FDC network was positive for the three stainings, it was considered a PrP^{Sc+}. The percentage of PrP^{Sc+} FDC networks in one sample per mice was considered as the incidence. This method had been used to determine the incidence of PrP^{Sc+} PP follicles in mice at 5, 10 and 15 weeks post orally infection (50 µl of a 1% of scrapie brain homogenate containing approximately 3.3 log10 i.c. ID_{50} units) [135, 205]. Data presented in Figure 4.3B, shows the median incidence of PrP^{Sc+} FDC networks in all groups at 5, 10 and 15 weeks post prion infection in the PP. Here, in the mice infected with prions alone, PrP^{Sc+} FDC networks were first detected from 5 weeks post-prion infection, increasing slightly in their abundance by 15 weeks (Figure 4.3A; Appendix 7.3.1). This analysis showed that co-infection with *H. polygyrus* appeared to have little influence on the early accumulation of prions in the PP. However, the incidence of PrP^{Sc+} FDC networks in the PP of mice co-infected with prions and *H. polygyrus* on the same day (day 0) was statistically significantly reduced at 15 weeks post prion infection ($p<0.034$). Therefore, co-infection with *H. polygyrus* had a limited influence on the early accumulation of prions upon FDC in the PP.

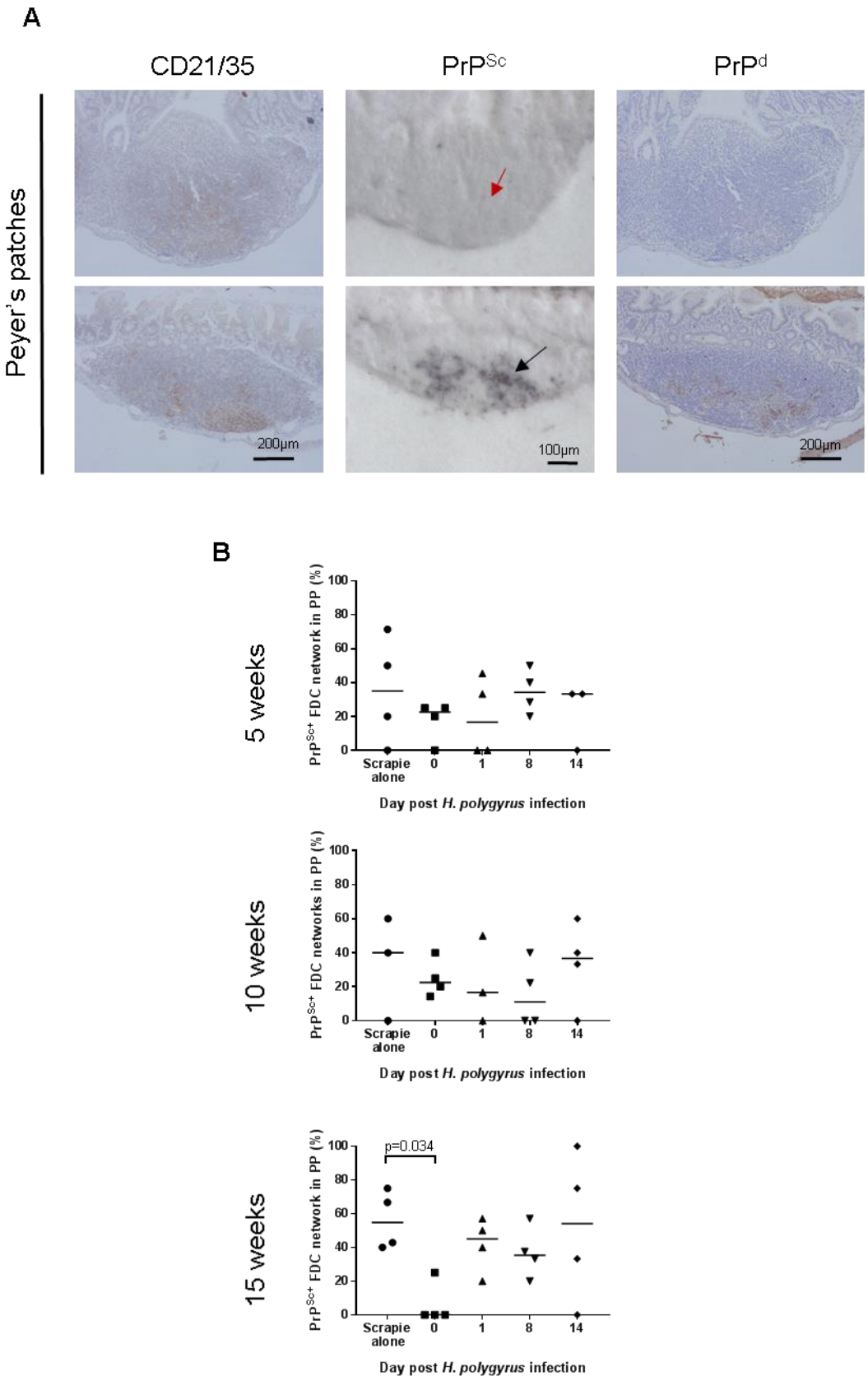
A
CD21/35
PrP^Sc
PrP^d
Peyer's patches
200µm
100µm
200µm
B
5 weeks
10 weeks
15 weeks
PrP^Sc+ FDC network in PP (%)
PrP^Sc+ FDC networks in PP (%)
Scrapie alone
0
1
8
14
Day post H. polygyrus infection
p=0.034

Figure 4.3 Effect of *H. polygyrus* co-infection on the early accumulation of PrP^{Sc} upon follicular dendritic cells (FDC) in Peyer's patches (PP). Female C57Bl/6 mice were orally infected with 200 L3 larvae, and then on days 0, 1, 8 or 14, the mice were subsequently orally infected with ME7 scrapie prions. PP were collected at 5, 10 and 15 weeks after prion infection and analysed by IHC and PET immunoblot. (A) Representative images of PP without (upper panels) and with (lower panels) high levels of disease-specific PrP (PrP^d, brown) in association with FDC ($CD21/35^+$ cells, brown). Analysis of adjacent sections by PET immunoblot analysis confirmed the absence (red arrow) or presence (black arrow) of prion specific PK-resistant PrP^{Sc} (blue). (B) Assessment of the incidence of FDC networks containing PrP^{Sc} in each group of mice at 5, 10 and 15 weeks after prion exposure. Each point represents mean data from individual mice (1-12 PP/mouse; 4 mice/group). Horizontal bar represents the median value of the group. Significant differences to the group infected with prions alone were compared by ANOVA, followed by Dunnett's multiple comparison test.

4.3.3 Effect of *H. polygyrus* infection on the early accumulation of prions in the mesenteric lymph nodes (MLN) and spleen.

After their initial accumulation in the PP, the prions subsequently spread to the MLN and spleen [206, 208]. Next, the influence of *H. polygyrus* infection on prion accumulation within the MLN and spleen was determined. Previous studies had shown that in the spleens and MLN, PrP^{Sc} accumulations in FDC networks had been detected at 70 days (10 weeks) post infection when using the same prion infective dose [205]. However, when prion (ME7) infection was by skin scarification, PrP^{Sc} accumulation in spleen was not detected until 80 days postinfection [315].

In control mice of this study, some evidence of PrP^{Sc+} FDC networks was detectable in the MLN at 5 weeks post-prion infection, but a greater incidence was observed by 15 weeks (Figure 4.4; Appendix 7.3.2). The incidence of PrP^{Sc+} FDC networks in the MLNs of mice given prions alone at this time point was statistically significantly greater than that observed in any of the mice that were co-infected with *H. polygyrus* (Figure 4.4; Appendix 7.3.2).

In contrast, in the spleens of mice infected with prions alone no PrP^{Sc+} FDC networks were detected. Contrary, in co-infected groups only limited numbers of PrP^{Sc+} FDC networks were observed suggesting that only limiting levels of prions had been disseminated to their spleens during this time. Furthermore, *H. polygyrus* infection had no statistically significant effect on the incidence of PrP^{Sc+} FDC networks in these spleens (Figure 4.5; Appendix 7.3.3).

Taken together, although co-infection with *H. polygyrus* had a limited influence on the early accumulation of prions upon FDC in the PP, it did significantly affect the dissemination of prions to the MLN.

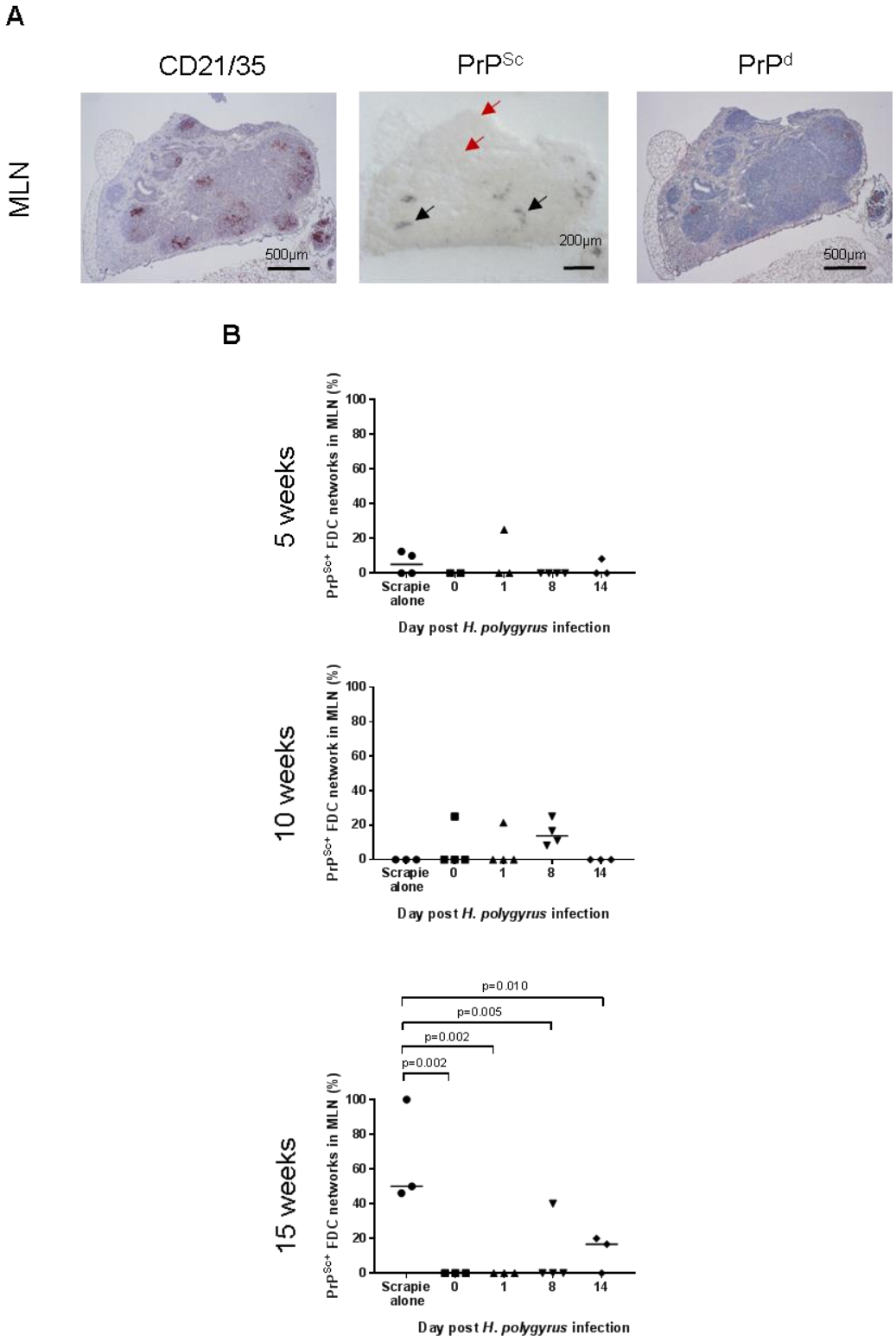
A
CD21/35
PrPSc
PrPd
MLN
500µm
200µm
500µm
B
5 weeks
10 weeks
15 weeks
PrPSc+ FDC networks in MLN (%)
PrPSc+ FDC network in MLN (%)
Scrapie alone
0
1
8
14
Day post H. polygyrus infection
p=0.010
p=0.005
p=0.002
p=0.002

Figure 4.4 Effect of *H. polygyrus* co-infection on the early accumulation of PrP^{Sc} upon follicular dendritic cells (FDC) in mesenteric lymph nodes (MLN). Female C57Bl/6 mice were orally infected with 200 L3 larvae, and then on days 0, 1, 8 or 14, the mice were subsequently orally infected with ME7 scrapie prions. MLN were collected at 5, 10 and 15 weeks after prion infection and analysed by IHC and PET immunoblot. (A) Representative image of MLN follicles without and with high levels of disease-specific PrP (PrP^{d}, brown) in association with FDC ($CD21/35^{+}$ cells, brown). Analysis of an adjacent section by PET immunoblot analysis confirmed the absence (red arrows) or presence (black arrows) of prion specific PK-resistant PrP^{Sc} (blue). (B) Assessment of the incidence of FDC networks containing PrP^{Sc} in each group of mice at 5, 10 and 15 weeks after prion exposure. Each point represents mean data from individual mice (2-3 MLN/mouse; 4 mice/group). Horizontal bar represents the median value of the group. Significant differences to the group infected with prions alone were compared by ANOVA, followed by Dunnett's multiple comparison test.

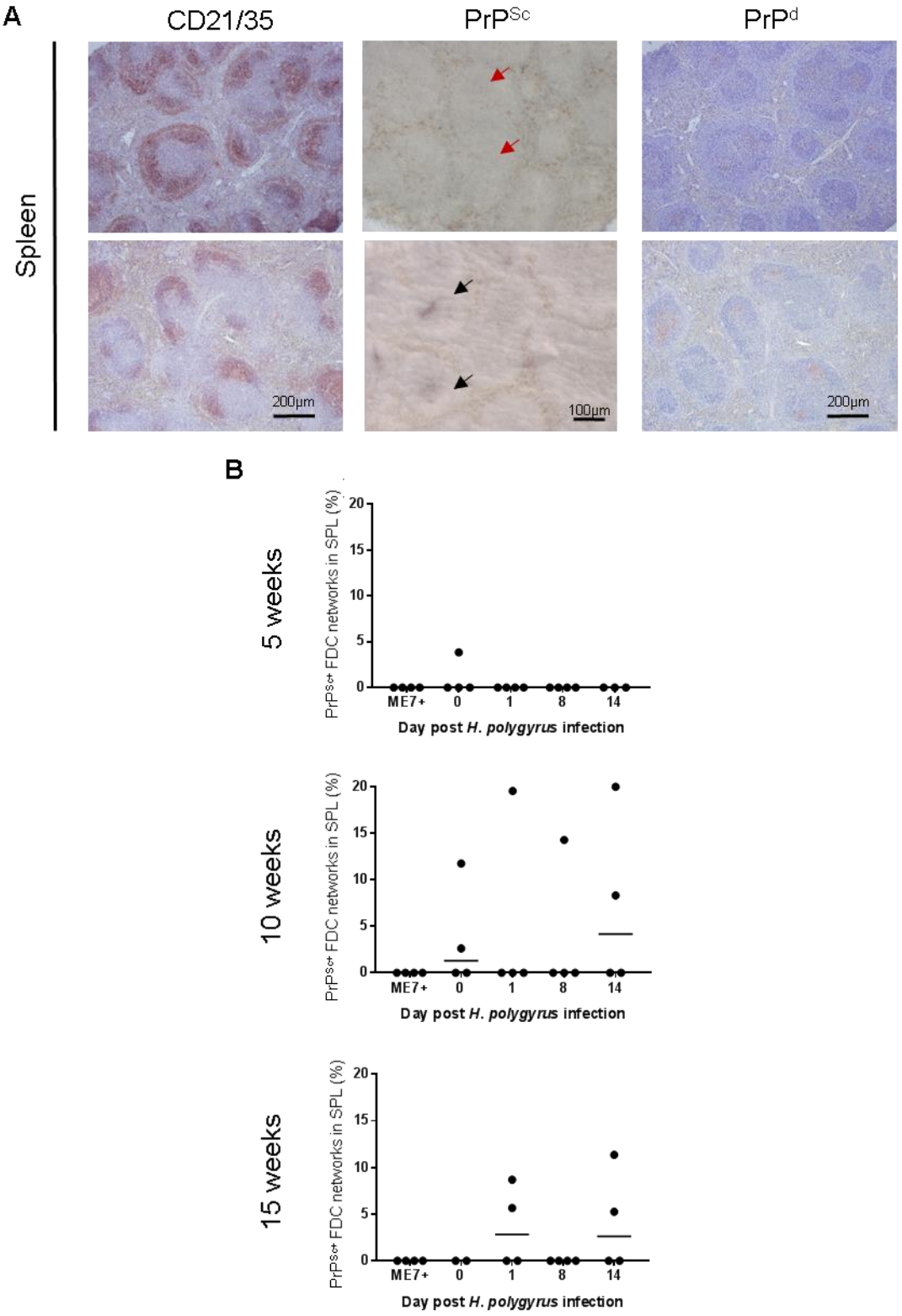
A
CD21/35
PrPSc
PrPd
Spleen
200µm
100µm
200µm
B
5 weeks
10 weeks
15 weeks
PrPSc+ FDC networks in SPL (%)
0
5
10
15
20
ME7+
0
1
8
14
Day post H. polygyrus infection

Figure 4.5 Effect of *H. polygyrus* co-infection on the early accumulation of PrP^{Sc} upon follicular dendritic cells (FDC) in the spleen. Female C57Bl/6 mice were orally infected with 200 L3 larvae, and then on days 0, 1, 8 or 14, the mice were subsequently orally infected with ME7 scrapie prions. Spleens were collected at 5, 10 and 15 weeks after prion infection and analysed by IHC and PET immunoblot. (A) Representative images of spleen without (upper panels) and with (lower panels) high levels of disease-specific PrP (PrP^{d}, brown) in association with FDC ($CD21/35^{+}$ cells, brown). Analysis of adjacent sections by PET immunoblot analysis confirmed the absence (red arrows) or presence (black arrows) of prion specific PK-resistant PrP^{Sc} (blue) (B) Assessment of the incidence of FDC networks containing PrP^{Sc} in each group of mice at 5, 10 and 15 weeks after prion exposure. Each point represents mean data from individual mice (4 mice/group). Horizontal bar represents median value of the group. Significant differences to the group infected with prions alone were compared by ANOVA, followed by Dunnett's multiple comparison test.

4.3.4 The granulomas induced in the gut wall by *H. polygyrus* infection do not accumulate PrP^{Sc} in prion-infected mice.

As Chapter 3 shows (Section 3.3.10), infection with the larval stages of *H. polygyrus* induces the development of granulomas in the wall of duodenum. Some experimentally-induced soft tissue granulomas have been shown to be capable of accumulating prions in prion-infected mice [234]. Data in this thesis show no evidence of FDC networks in granulomas induced by *H. polygyrus* as no CD 21/35 staining was detected (Figure 4.6A). However, Chapter 3 showed PrP^{C+} immunostaining on the periphery of the granulomas (Figure 3.20). This immunostaining corresponded to a dense network of PrP^{C}-expressing enteric nerves. Therefore, it raised the possibility that the granulomas induced by *H. polygyrus* might also be capable of accumulating prions in the intestines of prion-infected mice. To test this hypothesis, duodenal samples from the same mice used in Sections 4.3.2 & 4.3.3 were immunostained to detect PrP^{d}. PET immunoblot analysis of adjacent section was used to confirm the presence of PrP^{Sc}. Representative images of typical *H. polygyrus*-induced granulomas in the intestines of prion infected mice are presented in Figure 4.6. In this study, no PrP^{d} or PrP^{Sc} was detected in any of the granulomas at any time point throughout the prion infection (Figure 4.6B). This analysis clearly shows that the granulomas induced in the gut wall by *H. polygyrus* infection do not accumulate PrP^{Sc} in prion-infected mice.

A

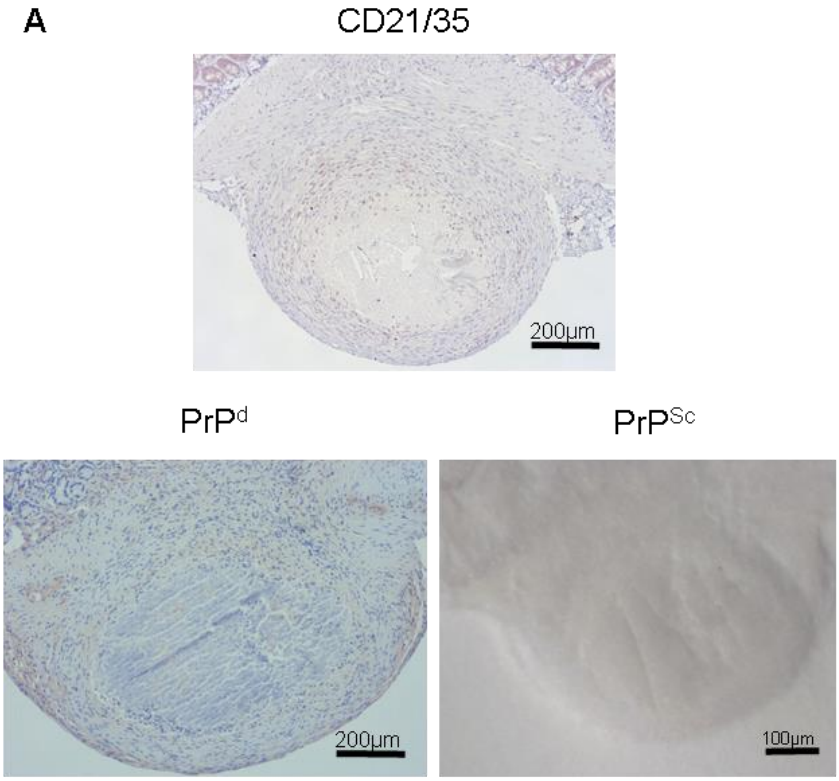

B

Weeks post prion infection	Incidence of PrP^{Sc+} granulomas
5	0/9
10	0/8
15	0/3

Figure 4.6 The granulomas induced in the gut after oral *H. polygyrus* are not sites of early PrP^{Sc} accumulation in mice co-infected with prions. Groups of 4 female C57Bl/6 mice were orally infected with 200 L3 larvae, and then on days 0, 1, 8 or 14, the mice were subsequently orally infected with ME7 scrapie prions. Small intestines were collected 5, 10 and 15 weeks after prion infection and analysed by IHC and PET immunoblot. (A) IHC analysis showed that no CD21/35 (brown), PrP^{d} (brown, left) or PrP^{Sc} (blue/black, right) accumulations were detected with the *H. polygyrus* induced granulomas in the gut wall. (B) Table shows the incidence of PrP^{Sc+} granulomas in the intestine at 5, 10 and 15 weeks after prion exposure.

4.3.5 Effect of *H. polygyrus* co-infection or prion disease susceptibility and disease duration.

As above C57BL/6J female mice (90 days old) were orally infected with 200 infective L3 by gavage. Then, on different days post *H. polygyrus* infection (days 0, 1, 8 and 14) groups of 8 mice were subsequently orally infected with a limiting dose of scrapie prions: 50 µl of a 1% dilution of scrapie brain homogenate prepared from mice terminally-affected with ME7 scrapie prions containing approximately 3.3 log10 i.c. ID_{50} units. A parallel group of 8 mice were orally infected with prions alone as a control. Each group of mice were clinically assessed weekly, from day 210 post prion infection, for the development of clinical signs of prion disease (Section 2.3) to terminal stage of the disease (Figure 4.7).

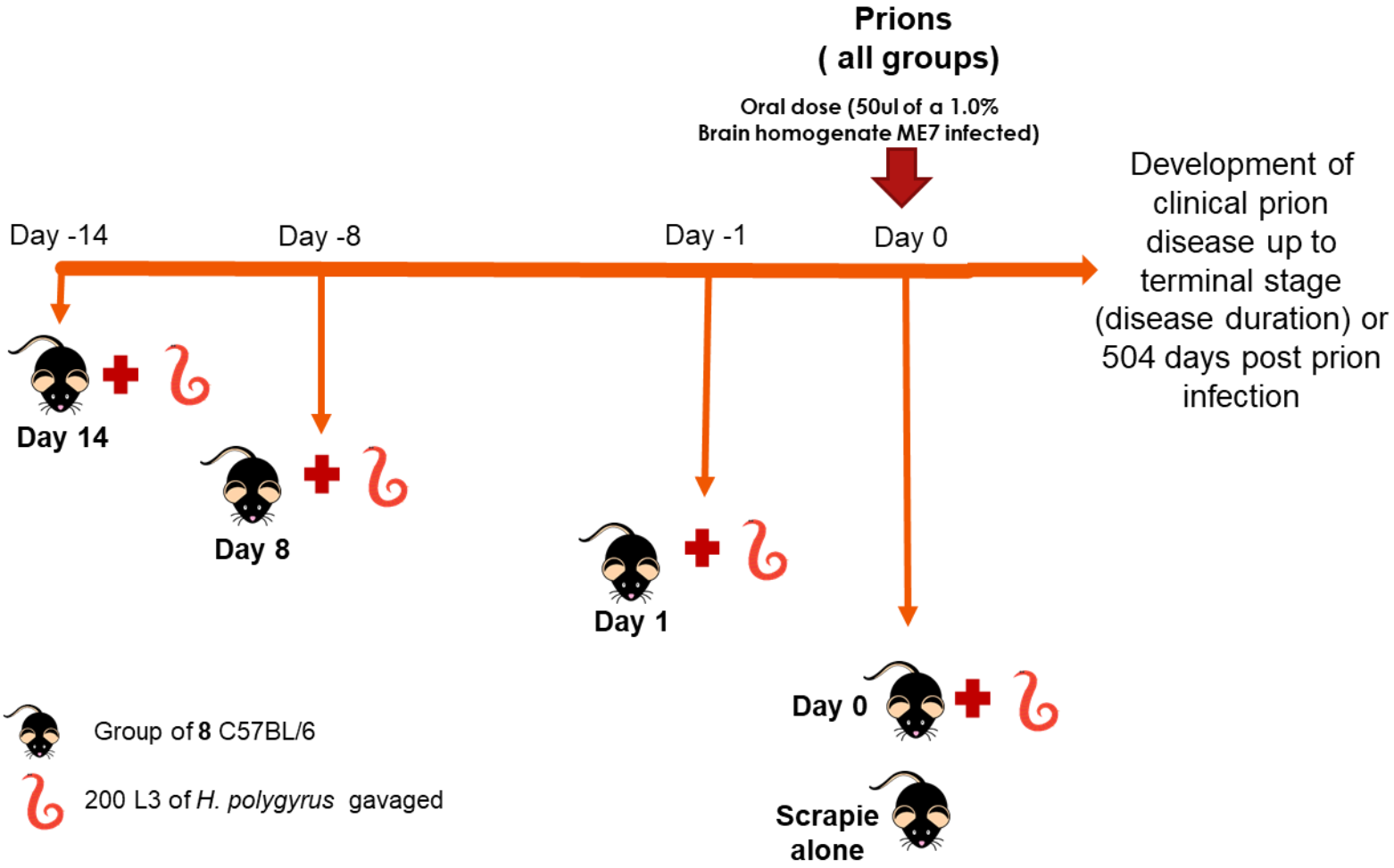
Prions
(all groups)
Oral dose (50ul of a 1.0%
Brain homogenate ME7 infected)
Development of clinical prion disease up to terminal stage (disease duration) or 504 days post prion infection
Day -14
Day -8
Day -1
Day 0
Day 14
Day 8
Day 1
Day 0
Scrapie alone
Group of 8 C57BL/6
200 L3 of H. polygyrus gavaged

Figure 4.7 Experimental design of *H. polygyrus* co-infection on prion disease susceptibility and disease duration. Groups of 8 female C57BL/6 mice were orally infected with 200 *H. polygyrus* L3, and on days 0, 1, 8 or 14 the mice were subsequently orally infected with ME7 scrapie prions. Also, a control group was infected with prions alone. Mice were monitored for clinical signs of prion disease; this was done weekly from day 210 post prion infection until the development of terminal stage of clinical prion disease or when the study was terminated at 504 days post prion infection.

First, for each mouse the time from prion infection to the time of cull due to development of terminal prion disease (survival) was determined. Survival curves for each group of co-infected mice compared to the prions alone group are presented in Figure 4.8. Half of the mice orally exposed to prions alone succumbed to terminal prion disease (Table 4.1 & Figure 4.8). It was considered that the mice developed clinical prion disease (Section 2.3) up to terminal stage when the animal wellbeing was compromised (e.g. poor body condition and inability to fed or have water). Further statistical analysis (Log-rank (Mantel-Cox) test) showed that co-infection with *H. polygyrus* did not have a significant effect on the survival time. Similarly, Fisher's exact test (each group was compared with the control) and chi-square test (all groups compared together) showed that the coinfection did not have a significant effect on the incidence (number animals which developed prion disease up to terminal stage from the all the survivals-infected in each group) of terminal prion disease irrespective of the time at which the mice were co-infected with prions (Figure 4.8).

Table 4.1 Clinical and histopathological incidence of prion disease, PrP^{Sc+} (spleen (SPL) and PP), PrP^{d} and vacuolation (brain).

Group	Clinical (+)	SPL PrP^{Sc+}	PP PrP^{Sc+}	Brain Vacuolation	Brain PrP^{d}
Scrapie alone	4/8	4/8	4/8	4/8	4/8
Day 0	4/7	2/5[a]	3[b]/7	4/7	4/6[a]
Day 1	6/7	6/7	4/5[a]	6/7	6/7
Day 8	3/5	2/4[a]	2/4[a]	3/5	3/5
Day 14	5/6	5/6	4[b]/6	5/6	5/6

a = tissue not available or not in optimal conditions for use
b = clinical (+) mouse missing was PrP^{d+} but not PrP^{Sc} detected
Incidence = number of positive animals/ total number of animals exposed to prions.

For each group of mice, the time from prion exposure to the first detectable onset of clinical signs, the incubation period (considered as positive score compatible with TSE), was determined (Appendix 7.3.4 & Figure 4.9A). The clinically positive control mice infected with prions alone presented clinical prion disease with a mean incubation period of 384 ± 10 days (Figure 4.9A). Further statistical analysis showed that *H. polygyrus* co-infection did not significantly influence the time taken to develop the first clinical signs of disease as the incubation periods for each group were similar to the control mice infected with prions alone.

Next, for each group of mice the duration of the clinical phase of the prion disease was determined: duration from the onset of clinical signs (incubation period) to the development of terminal prion disease. The mean duration of the clinical phase in control mice infected with prions alone was 25 ±7 days (Appendix 7.3.4 & Figure 4.9B). Although *H. polygyrus* co-infection did not significantly influence the duration of the clinical phase when mice were co-infected with prions on days 0, 1 and 14 post-*H. polygyrus*, the duration of clinical phase was statistically significantly longer when mice were co-infected with prions on day 8 post *H. polygyrus* infection 98 ±126 days (Figure 4.9B; $p<0.047$). However, this statistical difference appears to be influenced by only one mouse with a greatly extended survival time. Therefore, data show that *H. polygyrus* infection may under some circumstances prolong the clinical phase of prion disease in co-infected animals.

Finally, the effects of *H. polygyrus* infection on prion disease survival time was also considered: the time from prion infection to the time of cull due to development of terminal clinical signs of prion disease. The clinically positive control mice infected with prions alone succumbed to clinical prion disease with a mean time of 394 ± 14 days (Appendix 7.3.4 & Figure 4.9C). Although

H. polygyrus infection had no statistically significant influence on the survival times of any of the groups of mice which were co-infected with prions, the survival time of mice infected with prions on day 8 post *H. polygyrus* infection was ~47 days longer (441 ±21 days).

Together, these data show that despite the significant pathological disturbances in the small intestine caused by *H. polygyrus*, co-infection with prions only have modest effects; oral prion disease susceptibility (considered as disease incidence) and duration were increased in comparison with the scrapie alone control group.

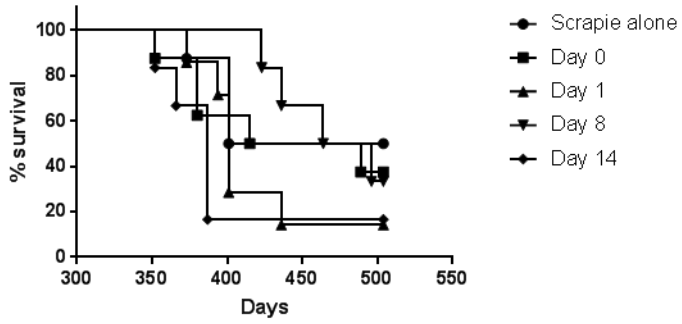
% survival
Days
Scrapie alone
Day 0
Day 1
Day 8
Day 14

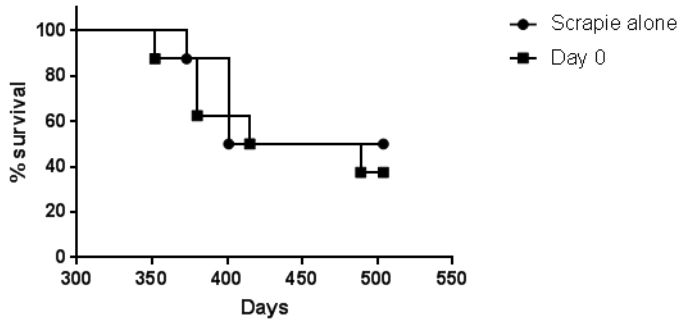
% survival
Days
Scrapie alone
Day 0

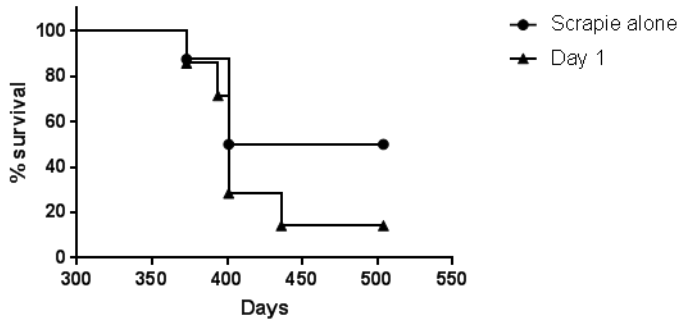
% survival
Days
Scrapie alone
Day 1

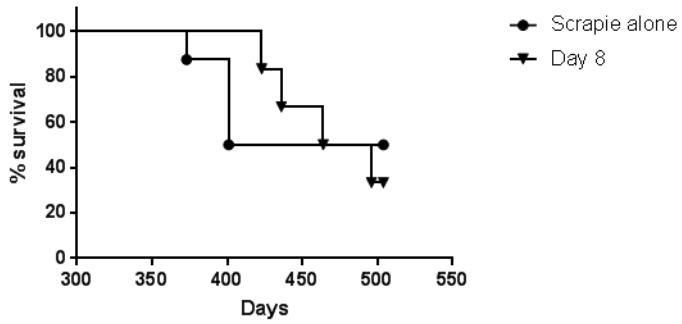
% survival
Days
Scrapie alone
Day 8

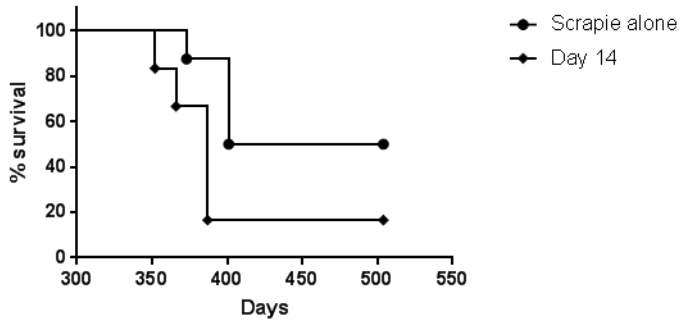
% survival
Days
Scrapie alone
Day 14

Figure 4.8 Effect of *H. polygyrus* co-infection on the susceptibility to oral prion infection. Female C57Bl/6 mice were orally infected with 200 L3 larvae, and then on days 0, 1, 8 or 14, the mice were subsequently orally infected with ME7 scrapie prions. Survival curves compare prion disease susceptibility for each group of mice. Each point represents the prion disease survival times for individual mice (6-8 mice/group). Significant differences were compared by Log-rank (Mantel-Cox) test.

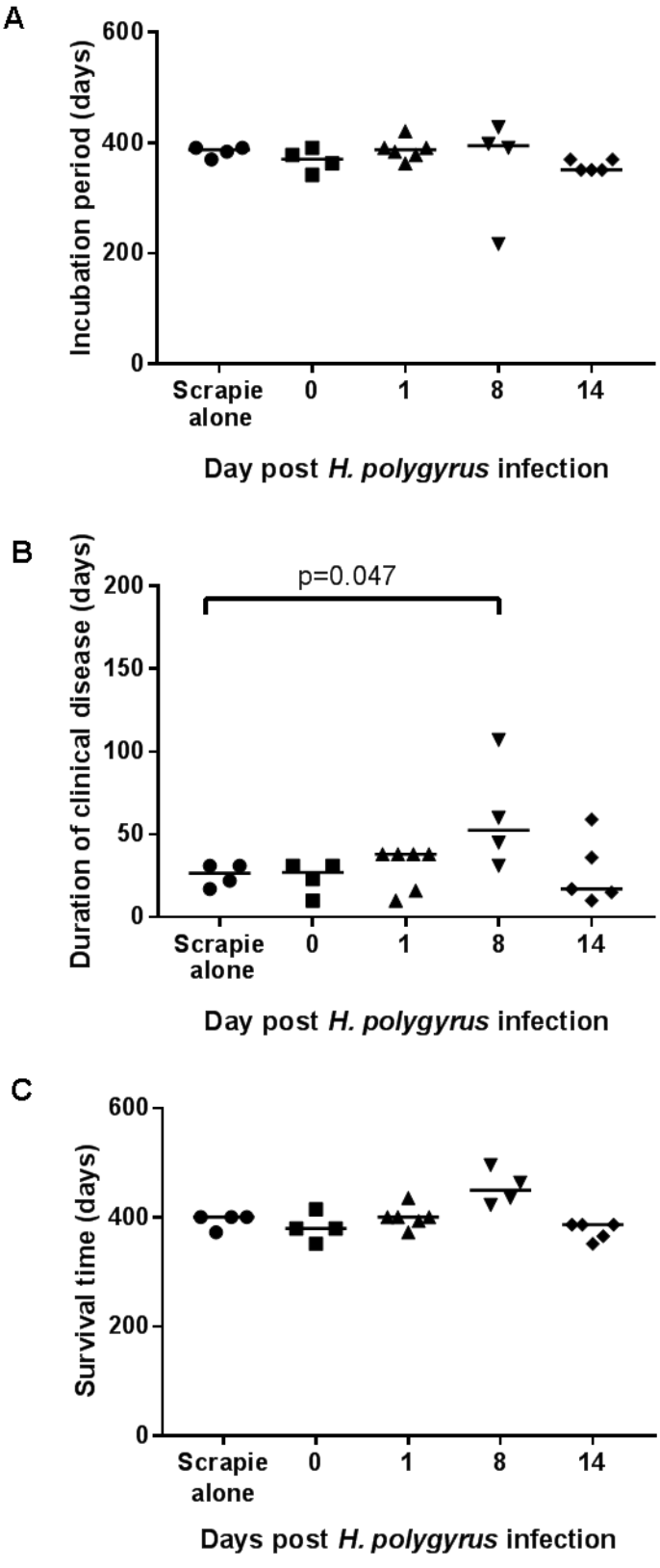
A
600
400
200
0
Incubation period (days)
Scrapie alone
0
1
8
14
Day post H. polygyrus infection
B
p=0.047
200
150
100
50
0
Duration of clinical disease (days)
Scrapie alone
0
1
8
14
Day post H. polygyrus infection
C
600
400
200
0
Survival time (days)
Scrapie alone
0
1
8
14
Days post H. polygyrus infection

Figure 4.9 Effect of *H. polygyrus* co-infection on the development of clinical prion disease. Female C57Bl/6 mice were orally infected with 200 L3 larvae, and then on days 0, 1, 8 or 14, the mice were subsequently orally infected with ME7 scrapie prions. The effects of *H. polygyrus* co-infection on (A) prion disease incubation period (time from prion exposure to onset of clinical signs), (B) duration of clinical disease, and (C) survival time (from prion infection to terminal disease) were determined for each mouse. Each point represents data from individual mice (4-6 mice/group). Horizontal bar represents the median time of each group. Significant differences to the group infected with prions alone were compared by ANOVA, followed by Dunnett's multiple comparison test.

4.3.6 Effect of *H. polygyrus* co-infection on the development of prion disease-specific neuropathology in the brain.

Next the effects of *H. polygyrus* co-infection on the development of the characteristic spongiform pathology (vacuolation), astrogliosis, microgliosis and PrP^{Sc} accumulation which are associated with terminal infection with ME7 scrapie prions were determined. Brains from each mouse from each group were stained using H&E (for assessment of spongiform pathology) or immunostained to detect PrP^{d}, $GFAP^{+}$ astrocytes and $Iba1^{+}$ microglia. All samples were blinded before assessment.

All the brains from the clinically-affected mice showed the characteristic histopathological signs of prion disease (Figure 4.10). In these brains, the most affected regions were the thalamus and the hippocampus with presence of vacuolation, PrP^{d} deposits, astrocytosis (GFAP), and reactive microglia (Iba1). None of these signs were detected in any of the clinically-negative mice (Figure 4.10).

The incidence of animals in each group that displayed prion disease-specific spongiform pathology is presented in Table 4.1. Then, the mean vacuolation score for each brain area in each group was compared (Figure 4.11). This analysis showed that the magnitude of the spongiform pathology in these regions was similar in the brains of clinically-affected mice from each group. However, in the hypothalamus of mice co-infected with *H. polygyrus* and prions on the same day (day 0), the magnitude of the vacuolation score was significantly reduced when compared with clinical positive control mice infected with prions alone (Figure 4.11B; $p<0.038$).

Brain sections from the same mice from each group were also immunostained to detect PrP^{d}, and the magnitude of its abundance was scored as described in

Sections 2.7.1 and 2.7.2. The incidence of PrP^d deposition observed in the brain was consistent with the incidence of vacuolation and presence of clinical signs of prion disease (Table 4.1). The mean score of the PrP^d deposition in brain area in each group was then compared (Figure 4.12). As above the magnitude of the PrP^d deposition was similar in the brains of clinically-affected mice from each group (Appendix 7.3.6). However, in the hippocampus of mice co-infected with *H. polygyrus* and prions on the same day (day 0), the magnitude of the PrP^d deposition was also significantly reduced when compared with clinical positive mice which were infected with prions alone (Figure 4.12; $p<0.014$). Although these significant differences may imply a biological effect, it is also important to consider that PrP^d deposition is accumulative. Mice co-infected on the same day (day 0) had a shorter survival time (382±26) than those from the prions alone group (394±14) (individual data of each mouse is available in the Appendix 7.3.6). Therefore, the shorted survival time may affect the accumulation of PrP^d deposition in affected areas. Figure 4.10 show the histopathological differences between clinical positive and clinical negative animals; differences in brain histopathological scoring are shown in Figure 2.1.

The type of the PrP^d deposition was also assessed using the criteria described in Section 2.7.1. This analysis showed that in the clinically-affected brains the PrP^d deposition was predominantly fine punctate and coarse in all groups (Appendix 7.3.6). *H. polygyrus* co-infection had no significant effect on the type of deposition presented in the brain when compared to mice infected with prions alone.

Next, brain sections from all mice from each group were immunostained to detect $GFAP^+$ astrocytes and the magnitude of the immunostaining was scored as described in Section 2.7.3 (Appendix 7.3.7). The mean GFAP

immunolabelling scores in each of the different brain areas were then compared (Figure 4.13). This analysis showed that *H. polygyrus* co-infection did not significantly influence the magnitude of the GFAP immunostaining detected in the brain, when compared to the brains from the mice infected with prions alone.

Finally, brain sections were immunostained to detect $Iba1^{+}$ microglia and the magnitude of the immunostaining scored as mentioned in Section 2.7.4. The mean Iba1 immunolabelling scores/group for each brain area are presented in Figure 4.14 (Appendix 7.3.7). This analysis also showed that *H. polygyrus* co-infection did not significantly influence the magnitude of the $Iba1^{+}$ immunostaining detected in the brain, when compared to the brains from the mice infected with prions alone.

Taken together, these data confirmed that all the mice which presented with positive clinical signs of prion disease also displayed the characteristic pathology of prions disease in their brains. None of the clinically negative animals showed any histopathological signs of prion disease in their brains suggesting they were free of prion disease and would have been unlikely to have developed prion disease had they survived longer. However, the possibility that these mice remained as subclinical carriers cannot be excluded. In the clinically-affected mice, the most affected regions of the brain with pathological changes were the thalamus and the hippocampus. Although the histopathological signs of prion disease were similar in all groups whether they were co-infected with *H. polygyrus* or not, significant effects were observed in the mice infected with prions and *H. polygyrus* on the same day, with significantly reduced vacuolation in the hypothalamus and PrP^{d} deposition in the hippocampus. However, the difference was only one point on the scale used, thus the biological significance remains to be determined in

the absence of any significant effect on disease susceptibility or the disease duration.

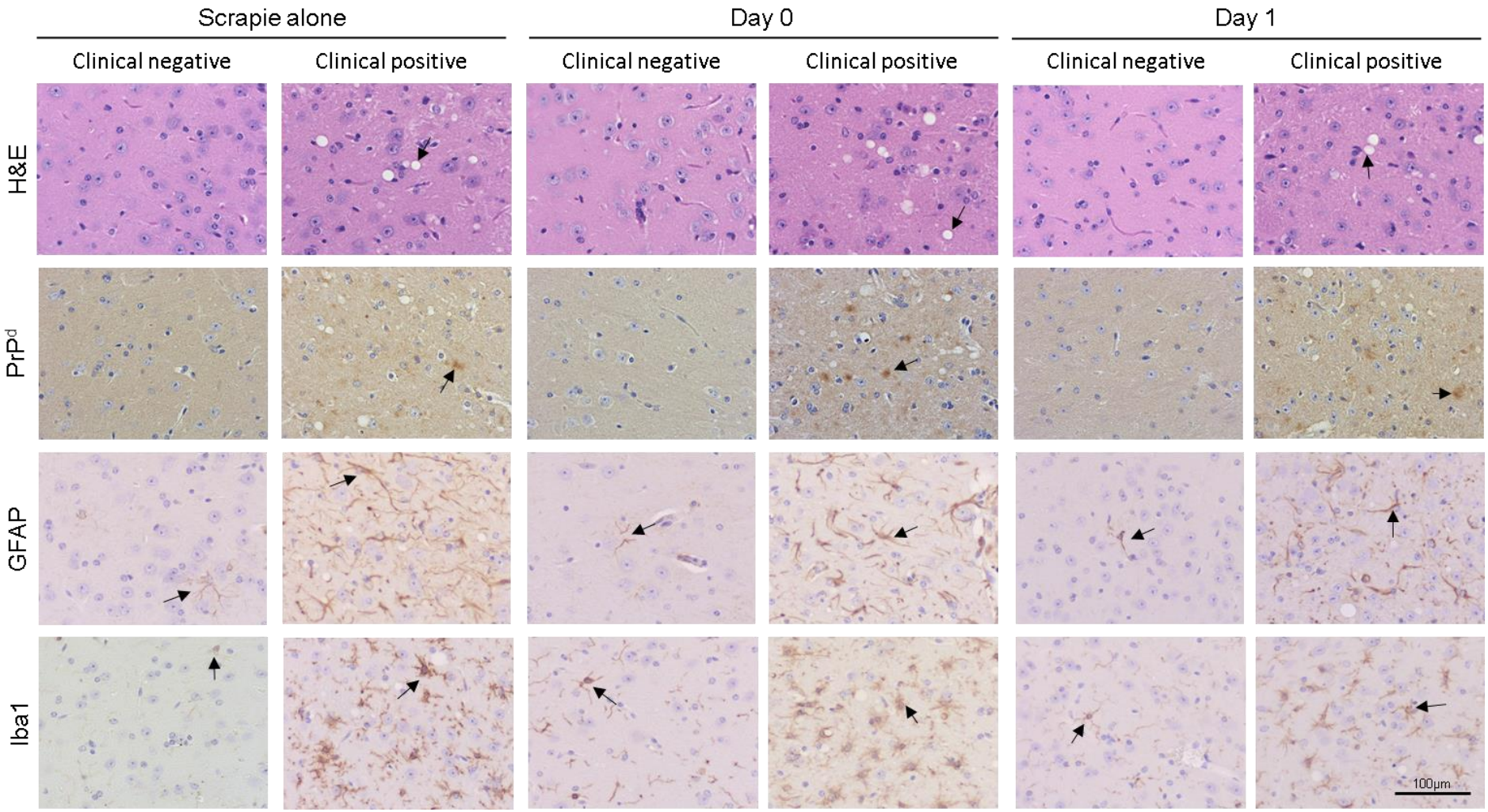
Scrapie alone
Day 0
Day 1
Clinical negative
Clinical positive
Clinical negative
Clinical positive
Clinical negative
Clinical positive
H&E
PrPd
GFAP
Iba1
100μm

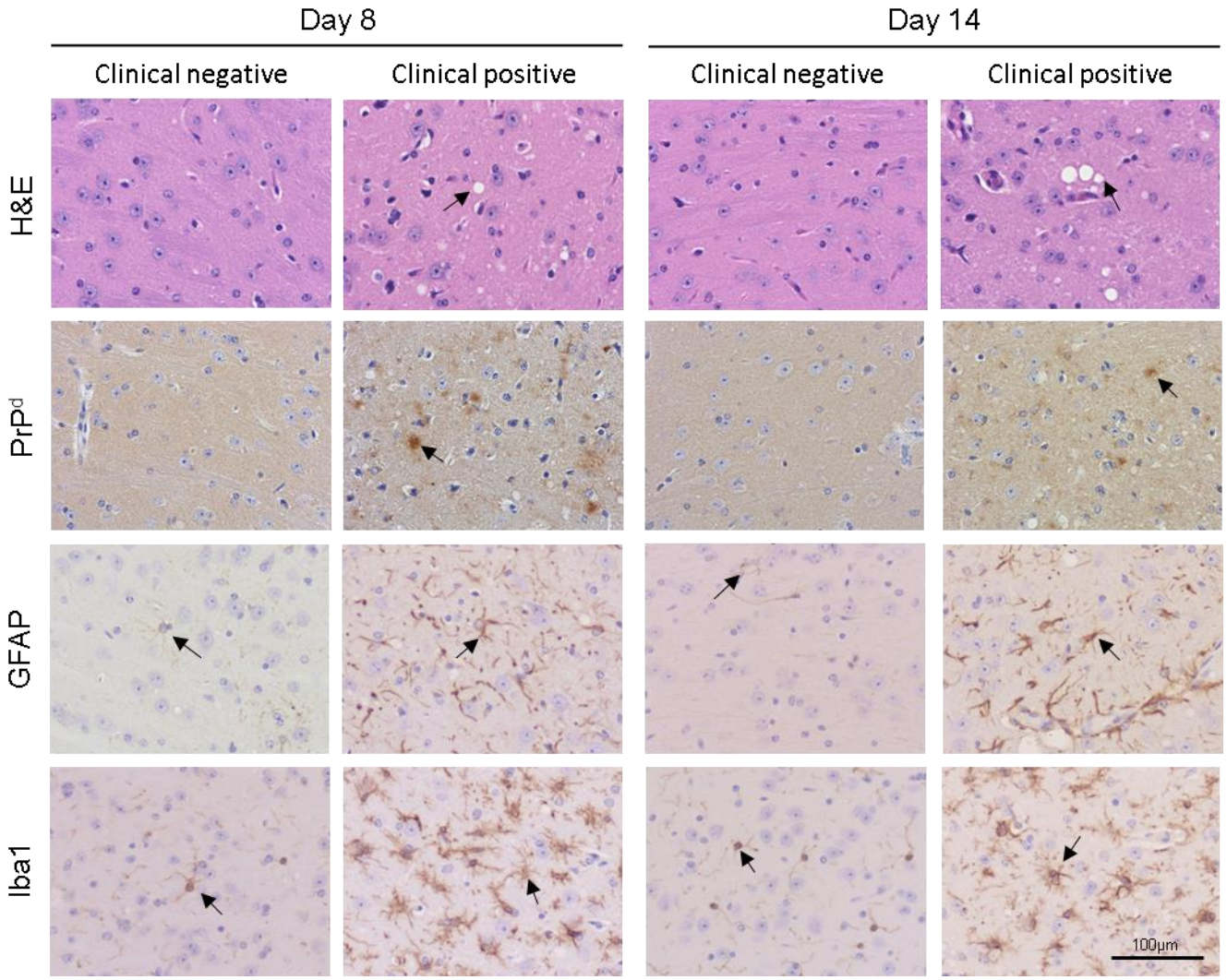
Day 8
Day 14
Clinical negative
Clinical positive
Clinical negative
Clinical positive
H&E
PrPd
GFAP
Iba1
100μm

Figure 4.10 Effect of *H. polygyrus* co-infection on the development of characteristic hallmarks of prion disease neuropathology. Female C57Bl/6 mice were orally infected with 200 L3 larvae, and then on days 0, 1, 8 or 14, the mice were subsequently orally infected with ME7 scrapie prions. Brains were collected from all mice with clinical signs of prion disease and clinically-negative survivors for IHC analysis. High levels of spongiform pathology (H&E, upper row) are evident as small holes in the tissue, heavy accumulations of PrP^d (brown staining deposition, second row), reactive astrocytes expressing GFAP (brown, third row) and active microglia expressing Iba1 (brown, bottom row) were detected in the brains of all the mice with clinical prion disease. Astrocytes and microglia are normally found in the brain, but in contrast with the pathological tissues they have thin dendrites and are less abundant. None of these histopathological signs of prion disease were detected in the brains of any of the clinically-negative mice up to at least 504 days after oral exposure. Images are only representative of a positive and a negative mice/group.

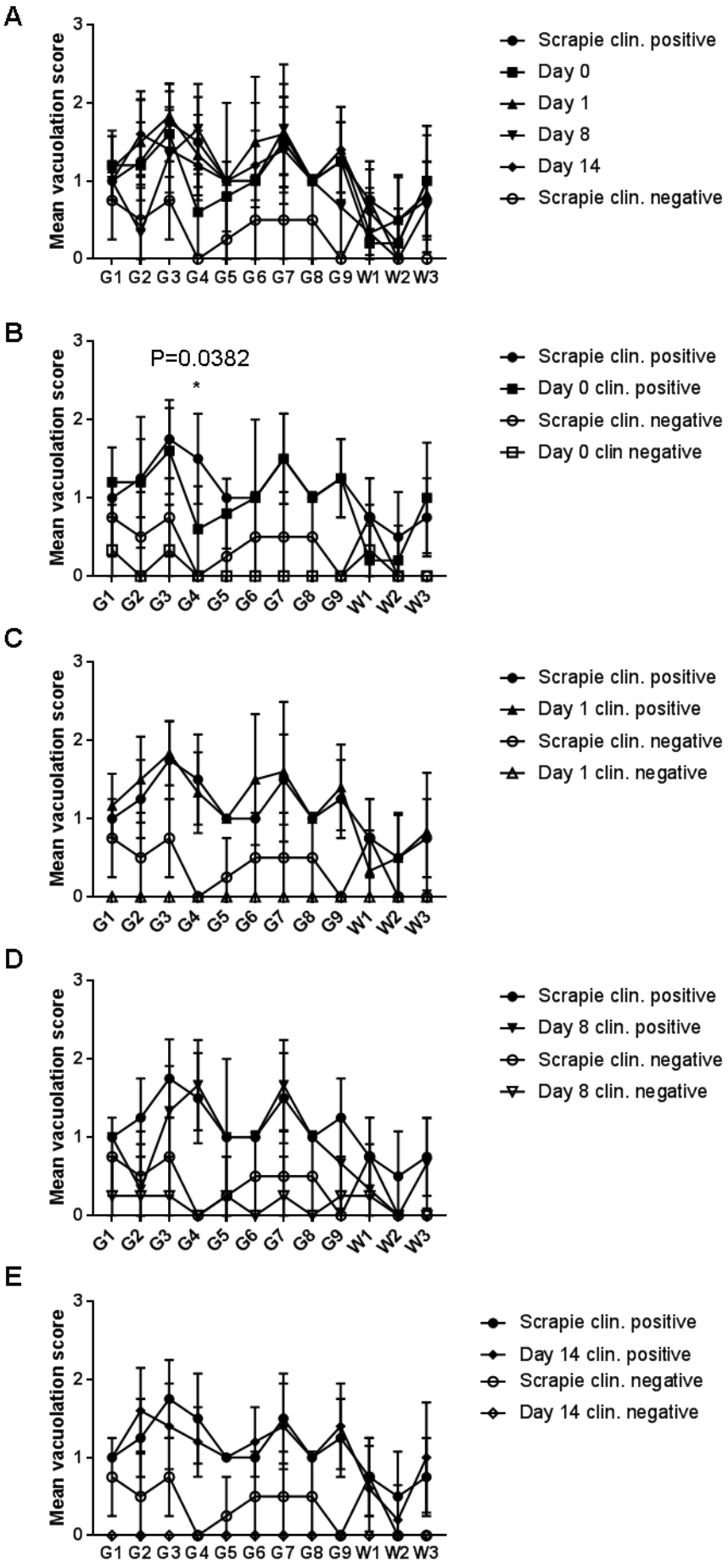
A
Mean vacuolation score
0
1
2
3
G1 G2 G3 G4 G5 G6 G7 G8 G9 W1 W2 W3
Scrapie clin. positive
Day 0
Day 1
Day 8
Day 14
Scrapie clin. negative
B
P=0.0382
*
Mean vacuolation score
Scrapie clin. positive
Day 0 clin. positive
Scrapie clin. negative
Day 0 clin negative
C
Mean vacuolation score
Scrapie clin. positive
Day 1 clin. positive
Scrapie clin. negative
Day 1 clin. negative
D
Mean vacuolation score
Scrapie clin. positive
Day 8 clin. positive
Scrapie clin. negative
Day 8 clin. negative
E
Mean vacuolation score
Scrapie clin. positive
Day 14 clin. positive
Scrapie clin. negative
Day 14 clin. negative

Figure 4.11 Effect of *H. polygyrus* co-infection on the development of spongiform pathology in prion infected mice. Female C57Bl/6 mice were orally infected with 200 L3 larvae, and then on days 0, 1, 8 or 14, the mice were subsequently orally infected with ME7 scrapie prions. Brains were collected from all mice with clinical signs of prion disease and clinically-negative survivors, and the H&E sections analysed. The severity and distribution of the vacuolation within each brain was scored on a scale of 1-5 in nine grey matter areas: G1, dorsal medulla; G2, cerebellar cortex; G3, superior colliculus; G4, hypothalamus; G5, thalamus; G6, hippocampus; G7, septum; G8, retrosplenial and adjacent motor cortex; G9, cingulate and adjacent motor cortex. (A) Mean vacuolation scores for all mouse groups. (B) Comparison of prions alone with the day 0 co-infection group. (C) Comparison of prions alone with the day 1 co-infection group. (D) Comparison of prions alone with the day 8 co-infection group. (E) Comparison of prions alone with the day 14 co-infection group. Each point represents the mean vacuolation score ± SD (3-6 clinical positive and 4 clinical negative mice/group). Significant differences to the group infected with prions alone were compared by ANOVA, followed by Dunnett's multiple comparison test.

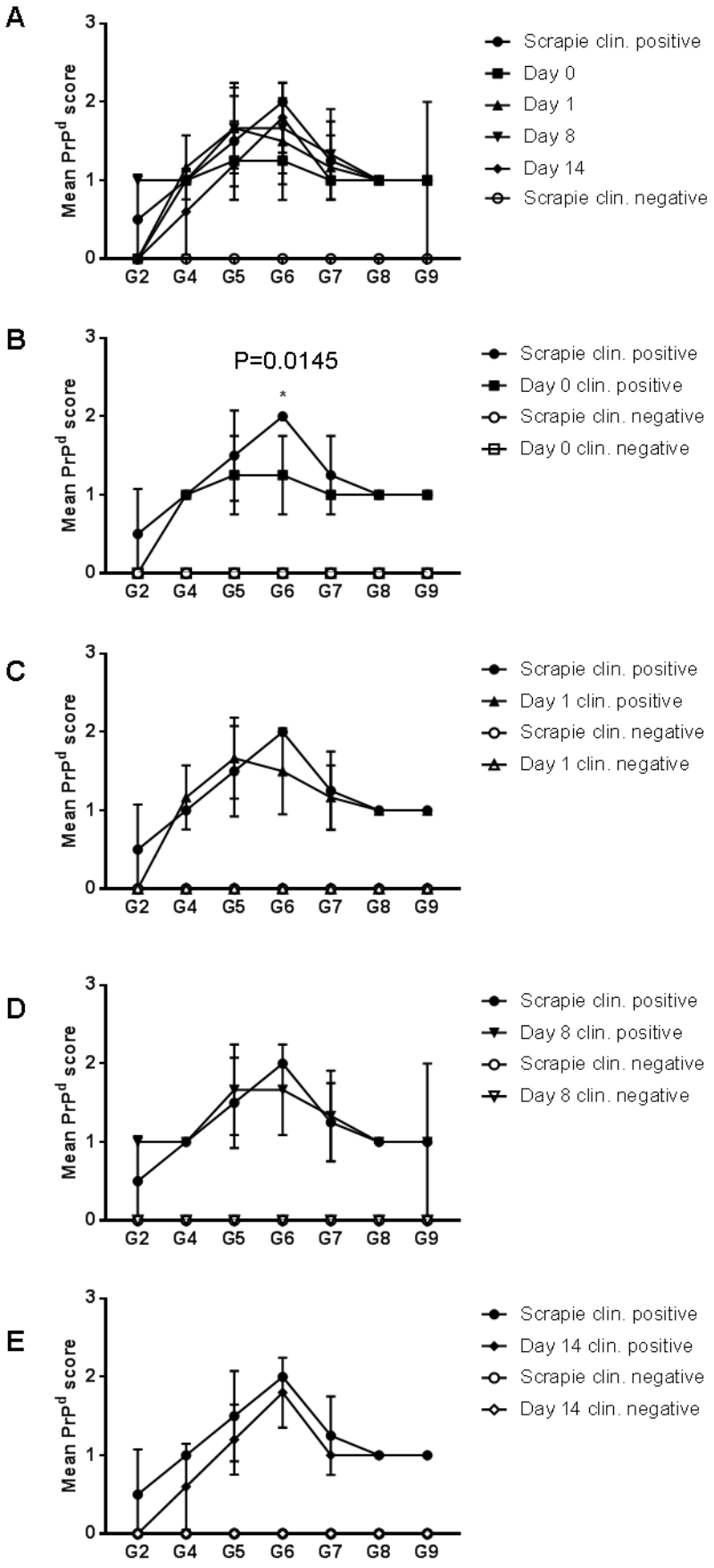
A
Mean PrPd score
3
2
1
0
G2 G4 G5 G6 G7 G8 G9
Scrapie clin. positive
Day 0
Day 1
Day 8
Day 14
Scrapie clin. negative
B
P=0.0145
*
Mean PrPd score
G2 G4 G5 G6 G7 G8 G9
Scrapie clin. positive
Day 0 clin. positive
Scrapie clin. negative
Day 0 clin. negative
C
Mean PrPd score
G2 G4 G5 G6 G7 G8 G9
Scrapie clin. positive
Day 1 clin. positive
Scrapie clin. negative
Day 1 clin. negative
D
Mean PrPd score
G2 G4 G5 G6 G7 G8 G9
Scrapie clin. positive
Day 8 clin. positive
Scrapie clin. negative
Day 8 clin. negative
E
Mean PrPd score
G2 G4 G5 G6 G7 G8 G9
Scrapie clin. positive
Day 14 clin. positive
Scrapie clin. negative
Day 14 clin. negative

Figure 4.12 Effect of *H. polygyrus* co-infection on the magnitude of the prion disease specific PrP^d accumulation in the brains of prion infected mice. Female C57Bl/6 mice were orally infected with 200 L3 larvae, and then on days 0, 1, 8 or 14, the mice were subsequently orally infected with ME7 scrapie prions. Brains were collected from all mice with clinical signs of prion disease and clinically-negative survivors, and immunostained to detect PrP^d. The severity and distribution of the PrP^d accumulation within each brain was scored on a scale of 1-3 in seven grey matter areas: G2, cerebellar cortex; G4, hypothalamus; G5, thalamus; G6, hippocampus; G7, septum; G8, retrosplenial and adjacent motor cortex; G9, cingulate and adjacent motor cortex. (A) Mean PrP^d accumulation scores for all mouse groups. (B) Comparison of prions alone with the day 0 co-infection group. (C) Comparison of prions alone with the day 1 co-infection group. (D) Comparison of prions alone with the day 8 co-infection group. (E) Comparison of prions alone with the day 14 co-infection group. Each point represents the mean PrP^d accumulation score ± SD (3-6 clinical positive and 4 clinical negative mice/group). Significant differences to the group infected with prions alone were compared by ANOVA, followed by Dunnett's multiple comparison test.

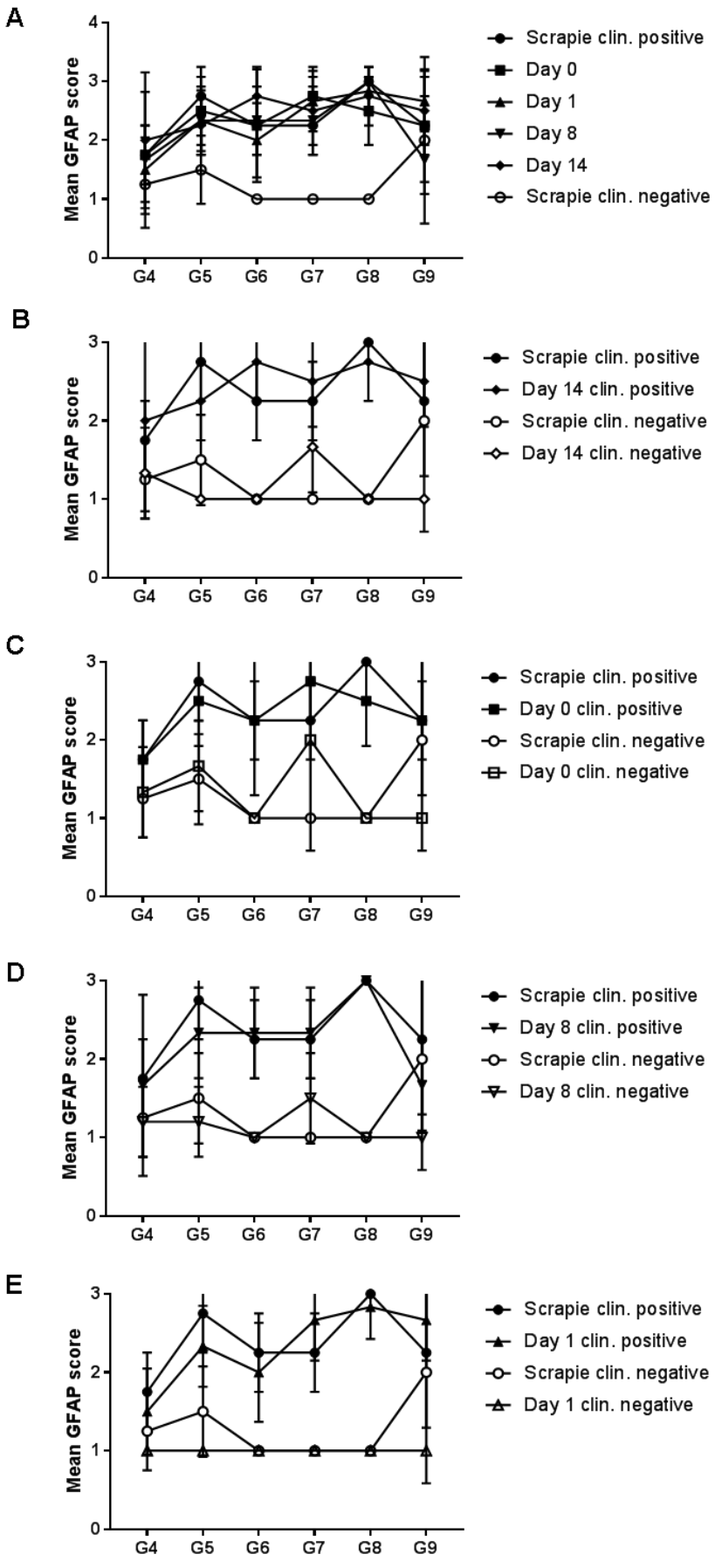
A
Mean GFAP score
0
1
2
3
4
G4
G5
G6
G7
G8
G9
Scrapie clin. positive
Day 0
Day 1
Day 8
Day 14
Scrapie clin. negative
B
Mean GFAP score
Scrapie clin. positive
Day 14 clin. positive
Scrapie clin. negative
Day 14 clin. negative
C
Mean GFAP score
Scrapie clin. positive
Day 0 clin. positive
Scrapie clin. negative
Day 0 clin. negative
D
Mean GFAP score
Scrapie clin. positive
Day 8 clin. positive
Scrapie clin. negative
Day 8 clin. negative
E
Mean GFAP score
Scrapie clin. positive
Day 1 clin. positive
Scrapie clin. negative
Day 1 clin. negative

Figure 4.13 Effect of *H. polygyrus* co-infection on the magnitude of astrocyte activation in the brains of prion infected mice. Groups of 8 female C57Bl/6 mice were orally infected with 200 L3 larvae, and then on days 0, 1, 8 or 14, the mice were subsequently orally infected with ME7 scrapie prions. Brains were collected from all mice with clinical signs of prion disease, or clinically-negative survivors, and immunostained to detect GFAP+ reactive astrocytes. The severity and distribution of the GFAP+ immunostaining within each brain was scored on a scale of 1-3 in six grey matter areas: G4, hypothalamus; G5, thalamus; G6, hippocampus; G7, septum; G8, retrosplenial and adjacent motor cortex; G9, cingulate and adjacent motor cortex. (A) Mean GFAP+ accumulation scores for all mouse groups. (B) Comparison of prions alone with the day 0 co-infection group. (C) Comparison of prions alone with the day 1 co-infection group. (D) Comparison of prions alone with the day 8 co-infection group. (E) Comparison of prions alone with the day 14 co-infection group. Each point represents the mean GFAP+ immunostaining score ± SD (3-6 clinical positive and 4 clinical negative mice/group). Significant differences to the group infected with prions alone were compared by ANOVA, followed by Dunnett's multiple comparison test.

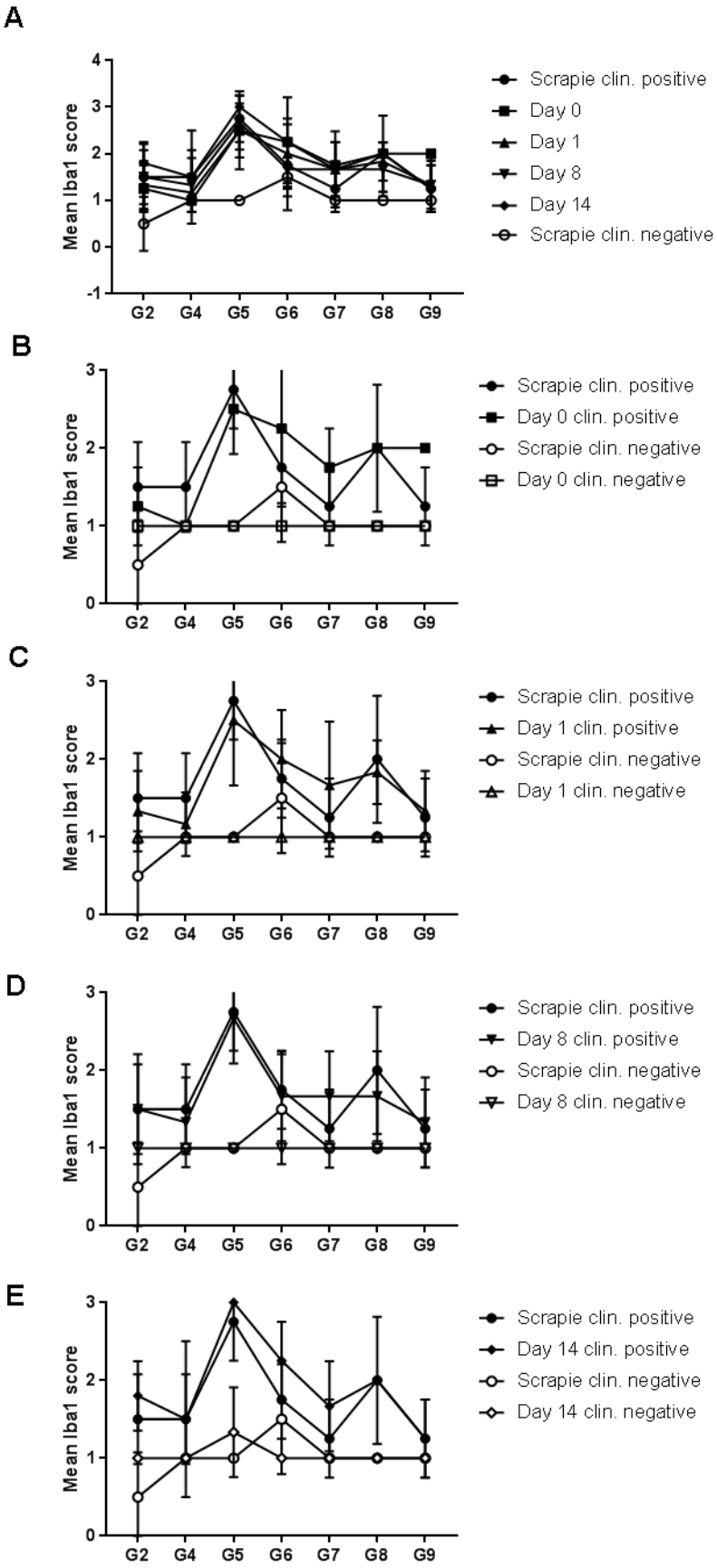
A
Mean Iba1 score
4
3
2
1
0
-1
G2
G4
G5
G6
G7
G8
G9
Scrapie clin. positive
Day 0
Day 1
Day 8
Day 14
Scrapie clin. negative
B
Mean Iba1 score
3
2
1
0
G2
G4
G5
G6
G7
G8
G9
Scrapie clin. positive
Day 0 clin. positive
Scrapie clin. negative
Day 0 clin. negative
C
Mean Iba1 score
3
2
1
0
G2
G4
G5
G6
G7
G8
G9
Scrapie clin. positive
Day 1 clin. positive
Scrapie clin. negative
Day 1 clin. negative
D
Mean Iba1 score
3
2
1
0
G2
G4
G5
G6
G7
G8
G9
Scrapie clin. positive
Day 8 clin. positive
Scrapie clin. negative
Day 8 clin. negative
E
Mean Iba1 score
3
2
1
0
G2
G4
G5
G6
G7
G8
G9
Scrapie clin. positive
Day 14 clin. positive
Scrapie clin. negative
Day 14 clin. negative

Figure 4.14 Effect of *H. polygyrus* co-infection on the magnitude of microglial activation in the brains of prion infected mice. Female C57Bl/6 mice were orally infected with 200 L3 larvae, and then on days 0, 1, 8 or 14, the mice were subsequently orally infected with ME7 scrapie prions. Brains were collected from all mice with clinical signs of prion disease and clinically-negative survivors, and immunostained to detect Iba1+ microglia. The severity and distribution of the Iba1+ immunostaining within each brain was scored on a scale of 1-3 in six grey matter areas: G4, hypothalamus; G5, thalamus; G6, hippocampus; G7, septum; G8, retrosplenial and adjacent motor cortex; G9, cingulate and adjacent motor cortex. (A) Mean PrP^d accumulation scores for all mouse groups. (B) Comparison of prions alone with the day 0 co-infection group. (C) Comparison of prions alone with the day 1 co-infection group. (D) Comparison of prions alone with the day 8 co-infection group. (E) Comparison of prions alone with the day 14 co-infection group. Each point represents the mean Iba1+ immunostaining score ± SD (3-6 clinical positive and 4 clinical negative mice/group). Significant differences to the group infected with prions alone were compared by ANOVA, followed by Dennett's multiple comparison test.

4.3.7 PrP^{Sc} deposition in PP and spleens at the terminal stage of prion disease

In mice orally infected with ME7 scrapie prions, PrP^{Sc} accumulation is maintained upon FDC in the PP and spleen until the clinical phase [125, 194, 195, 341]. The PP and spleens from each animal collected either at the end of the clinical stage or the end of the experiment (for clinically negative survivors) were analysed by IHC and PET immunoblotting to detect FDC ($CD21/35^{+}$ cells), PrP^{d} and PrP^{Sc} (Figure 4.15 & Appendix 7.3.5). The incidence of PrP^{Sc+} FDC in each tissue is shown in Table 4.1. This analysis confirmed that FDC-associated PrP^{Sc} accumulations were detected in all the PP and spleens collected from the mice with clinical prion disease. Co-infection with *H. polygyrus* did not influence the incidence of the PrP^{Sc+} FDC in PP and spleen at the terminal stage of the disease when compared to those from mice infected with prions alone. Furthermore, no signs of PrP^{Sc} accumulation were detected in any of the tissues from the clinically negative mice suggesting these mice were free of prion infection.

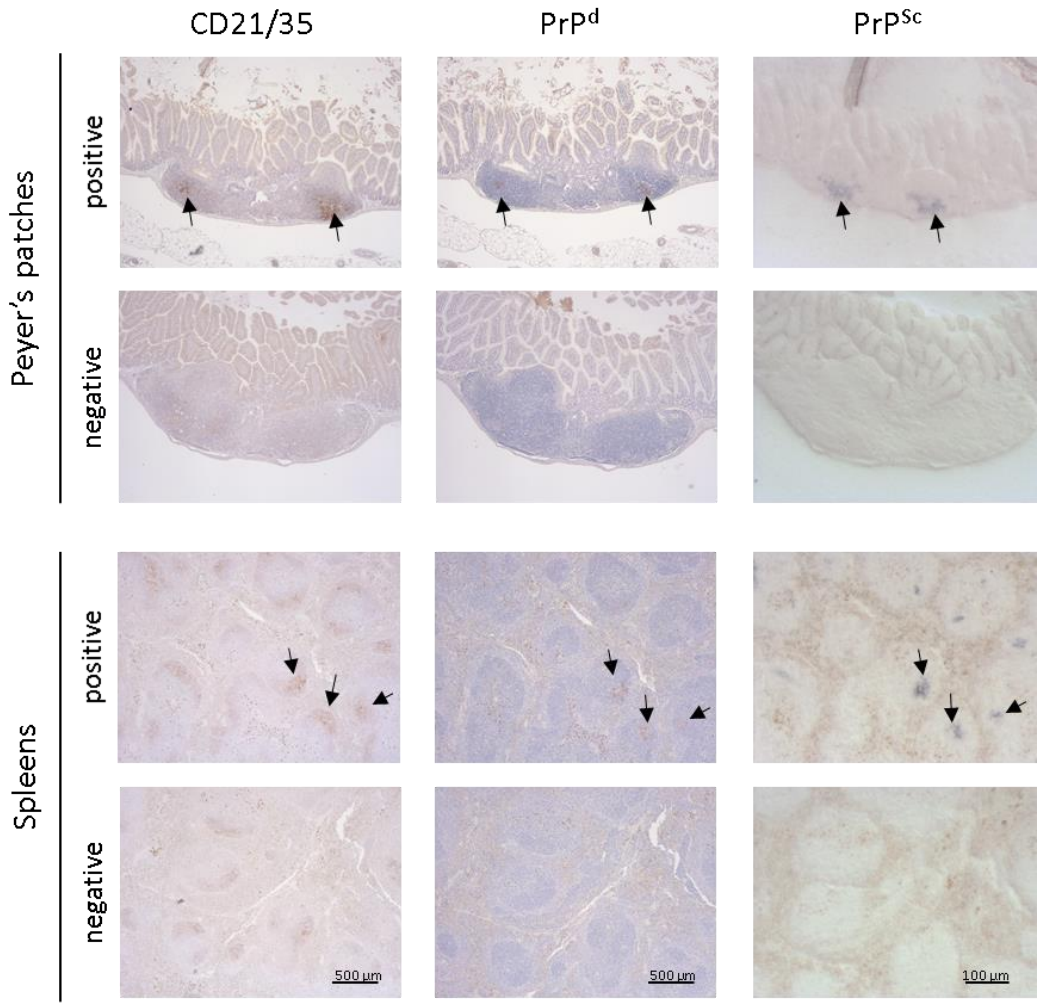

Figure 4.15 Effect of *H. polygyrus* co-infection on the accumulation of PrP^{Sc} upon follicular dendritic cells (FDC) in Peyer's patches (PP) and the spleen. Female C57Bl/6 mice were orally infected with 200 L3 larvae, and then on days 0, 1, 8 or 14, the mice were subsequently orally infected with ME7 scrapie prions. PP and spleens were collected from all mice with clinical signs of prion disease and clinically-negative survivors, and analysed by IHC and PET blot. Representative images of PP and spleen from clinically positive and negative animals are shown. In all PP and spleens from mice with positive clinical signs of prion disease, high levels of disease-specific PrP^d (PrP^d, brown) were detected in association with FDC (CD21/35+ cells, brown). Analysis of adjacent sections by PET immunoblot analysis confirmed the presence of prion specific PK-resistant PrP^{Sc} (blue/black, black arrow, right panels). No PrP^d or PrP^{Sc} accumulations were detected in association with FDC in any of the tissues from the clinically-negative survivors.

4.4 Discussion

In this chapter the effect of *H. polygyrus* infection in the small intestine on oral prion disease susceptibility and duration was assessed. Groups of mice were first orally infected with *H. polygyrus* and either on the same day (day 0) or on days 1, 8 or 14 post infection, the mice were subsequently orally co-infected with ME7 scrapie prions. The effect of *H. polygyrus* co-infection on the early accumulation of prions upon FDC in the PP, MLN, and spleen were then determined, as well the subsequent effects on prion disease susceptibility and duration. The results showed that co-infection with *H. polygyrus* had only a limited influence on the early accumulation of prions upon FDC in the PP, however it did appear to restrict its dissemination to the MLN. Despite of this, co-infection with *H. polygyrus* did not affect oral prion disease susceptibility (incidence of disease). Although the histopathological signs of prion disease were similar in all groups whether they were co-infected with *H. polygyrus* or not, a significant reduction in the magnitude of the spongiform pathology and PrP^{d} accumulation was detected in certain brain regions when the mice co-infected with prions and *H. polygyrus* on the same day. Therefore, although data in Chapter 3 showed that oral infection with *H. polygyrus* causes significant pathological disturbances in the small intestine, data in this chapter showed that co-infection with *H. polygyrus* had only a modest influence on oral prion disease pathogenesis and susceptibility.

In the previous chapter it was shown that *H. polygyrus* infection specifically affected the microarchitecture of the small intestine and the GALT within it. Given that small intestine GALT are important sites of prion uptake, accumulation and replication after oral exposure [124, 125, 194, 195, 369], the effects of a small intestine-restricted parasitic infection (*H. polygyrus*) on prion disease pathogenesis and susceptibility were studied. After oral exposure the

prions cross through the specialised enterocytes or M cells in the epithelium covering the PP [139, 369, 370]. Afterwards the prions are then acquired by mononuclear phagocytes in the subepithelial dome region [139] of the PP from where they are subsequently propagated to the FDC in the B cell follicles of the PP and on towards other tissues via the lymph and blood to the MLN and spleen [333, 371-373]. Early detection of PrP^{Sc} by cryoelectron microscopy has shown PrP^{Sc} accumulation upon FDC in PP as early as 7-21 days post infection, which subsequently spreads to the myenteric plexus neurons by day 21 [139]. In this chapter PET immunoblot analysis confirmed the presence of PrP^{Sc} upon FDC in PP from 5 weeks post prion infection. *H. polygyrus* co-infection had little influence on the accumulation of PrP^{Sc} within PP except when the mice were co-infected with *H. polygyrus* and prions on the same day, where a significant reduction in the incidence of PrP^{Sc}-positive FDC networks at 15 weeks post prion infection was observed. However, this result may be due to the number of PP follicles sampled. For this analysis, all the visible PP of each mouse were collected and processed. However, the final number of PP follicles suitable for analysis (FDC^{+}) in sections ranged from 1-12 per mouse (Appendix 7.3.1). Therefore, the probability of detecting PrP^{Sc+} FDC was greater when larger numbers of follicles were available. Further analyses with more tissue sections from these mice may be needed to corroborate this result. However, given that mice with negative PP were also negative in the other tissue samples, the possibility that these animals were negative due the prion limiting dose remains.

Following their replication upon FDC in the PP, the prions are subsequently disseminated to the MLN and spleen. In mice co-infected with *H. polygyrus* the abundance of PrP^{Sc+} FDC in the MLN after prion exposure was significantly reduced in comparison with control mice group infected with prions alone at

15 weeks post prion infection. The absent or low detection of PrP^{Sc} in the MLN of these co-infected mice (Appendix 7.3.2) may be a consequence of the effects of *H. polygyrus* infection on the MLN. For example the migration of CD11c CD8α DC from the lamina propria to the MLN is reported to be reduced in *H. polygyrus* infected mice [374]. Within the MLN changes to the positioning of $CD11c^+$ DC from the T cell areas to below the sub capsular sinus in the inter-follicular areas and to the T cell-B borders have been described [374, 375]. As $CD11c^+$ DC have been proposed to play an important role in the initial delivery of prions to the FDC within the draining lymphoid tissues [180, 205, 376], the reduced detection of PrP^{Sc} deposition in MLN 15 weeks after scrapie infection may be a consequence of *H. polygyrus* infection on $CD11c^+$ cells. It is also possible that this effect could be related to the increased abundance of $CD68^+$ cells (macrophages) in the PP after *H. polygyrus* infection described in the previous chapter (Figure 3.15). In the lymph nodes, macrophages have been suggested to phagocytose PrP^{Sc} form FDC [186, 377, 378]. Since macrophages and DC can phagocytose PrP^{Sc} and degrade prions [178, 379], the increased number or activation of macrophages in the PP and MLN during *H. polygyrus* infection may reduce the amount of PrP^{Sc} transported to the MLN or replication within it. During chronic *H. polygyrus* infection, there are high levels of Foxp3 regulatory T cells (Treg) in the MLN and spleen [294]. Therefore, *H. polygyrus* induced Treg may down regulate host immune responses in MLN and spleen, resulting in the low levels of PrP^{Sc} detected in these organs in some of the co-infected mice.

It had been suggested that after prions are orally acquired, they need to replicate in PP before dissemination to MLN and spleen before prions are found in the CNS [125]. In this context, the spleen had special consideration in

prion pathogenesis due the amount of FDC. However, splenectomised mice had been shown to develop the disease [205].

In the PP, the lack of $CD11c^{+}$ cells impedes prion accumulation within them [211]. However, this only reduces the susceptibility to develop prion disease [211]. Therefore, although prion replication in the PP may be needed to increase pathogenicity of the prions to infect a host, this may not be necessary to develop the disease. In this study, prion accumulation in the MLN was restricted at early time; however, the susceptibility to prion disease was not altered. This is compatible with the concept that prion replication over MLN may not be essential [125].

Studies suggest that there is a close relation and communication between the gut and the nervous system. Interactions between enteric microbiota and nervous system had been related with autism or anxiety-depressive disorders [380]. Furthermore, intestinal macrophages may have direct communication with the nervous system [381, 382]. Specifically, during *H. polygyrus* infection, it has been shown that mucosal neurons express neuromedin U (NMU) [383]. This neuropeptide is express by cholinergic neurons in the gastrointestinal tract and is closely related with worm expulsion by regulating the activities of innate lymphoid cells, regulating inflammation, repairing tissue, and therefore, facilitating the worm expulsion [383, 384]. Considering that acetylcholinesterase is among the excretory secretory products of *H. polygyrus* [250], it may be possible to speculate that this enzyme may block the activation of the cholinergic neurons that express NMU and therefore influence the severity of prion disease. Another possibility is that *H. polygyrus* infection, which drives a predominantly Th2 response [256], is mainly activating NMU-expressing neurons, and given their overexcitability they may not increase prions disease characteristics. Whether prion disease itself also affects the

activities of the NMU-expressing neurones is not known, but potential effects on this pathway may explain the effects of co-infection with prions on worm burden.

Although the number of eggs is not necessarily related to the number of worms [385], this parameter is used as an indicator of the worm infection. Here, the egg burden was altered in its number and duration by prion co-infection (Figure 4.1). This alteration were apparently related with the stage of *H. polygyrus* infection at which prions were administrated. This has not been reported before, but some speculations are presented ahead. Mice infected with prions at day 1 after *H. polygyrus* infection had a reduced egg burden. Also, in the same group and in mice infected with prions and *H. polygyrus* on the same day, eggs were detected in the faeces for up to 4 weeks (17±19 eggs/g of faeces) after *H. polygyrus* oral exposure. This means that they have a shorter egg output. C57BL/6 mice are considered to be intermediate responders to *H. polygyrus* which takes from 8 to 20 weeks to clear worm burden infection [245, 386]. Similar to the groups which were infected with prions at days 8 and 14 post *H. polygyrus* infection; in which the presence of eggs in faeces were detected until 16-20 weeks (23±25 eggs/g of faeces) after parasite exposure. In Chapter 3 no effects were detected in duodenum epithelium at day 1 post *H. polygyrus*. Therefore, the reduced egg burden may suggest that either there was a prion-parasite interaction or both infections may have an immune synergic effect which reduces worm fertility or influences early worm expulsion. Prion-worm interaction has been suggested before. Even more, in a study in which different developmental stages of a fly larvae (*Sacrophaga canaria*) were fed with brains of hamsters infected with prions, the consumption of infected larvae proved to transmit prion disease to other hamsters [387].

A third effect was noticed when the maximum egg burden was reach later in time (day 21) on mice infected with prions at day 8 post *H. polygyrus* infection. It is important to notice that at the time of prion infection, worms were on their second moult stage and ready to break out into the intestinal lumen. So, if prion co-infection delay adult worms to emerge or delay worm mating, both are just speculative explanations.

Regarding the apparent increase egg output in mice co-infected with prions at day 14 post *H. polygyrus* (Figure 4.1), it is worth to clarify that this result is caused by an individual effect. Although the mean number of eggs in faeces is 26932, the standard deviation was very wide (±1534 eggs/g. of faeces); and these mice had not been infected with prions at the time of the first measurement (day 14). Therefore, these data need to be interpreted with caution.

As mentioned previously, it has been suggested that chronic inflammation may favour prion replication in inflamed organs such as mammary gland, kidney, lung and liver. However, in these circumstances PrP^{Sc} accumulation was dependent upon the presence of newly formed lymphoid structures [110, 313, 388]. Chronic inflammation can lead to development of granulomas. These lympho-follicular inflammatory sites are developed during *H. polygyrus* infection. It has been suggested that prion can accumulate in soft tissue granulomas even in the absence of FDC [234]. However, in this study no PrP^{Sc} was detected in the worm-induced granulomas. Although this may be contradictory, it is consistent with a study in sheep where no PrP^{Sc} was detected in granulomas [389]. Differences in these findings may be related to the type of granuloma. These structures are a common pathological finding in chronic inflammatory process and can have different origins (bacterial, parasites foreign bodies) which seem to be reflected in some histopathological

differences [305, 390, 391]. Therefore, these contradictory findings may be associated with differences between an induced and a natural granuloma [302], and possibly to the area of the body where the granulomas are formed.

Although in this chapter, the pathology of *H. polygyrus* in the small intestine epithelium seems to have a limited effect with statistical significance on prion disease, results suggest that there may be a significant biological effect of this coinfection. Table 4.1 show that prion infection may enhance prion disease susceptibility. Furthermore, the stage of *H. polygyrus* infection at which mice were co-infected with prions seems to influence the incidence of clinical disease. Evidence show that mice co-infected on day 0 and 8 post *H. polygyrus* had an incidence of 57% and 60% of clinical positive prion disease, while mice co-infected on day 1 and 14 post *H. polygyrus* had an incidence of 83% and 85%.

Despite causing significant histopathological disturbances to the duodenum and within PP, coinfection with *H. polygyrus* did not significantly influence prion disease susceptibility, survival times or the development of neuropathology in the brain. Data from this study suggest that gastrointestinal helminth infections specifically in the small intestine may have little influence on susceptibility to orally acquired prion infections.

Chapter 5. General discussion

5.1 Introduction

Prion diseases are progressive neurodegenerative diseases which can affect human and animals with fatal consequences. Although their origin can be sporadic or genetic, some are caused by the infectious prion particle (PrP^{Sc}) [392-395]. This is the pathological infectious form of the cellular prion protein (PrP^{C}) which can be normally found in different tissues such as synaptic membranes of neurons and astrocytes, muscle, kidney, heart, secondary lymphoid organs and gastrointestinal tract [64, 396-399]. Although the exact route of exposure of infectious prions is unclear, many may be orally acquired, such as following consumption of contaminated food or pasture. While some gaps still exist in the understanding of pathogenesis following infection of the host, the requirement for certain key cell types to facilitate the spread of prions from the intestine to the central nervous system has been demonstrated. Studies of experimental mice orally infected with prions show that the prions are first transported across the gut epithelium in the small intestine and into the Peyer's patches (PP) by M cells [135, 198, 369]. Once the prions are shed into the underlying subepithelial dome region of the PP they are then taken up by mononuclear phagocytes or dendritic cells (DC) [211, 400, 401]. If the prions are phagocytosed by dendritic cells, data imply that they are most-likely destroyed [178, 378, 379]. If the prions are acquired by DC, they can be carried to the follicular dendritic cells (FDC) in the B cell follicles where they replicate [186, 340]. Prions replicate upon FDC at early stage of the infection before infecting the peripheral nervous system, through which they spread to the central nervous system (CNS). Since the early replication of prions in the small intestinal gut associated lymphoid tissues (GALT) is essential for the prions to establish host infection [124], factors such as inflammation may significantly influence prion disease pathogenesis. However, the effects that

co-infection or inflammation specifically in the small intestine may have on oral prion disease pathogenesis are not known. Therefore, the aim of this thesis was to test the hypothesis that a congruent infection with a gastro-intestinal pathogen specifically in the small intestine may significantly influence susceptibility to an orally-acquired prion infection.

In order to test this hypothesis, the natural mouse intestinal helminth pathogen *H. polygyrus* was used. This helminth was considered ideal for co-infection with prions as it establishes infection specifically in the small intestine (duodenum) where it induces a chronic infection which is cleared from the host (C57BL/6) within 8-20 weeks [386]. The strain of the mouse determines resistance or susceptibility to the *H. polygyrus* infection. While CBA or A/J mice are slow responders which can host *H. polygyrus* infection for more than 20 weeks [402-406], other strains such as SJL and SWR can clear the infection within 4-6 weeks and are considered fast responsive [286, 402, 405, 407, 408]. However, there is a range of intermediate responders including C57BL/6 (used in this study), BALB and NIH [386, 409]. Oral infection with *H. polygyrus* also leads to the development of significant pathology in the gut epithelium and induces the formation of granulomas in the gut wall. Furthermore, it has been shown that *H. polygyrus* infection can modulate other immune responses, including allergy and autoimmune inflammation [289, 410].

H. polygyrus induces a polarized Th2 response that includes goblet cell hyperplasia, mastocytosis, enteritis and increased smooth muscle contractions and granulomas are normally developed during the infection [260, 269, 407, 411]. However, little was known of the effects of *H. polygyrus* on the microarchitecture of the GALT and the status of key cell types which are known to play an important role in oral prion disease pathogenesis, such as M

cells, FDC and enteric nerves. Therefore, the aim of the studies described in Chapter 3 was to provide a detailed characterization of the effects of oral *H. polygyrus* infection on the microarchitecture of the gut and the GALT. As mentioned above, specific attention was given to the effects of infection on the cells which prions exploit in the intestine to establish host infection, including: M cells, macrophages, DC, FDC and enteric nerves. Data from those studies were then used to inform the design of the experiments described in Chapter 4, which aimed to test the hypothesis that a small intestine-restricted pathogen such as *H. polygyrus* might significantly influence oral prion disease pathogenesis and susceptibility. Data from these studies revealed that although oral *H. polygyrus* infection caused significant disturbances to the microarchitecture of the small intestine and the GALT within it, these changes had limited effects on oral prion disease pathogenesis and susceptibility. When mice were coinfected with *H. polygyrus* and prions, the presence of *H. polygyrus* eggs in faeces suggest that parasite infection was cleared faster. Data also suggested that the early PrP^{Sc} detection within MLN follicular dendritic cell network was reduced in some mice. In some animals the duration of clinical prion disease was longer, and in the brain, the accumulation of PrP^{d} and the spongiform pathology were reduced. However, despite these effects co-infection did not affect oral prion disease susceptibility.

A number of experimental co-infections with different pathogens and prions have previously been performed. In experimental viral co-infections in mice, such as intranasal co-infection with Piry-arbovirus virus at 15 weeks post intracranial ME7 scrapie prion infection, the microglial inflammatory response is increased, but no behavioral changes related to these were detected [412]. In the co-infection of mice with murine Friend leukemia virus (retrovirus) and 22L scrapie prions (inoculated intraperitoneal) on the same day, no effects on

prion disease pathology were detected; even though scrapie infectivity was increased in an *in vitro* model [240]. However, when mice were co-infected with MAdV (mice adenovirus) and scrapie at a later time point (after 128 days), susceptibility to prion disease increased [239]. Similarly, oral co-infection with the bacterial pathogen *S. typhimurium* and RML6 scrapie prions showed an increased prion disease susceptibility associated with the acute inflammation in the cecum and colon caused by *Salmonella* [413]. Despite that this subspecie of *Salmonella* induced a moderate, acute suppurative inflammation restricted to the caecum and colon [414]; studies with S. *typhimurium* administered in gut loops, induced M cells differentiation in murine PP [415]. M cells are an entry site of prions [416], and its differentiation during *S. typhimurium* infection is dependent on the phosphatase activity of SopB, which is an essential protein that mediates the RANKL; this mediate the transformation of epithelial cells into M cells [415]. Contrary, previous studies with the large intestinal parasite *Trichuris muris* did not have a significant impact on orally acquired ME7 prion disease in C57BL/6J mice [124]. These results suggest that the pathogen, prion strain, timing of infection as well as the inoculation route may play an important role in the ability of a co-infection to alter prion disease development.

Certain factors have been shown to modify prion disease pathogenesis, or the distribution of prions in the host. For example, prions have been shown to be able to accumulate in certain chronically inflamed tissues within prion-infected hosts. These include ectopic/tertiary lymphoid tissues induced in the liver, kidney, pancreas, lung and mammary gland, as well as soft-tissue granulomas [235, 389, 417]. However, the increased number of colonic isolated lymphoid follicles (ILF) caused by *T. muris* did not influence prion disease susceptibility or disease onset even though there was increased accumulation

of PrP^{Sc} in the large intestine GALT at an earlier time post prion infection (15 weeks). Other indirect effects of the inflammatory response may be critical such as the increased differentiation of M cells found in the presence of *Salmonella* infection [415] or cholera toxin [418]. Therefore, that fact that these aspects were not altered at the time of infection may underlie the reason why *H. polygyrus* did not alter significantly oral prion disease susceptibility.

5.2 **Results**

5.2.1 Effect of *H. polygyrus* infection on ILF

ILF are dynamic structures that similar to PP are in direct contact with the intestinal lumen. These structures have a FAE with M cells and a B cell-containing germinal centre [335, 419]. They are also capable of inducing specific immune responses to antigens within the gut lumen [334, 419]. Data in this thesis showed that *H. polygyrus* infection reduced the number of ILF in the duodenum and colon on day 14 after infection (Figures 3.9 and 3.11). This is the first study to show this effect of *H. polygyrus* infection. This contrasts with the effects of inflammation [420], commensal bacteria [421] and the large intestine restricted helminth *T. muris* [422] that have been shown to stimulate ILF maturation. Neo-formation of ILF is dependent on RANKL to transform the gut villus epithelium into FAE in the small intestine [127, 130, 335], and the migration of B cells to the neo-lymphoid sites [423]. During *H. polygyrus* infection the Th2 response in the MLN is accompanied by an increased accumulation of B cells [403, 424], where these cells are retained and as a consequence depleted from other peripheral lymph nodes [353]; therefore, the effect on ILF may due to a downregulation or blocking of neo-formation of ILF by B cell sequestration. In the absence of PP, ILF were able to substitute PP function and accumulate ME7 prions when administered orally [125]. Furthermore, mice which only had ILF developed prion disease similar disease incidences and survival times as intact control mice [125]. Therefore, the reduction of ILF in the presence of *H. polygyrus* infection could have had the potential to reduce the uptake of orally-acquired prions from the intestinal lumen.

5.2.2 Effect of *H. polygyrus* infection on M cells

M cells are antigen sampling epithelial cells in the epithelium that overlies GALT. These cells also play an essential role in the initial uptake of prions from the gut lumen [135, 369, 416]. B cells may play an important role in M cell differentiation as in their absence, specifically a $CD11c^+$ population, there is a reduction of M cells [425][426]. Subepithelial dome stromal cells express RANKL which is essential for M cell differentiation [130, 427, 428]. Also, the transcription factor Spi-B is expressed on M cell differentiation [429]; although other pathways may also be involved in M cell differentiation as Spi-B may not be sufficient to induce differentiation [430, 431]. Bacteria like *Streptococcus pneumoniae* in rabbits or *S. typhimurium* in mice can activate M cell differentiation [346, 432, 433]. In the case of *Salmonella*, the increased density of M cells in the FAE is associated with SopB protein which induces the FAE enterocyte transition by activating tWnt/B-catenin signal that leads to the activation of the RANKL and its receptor [434].

In this thesis, contrary to what would be expected in bacterial infections, the density of M cells was increased at a late time post infection with *H. polygyrus* on day 35. This late response may be attributed to *H. polygyrus* immunomodulatory effects through their excretory-secretory products. Although the effect of these on M cells have not been studied, it is known that other helminths such as *Schistosoma mansoni* can reduce the severity of collagen-induced arthritis by downregulation of IFNγ, and the upregulation of the Th2 response (IL4), as well as the anti-inflammatory cytokine (IL10) [435]. In this model, where *S. mansoni* was administered before the induction of arthritis, the gene expression of cytokines (IL-1, IL-6, IL-10, TNFα, and TGFβ), Foxp3 and RANKL were measured. The results showed a significant reduction of RANKL expression in *S. mansoni*/collagen-induced arthritis mice

[435]. Considering the role of RANKL in M cell differentiation it may be possible that *H. polygyrus* may also have a similarly immunomodulatory effect, which suppress M cell hyperplasia. Furthermore, it had also been shown that *H. polygyrus* also had immunomodulatory effects in arthritis models, although RANKL levels were not measured [436].

In contrast, the increased density of M cells may be attributed to the inflammation induced by *H. polygyrus* infection. It is known that inflammation is another factor known to increase M cell density [337, 437]. *H. polygyrus* infection causes goblet cells hyperplasia and crypt hypertrophy. These changes may affect cell differentiation. Studies suggest that all the intestinal epithelial cells have the same origin in the intestinal epithelial stem cells, located in the intestinal crypts [428]. Therefore, it is possible that when mice clear *H. polygyrus* infection and goblet cell density is reduced there is a reciprocal compensatory increase in M cell differentiation.

5.2.3 Effect of *H. polygyrus* infection on FDC

FDC are stromal cells derived from vascular mural cells [438], and located in the B cell follicles within secondary lymphoid organs (PP, MLN, spleen etc.) [438, 439] and tertiary lymphoid organs [440]. These can develop in non-lymphoid tissues under chronic inflammation in autoimmune diseases such as rheumatoid arthritis or chronic infections as hepatitis [420, 440, 441]. FDC are mutually dependent on B cells; while FDC provide CXCL13 to aggregate B cells expressing CXCR5 [442], B cells provide lymphotoxin and TNFα which promotes FDC maturation and maintenance [199, 200, 202, 443-445].

FDC capture and retain unprocessed antigens in the form of immune complexes [446]. In prion infection FDC act as prion accumulation and

replication sites [204, 447]. This is similar to the pathway of HIV dissemination [448]. FDC activation had also been shown to be influenced by commensal bacterial products in synergy with retinoic acid [449]. During *H. polygyrus* infection, data in this thesis suggested that FDC size was increased. It would be interesting to explore the possibility that these cells are proliferating or just expanding. The importance of this finding is that as FDC are sites of prion accumulation and replication, and their increased size or number during prion disease may provide additional sites of prion replication in lymphoid tissues.

During *H. polygyrus* infection, there are changes in the villi and disruption of the epithelium. Thus, antigens could enter through the damaged epithelium. However, there was no increase in prion replication in the PP. This suggests that if the prions enter through the disrupted epithelium, prions were not taken to the FDC in the GALT. Likewise, mice that lack GALT but have M cells only in the villous epithelium do not accumulate prions in the MLN, suggesting this uptake through the villous epithelium does not deliver prions to FDC in the MLN [137]. It is also possible that prions do not enter through the damaged epithelium due to reduced exposure by the increased peristalsis and mucus production.

5.2.4 Effect of *H. polygyrus* on mononuclear phagocytes

In the intestine mononuclear phagocytes (DC and macrophages) are typically found in the lamina propria and in the PP [450]. They also maintain a close interaction with the MLN to maintain the homeostasis of the gut by regulating inflammation and controlling infections [450, 451]. Their positioning in the lamina propria enables them to sample antigens from the intestinal lumen which they subsequently carry to lymphocytes to induce an immune response [173, 179, 312, 366]. In prion pathogenesis, DC can also acquire prions [210, 452]. $CD11c^+$ cells transport prions to the FDC and in the absence of DC expressing CXCR5, which attract DC to the B cell follicles, prion disease susceptibility is reduced [205]. Furthermore, in the absence of $CD11c^+$ cells the early accumulation of prions in the GALT is blocked [180]. Macrophages have also been shown to have prion clearance properties [453, 454]. In this study, during *H. polygyrus* infection the distribution of these cells was significantly altered. While in the lamina propria $CD11c^+$ cells were reduced on day 8, there was an increased density of $CD11b^+$ cells on day 21 and in the PP, and $CD68^+$ cells were increased on day 14. Studies have reported that during *H. polygyrus* infection, $CD11c^+$ cells migrate from the intestine to the mesenteric lymph nodes [375, 455, 456]. Therefore, it could be possible that mice co-infected with prions on that day could have an increased uptake due the damage of the epithelium; however, their transport to lymphoid organs may be limited by the reduced $CD11c^+$ cells available. The increased detection of $CD11b^+$ and $CD68^+$ cells was later, on days 14 and 21. It has been described that *H. polygyrus* can activate macrophages by alternative and classical pathways from day 7 in colon; and their antimicrobial activity against *Citrobacter rodentium* was reduced in a co-infected model [401]. Also, the increased number of macrophages had been associated with the presence of granulomas [401].

Therefore, although it is known that *H. polygyrus* can activate macrophages in its host, their function may also be limited. This effect may be reflected in increased prion pathology as macrophages may not be able to degrade prions at early times. However, most of the studies on *H. polygyrus* do not study the chronic infection and there is limited information regarding later time points. Also, it is possible that the increased number of macrophages in the lamina propria may have limited prion uptake from the disrupted epithelium when prion co-infection occurred on day 14 post *H. polygyrus,* and that could explain why no significant effects were detected. Within the PP, the increase detection of $CD68^+$ cells may correspond to tingible body macrophages. They clear the apoptotic B cells in the germinal centres, but prions have been identified within them [139]. As they can degrade prions [400], they may have stopped prion dissemination to other lymphoid organs.

5.2.5 Does prion infection alter *H. polygyrus* pathogenesis?

Interestingly, prion infection appeared to influence *H. polygyrus* egg burden. Although the main objective of this study was to determine the effect of *H. polygyrus* on prion disease, different trends in the egg burden of each group were noted. These results suggest that there may be an influence of the prion infection over *H. polygyrus* infection which may need further studies as these have not been reported before.

Although the cause of this effect is unknown, it may be possible that prions may affect *H. polygyrus* viability on their larval stage, the host immune response to *H. polygyrus* or the worm fecundity. It is important to consider that egg burden may be influenced by the worm burden, the worm fertility (e.g. sex-ratio of adult parasites or mating success), and the relation of food intake-

faecal egestion (food deprivation increases eggs/g of faeces output) [385]. In the groups of mice that were co-infected with prions on the same day or one day after *H. polygyrus*, there was a shorter time of egg production (4weeks); while in the mice co-infected with prions on day 1 after *H. polygyrus,* a marked reduction in the egg production was detected. At this time, it is possible that the worms and the prions get in contact with each other. It is known that worms also have a nervous system; and possibly this interaction may have affected the larva in some way that is reflected on the adult stage of the worms. Although evidence show the opposite as no PrP^{Sc} was detected by ELISA in adult worms (*H. contortus, T. circumcincta, Chabertia ovina, Cooperia curticei,* and *Oesophagostomum venulosum)* collected from necropsied ewes with clinical scrapie; neither *H. polygyrus* larvae hatched from eggs from prion infected mice transmit prion disease [457]; evidence suggest that some insect larvae (*Sacrophaga canaria*; fly larvae) can accumulate PrP^{Sc} and transmit prion disease. Whether prions can affect *H. polygyrus* larval viability or egg production remains to be determined. Despite that all the groups in this study underwent the same procedure, they were under different stage of *H. polygyrus* when caged individually in a bedding-less environment for prion infection. This stress may have also impacted the result by modifying the host immune response, causing a faster clearance, affect worm viability and egg production. It may also be possible that the adult worm burden is modified in some other pathway by the effect of prions in the nervous system. Thus, considering that *H. polygyrus* acts on the enteric neurons to activate NMU neuropeptide, [383], prion infection of these may have altered the immune response.

5.2.6 Limited detection of PrP^{Sc} in MLN in *H. polygyrus*-prion co-infection

At 15 weeks after prion infection the incidence of PrP^{Sc+} FDC in the MLN of mice co-infected with *H. polygyrus* and prions was lower when compared with those infected with prions alone. During *H. polygyrus* infection, the migration of $CD11c^+$ cells to the MLN is reduced [458]. While most of this is likely from the lamina propria, it is known that DC are able to carry live enteric bacteria like *Enterobacter cloacae* within them from the PP to the MLN [324]. $CD11c^+$ cells had also been shown to be essential for an appropriate infection and prion pathogenesis from the intestine lumen to the lymphoid organs [180, 376]; therefore, if their migration is impaired so may be prion translocation. As accumulation of prions in the secondary lymphoid organs is necessary for efficient prion disease development [125, 193, 348], if this is impeded, normal prion disease pathogeny will likely do too. However, as presented in this thesis, the lack of dissemination to the MLN did not affect the onset of prion disease or any other parameter of pathogenesis. Consistent with previous data [125], this suggests that the MLN are not essential sites of prion replication or accumulation and its necessity for prion disease pathogenesis may be limited after oral exposure. A similar conclusion was derived in a separate study using mice with a CXCR5 deficiency restricted to $CD11c^+$ cells in which the susceptibility to prion disease was reduced, but the early accumulation of prions in MLN was not impaired [205].

Similarly, B cells had been implicated in the transport of prions from the FDC in the germinal centres of draining lymph nodes to non-draining lymphoid organs. This was demonstrated in mice treated with modulator or B cell restricted sphingosine 1-phosphate receptor (S1PR), which result in blocked prion dissemination [315]. S1PR control the egress of B and T cells from the

secondary lymphoid organs, and when blocked retain the lymphocytes within the lymphoid organ [459]. In chapter 3 of this thesis it was shown that during *H. polygyrus* infection, the number of ILF (B cell follicles) was almost ablated in the duodenum and colon. This suggests that B cell migration to the gut may be reduced during *H. polygyrus* infection leading to reduced dissemination to the MLN by B cells.

5.2.7 Effect of *H. polygyrus*-prion co-infection on the terminal stage of prion disease

As expected, only mice with clinical signs of prion disease at the time of cull had any pathological signs of prion disease in their tissues. The clinical positive mice from the co-infected groups did not show significant statistical differences in the incubation period or the survival time when compared to the group given prions alone. However, when mice were co-infected with prions on day 8 after *H. polygyrus* infection the duration of the clinical disease was longer. This could be due to the increased number of mononuclear phagocytes and the reduction of $CD11c^{+}$ cells on this day. This may have limited the amount of prion particles that are taken to the FDC [211] and by limiting the number of infective particles, then less prions may get to the nerves. Although they developed the disease, this reduction may explain why it took longer to reach the terminal stage. Another potential factor to consider is intestinal peristalsis. This is considered to be increased during *H. polygyrus* infection [269], therefore, the intestinal contents are cleared in shorter time. If the intestinal contents including the prions flow faster, then the exposure time for prions to be uptaken may be reduced and they will be evacuated. Other considerations may be that the nerve-gut communication control prion neuroinvasion route. The expression of NMU which is a regulatory

neuropeptide of inflammation, tissue repair and worm expulsion [383], is expressed by the mucosal neurons during *H. polygyrus* infection [382]. Therefore, when mice are co-infected with *H. polygyrus* and prions on the same day, the transport of prions to the brain or through it may have been be altered. There are also numerous connections between the gut and brain. An example of this are the changes in cognition and behaviour attributed to the changes in microbiota induced by helminth infection [460]. However, even though *H. polygyrus* can modify gut microbiota composition [461], the microbiota on prion disease may have a little or no impact on prion pathogenesis [462, 463].

The survival times in this study can be compared with a similar study designed to determine whether a nematode infection could modify the scrapie incubation time. This was a similar study that used C57BL mice and co-infected them with *H. polygyrus.* It differentiates from this thesis because in most groups, mice were first infected with scrapie (orally with 100 µl of a 2% or intraperitoneally with 100 µl of a 1% suspension of scrapie (C506-M3)-infected mouse brain (corresponding to 10^5 ID_{50})) on day 0. Mice that were orally infected with prions received 200 L3 larvae of *H. polygyrus* infection either on day -7, +60 or +150 or repeatedly infected at those times [457]. The results were that mice inoculated with scrapie by oral route had a significantly longer survival times (313 days; except for group +150 (307 days)) in all parasitized groups compared to the unparasitized control group (301 days) [457]. However, parasite infection did not significantly change the survival time (244 days) in animals inoculated with scrapie by the intraperitoneal route in comparison with its control (339 days) [457]. These is similar to the findings in this thesis where the survival time (Figure 4.9) was 394 ±14 days for the scrapie alone group and 455 ±32 days for mice infected with prions at day 8 post *H. polygyrus* infection. Nevertheless, this parameter

was not statistically significant. This may be explained by the wide standard deviation which result from a small sample number. While here only 8 mice were used, the other study used 14. Also, these studies used a different prion strain. Despite that the results in this thesis do not have statistical significance, the results suggest a similar trend of longer survival time when co-infected with prions on day 8 post *H. polygyrus* infection.

5.2.8 Prions do not accumulate or replicate in granulomas formed during *H. polygyrus* infection.

Contrary to expectation, no PrP^{Sc} was detected in the granulomas induced by *H. polygyrus* infection. It has been suggested that prions can accumulate and replicate in chronic inflamed tissues in granulomas, even in the absence of FDC [234]. This result was not reproducible in this study. However, important differences between these studies such as the origin of the granulomas, their site of induction and experimental design may help explain the differing results observed. In this study, granulomas were formed as a natural host response to a parasitic infection. In the other study, the granulomas were induced through the administration of complete Freud's adjuvant (CFA) or Zymosan resuspended in paraffin oil (Z/PFO) [234]. The origin of the granulomas is reflected in their structure [305]. Granulomas formed by CFA inoculation alone have minimal interstitial changes in comparison with the ones generated using CFA and bacillus Calmette-Guérin [464]. Although all granulomas independently of their origin share similar characteristic features, such as mononuclear macrophage compact collection, epithelioid cells, and with ageing fibroblast capsule [465], data in this thesis imply that the location of the granulomas may also have a particular influence in their histopathological composition. In this study the formation of granulomas took

place in a soft tissue. Other studies in different soft tissue (mammary gland) also did not report any prion replication in granulomas [389]. These contrast with the apparent ability of granulomas in the skin to accumulate prions [234]. However, the skin may itself be a site of prion accumulation [466]. Finally, the experimental design may also be a key difference. While in this thesis the prion infection was established before, after and during the formation of granulomas, in the Heikenwalder [417] study the prions were administered in granulomas induced 50 days before and boosted at 25 days.

5.2.9 Helminth effects on other prion diseases and hosts

Findings in this thesis show that helminth infection has a limited statistical effect on prion disease susceptibility. Like *H. polygyrus*, there are many other helminths that may have a similar effect in hosts like human, sheep or deer. For example, it may be possible to think that helminths that affect deer, cattle and sheep such as *H. contortus, Teladorsagia circumcincta* which affects the abomasum; *Nematodirus* spp. that affect the small intestine; *Trichuris* spp. which affect the caecum and large intestine; *Capillaria* spp. which is a migratory parasite that affect the lung and the intestine; or *Chabertia* spp. which affect all the intestinal tract [467], may behave similarly to *H. polygyrus* in a prion co-infection. However, helminths have evolved with their host and adaptation strategies vary between host and helminth species. For example, parasites such as *Ancylostoma duodenale* (human parasite) and *Haemonchus contortus* (ruminant parasite) differ from *H. polygyrus* in the way they attach and feed. Others may induce chronic inflammation and the formation of tertiary lymphoid organs which may influence prion accumulation. These specific characteristics may explain why parasites such as *H. contortus* from

scrapie infected sheep can transmit scrapie into mouse *[468]*; or why sheep infected with *T. circumcincta* (abomasum parasite) developed scrapie symptoms at a younger age [469], but prion disease susceptibility was not affected in naturally infected scrapie sheep which received either monthly doses (20,000 infective larvae (L3)) or repeatedly doses (10,000 L3 at 6, 8 and 14 months old) of *T. circumcincta* [457]. Therefore, these differences between the pathogenesis of different helminths may limit the applicability of comparing the results in the thesis with natural infections.

5.3 Concluding remarks

Together, the data presented in this thesis shows that co-infection with *H. polygyrus* has only limited effect on oral prion disease susceptibility and disease duration. However, this complex model (*H. polygyrus*-prion co-infection) did reveal some interesting insights of the interactions between these pathogens in the intestine such as limited prion accumulation on MLN or the longer duration of the clinical phase of prion disease. Prion disease may also affect *H. polygyrus* egg burdens. Thus, although the early accumulation of prions in the GALT in the small intestine is essential for efficient neuroinavsion after oral exposure, data in this thesis show that the pathology caused in the small intestine by infection with a helminth such *H. polygyrus* does not affect prion disease susceptibility.

References

1. Prusiner, S.B., *Prions.* Proc. Natl. Acad. Sci. USA, 1998. **95**: p. 13363-13383.
2. Zabel, M.D. and C. Reid, *A brief history of prions.* Pathog Dis, 2015. **73**(9): p. ftv087.
3. Gajdusek, D.C., *Slow-virus infections of the nervous system.* N Engl J Med, 1967. **276**(7): p. 392-400.
4. Hunter, G.D. and G.C. Millson, *Studies on the heat stability and chromatographic behaviour of the scrapie agent.* J Gen Microbiol, 1964. **37**: p. 251-8.
5. Pattison, I.H., *Resistance of the scrapie agent to formalin.* J Comp Pathol, 1965. **75**: p. 159-64.
6. Prusiner, S.B., *Novel proteinaceous infectious particles cause scrapie.* Science, 1982. **216**(4542): p. 136-44.
7. Alper, T., D.A. Haig, and M.C. Clarke, *The exceptionally small size of the scrapie agent.* Biochem Biophys Res Commun, 1966. **22**(3): p. 278-84.
8. Alper, T., et al., *Does the agent of scrapie replicate without nucleic acid?* Nature, 1967. **214**(5090): p. 764-6.
9. Pattison, I.H. and K.M. Jones, *The possible nature of the transmissible agent of scrapie.* Vet Rec, 1967. **80**(1): p. 2-9.
10. Griffith, J.S., *Self-replication and scrapie.* Nature, 1967. **215**(5105): p. 1043-4.
11. Prusiner, S.B., et al., *Partial purification and evidence for multiple molecular forms of the scrapie agent.* Biochemistry, 1978. **17**(23): p. 4993-9.
12. Hunter, G.D., et al., *Further studies of the infectivity and stability of extracts and homogenates derived from scrapie affected mouse brains.* J Comp Pathol, 1969. **79**(1): p. 101-8.
13. Chesebro, B., et al., *Identification of scrapie prion protein-specific mRNA in scrapie-infected and uninfected brain.* Nature, 1985. **315**(6017): p. 331-3.
14. Locht, C., et al., *Molecular cloning and complete sequence of prion protein cDNA from mouse brain infected with the scrapie agent.* Proc Natl Acad Sci U S A, 1986. **83**(17): p. 6372-6.
15. Bueler, H., et al., *Mice devoid of PrP are resistant to scrapie.* Cell, 1993. **73**(7): p. 1339-47.
16. Schneider, K., et al., *The early history of the transmissible spongiform encephalopathies exemplified by scrapie.* Brain Res Bull, 2008. **77**(6): p. 343-55.
17. Crowder, L.A., et al., *Creutzfeldt-Jakob disease lookback study: 21 years of surveillance for transfusion transmission risk.* Transfusion, 2017. **57**(8): p. 1875-1878.
18. Imran, M. and S. Mahmood, *An overview of human prion diseases.* Virol J, 2011. **8**: p. 559.
19. Shi, Q., et al., *The Features of Genetic Prion Diseases Based on Chinese Surveillance Program.* PLoS One, 2015. **10**(10): p. e0139552.
20. Mastrianni, J.A., *The genetics of prion diseases.* Genet Med, 2010. **12**(4): p. 187-95.
21. Bonda, D.J., et al., *Human prion diseases: surgical lessons learned from iatrogenic prion transmission.* Neurosurg Focus, 2016. **41**(1): p. E10.
22. Collinge, J., *Variant Creutzfeldt-Jakob disease.* Lancet, 1999. **354**(9175): p. 317-23.
23. Collinge, J., et al., *Molecular analysis of prion strain variation and the aetiology of 'new variant' CJD.* Nature, 1996. **383**(6602): p. 685-90.
24. Liberski, P.P., *Gerstmann-Straussler-Scheinker disease.* Adv Exp Med Biol, 2012. **724**: p. 128-37.

25. Gajdusek, D.C. and V. Zigas, *Degenerative disease of the central nervous system in New Guinea; the endemic occurrence of kuru in the native population.* N Engl J Med, 1957. **257**(20): p. 974-8.
26. Mead, S., et al., *A novel prion disease associated with diarrhea and autonomic neuropathy.* N Engl J Med, 2013. **369**(20): p. 1904-14.
27. Montagna, P., et al., *Familial and sporadic fatal insomnia.* Lancet Neurol, 2003. **2**(3): p. 167-76.
28. Lugaresi, E., et al., *Fatal familial insomnia and dysautonomia with selective degeneration of thalamic nuclei.* N Engl J Med, 1986. **315**(16): p. 997-1003.
29. Sigurdson, C.J. and A. Aguzzi, *Chronic wasting disease.* Biochim Biophys Acta, 2007. **1772**(6): p. 610-618.
30. Mathiason, C.K., et al., *Susceptibility of domestic cats to chronic wasting disease.* J Virol, 2013. **87**(4): p. 1947-56.
31. Singh, N., et al., *Redox control of prion and disease pathogenesis.* Antioxidants & redox signaling, 2010. **12**(11): p. 1271-94.
32. Mead, S., et al., *Balancing selection at the prion protein gene consistent with prehistoric kurulike epidemics.* Science, 2003. **300**(5619): p. 640-3.
33. Chen, C. and X.P. Dong, *Epidemiological characteristics of human prion diseases.* Infect Dis Poverty, 2016. **5**(1): p. 47.
34. Gill, O.N., et al., *Prevalent abnormal prion protein in human appendixes after bovine spongiform encephalopathy epizootic: large scale survey.* BMJ (Clinical research ed.), 2013. **347**: p. f5675.
35. Garske, T. and A.C. Ghani, *Uncertainty in the tail of the variant Creutzfeldt-Jakob disease epidemic in the UK.* PLoS One, 2010. **5**(12): p. e15626.
36. Bruce, M.E., et al., *Transmissions to mice indicate that 'new variant' CJD is caused by the BSE agent.* Nature, 1997. **389**(6650): p. 498-501.
37. Hunter, N., et al., *Transmission of prion diseases by blood transfusion.* J Gen Virol, 2002. **83**(Pt 11): p. 2897-905.
38. Greenlee, J.J. and M.H. Greenlee, *The transmissible spongiform encephalopathies of livestock.* ILAR journal / National Research Council, Institute of Laboratory Animal Resources, 2015. **56**(1): p. 7-25.
39. Krasnianski, A., et al., *Clinical findings and diagnosis in genetic prion diseases in Germany.* Eur J Epidemiol, 2016. **31**(2): p. 187-96.
40. Geschwind, M.D., *Prion Diseases.* Continuum (Minneap Minn), 2015. **21**(6 Neuroinfectious Disease): p. 1612-38.
41. Bae, S.E., et al., *Correlation analysis for the incubation period of prion disease.* Prion, 2012. **6**(3): p. 276-81.
42. Krasnianski, A., et al., *Clinical findings and diagnostic tests in Creutzfeldt-Jakob disease and variant Creutzfeldt-Jakob disease.* Folia Neuropathol, 2004. **42 Suppl B**: p. 24-38.
43. Collinge, J., *Molecular neurology of prion disease.* Journal of neurology, neurosurgery, and psychiatry, 2005. **76**(7): p. 906-19.
44. Manson, J., et al., *The prion protein gene: a role in mouse embryogenesis?* Development, 1992. **115**(1): p. 117-22.
45. Hornemann, S., et al., *Recombinant full-length murine prion protein, mPrP(23-231): purification and spectroscopic characterization.* FEBS Lett, 1997. **413**(2): p. 277-81.
46. Stahl, N., et al., *Scrapie prion protein contains a phosphatidylinositol glycolipid.* Cell, 1987. **51**(2): p. 229-40.
47. Riek, R., et al., *NMR structure of the mouse prion protein domain PrP(121-231).* Nature, 1996. **382**(6587): p. 180-2.

48. Aguzzi, A. and M. Heikenwalder, *Pathogenesis of prion diseases: current status and future outlook.* Nature Reviews Microbiology, 2006. **4**: p. 765-775.
49. Riek, R., et al., *NMR characterization of the full-length recombinant murine prion protein, mPrP(23-231).* FEBS letters, 1997. **413**(2): p. 282-8.
50. Gossert, A.D., et al., *Prion protein NMR structures of elk and of mouse/elk hybrids.* Proc Natl Acad Sci U S A, 2005. **102**(3): p. 646-50.
51. Brockes, J.P., *Topics in prion cell biology.* Curr Opin Neurobiol, 1999. **9**(5): p. 571-7.
52. Strumbo, B., et al., *Molecular cloning of the cDNA coding for Xenopus laevis prion protein.* FEBS Lett, 2001. **508**(2): p. 170-4.
53. Simonic, T., et al., *cDNA cloning of turtle prion protein.* FEBS Lett, 2000. **469**(1): p. 33-8.
54. Collinge, J., et al., *Prion protein is necessary for normal synaptic function.* Nature, 1994. **370**(6487): p. 295-7.
55. Carleton, A., et al., *Dose-dependent, prion protein (PrP)-mediated facilitation of excitatory synaptic transmission in the mouse hippocampus.* Pflugers Arch, 2001. **442**(2): p. 223-9.
56. Criado, J.R., et al., *Mice devoid of prion protein have cognitive deficits that are rescued by reconstitution of PrP in neurons.* Neurobiol Dis, 2005. **19**(1-2): p. 255-65.
57. Coitinho, A.S., et al., *Cellular prion protein ablation impairs behavior as a function of age.* Neuroreport, 2003. **14**(10): p. 1375-9.
58. Herms, J.W., et al., *Altered intracellular calcium homeostasis in cerebellar granule cells of prion protein-deficient mice.* J Neurochem, 2000. **75**(4): p. 1487-92.
59. Fuhrmann, M., et al., *Loss of the cellular prion protein affects the Ca2+ homeostasis in hippocampal CA1 neurons.* J Neurochem, 2006. **98**(6): p. 1876-85.
60. Tobler, I., et al., *Altered circadian activity rhythms and sleep in mice devoid of prion protein.* Nature, 1996. **380**(6575): p. 639-42.
61. Weise, J., et al., *Deletion of cellular prion protein results in reduced Akt activation, enhanced postischemic caspase-3 activation, and exacerbation of ischemic brain injury.* Stroke, 2006. **37**(5): p. 1296-300.
62. Doeppner, T.R., et al., *Cellular prion protein promotes post-ischemic neuronal survival, angioneurogenesis and enhances neural progenitor cell homing via proteasome inhibition.* Cell Death Dis, 2015. **6**: p. e2024.
63. Bremer, J., et al., *Axonal prion protein is required for peripheral myelin maintenance.* Nat Neurosci, 2010. **13**(3): p. 310-8.
64. Ford, M.J., et al., *Selective expression of prion protein in peripheral tissues of the adult mouse.* Neuroscience, 2002. **113**(1): p. 177-92.
65. McBride, P.A., et al., *PrP protein is associated with follicular dendritic cells of spleens and lymph nodes in uninfected and scrapie-infected mice.* J Pathol, 1992. **168**(4): p. 413-8.
66. Burthem, J., et al., *The normal cellular prion protein is strongly expressed by myeloid dendritic cells.* Blood, 2001. **98**(13): p. 3733-8.
67. Marcos, Z., et al., *Comparative study of PrPc expression in rat, monkey, and cow gastrointestinal tract.* Ann N Y Acad Sci, 2005. **1040**: p. 391-4.
68. Austbo, L., et al., *Lymphoid follicles of the ileal Peyer's patch of lambs express low levels of PrP, as demonstrated by quantitative real-time RT-PCR on microdissected tissue compartments, in situ hybridization and immunohistochemistry.* J Gen Virol, 2006. **87**(Pt 11): p. 3463-71.
69. Morel, E., et al., *The cellular prion protein PrPc is expressed in human enterocytes in cell-cell junctional domains.* J Biol Chem, 2004. **279**(2): p. 1499-505.

70. Petit, C.S., et al., *Requirement of cellular prion protein for intestinal barrier function and mislocalization in patients with inflammatory bowel disease.* Gastroenterology, 2012. **143**(1): p. 122-32.e15.
71. Petit, C.S., et al., *Roles of the cellular prion protein in the regulation of cell-cell junctions and barrier function.* Tissue Barriers, 2013. **1**(2): p. e24377.
72. Li, R., et al., *The expression and potential function of cellular prion protein in human lymphocytes.* Cell Immunol, 2001. **207**(1): p. 49-58.
73. Dodelet, V.C. and N.R. Cashman, *Prion protein expression in human leukocyte differentiation.* Blood, 1998. **91**(5): p. 1556-61.
74. Durig, J., et al., *Differential constitutive and activation-dependent expression of prion protein in human peripheral blood leucocytes.* Br J Haematol, 2000. **108**(3): p. 488-95.
75. Ballerini, C., et al., *Functional implication of cellular prion protein in antigen-driven interactions between T cells and dendritic cells.* J Immunol, 2006. **176**(12): p. 7254-62.
76. Aguzzi, A., C. Sigurdson, and M. Heikenwaelder, *Molecular mechanisms of prion pathogenesis.* Annual review of pathology, 2008. **3**: p. 11-40.
77. Aguzzi, A. and M. Polymenidou, *Mammalian prion biology: one century of evolving concepts.* Cell, 2004. **116**(2): p. 313-27.
78. Cohen, F.E., et al., *Structural clues to prion replication.* Science, 1994. **264**(5158): p. 530-1.
79. Tanaka, M., et al., *Conformational variations in an infectious protein determine prion strain differences.* Nature, 2004. **428**(6980): p. 323-8.
80. Morales, R., K. Abid, and C. Soto, *The prion strain phenomenon: molecular basis and unprecedented features.* Biochim Biophys Acta, 2007. **1772**(6): p. 681-91.
81. Fraser, H. and A.G. Dickinson, *Scrapie in mice. Agent-strain differences in the distribution and intensity of grey matter vacuolation.* Journal of comparative pathology, 1973. **83**(1): p. 29-40.
82. Bruce, M.E., et al., *PrP in pathology and pathogenesis in scrapie-infected mice.* Mol Neurobiol, 1994. **8**(2-3): p. 105-12.
83. Safar, J., et al., *Molecular mass, biochemical composition, and physicochemical behavior of the infectious form of the scrapie precursor protein monomer.* Proc Natl Acad Sci U S A, 1990. **87**(16): p. 6373-7.
84. Kascsak, R.J., et al., *Biochemical differences among scrapie-associated fibrils support the biological diversity of scrapie agents.* J Gen Virol, 1985. **66 (Pt 8)**: p. 1715-22.
85. Bessen, R.A. and R.F. Marsh, *Biochemical and physical properties of the prion protein from two strains of the transmissible mink encephalopathy agent.* J Virol, 1992. **66**(4): p. 2096-101.
86. Gonzalez, L., et al., *Variability in disease phenotypes within a single PRNP genotype suggests the existence of multiple natural sheep scrapie strains within Europe.* J Gen Virol, 2010. **91**(Pt 10): p. 2630-41.
87. Gonzalez, L., et al., *Effects of agent strain and host genotype on PrP accumulation in the brain of sheep naturally and experimentally affected with scrapie.* J Comp Pathol, 2002. **126**(1): p. 17-29.
88. Sakudo, A. and T. Onodera, *Prion protein (PrP) gene-knockout cell lines: insight into functions of the PrP.* Front Cell Dev Biol, 2014. **2**: p. 75.
89. Makrinou, E., J. Collinge, and M. Antoniou, *Genomic characterization of the human prion protein (PrP) gene locus.* Mamm Genome, 2002. **13**(12): p. 696-703.
90. Kretzschmar, H.A., et al., *Molecular cloning of a human prion protein cDNA.* Dna, 1986. **5**(4): p. 315-24.

91. Puckett, C., et al., *Genomic structure of the human prion protein gene.* Am J Hum Genet, 1991. **49**(2): p. 320-9.
92. Lee, I.Y., et al., *Complete genomic sequence and analysis of the prion protein gene region from three mammalian species.* Genome Res, 1998. **8**(10): p. 1022-37.
93. Gonzalez, L., et al., *Susceptibility to scrapie and disease phenotype in sheep: cross-PRNP genotype experimental transmissions with natural sources.* Vet Res, 2012. **43**: p. 55.
94. Fraser, H. and A.G. Dickinson, *The sequential development of the brain lesion of scrapie in three strains of mice.* J Comp Pathol, 1968. **78**(3): p. 301-11.
95. Langeveld, J.P., et al., *Prion Type-Dependent Deposition of PRNP Allelic Products in Heterozygous Sheep.* J Virol, 2015. **90**(2): p. 805-12.
96. Monari, L., et al., *Fatal familial insomnia and familial Creutzfeldt-Jakob disease: different prion proteins determined by a DNA polymorphism.* Proc Natl Acad Sci U S A, 1994. **91**(7): p. 2839-42.
97. Le Dur, A., et al., *A newly identified type of scrapie agent can naturally infect sheep with resistant PrP genotypes.* Proc Natl Acad Sci U S A, 2005. **102**(44): p. 16031-6.
98. Telling, G.C., *Transgenic mouse models and prion strains.* Top Curr Chem, 2011. **305**: p. 79-99.
99. Bruce, M.E., P.A. McBride, and C.F. Farquhar, *Precise targeting of the pathology of the sialoglycoprotein, PrP, and vacuolar degeneration in mouse scrapie.* Neurosci Lett, 1989. **102**(1): p. 1-6.
100. Dickinson, A.G. and V.M. Meikle, *Host-genotype and agent effects in scrapie incubation: change in allelic interaction with different strains of agent.* Mol Gen Genet, 1971. **112**(1): p. 73-9.
101. Bruce, M.E., *Scrapie strain variation and mutation.* Br Med Bull, 1993. **49**(4): p. 822-38.
102. Bruce, M.E., et al., *Strain characterization of natural sheep scrapie and comparison with BSE.* J Gen Virol, 2002. **83**(Pt 3): p. 695-704.
103. Asante, E.A., et al., *BSE prions propagate as either variant CJD-like or sporadic CJD-like prion strains in transgenic mice expressing human prion protein.* Embo j, 2002. **21**(23): p. 6358-66.
104. Wadsworth, J.D., et al., *Human prion protein with valine 129 prevents expression of variant CJD phenotype.* Science, 2004. **306**(5702): p. 1793-6.
105. Notari, S., et al., *Assessing prion infectivity of human urine in sporadic Creutzfeldt-Jakob disease.* Emerg Infect Dis, 2012. **18**(1): p. 21-8.
106. John, T.R., H.M. Schatzl, and S. Gilch, *Early detection of chronic wasting disease prions in urine of pre-symptomatic deer by real-time quaking-induced conversion assay.* Prion, 2013. **7**(3): p. 253-8.
107. Moda, F., et al., *Prions in the urine of patients with variant Creutzfeldt-Jakob disease.* N Engl J Med, 2014. **371**(6): p. 530-9.
108. Tamguney, G., et al., *Salivary prions in sheep and deer.* Prion, 2012. **6**(1): p. 52-61.
109. Seeger, H., et al., *Coincident scrapie infection and nephritis lead to urinary prion excretion.* Science, 2005. **310** p. 324-326.
110. Ligios, C., et al., *Sheep with scrapie and mastitis transmit infectious prions through the milk.* Journal of virology, 2011. **85**(2): p. 1136-9.
111. Konold, T., et al., *Evidence of effective scrapie transmission via colostrum and milk in sheep.* BMC veterinary research, 2013. **9**: p. 99.
112. Lacroux, C., et al., *Prions in milk from ewes incubating natural scrapie.* PLoS pathogens, 2008. **4**(12): p. e1000238.

113. Vascellari, M., et al., *PrPSc in salivary glands of scrapie-affected sheep.* Journal of virology, 2007. **81**(9): p. 4872-6.
114. Mathiason, C.K., et al., *Infectious prions in the saliva and blood of deer with chronic wasting disease.* Science, 2006. **314**(5796): p. 133-6.
115. Murayama, Y., et al., *Urinary excretion and blood level of prions in scrapie-infected hamsters.* J Gen Virol, 2007. **88**(Pt 10): p. 2890-8.
116. Safar, J.G., et al., *Transmission and detection of prions in feces.* J Infect Dis, 2008. **198**(1): p. 81-9.
117. Pattison, I.H., et al., *Spread of scrapie to sheep and goats by oral dosing with foetal membranes from scrapie-affected sheep.* Vet Rec, 1972. **90**(17): p. 465-8.
118. Castilla, J., et al., *Vertical tansmission of bovine spongiform encephalopathy prions evaluated in a transgenic mouse model.* Journal of virology, 2005. **79**(13): p. 8665-8668.
119. Urwin, P.J., et al., *Creutzfeldt-Jakob disease and blood transfusion: updated results of the UK Transfusion Medicine Epidemiology Review Study.* Vox Sang, 2016. **110**(4): p. 310-6.
120. Bougard, D., et al., *Detection of prions in the plasma of presymptomatic and symptomatic patients with variant Creutzfeldt-Jakob disease.* Sci Transl Med, 2016. **8**(370): p. 370ra182.
121. Concha-Marambio, L., et al., *Detection of prions in blood from patients with variant Creutzfeldt-Jakob disease.* Sci Transl Med, 2016. **8**(370): p. 370ra183.
122. Maddox, R.A., et al., *Creutzfeldt-Jakob disease in recipients of corneal transplants.* Cornea, 2008. **27**(7): p. 851-4.
123. Thomas, J.G., C.E. Chenoweth, and S.E. Sullivan, *Iatrogenic Creutzfeldt-Jakob disease via surgical instruments.* J Clin Neurosci, 2013. **20**(9): p. 1207-12.
124. Donaldson, D., K. Else, and N. Mabbott, *The gut-associated lymphoid tissues in small intestine, not the large intestine, play a critical role in oral prion disease pathogenesis.* Immunology, 2014. **143**: p. 37-37.
125. Glaysher, B.R. and N.A. Mabbott, *Role of the GALT in scrapie agent neuroinvasion from the intestine.* The Journal of Immunology, 2007. **178** p. 3757-3766.
126. Mabbott, N.A. and G.G. MacPherson, *Prions and their lethal journey to the brain.* Nature Reviews Microbiology, 2006. **4** p. 201-211
127. Knoop, K.A., et al., *Distinct developmental requirements for isolated lymphoid follicle formation in the small and large intestine: RANKL is essential only in the small intestine.* Am J Pathol, 2011. **179**(4): p. 1861-71.
128. Allan, C.H. and J.S. Trier, *Structure and permeability differ in subepithelial villus and Peyer's patch follicle capillaries.* Gastroenterology, 1991. **100**(5 Pt 1): p. 1172-9.
129. Mabbott, N.A., et al., *Microfold (M) cells: important immunosurveillance posts in the intestinal epithelium.* Nature Mucosal Immunology, 2013. **6**(4): p. 666-677.
130. Taylor, R.T., et al., *Lymphotoxin-independent expression of TNF-related activation-induced cytokine by stromal cells in cryptopatches, isolated lymphoid follicles, and Peyer's patches.* J Immunol, 2007. **178**(9): p. 5659-67.
131. Katakai, T., et al., *Organizer-like reticular stromal cell layer common to adult secondary lymphoid organs.* J Immunol, 2008. **181**(9): p. 6189-200.
132. Wolf, J.L., et al., *Intestinal M cells: a pathway for entry of reovirus into the host.* Science, 1981. **212**(4493): p. 471-2.
133. Takahashi, Y., et al., *Nonhuman primate intestinal villous M-like cells: an effective poliovirus entry site.* Biochemical and biophysical research communications, 2008. **368**(3): p. 501-7.

134. Ponnusamy, D., et al., *Mycobacterium avium subsp. paratuberculosis invades through M cells and enterocytes across ileal and jejunal mucosa of lambs.* Research in veterinary science, 2013. **94**(2): p. 306-12.
135. Donaldson, D.S., et al., *M cell-depletion blocks oral prion disease pathogenesis.* Nature Mucosal Imunology., 2012. **5**(2): p. 216-225.
136. S., W., et al., *Resistance of Chemokine Receptor 6-Deficient Mice to Yersinia Enterocolitica Infection : Evidence of Defective M-Cell Formation in Vivo.* Am J Pathol., 2008 **3** (172): p. 671-680.
137. Donaldson, D.S., et al., *Increased Abundance of M Cells in the Gut Epithelium Dramatically Enhances Oral Prion Disease Susceptibility.* PLoS Pathog, 2016. **12**(12): p. e1006075.
138. Mostov, K., T. Su, and M. ter Beest, *Polarized epithelial membrane traffic: conservation and plasticity.* Nat Cell Biol, 2003. **5**(4): p. 287-93.
139. Kujala, P., et al., *Prion uptake in the gut: identification of the first uptake and replication sites.* PLoS Pathogens, 2011. **7**(12): p. e1002449.
140. Morel, E., et al., *Bovine prion is endocytosed by human enterocytes via the 37 kDa/67 kDa laminin receptor.* Am J Pathol, 2005. **167**(4): p. 1033-42.
141. Gutknecht, M.F. and A.H. Bouton, *Functional significance of mononuclear phagocyte populations generated through adult hematopoiesis.* J Leukoc Biol, 2014. **96**(6): p. 969-80.
142. Hume, D.A., *The mononuclear phagocyte system.* Curr Opin Immunol, 2006. **18**(1): p. 49-53.
143. Pollard, J.W., *Trophic macrophages in development and disease.* Nat Rev Immunol, 2009. **9**(4): p. 259-70.
144. Hume, D.A., et al., *The mononuclear phagocyte system revisited.* J Leukoc Biol, 2002. **72**(4): p. 621-7.
145. Epelman, S., K.J. Lavine, and G.J. Randolph, *Origin and functions of tissue macrophages.* Immunity, 2014. **41**(1): p. 21-35.
146. Ginhoux, F., et al., *Fate mapping analysis reveals that adult microglia derive from primitive macrophages.* Science, 2010. **330**(6005): p. 841-5.
147. Schulz, C., et al., *A lineage of myeloid cells independent of Myb and hematopoietic stem cells.* Science, 2012. **336**(6077): p. 86-90.
148. Yona, S., et al., *Fate mapping reveals origins and dynamics of monocytes and tissue macrophages under homeostasis.* Immunity, 2013. **38**(1): p. 79-91.
149. Epelman, S., et al., *Embryonic and adult-derived resident cardiac macrophages are maintained through distinct mechanisms at steady state and during inflammation.* Immunity, 2014. **40**(1): p. 91-104.
150. Da Silva, C., et al., *The Peyer's Patch Mononuclear Phagocyte System at Steady State and during Infection.* Front Immunol, 2017. **8**: p. 1254.
151. Schulz, O. and O. Pabst, *Antigen sampling in the small intestine.* Trends Immunol, 2013. **34**(4): p. 155-61.
152. Cerovic, V., et al., *Intestinal macrophages and dendritic cells: what's the difference?* Trends Immunol, 2014. **35**(6): p. 270-7.
153. Vremec, D. and K. Shortman, *Dendritic cell subtypes in mouse lymphoid organs: cross-correlation of surface markers, changes with incubation, and differences among thymus, spleen, and lymph nodes.* J Immunol, 1997. **159**(2): p. 565-73.
154. Guilliams, M., et al., *Dendritic cells, monocytes and macrophages: a unified nomenclature based on ontogeny.* Nat Rev Immunol, 2014. **14**(8): p. 571-8.
155. Sancho, D., et al., *Tumor therapy in mice via antigen targeting to a novel, DC-restricted C-type lectin.* J Clin Invest, 2008. **118**(6): p. 2098-110.

156. Huysamen, C., et al., *CLEC9A is a novel activation C-type lectin-like receptor expressed on BDCA3+ dendritic cells and a subset of monocytes.* J Biol Chem, 2008. **283**(24): p. 16693-701.
157. Caminschi, I., et al., *The dendritic cell subtype-restricted C-type lectin Clec9A is a target for vaccine enhancement.* Blood, 2008. **112**(8): p. 3264-73.
158. Dorner, B.G., et al., *Selective expression of the chemokine receptor XCR1 on cross-presenting dendritic cells determines cooperation with CD8+ T cells.* Immunity, 2009. **31**(5): p. 823-33.
159. Crozat, K., et al., *The XC chemokine receptor 1 is a conserved selective marker of mammalian cells homologous to mouse CD8alpha+ dendritic cells.* J Exp Med, 2010. **207**(6): p. 1283-92.
160. Bachem, A., et al., *Superior antigen cross-presentation and XCR1 expression define human CD11c+CD141+ cells as homologues of mouse CD8+ dendritic cells.* J Exp Med, 2010. **207**(6): p. 1273-81.
161. Gurka, S., et al., *Mouse Conventional Dendritic Cells Can be Universally Classified Based on the Mutually Exclusive Expression of XCR1 and SIRPalpha.* Front Immunol, 2015. **6**: p. 35.
162. Iwasaki, A. and B.L. Kelsall, *Localization of distinct Peyer's patch dendritic cell subsets and their recruitment by chemokines macrophage inflammatory protein (MIP)-3alpha, MIP-3beta, and secondary lymphoid organ chemokine.* J Exp Med, 2000. **191**(8): p. 1381-94.
163. Iwasaki, A. and B.L. Kelsall, *Unique functions of CD11b+, CD8 alpha+, and double-negative Peyer's patch dendritic cells.* J Immunol, 2001. **166**(8): p. 4884-90.
164. Bonnardel, J., et al., *Distribution, location, and transcriptional profile of Peyer's patch conventional DC subsets at steady state and under TLR7 ligand stimulation.* Mucosal Immunol, 2017. **10**(6): p. 1412-1430.
165. Anjuere, F., et al., *Definition of dendritic cell subpopulations present in the spleen, Peyer's patches, lymph nodes, and skin of the mouse.* Blood, 1999. **93**(2): p. 590-8.
166. Bonnardel, J., et al., *Innate and adaptive immune functions of peyer's patch monocyte-derived cells.* Cell Rep, 2015. **11**(5): p. 770-84.
167. Bonnardel, J., et al., *Gene expression profiling of the Peyer's patch mononuclear phagocyte system.* Genom Data, 2015. **5**: p. 21-4.
168. Lelouard, H., et al., *Pathogenic bacteria and dead cells are internalized by a unique subset of Peyer's patch dendritic cells that express lysozyme.* Gastroenterology, 2010. **138**(1): p. 173-84.e1-3.
169. Chistiakov, D.A., et al., *Myeloid dendritic cells: Development, functions, and role in atherosclerotic inflammation.* Immunobiology, 2015. **220**(6): p. 833-44.
170. Contractor, N., et al., *Cutting edge: Peyer's patch plasmacytoid dendritic cells (pDCs) produce low levels of type I interferons: possible role for IL-10, TGFbeta, and prostaglandin E2 in conditioning a unique mucosal pDC phenotype.* J Immunol, 2007. **179**(5): p. 2690-4.
171. Li, H.S., et al., *Cell-intrinsic role for IFN-alpha-STAT1 signals in regulating murine Peyer patch plasmacytoid dendritic cells and conditioning an inflammatory response.* Blood, 2011. **118**(14): p. 3879-89.
172. Bradford, B.M., et al., *Defining the anatomical localisation of subsets of the murine mononuclear phagocyte system using integrin alpha X (Itgax, CD11c) and colony stimulating factor 1 receptor (Csf1r, CD115) expression fails to discriminate dendritic cells from macrophages.* Immunobiology, 2011. **216**(11): p. 1228-37.

173. Lelouard, H., et al., *Peyer's patch dendritic cells sample antigens by extending dendrites through M cell-specific transcellular pores.* Gastroenterology, 2012. **142**(3): p. 592-601.e3.
174. Farache, J., *Luminal bacteria recruit CD103+ dendritic cells into the intestinal epithelium to sample bacterial antigens for presentation.* Immunity, 2013. **38**: p. 581-595.
175. Knoop, K.A., et al., *Microbial sensing by goblet cells controls immune surveillance of luminal antigens in the colon.* Mucosal Immunol, 2015. **8**(1): p. 198-210.
176. Jang, M.H., *Intestinal villous M cells: an antigen entry site in the mucosal epithelium.* Proc. Natl. Acad. Sci. USA, 2004. **101**: p. 6110-6115.
177. Cerovic, V., et al., *Lymph-borne CD8alpha+ dendritic cells are uniquely able to cross-prime CD8+ T cells with antigen acquired from intestinal epithelial cells.* Mucosal Immunol, 2015. **8**(1): p. 38-48.
178. Luhr, K.M., et al., *Processing and degradation of exogenous prion protein by CD11c(+) myeloid dendritic cells in vitro.* J Virol, 2002. **76**(23): p. 12259-64.
179. Wykes, M., et al., *Dendritic cells interact directly with naive B lymphocytes to transfer antigen and initiate class switching in a primary T-dependent response.* J Immunol, 1998. **161**(3): p. 1313-9.
180. Raymond, C.R., P. Aucouturier, and N.A. Mabbott, *In vivo deplation of CD11c+ cells impairs scrapie agent neuroinvasion from the intestine.* Journal of Immunology, 2007. **179**: p. 7758-7766.
181. Rivollier, A., et al., *Inflammation switches the differentiation program of Ly6Chi monocytes from antiinflammatory macrophages to inflammatory dendritic cells in the colon.* J Exp Med, 2012. **209**(1): p. 139-55.
182. Gross, M., T.M. Salame, and S. Jung, *Guardians of the Gut - Murine Intestinal Macrophages and Dendritic Cells.* Front Immunol, 2015. **6**: p. 254.
183. Muller, P.A., et al., *Crosstalk between muscularis macrophages and enteric neurons regulates gastrointestinal motility.* Cell, 2014. **158**(2): p. 300-313.
184. Veiga-Fernandes, H. and D. Mucida, *Neuro-Immune Interactions at Barrier Surfaces.* Cell, 2016. **165**(4): p. 801-11.
185. Beekes, M. and P.A. McBride, *Early accumulation of pathological PrP in the enteric nervous system and gut-associated lymphoid tissue of hamsters orally infected with scrapie.* Neurosci Lett, 2000. **278**(3): p. 181-4.
186. Sassa, Y., Y. Inoshima, and N. Ishiguro, *Bovine macrophage degradation of scrapie and BSE PrPSc.* Vet Immunol Immunopathol, 2010. **133**(1): p. 33-9.
187. Roozendaal, R., R.E. Mebius, and G. Kraal, *The conduit system of the lymph node.* Int Immunol, 2008. **20**(12): p. 1483-7.
188. Buettner, M., R. Pabst, and U. Bode, *Stromal cell heterogeneity in lymphoid organs.* Trends Immunol, 2010. **31**(2): p. 80-6.
189. Mebius, R.E. and G. Kraal, *Structure and function of the spleen.* Nat Rev Immunol, 2005. **5**(8): p. 606-16.
190. Mueller, S.N. and R.N. Germain, *Stromal cell contributions to the homeostasis and functionality of the immune system.* Nat Rev Immunol, 2009. **9**(9): p. 618-29.
191. Mabbott, N.A., *Prion pathogenesis and secondary lymphoid organs (SLO): Tracking the SLO spread of prions to the brain.* Prion, 2012. **6**(4): p. 322-333.
192. Imazeki, N., A. Senoo, and Y. Fuse, *Is the follicular dendritic cell a primarily stationary cell?* Immunology, 1992. **76**(3): p. 508-10.
193. Mabbott, N.A., et al., *Follicular dendritic cell dedifferentiation by treatment with an inhibitor of the lymphotoxin pathway dramatically reduces scrapie susceptibility.* Journal of virology, 2003. **77**(12): p. 6845-54.

194. Andreoletti, O., et al., *Early accumulation of PrP(Sc) in gut-associated lymphoid and nervous tissues of susceptible sheep from a Romanov flock with natural scrapie.* J Gen Virol, 2000. **81**(Pt 12): p. 3115-26.
195. Sigurdson, C.J., et al., *Oral transmission and early lymphoid tropism of chronic wasting disease PrPres in mule deer fawns (Odocoileus hemionus).* J Gen Virol, 1999. **80 (Pt 10)**: p. 2757-64.
196. Klein, M.A., et al., *Complement facilitates early prion pathogenesis.* Nat Med, 2001. **7**(4): p. 488-92.
197. Mabbott, N.A., et al., *Temporary depletion of complement component C3 or genetic deficiency of C1q significantly delays onset of scrapie.* Nat Med, 2001. **7**(4): p. 485-7.
198. Donaldson, D.S., K.J. Else, and N.A. Mabbott, *The gut-associated lymphoid tissues in the small intestine, not the large intestine, play a major role in oral prion disease pathogenesis.* J Virol, 2015.
199. Futterer, A., et al., *The lymphotoxin beta receptor controls organogenesis and affinity maturation in peripheral lymphoid tissues.* Immunity, 1998. **9**(1): p. 59-70.
200. Koni, P.A., et al., *Distinct roles in lymphoid organogenesis for lymphotoxins alpha and beta revealed in lymphotoxin beta-deficient mice.* Immunity, 1997. **6**(4): p. 491-500.
201. Korner, H., et al., *Distinct roles for lymphotoxin-alpha and tumor necrosis factor in organogenesis and spatial organization of lymphoid tissue.* Eur J Immunol, 1997. **27**(10): p. 2600-9.
202. De Togni, P., et al., *Abnormal development of peripheral lymphoid organs in mice deficient in lymphotoxin.* Science, 1994. **264**(5159): p. 703-7.
203. Rennert, P.D., et al., *Surface lymphotoxin alpha/beta complex is required for the development of peripheral lymphoid organs.* J Exp Med, 1996. **184**(5): p. 1999-2006.
204. Prinz, M., et al., *Lymph nodal prion replication and neuroinvasion in mice devoid of follicular dendritic cells.* Proc Natl Acad Sci U S A, 2002. **99**(2): p. 919-24.
205. Bradford, B.M., B. Reizis, and N.A. Mabbott, *Oral Prion Disease Pathogenesis Is Impeded in the Specific Absence of CXCR5-Expressing Dendritic Cells.* J Virol, 2017. **91**(10).
206. McBride, P.A., et al., *Early spread of scrapie from the gastrointestinal tract to the central nervous system involves autonomic fibers of the splanchnic and vagus nerves.* J Virol, 2001. **75**(19): p. 9320-7.
207. Glatzel, M., et al., *Sympathetic innervation of lymphoreticular organs is rate limiting for prion neuroinvasion.* Neuron, 2001. **31**(1): p. 25-34.
208. Kujala, P., et al., *Prion uptake in the gut: identification of the first uptake and replication sites.* PLoS Pathogens, 2011. **7**.
209. Prinz, M., et al., *Positioning of follicular dendritic cells within the spleen controls prion neuroinvasion.* Nature, 2003. **425**(6961): p. 957-62.
210. Aucouturier, P., et al., *Infected splenic dendritic cells are sufficient for prion transmission to the CNS in mouse scrapie.* J Clin Invest, 2001. **108**(5): p. 703-8.
211. Raymond, C.R. and N.A. Mabbott, *Assessing the involvement of migratory dendritic cells in the transfer of the scrapie agent from the immune to peripheral nervous systems.* J Neuroimmunol, 2007. **187**(1-2): p. 114-25.
212. Bowen, R.L. and C.S. Atwood, *Living and dying for sex. A theory of aging based on the modulation of cell cycle signaling by reproductive hormones.* Gerontology, 2004. **50**(5): p. 265-90.
213. Hedden, T. and J.D. Gabrieli, *Insights into the ageing mind: a view from cognitive neuroscience.* Nat Rev Neurosci, 2004. **5**(2): p. 87-96.
214. Peters, R., *Ageing and the brain.* Postgrad Med J, 2006. **82**(964): p. 84-8.

215. Kobayashi, A., et al., *The functional maturation of M cells is dramatically reduced in the Peyer's patches of aged mice.* Mucosal Immunology, 2013,. **6**(5): p. 1027-1037
216. St Rose, S.G., et al., *Comparative evidence for a link between Peyer's patch development and susceptibility to transmissible spongiform encephalopathies.* BMC Infect Dis, 2006. **6**: p. 5.
217. Szakal, A.K., et al., *Kinetics of germinal center development in lymph nodes of young and aging immune mice.* Anat Rec, 1990. **227**(4): p. 475-85.
218. Turner, V.M. and N.A. Mabbott, *Structural and functional changes to lymph nodes in ageing mice.* Immunology, 2017. **151**(2): p. 239-247.
219. Turner, V.M. and N.A. Mabbott, *Ageing adversely affects the migration and function of marginal zone B cells.* Immunology, 2017. **151**(3): p. 349-362.
220. Aw, D., et al., *Disorganization of the splenic microanatomy in ageing mice.* Immunology, 2016. **148**(1): p. 92-101.
221. Birjandi, S.Z., et al., *Alterations in marginal zone macrophages and marginal zone B cells in old mice.* J Immunol, 2011. **186**(6): p. 3441-51.
222. Brown, K.L., et al., *The effects of host age on the transport of complement-bound complexes to the spleen and the pathogenesis of intravenous scrapie infection.* J Virol, 2012. **86**(1): p. 25-35.
223. Mackay, G.A., R.S. Knight, and J.W. Ironside, *The molecular epidemiology of variant CJD.* Int J Mol Epidemiol Genet, 2011. **2**(3): p. 217-27.
224. Will, R.G., *Acquired prion disease: iatrogenic CJD, variant CJD, kuru.* Br Med Bull, 2003. **66**: p. 255-65.
225. Filaretova, L.P., et al., *A wider view on gastric erosion: detailed evaluation of complex somatic and behavioral changes in rats treated with indomethacin at gastric ulcerogenic dose.* Endocrine regulations, 2014. **48**(4): p. 163-72.
226. Walter, B.M., P. Born, and J. Winker, *Ascaris lumbricoides causing obscure gastrointestinal bleeding detected by double-balloon enteroscopy.* Endoscopy, 2015. **47**(1): p. E354-5.
227. Mohammadi, R., et al., *The relationship between intestinal parasites and some immune-mediated intestinal conditions.* Gastroenterology and hepatology from bed to bench, 2015. **8**(2): p. 123-31.
228. Ricciotti, E. and G.A. FitzGerald, *Prostaglandins and inflammation.* Arterioscler Thromb Vasc Biol, 2011. **31**(5): p. 986-1000.
229. Drini, M., *Peptic ulcer disease and non-steroidal anti-inflammatory drugs.* Aust Prescr, 2017. **40**(3): p. 91-93.
230. Brune, K. and P. Patrignani, *New insights into the use of currently available non-steroidal anti-inflammatory drugs.* J Pain Res, 2015. **8**: p. 105-18.
231. Russell, R.I., *Non-steroidal anti-inflammatory drugs and gastrointestinal damage-problems and solutions.* Postgrad Med J, 2001. **77**(904): p. 82-8.
232. Wyatt, J., et al., *Intestinal permeability and the prediction of relapse in Crohn's disease.* Lancet, 1993. **341**(8858): p. 1437-9.
233. Schulzke, J.D., et al., *Epithelial tight junctions in intestinal inflammation.* Ann N Y Acad Sci, 2009. **1165**: p. 294-300.
234. Heikenwalder, M., et al., *Lymphotoxin-dependant prion replication in inflamatory stromal cells of granulomas.* Immunity, 2008. **29**: p. 998-1008.
235. Heikenwalder, M., et al., *Chronic lymphocytic inflammation specifies the organ tropism of prions.* Science, 2005. **307**(5712): p. 1107-10.
236. Sipos, F. and G. Muzes, *Isolated lymphoid follicles in colon: switch points between inflammation and colorectal cancer?* World J Gastroenterol, 2011. **17**(13): p. 1666-73.

237. Buettner, M. and M. Lochner, *Development and Function of Secondary and Tertiary Lymphoid Organs in the Small Intestine and the Colon.* Front Immunol, 2016. **7**: p. 342.
238. Friedman-Levi, Y., et al., *Fatal neurological disease in scrapie-infected mice induced for experimental autoimmune encephalomyelitis.* J Virol, 2007. **81**(18): p. 9942-9.
239. Ehresmann, D.W. and R.N. Hogan, *Acceleration of scrapie disease in mice by an adenovirus.* Intervirology, 1986. **25**(2): p. 103-10.
240. Leblanc, P., et al., *Co-infection with the friend retrovirus and mouse scrapie does not alter prion disease pathogenesis in susceptible mice.* PLoS One, 2012. **7**(1): p. e30872.
241. Salazar, E., et al., *Detection of PrPSc in lung and mammary gland is favored by the presence of Visna/maedi virus lesions in naturally coinfected sheep.* Vet Res, 2010. **41**(5): p. 58.
242. Sigurdson, C.J., et al., *Bacterial colitis increases susceptibility to oral prion disease.* Journal of Infectious Diseases, 2009. **199**(2).
243. Behnke, J.M., D.M. Menge, and H. Noyes, *Heligmosomoides bakeri: a model for exploring the biology and genetics of resistance to chronic gastrointestinal nematode infections.* Parasitology, 2009. **136**: p. 1565-1580
244. Behnke, J.M., et al., *Genetic variation in resistance to repeated infections with Heligmosomoides polygyrus bakeri, in inbred mouse strains selected for the mouse genome project.* Parasite Immunology, 2006. **28**(3): p. 85-94.
245. Reynolds, L.A., K.J. Filbey, and R.M. Maizels, *Immunity to the model intestinal helminth parasite Heligmosomoides polygyrus.* Semin Immunopathol, 2012. **34**(6): p. 829-46.
246. Maizels, R.M., J.P. Hewitson, and K.A. Smith, *Susceptibility and immunity to helminth parasites.* Current opinion in immunology, 2012. **24**(4): p. 459-66.
247. Gouy de Bellocq, J., et al., *Phylogeny of the Trichostrongylina (Nematoda) inferred from 28S rDNA sequences.* Molecular phylogenetics and evolution, 2001. **19**(3): p. 430-42.
248. Telford, G., et al., *Heligmosomoides polygyrus immunomodulatory factor (IMF), tragets T lymphocytes.* Parasite Immunology, 1998. **20**: p. 601-611.
249. Bansemir, A.D. and M.V. Sukhdeo, *Villus length influences habitat selection by Heligmosomoides polygyrus.* Parasitology, 1996. **113**(3): p. 311-316.
250. Maizels, R.M., et al., *Immune modulation and modulators in Heligmosomoides polygyrus infection.* Experimental Parasitology, 2012. **132**: p. 72-89.
251. Cywinska, A., K. Czuminska, and A. Schollenberger, *Granulomatous inflammation during Heligmosomoides polygyrus primary infections in FVB mice.* J Helminthol, 2004. **78**(1): p. 17-24.
252. Bansemir, A.D. and M.V. Sukhdeo, *The food resource of adult Heligmosomoides polygyrus in the small intestine.* The Journal of parasitology, 1994. **80**(1): p. 24-8.
253. Anthony, R.M., et al., *Memory T(H)2 cells induce alternatively activated macrophages to mediate protection against nematode parasites.* Nature medicine, 2006. **12**(8): p. 955-60.
254. Rausch, S., et al., *Small intestinal nematode infection of mice is associated with increased enterobacterial loads alongside the intestinal tract.* PLoS One, 2013. **8**(9): p. e74026.
255. B., L., et al., *Regulation of T(H)2 development by CXCR5+ dendritic cells and lymphotoxin-expressing B cells.* Nature immunology, 2012. **13**(7): p. 681-90.

256. Filbey, K.J., et al., *Innate and adaptive type 2 immune cell responses in genetically controlled resistance to intestinal helminth infection.* Immunology and cell biology, 2014. **92**(5): p. 436-448.
257. Chaicumpa, V., et al., *Induction of immunity in mice to the nematode parasite, Nematospiroides dubius.* Aust J Exp Biol Med Sci, 1977. **55**(4): p. 393-400.
258. Prowse, S.J., et al., *The development of resistance in different inbred strains of mice to infection with Nematospiroides dubius.* Parasite Immunology, 1979. **1**(4): p. 277-288.
259. Sugawara, Y., et al., *Th2 immune responses and alternatively activated macrophages (AAMacs) in helminth infection in aged mice.* J Vet Med Sci. , 2011. **73**(4): p. 511-5116.
260. Hashimoto, K., et al., *Depleted intestinal goblet cells and severe pathological changes in SCID mice infected with Heligmosomoides polygyrus.* Parasite Immunol, 2009. **31**(8): p. 457-65.
261. Kim, Y.S. and S.B. Ho, *Intestinal goblet cells and mucins in health and disease: recent insights and progress.* Curr. Gastroenterol. Rep., 2010. **12**: p. 319-330.
262. Hasnain, S.Z., et al., *Mucin gene deficiency in mice impairs host resistance to an enteric parasitic infection.* Gastroenterology, 2010. **138**(5): p. 1763-71.
263. Hasnain, S.Z., et al., *Muc5ac: a critical component mediating the rejection of enteric nematodes.* The Journal of experimental medicine, 2011. **208**(5): p. 893-900.
264. Artis, D., et al., *RELMbeta/FIZZ2 is a goblet cell-specific immune-effector molecule in the gastrointestinal tract.* Proc Natl Acad Sci U S A, 2004. **101**(37): p. 13596-600.
265. Herbert, D.R., et al., *Intestinal epithelial cell secretion of RELM-beta protects against gastrointestinal worm infection.* J Exp Med, 2009. **206**(13): p. 2947-57.
266. Kawabata, A., et al., *In vivo evidence that protease-activated receptors 1 and 2 modulate gastrointestinal transit in the mouse.* Br J Pharmacol, 2001. **133**(8): p. 1213-8.
267. Cocks, T.M., et al., *Protease-activated receptors mediate apamin-sensitive relaxation of mouse and guinea pig gastrointestinal smooth muscle.* Gastroenterology, 1999. **116**(3): p. 586-92.
268. Kawabata, A., et al., *Modulation by protease-activated receptors of the rat duodenal motility in vitro: possible mechanisms underlying the evoked contraction and relaxation.* Br J Pharmacol, 1999. **128**(4): p. 865-72.
269. Shea-Donohue, T., et al., *Role of enteric nerves in immune-mediated changes in protease-activated receptor 2 effects on gut function.* Neurogastroenterol Motil, 2010. **22**(10): p. 1138-e291.
270. Akiho, H., et al., *Role of IL-4, IL-13, and STAT6 in inflammation-induced hypercontractility of murine smooth muscle cells.* Am J Physiol Gastrointest Liver Physiol, 2002. **282**(2): p. G226-32.
271. Urban, J.F., Jr., et al., *Interleukin 4 is important in protective immunity to a gastrointestinal nematode infection in mice.* Proc Natl Acad Sci U S A, 1991. **88**(13): p. 5513-7.
272. Anthony, R.M., et al., *Protective immune mechanisms in helminth infection.* Nat Rev Immunol, 2007. **7**(12): p. 975-87.
273. Zhu, J. and W.E. Paul, *CD4 T cells: fates, functions, and faults.* Blood, 2008. **112**(5): p. 1557-69.
274. MacDonald, A.S. and R.M. Maizels, *Alarming dendritic cells for Th2 induction.* J Exp Med, 2008. **205**(1): p. 13-7.
275. Paul, W.E. and J. Zhu, *How are T(H)2-type immune responses initiated and amplified?* Nat Rev Immunol, 2010. **10**(4): p. 225-35.

276. Modolell, M., et al., *Reciprocal regulation of the nitric oxide synthase/arginase balance in mouse bone marrow-derived macrophages by TH1 and TH2 cytokines.* Eur J Immunol, 1995. **25**(4): p. 1101-4.
277. Pesce, J., et al., *The IL-21 receptor augments Th2 effector function and alternative macrophage activation.* J Clin Invest, 2006. **116**(7): p. 2044-55.
278. Park-Min, K.H., T.T. Antoniv, and L.B. Ivashkiv, *Regulation of macrophage phenotype by long-term exposure to IL-10.* Immunobiology, 2005. **210**(2-4): p. 77-86.
279. Gordon, S., *Alternative activation of macrophages.* Nat Rev Immunol, 2003. **3**(1): p. 23-35.
280. Zhao, A., et al., *Th2 cytokine-induced alterations in intestinal smooth muscle function depend on alternatively activated macrophages.* Gastroenterology, 2008. **135**(1): p. 217-225.e1.
281. Martin, P. and S.J. Leibovich, *Inflammatory cells during wound repair: the good, the bad and the ugly.* Trends Cell Biol, 2005. **15**(11): p. 599-607.
282. Krystel-Whittemore, M., K.N. Dileepan, and J.G. Wood, *Mast Cell: A Multi-Functional Master Cell.* Front Immunol, 2015. **6**: p. 620.
283. Morimoto, M. and K. Utsumiya, *Enhanced protection against Heligmosomoides polygyrus in IL-2 receptor beta-chain overexpressed transgenic mice with intestinal mastocytosis.* J Vet Med Sci, 2011. **73**(6): p. 849-51.
284. Hashimoto, K., et al., *Immunity-mediated regulation of fecundity in the nematode Heligmosomoides polygyrus--the potential role of mast cells.* Parasitology, 2010. **137**(5): p. 881-7.
285. Snoek, S.A., et al., *Mast cells trigger epithelial barrier dysfunction, bacterial translocation and postoperative ileus in a mouse model.* Neurogastroenterol Motil, 2012. **24**(2): p. 172-84, e91.
286. Ben-Smith, A., D.A. Lammas, and J.M. Behnke, *The relative involvement of Th1 and Th2 associated immune responses in the expulsion of a primary infection of Heligmosomoides polygyrus in mice of differing response phenotype.* J Helminthol, 2003. **77**(2): p. 133-46.
287. McDermott, J.R., et al., *Mast cells disrupt epithelial barrier function during enteric nematode infection.* Proc Natl Acad Sci U S A, 2003. **100**(13): p. 7761-6.
288. Harris, N. and W.C. Gause, *To B or not to B: B cells and the Th2-type immune response to helminths.* Trends Immunol, 2011. **32**(2): p. 80-8.
289. Wilson, M.S., et al., *Helminth-induced $CD19^{+}$ $CD23^{hi}$ B cells modulate experimental allergic and autoimmune inflammation.* European Journal of Immunology., 2010. **40**: p. 1682-1696.
290. Chapman, C.B., et al., *IgG1 hypergammaglobulinaemia in chronic parasitic infections in mice: magnitude of the response in mice infected with various parasites.* Aust J Exp Biol Med Sci, 1979. **57**(4): p. 369-87.
291. McCoy, K.D., et al., *Polyclonal and specific antibodies mediate protective immunity against enteric helminth infection.* Cell Host Microbe, 2008. **4**(4): p. 362-73.
292. Harris, N.L., et al., *Mechanisms of neonatal mucosal antibody protection.* J Immunol, 2006. **177**(9): p. 6256-62.
293. Wahid, F.N., M. Robinson, and J.M. Behnke, *Immunological relationships during primary infection with Heligmosomoides polygyrus (Nematospiroides dubius): expulsion of adult worms from fast responder syngeneic and hybrid strains of mice.* Parasitology, 1989. **98 Pt 3**: p. 459-69.
294. Grainger, J.R., et al., *Helminth secretions induce de novo T cell Foxp3 expression and regulatory function through the TGF-beta pathway.* J Exp Med, 2010. **207**(11): p. 2331-41.

295. Grainger, J.R., et al., *Helminth secretions induce de novo T cell Foxp3 expression and regulatory function through the TGF-β pathway.* J Exp Med. , 2010. **207**(11): p. 2331-2341.
296. Segura, M., et al., *Impairment of dendritic cell function by excretory-secretory products: a potential mechanism for nematode-induced immunosuppression.* European Journal of Immunology., 2007. **37**(7): p. 1887-1904.
297. McSorley, H.J., et al., *Blockade of IL-33 release and suppression of type 2 innate lymphoid cell responses by helminth secreted products in airway allergy.* Mucosal Immunol, 2014. **7**(5): p. 1068-78.
298. Telford, G., et al., *Heligmosomoides polygyrus immunomodulatory factor (IMF), targets T-lymphocytes.* Parasite Immunol, 1998. **20**(12): p. 601-11.
299. Moreno, Y., et al., *Proteomic analysis of excretory-secretory products of Heligmosomoides polygyrus assessed with next-generation sequencing transcriptomic information.* PLoS Negl Trop Dis, 2011. **5**(10): p. e1370.
300. Lawrence, C.E. and D.I. Pritchard, *Differential secretion of acetylcholinesterase and proteases during the development of Heligmosomoides polygyrus.* Int J Parasitol, 1993. **23**(3): p. 309-14.
301. Bustos, J.A., H.H. Garcia, and O.H. Del Brutto, *Reliability of Diagnostic Criteria for Neurocysticercosis for Patients with Ventricular Cystic Lesions or Granulomas: A systematic review.* Am J Trop Med Hyg, 2017.
302. Amaral, K.B., et al., *Histological assessment of granulomas in natural and experimental Schistosoma mansoni infections using whole slide imaging.* PLoS One, 2017. **12**(9): p. e0184696.
303. Khurana, S., et al., *Pulmonary foreign body granulomatosis in a chronic user of powder cocaine.* J Bras Pneumol, 2017: p. 0.
304. Jain, D., et al., *Pathology of pulmonary tuberculosis and non-tuberculous mycobacterial lung disease: Facts, misconceptions, and practical tips for pathologists.* Semin Diagn Pathol, 2017.
305. Shah K., Pritt B, and A. M, *Histopathologic review of granulomatous inflammation.* J of Clin. Tuberculosis and Other Mycobacterium Diseases, 2017. **7**: p. 1-12.
306. Heresbach, D., et al., *Frequency and significance of granulomas in a cohort of incident cases of Crohn's disease.* Gut, 2005. **54**(2): p. 215-22.
307. Brown, I.S., et al., *Histopathological findings of extra-ileal manifestations at initial diagnosis of Crohn's disease-related ileitis.* Virchows Arch, 2016. **469**(5): p. 515-522.
308. James, D.G., *A clinicopathological classification of granulomatous disorders.* Postgrad Med J, 2000. **76**(898): p. 457-65.
309. Brown, I. and M.P. Kumarasinghe, *Granulomas in the gastrointestinal tract: deciphering the Pandora's box.* Virchows Arch, 2017.
310. Morimoto, M., et al., *Peripheral CD4 T cells rapidly accumulate at the host: parasite interface during an inflammatory Th2 memory response.* J Immunol, 2004. **172**(4): p. 2424-30.
311. Esser-von Bieren, J., et al., *Antibody-mediated trapping of helminth larvae requires CD11b and Fcgamma receptor I.* J Immunol, 2015. **194**(3): p. 1154-63.
312. Farache, J., et al., *Luminal bacteria recruit CD103+ dendritic cells into the intestinal epithelium to sample bacterial antigens for presentation.* Immunity, 2013. **38**(3): p. 581-95.
313. Heikenwalder, M., et al., *Chronic lymphocytic inflammation specifies the organ tropism of prions.* Science, 2005. **307**(1107): p. 1107-1110.

314. Prinz, M., et al., *Oral prion infection requires normal numbers of Peyer's patches but not of enteric lymphocytes.* The American journal of pathology, 2003. **162**(4): p. 1103-11.
315. Mok, S.W., et al., *B Cell-specific S1PR1 deficiency blocks prion dissemination between secondary lymphoid organs'* Journal of Immunology 2012. **188**(10): p. 5032-5040.
316. Farquhar, C.F., R.A. Somerville, and L.A. Ritchie, *Post-mortem immunodiagnosis of scrapie and bovine spongiform encephalopathy.* Journal of Virology Methods, 1989. **24**(1-2): p. 215- 221.
317. Schulz-Schaeffer, W.J., et al., *The paraffin-embedded tissue blot detects PrP(Sc) early in the incubation time in prion diseases.* Am J Pathol, 2000. **156**(1): p. 51-6.
318. Landsverk, T., *The follicle-associated epithelium of the ileal Peyer's patch in ruminants is distinguished by its shedding of 50 nm particles.* Immunol Cell Biol, 1987. **65 (Pt 3)**: p. 251-61.
319. Parsons, K.R., A.P. Bland, and G.A. Hall, *Follicle associated epithelium of the gut associated lymphoid tissue of cattle.* Vet Pathol, 1991. **28**(1): p. 22-9.
320. Neutra, M.R. and J.P. Kraehenbuhl, *The role of transepithelial transport by M cells in microbial invasion and host defense.* J Cell Sci Suppl, 1993. **17**: p. 209-15.
321. Rescigno, M., et al., *Dendritic cell express tight junction proteins and penetrate gut epithelial monolayers to sample bacteria.* Nature Immunology, 2001. **2**(4): p. 361-367.
322. Niess, J.H., et al., *CX3CR1-mediated dendritic cell access to the intestinal lumen and bacterial clearance.* Science, 2005. **307**(5707): p. 254-8.
323. McDole, J.R., et al., *Goblet cells deliver luminal antigen to CD103^{+} dendritic cells in the small intestine.* Nature, 2012. **483**: p. 345-349.
324. Macpherson, A.J. and T. Uhr, *Induction of protective IgA by intestinal dendritic cells carrying commensal bacteria.* Science, 2004. **303**(5664): p. 1662-5.
325. Fernandez-Blanco, J.A., et al., *Changes in Epithelial Barrier Function in Response to Parasitic Infection: Implications for IBD Pathogenesis.* J Crohns Colitis, 2015. **9**(6): p. 463-76.
326. Buchheister, S., et al., *CD14 Plays a Protective Role in Experimental Inflammatory Bowel Disease by Enhancing Intestinal Barrier Function.* Am J Pathol, 2017. **187**(5): p. 1106-1120.
327. Soderholm, J.D., et al., *Increased epithelial uptake of protein antigens in the ileum of Crohn's disease mediated by tumour necrosis factor alpha.* Gut, 2004. **53**(12): p. 1817-24.
328. Keita, A.V. and J.D. Soderholm, *Barrier dysfunction and bacterial uptake in the follicle-associated epithelium of ileal Crohn's disease.* Ann N Y Acad Sci, 2012. **1258**: p. 125-34.
329. Bischoff, S.C., et al., *Intestinal permeability--a new target for disease prevention and therapy.* BMC Gastroenterol, 2014. **14**: p. 189.
330. Groschwitz, K.R. and S.P. Hogan, *Intestinal barrier function: molecular regulation and disease pathogenesis.* J Allergy Clin Immunol, 2009. **124**(1): p. 3-20; quiz 21-2.
331. Kaatz, M., et al., *Spread of classic BSE prions from the gut via the peripheral nervous system to the brain.* Am J Pathol, 2012. **181**(2): p. 515-24.
332. Hoffmann, C., et al., *Prions spread via the autonomic nervous system from the gut to the central nervous system in cattle incubating bovine spongiform encephalopathy.* J Gen Virol, 2007. **88**(Pt 3): p. 1048-55.
333. Glaysher, B.R. and N.A. Mabbott, *Isolated lymphoid follicle maturation induces the development of follicular dendritic cells.* Immunology, 2007. **120**(3): p. 336-44.

334. Knoop, K.A. and R.D. Newberry, *Isolated Lymphoid Follicles are Dynamic Reservoirs for the Induction of Intestinal IgA.* Front Immunol, 2012. **3**: p. 84.
335. Lorenz, R.G. and R.D. Newberry, *Isolated lymphoid follicles can function as sites for induction of mucosal immune responses.* Ann N Y Acad Sci, 2004. **1029**: p. 44-57.
336. Rios, D., et al., *Antigen sampling by intestinal M cells is the principal pathway initiating mucosal IgA production to commensal enteric bacteria.* Mucosal Immunol, 2016. **9**(4): p. 907-16.
337. Kucharzik, T., et al., *Role of M cells in intestinal barrier function.* Ann N Y Acad Sci, 2000. **915**: p. 171-83.
338. Jung, C., J.P. Hugot, and F. Barreau, *Peyer's Patches: The Immune Sensors of the Intestine.* Int J Inflam, 2010. **2010**: p. 823710.
339. Chieppa, M., et al., *Dynamic imaging of dendritic cell extension into the small bowel lumen in response to epithelial cell TLR engagement.* J. Exp. Med., 2006. **203**: p. 2841-2852.
340. Montrasio, F., et al., *Impaired prion replication in spleens of mice lacking functional follicular dendritic cells.* Science, 2000. **288**(5469): p. 1257-9.
341. McCulloch, L., et al., *Follicular dendritic cell-specific prion protein (PrP) expression alone is sufficient to sustain prion infection in the spleen.* PLoS pathogens, 2011. **7**(12): p. e1002402.
342. Knoop, K.A., M.J. Miller, and R.D. Newberry, *Transepithelial antigen delivery in the small intestine: different paths, different outcomes.* Curr. Opin. Gastroenterol., 2013. **29**: p. 112-118.
343. Bellinger-Kawahara, C.G., et al., *Scrapie prion liposomes and rods exhibit target sizes of 55,000 Da.* Virology, 1988. **164**(2): p. 537-41.
344. Gabizon, R., M.P. McKinley, and S.B. Prusiner, *Purified prion proteins and scrapie infectivity copartition into liposomes.* Proc Natl Acad Sci U S A, 1987. **84**(12): p. 4017-21.
345. Gibbs, C.J., Jr., D.C. Gajdusek, and R. Latarjet, *Unusual resistance to ionizing radiation of the viruses of kuru, Creutzfeldt-Jakob disease, and scrapie.* Proc Natl Acad Sci U S A, 1978. **75**(12): p. 6268-70.
346. Meynell, H.M., et al., *Up-regulation of microsphere transport across the follicle-associated epithelium of Peyer's patch by exposure to Streptococcus pneumoniae R36a.* The FASEB Journal., 1999. **13**: p. 611-619.
347. *Correction: Increased Abundance of M Cells in the Gut Epithelium Dramatically Enhances Oral Prion Disease Susceptibility.* PLoS Pathog, 2017. **13**(2): p. e1006222.
348. McCulloch, L., et al., *Follicular dendritic cell-specific prion protein (PrP^c) expression alone is sufficient to sustain prion infection in spleen.* Plos Pathogens., 2011. **7**(12).
349. Kim, J.J. and W.I. Khan, *Goblet cells and mucins: role in innate defense in enteric infections.* Pathogens, 2013. **2**: p. 55-70.
350. Zhao, A., et al., *Dependence of IL-4, IL-13, and nematode-induced alterations in murine small intestinal smooth muscle contractility on Stat6 and enteric nerves.* J Immunol, 2003. **171**(2): p. 948-54.
351. Ermund, A., et al., *Mucus properties and goblet cell quantification in mouse, rat and human ileal Peyer's patches.* PLoS One, 2013. **8**(12): p. e83688.
352. Rausch, S., et al., *Functional analysis of effector and regulatory T cells in a parasitic nematode infection.* Infective Immunology 2008. **76**(5): p. 1908-1919.
353. King, I.L., et al., *Intestinal helminth infection impacts the systemic distribution and function of the naive lymphocyte pool.* Mucosal Immunol, 2017. **10**(5): p. 1160-1168.
354. Schreiber, H.A., et al., *Inflammatory dendritic cells migrate in and out of transplanted chronic mycobacterial granulomas in mice.* J Clin Invest, 2011. **121**(10): p. 3902-13.

355. Copin, R., et al., *In situ microscopy analysis reveals local innate immune response developed around Brucella infected cells in resistant and susceptible mice.* PLoS Pathog, 2012. **8**(3): p. e1002575.
356. Donskow-Lysoniewska, K., et al., *Colitis promotes adaptation of an intestinal nematode: a Heligmosomoides polygyrus mouse model system.* PLoS One, 2013. **8**(10): p. e78034.
357. van Keulen, L.J., et al., *Immunohistochemical detection of prion protein in lymphoid tissues of sheep with natural scrapie.* J Clin Microbiol, 1996. **34**(5): p. 1228-31.
358. Sigurdson, C.J., et al., *PrP(CWD) lymphoid cell targets in early and advanced chronic wasting disease of mule deer.* J Gen Virol, 2002. **83**(Pt 10): p. 2617-28.
359. Mohan, J., M.E. Bruce, and N.A. Mabbott, *Neuroinvasion by scrapie following inoculation via the skin is independent of migratory Langerhans cells.* J Virol, 2005. **79**(3): p. 1888-97.
360. Brown, K.L., et al., *Scrapie replication in lymphoid tissues depends on prion protein-expressing follicular dendritic cells.* Nat Med, 1999. **5**(11): p. 1308-12.
361. Okamoto, M., et al., *Experimental transmission of abnormal prion protein (PrPsc) in the small intestinal epithelial cells of neonatal mice.* Vet Pathol, 2003. **40**(6): p. 723-7.
362. Nicoletti, C., M. Regoli, and E. Bertelli, *Dendritic cells in the gut: to sample and to exclude?* Mucosal Immunol, 2009. **2**(5): p. 462.
363. Owen, R.L. and A.L. Jones, *Epithelial cell specialization within human Peyer's patches: an ultrastructural study of intestinal lymphoid follicles.* Gastroenterology, 1974. **66**(2): p. 189-203.
364. Owen, R.L., *Uptake and transport of intestinal macromolecules and microorganisms by M cells in Peyer's patches--a personal and historical perspective.* Semin Immunol, 1999. **11**(3): p. 157-63.
365. Debard, N., et al., *Effect of mature lymphocytes and lymphotoxin on the development of the follicle-associated epithelium and M cells in mouse Peyer's patches.* Gastroenterology, 2001. **120**(5): p. 1173-82.
366. Phan, T.G., et al., *Immune complex relay by subcapsular sinus macrophages and noncognate B cells drives antibody affinity maturation.* Nat Immunol, 2009. **10**(7): p. 786-93.
367. Kovacs, G.G., et al., *Creutzfeldt-Jakob disease and inclusion body myositis: abundant disease-associated prion protein in muscle.* Ann Neurol, 2004. **55**(1): p. 121-5.
368. Gabizon, R., et al., *Insoluble wild-type and protease-resistant mutant prion protein in brains of patients with inherited prion disease.* Nat Med, 1996. **2**(1): p. 59-64.
369. Heppner, F.L., et al., *Transepithelial prion transport by M cells.* Nat Med, 2001. **7**(9): p. 976-7.
370. Foster, N. and G.G. Macpherson, *Murine cecal patch M cells transport infectious prions in vivo.* J Infect Dis, 2010. **202**(12): p. 1916-9.
371. Lacroux, C., et al., *Preclinical detection of variant CJD and BSE prions in blood.* PLoS Pathog, 2014. **10**(6): p. e1004202.
372. Saa, P., et al., *First demonstration of transmissible spongiform encephalopathy-associated prion protein (PrPTSE) in extracellular vesicles from plasma of mice infected with mouse-adapted variant Creutzfeldt-Jakob disease by in vitro amplification.* J Biol Chem, 2014. **289**(42): p. 29247-60.
373. Properzi, F., et al., *Detection of exosomal prions in blood by immunochemistry techniques.* J Gen Virol, 2015. **96**(Pt 7): p. 1969-74.
374. León, B., et al., *Regulation of TH2 development by CXCR5+ dendritic cells and lymphotoxin-expressing B cells.* Nature Immunology 2012. **13** (7).

375. Balic, A., et al., *Dynamics of CD11c(+) dendritic cell subsets in lymph nodes draining the site of intestinal nematode infection.* Immunol Lett, 2009. **127**(1): p. 68-75.
376. Cordier-Dirikoc, S. and J. Chabry, *Temporary depletion of CD11c+ dendritic cells delays lymphoinvasion after intraperitonal scrapie infection.* J Virol, 2008. **82**(17): p. 8933-6.
377. Herrmann, L.M., et al., *CD21-positive follicular dendritic cells: A possible source of PrPSc in lymph node macrophages of scrapie-infected sheep.* Am J Pathol, 2003. **162**(4): p. 1075-81.
378. Luhr, K.M., et al., *Scrapie protein degradation by cysteine proteases in CD11c+ dendritic cells and GT1-1 neuronal cells.* J Virol, 2004. **78**(9): p. 4776-82.
379. McGovern, G. and M. Jeffrey, *Scrapie-specific pathology of sheep lymphoid tissues.* PLoS One, 2007. **2**(12): p. e1304.
380. Carabotti, M., et al., *The gut-brain axis: interactions between enteric microbiota, central and enteric nervous systems.* Ann Gastroenterol, 2015. **28**(2): p. 203-209.
381. Verheijden, S., S. De Schepper, and G.E. Boeckxstaens, *Neuron-macrophage crosstalk in the intestine: a "microglia" perspective.* Front Cell Neurosci, 2015. **9**: p. 403.
382. Ray, K., *Neurogastroenterology: Enteric neurons and macrophage crosstalk.* Nat Rev Gastroenterol Hepatol, 2016. **13**(3): p. 123.
383. Klose, C.S.N., et al., *The neuropeptide neuromedin U stimulates innate lymphoid cells and type 2 inflammation.* Nature, 2017. **549**(7671): p. 282-286.
384. Cardoso, V., et al., *Neuronal regulation of type 2 innate lymphoid cells via neuromedin U.* Nature, 2017. **549**(7671): p. 277-281.
385. Keymer, A.E. and R.W. Hiorns, *Faecal egg counts and nematode fecundity: Heligmosomoides polygyrus and laboratory mice.* Parasitology, 1986. **93 (Pt 1)**: p. 189-203.
386. Wakelin, D. and A.M. Donachie, *Genetic control of eosinophilia. Mouse strain variation in response to antigens of parasite origin.* Clin Exp Immunol, 1983. **51**(2): p. 239-46.
387. Post, K., et al., *Fly larvae and pupae as vectors for scrapie.* Lancet, 1999. **354**(9194): p. 1969-70.
388. Lacroux, C., et al., *Prions in milk from ewes incubating natural scrapie.* PLoS Pathogens, 2008. **4**(12).
389. Maestrale, C., et al., *A lympho-follicular microenvironment is required for pathological prion protein deposition in chronically inflamed tissues from scrapie-affected sheep.* PLoS One, 2013. **8**(5): p. e62830.
390. van den Oord, J.J., C. de Wolf-Peeters, and V.J. Desmet, *Cellular composition of suppurative granulomas: an immunohistochemical study of suppurative granulomatous lymphadenitis.* Hum Pathol, 1985. **16**(10): p. 1009-14.
391. DG, J., *A clinicopathological classification of granulomatous disorders.* Postgraduate Medical Journal 2000. **76**: p. 457-465.
392. Colchester, A.C. and N.T. Colchester, *The origin of bovine spongiform encephalopathy: the human prion disease hypothesis.* Lancet, 2005. **366**(9488): p. 856-61.
393. Knight, R., *Infectious and Sporadic Prion Diseases.* Prog Mol Biol Transl Sci, 2017. **150**: p. 293-318.
394. Carlson, G.A., *Prion Protein and Genetic Susceptibility to Diseases Caused by Its Misfolding.* Prog Mol Biol Transl Sci, 2017. **150**: p. 123-145.
395. Kim, M.O., et al., *Genetic PrP Prion Diseases.* Cold Spring Harb Perspect Biol, 2017.
396. Oesch, B., et al., *A cellular gene encodes scrapie PrP 27-30 protein.* Cell, 1985. **40**(4): p. 735-46.

397. Harris, D.A., P. Lele, and W.D. Snider, *Localization of the mRNA for a chicken prion protein by in situ hybridization.* Proceedings of the National Academy of Sciences of the United States of America, 1993. **90**(9): p. 4309-13.
398. Aguzzi, A. and M. Heikenwalder, *Prions, cytokines, and chemokines: a meeting in lymphoid organs.* Immunity, 2005. **22**: p. 145-154.
399. Dlakic, W.M., E. Grigg, and R.A. Bessen, *Prion infection of muscle cells in vitro.* Journal of virology, 2007. **81**(9): p. 4615-4624.
400. Wathne, G.J. and N.A. Mabbott, *The diverse roles of mononuclear phagocytes in prion disease pathogenesis.* Prion, 2012. **6**(2): p. 124-133.
401. Weng, M., et al., *Alternatively activated macrophages in intestinal helminth infection: effects on concurrent bacterial colitis.* Journal of Immunology 2007. **179**(7): p. 4721-4731.
402. Lawrence, C.E. and D.I. Pritchard, *Immune response profiles in responsive and non-responsive mouse strains infected with Heligmosomoides polygyrus.* Int J Parasitol, 1994. **24**(4): p. 487-94.
403. Parker, S.J. and C.J. Inchley, *Heligmosomoides polygyrus: influence of infection on lymphocyte subpopulations in mouse mesenteric lymph nodes.* Exp Parasitol, 1990. **71**(3): p. 249-58.
404. Behnke, J.M. and H.A. Parish, *Nematospiroides dubius: arrested development of larvae in immune mice.* Exp Parasitol, 1979. **47**(1): p. 116-27.
405. Behnke, J.M., et al., *Cellular and serological responses in resistant and susceptible mice exposed to repeated infection with Heligmosomoides polygyrus bakeri.* Parasite Immunol, 2003. **25**(6): p. 333-40.
406. Behnke, J.M. and M. Robinson, *Genetic control of immunity to Nematospiroides dubius: a 9-day anthelmintic abbreviated immunizing regime which separates weak and strong responder strains of mice.* Parasite Immunol, 1985. **7**(3): p. 235-53.
407. Wahid, F.N., et al., *Immunological relationships during primary infection with Heligmosomoides polygyrus: Th2 cytokines and primary response phenotype.* Parasitology, 1994. **108**(4): p. 461-471.
408. Ben-Smith, A., et al., *The relationship between circulating and intestinal Heligmosomoides polygyrus-specific IgG1 and IgA and resistance to primary infection.* Parasite Immunology 1999. **21**(8): p. 383-395.
409. Ali, N.M., J.M. Behnke, and B.R. Manger, *The pattern of peripheral blood leucocyte changes in mice infected with Nematospiroides dubius.* J Helminthol, 1985. **59**(1): p. 83-93.
410. Urban, J.F., Jr., I.M. Katona, and F.D. Finkelman, *Heligmosomoides polygyrus: CD4+ but not CD8+ T cells regulate the IgE response and protective immunity in mice.* Exp Parasitol, 1991. **73**(4): p. 500-11.
411. Reynolds, L.A., K.J. Fibey, and R.M. Maizels, *Immunity to the model intestinal helminth parasite Heligmosomoides polygyrus.* Seminars in Immunopathology., 2012. **34**: p. 829-846.
412. Lins, N., et al., *Virus Infections on Prion Diseased Mice Exacerbate Inflammatory Microglial Response.* Oxid Med Cell Longev, 2016. **2016**: p. 3974648.
413. Sigurdson, C.J., et al., *Bacterial colitis increases susceptibility to oral prion disease.* The Journal of infectious diseases, 2009. **199**(2): p. 243-52.
414. Hapfelmeier, S., et al., *The Salmonella pathogenicity island (SPI)-2 and SPI-1 type III secretion systems allow Salmonella serovar typhimurium to trigger colitis via MyD88-dependent and MyD88-independent mechanisms.* J Immunol, 2005. **174**(3): p. 1675-85.

415. Tahoun, A., et al., *Salmonella transforms follicle-associated epithelial cells into M cells to promote intestinal invasion.* Cell Host & Microbe, 2012. **12**(5): p. 645-656
416. Takakura, I., et al., *Orally administered prion protein is incorporated by m cells and spreads into lymphoid tissues with macrophages in prion protein knockout mice.* Am J Pathol, 2011. **179**(3): p. 1301-9.
417. Heikenwalder, M., et al., *Lymphotoxin-dependent prion replication in inflammatory stromal cells of granulomas.* Immunity 2008. **29**: p. 998-1008.
418. Terahara, K., *Comprehensive gene expression profiling of Peyer/'s patch M cells, villous M-like cells, and intestinal epithelial cells.* J. Immunol., 2008. **180**: p. 7840-7846.
419. Hamada, H., et al., *Identification of multiple isolated lymphoid follicles on the antimesenteric wall of the mouse small intestine.* J Immunol, 2002. **168**(1): p. 57-64.
420. Aloisi, F. and R. Pujol-Borrell, *Lymphoid neogenesis in chronic inflammatory diseases.* Nat Rev Immunol, 2006. **6**(3): p. 205-17.
421. Bouskra, D., et al., *Lymphoid tissue genesis induced by commensals through NOD1 regulates intestinal homeostasis.* Nature, 2008. **456**(7221): p. 507-10.
422. Little, M.C., et al., *The characterization of intraepithelial lymphocytes, lamina propria leukocytes, and isolated lymphoid follicles in the large intestine of mice infected with the intestinal nematode parasite Trichuris muris.* J Immunol, 2005. **175**(10): p. 6713-22.
423. Suzuki, K., et al., *Two distinctive pathways for recruitment of naive and primed IgM+ B cells to the gut lamina propria.* Proc Natl Acad Sci U S A, 2005. **102**(7): p. 2482-6.
424. Mosconi, I., et al., *Parasite Proximity Drives the Expansion of Regulatory T Cells in Peyer's Patches following Intestinal Helminth Infection.* Infection and immunity, 2015. **83**(9): p. 3657-65.
425. Golovkina, T.V., et al., *Organogenic role of B lymphocytes in mucosal immunity.* Science, 1999. **286**(5446): p. 1965-8.
426. Ebisawa, M., et al., *CCR6hiCD11c(int) B cells promote M-cell differentiation in Peyer's patch.* Int Immunol, 2011. **23**(4): p. 261-9.
427. Knoop, K.A., *RANKL is necessary and sufficient to initiate development of antigen-sampling M cells in the intestinal epithelium.* J. Immunol., 2009. **183**: p. 5738-5747.
428. Kanaya, T. and H. Ohno, *The Mechanisms of M-cell Differentiation.* Biosci Microbiota Food Health, 2014. **33**(3): p. 91-7.
429. Kanaya, T., et al., *The Ets transcription factor Spi-B is essential for the differentiation of intestinal microfold cells.* Nat Immunol, 2012. **13**(8): p. 729-36.
430. Sato, S., et al., *Transcription factor Spi-B-dependent and -independent pathways for the development of Peyer's patch M cells.* Mucosal Immunol, 2013. **6**(4): p. 838-46.
431. de Lau, W., et al., *Peyer's patch M cells derived from Lgr5(+) stem cells require SpiB and are induced by RankL in cultured "miniguts".* Mol Cell Biol, 2012. **32**(18): p. 3639-47.
432. Savidge, T.C., et al., *Salmonella-induced M-cell formation in germ-free mouse Peyer's patch tissue.* Am J Pathol, 1991. **139**(1): p. 177-84.
433. Borghesi, C., et al., *Modifications of the follicle-associated epithelium by short-term exposure to a non-intestinal bacterium.* J Pathol, 1996. **180**(3): p. 326-32.
434. Tahoun, A., et al., *Salmonella transforms follicle-associated epithelial cells into M cells to promote intestinal invasion.* Cell host & microbe, 2012. **12**(5): p. 645-56.
435. Osada, Y., et al., *Schistosoma mansoni infection reduces severity of collagen-induced arthritis via down-regulation of pro-inflammatory mediators.* Int J Parasitol, 2009. **39**(4): p. 457-64.

436. Salinas-Carmona, M.C., et al., *Spontaneous arthritis in MRL/lpr mice is aggravated by Staphylococcus aureus and ameliorated by Nippostrongylus brasiliensis infections.* Autoimmunity, 2009. **42**(1): p. 25-32.
437. Bennett, K.M., et al., *Induction of Colonic M Cells during Intestinal Inflammation.* Am J Pathol, 2016. **186**(5): p. 1166-79.
438. Krautler, N.J., et al., *Follicular dendritic cells emerge from ubiquitous perivascular precursors.* Cell, 2012. **150**(1): p. 194-206.
439. Heesters, B.A., R.C. Myers, and M.C. Carroll, *Follicular dendritic cells: dynamic antigen libraries.* Nat Rev Immunol, 2014. **14**(7): p. 495-504.
440. Neyt, K., et al., *Tertiary lymphoid organs in infection and autoimmunity.* Trends Immunol, 2012. **33**(6): p. 297-305.
441. Dieu-Nosjean, M.C., et al., *Tertiary lymphoid structures in cancer and beyond.* Trends Immunol, 2014. **35**(11): p. 571-80.
442. Cyster, J.G., et al., *Follicular stromal cells and lymphocyte homing to follicles.* Immunol Rev, 2000. **176**: p. 181-93.
443. Fu, Y.X. and D.D. Chaplin, *Development and maturation of secondary lymphoid tissues.* Annu Rev Immunol, 1999. **17**: p. 399-433.
444. Le Hir, M., et al., *Differentiation of follicular dendritic cells and full antibody responses require tumor necrosis factor receptor-1 signaling.* J Exp Med, 1996. **183**(5): p. 2367-72.
445. Marino, M.W., et al., *Characterization of tumor necrosis factor-deficient mice.* Proc Natl Acad Sci U S A, 1997. **94**(15): p. 8093-8.
446. Aguzzi, A. and N.J. Krautler, *Characterizing follicular dendritic cells: A progress report.* Eur J Immunol, 2010. **40**(8): p. 2134-8.
447. Jeffrey, M., et al., *Sites of prion protein accumulation in scrapie-infected mouse spleen revealed by immuno-electron microscopy.* J Pathol, 2000. **191**(3): p. 323-32.
448. Parmentier, H.K., et al., *HIV-1 infection and virus production in follicular dendritic cells in lymph nodes. A case report, with analysis of isolated follicular dendritic cells.* Am J Pathol, 1990. **137**(2): p. 247-51.
449. Suzuki, K., et al., *The sensing of environmental stimuli by follicular dendritic cells promotes immunoglobulin A generation in the gut.* Immunity, 2010. **33**(1): p. 71-83.
450. Joeris, T., et al., *Diversity and functions of intestinal mononuclear phagocytes.* Mucosal Immunol, 2017. **10**(4): p. 845-864.
451. Houston, S.A., et al., *The lymph nodes draining the small intestine and colon are anatomically separate and immunologically distinct.* Mucosal Immunol, 2016. **9**(2): p. 468-78.
452. Miyazawa, K., et al., *Immunohistochemical characterization of cell types expressing the cellular prion protein in the small intestine of cattle and mice.* Histochem Cell Biol, 2007. **127**(3): p. 291-301.
453. Carp, R.I. and S.M. Callahan, *Effect of mouse peritoneal macrophages on scrapie infectivity during extended in vitro incubation.* Intervirology, 1982. **17**(4): p. 201-7.
454. Maignien, T., et al., *Role of gut macrophages in mice orally contaminated with scrapie or BSE.* Int J Pharm, 2005. **298**(2): p. 293-304.
455. Li, Z., et al., *The phenotype and function of naturally existing regulatory dendritic cells in nematode-infected mice.* Int J Parasitol, 2011. **41**(11): p. 1129-37.
456. Smith, K.A., et al., *Chronic helminth infection promotes immune regulation in vivo through dominance of CD11cloCD103- dendritic cells.* J Immunol, 2011. **186**(12): p. 7098-109.
457. Gruner, L., et al., *Nematode parasites and scrapie: experiments in sheep and mice.* Parasitology research, 2004. **93**(6): p. 493-8.

458. Leon, B., et al., *Regulation of T(H)2 development by CXCR5+ dendritic cells and lymphotoxin-expressing B cells.* Nat Immunol, 2012. **13**(7): p. 681-90.
459. Matloubian, M., et al., *Lymphocyte egress from thymus and peripheral lymphoid organs is dependent on S1P receptor 1.* Nature, 2004. **427**(6972): p. 355-60.
460. Guernier, V., et al., *Gut microbiota disturbance during helminth infection: can it affect cognition and behaviour of children?* BMC Infect Dis, 2017. **17**(1): p. 58.
461. Walk, S.T., et al., *Alteration of the murine gut microbiota during infection with the parasitic helminth Heligmosomoides polygyrus.* Inflamm Bowel Dis, 2010. **16**(11): p. 1841-9.
462. Bradford, B.M., L. Tetlow, and N.A. Mabbott, *Prion disease pathogenesis in the absence of the commensal microbiota.* J Gen Virol, 2017. **98**(7): p. 1943-1952.
463. Donaldson, D.S. and N.A. Mabbott, *The influence of the commensal and pathogenic gut microbiota on prion disease pathogenesis.* J Gen Virol, 2016. **97**(8): p. 1725-38.
464. Chang, J.C., J. Jagirdar, and M. Lesser, *Long-term evolution of BCG- and CFA-induced granulomas in rat lungs. Correlation of histologic features with cells in bronchoalveolar lavage samples.* Am J Pathol, 1986. **125**(1): p. 16-27.
465. Zumla, A. and D.G. James, *Granulomatous infections: etiology and classification.* Clin Infect Dis, 1996. **23**(1): p. 146-58.
466. Thomzig, A., et al., *Accumulation of pathological prion protein PrPSc in the skin of animals with experimental and natural scrapie.* PLoS Pathog, 2007. **3**(5): p. e66.
467. Pato, F.J., et al., *Gastrointestinal nematode infections in roe deer (Capreolus capreolus) from the NW of the Iberian Peninsula: assessment of some risk factors.* Vet Parasitol, 2013. **196**(1-2): p. 136-42.
468. Hourrigan, J.L., *Experimentally induced bovine spongiform encephalopathy in cattle in Mission, Tex, and the control of scrapie.* J Am Vet Med Assoc, 1990. **196**(10): p. 1678-9.
469. Elsen, J.M., et al., *Genetic susceptibility and transmission factors in scrapie: detailed analysis of an epidemic in a closed flock of Romanov.* Arch Virol, 1999. **144**(3): p. 431-45.
470. McGhee, M.B., et al., *Studies on cross-transmission and pathogenicity of Haemonchus contortus in white-tailed deer, domestic cattle and sheep.* J Wildl Dis, 1981. **17**(3): p. 353-64.

Appendix

7.1 Multiple colour backgrounds (Image J macro)

```
// Generic multiple colour macro for assisting setting of thresholds

// Analyses pixel intensities along a line selection

// for a series of greyscale slices in a stack, each corresponding to a colour channel

// Expandable to any number of colour channels (slices)


// Check for RGB image and convert to greyscale stack

// Breaks if image name includes "(RGB)"

image = getImageID(); selectImage(image); info = getInfo();

if (indexOf(info, "(RGB)") >1) {

        getLine(x1,y1,x2,y2,width);

        run("RGB Split");

        run("Convert Images to Stack");

        makeLine(x1,y1,x2,y2);}


Greyscales = 255; if (indexOf(info, "pixel: 16")>1) {Greyscales = 65535;}


setLineWidth(1);

getLine(startx, starty, endx, endy, temp);
```

```
stack = getImageID();


selectImage(stack); slices = nSlices();


for (i =0; i<slices; i++) {
        selectImage(stack);
        slice = "slice="+(i+1);
        run("Set Slice...", slice);
        ydata = getProfile();
        Plot.create(slice, "pixels", "intensity");
        Plot.setLimits(0, ydata.length, 0, Greyscales);
        Plot.setLineWidth(1);
        Plot.setColor("red");
        Plot.add("line", ydata);
        Plot.show();
```

7.2 Multiple colour analysis (Image J macro)

```
// Generic multiple colour co-localisation analysis macro

// Analyses a series of greyscale slices in a stack, each corresponding to a colour channel

// Expandable to any number of colour channels (slices)

// Provides number of pixels above threshold for each combination of colour channels

// Data provided is in bins corresponding to (for three channels):

//

// Bin  Ch 1  Ch 2  Ch 3

// 0    -     -     -

// 1    +     -     -

// 2    -     +     -

// 3    +     +     -

// 4    -     -     +

// 5    +     -     +

// 6    -     +     +

// 7    +     +     +
```

```
// Set threshold values for each colour channel (each slice)
// Add extra thresholds for more than 5 channels
Threshold = newArray(6);

Threshold[1] = 80;
Threshold[2] = 60;
Threshold[3] = 50;
Threshold[4] = 50;
Threshold[5] = 50;

// Check for RGB image and convert to greyscale stack
// Where Ch 1 = red, Ch 2 = green, Ch 3 = blue
// Breaks if image name includes "(RGB)"
image = getImageID(); selectImage(image); info = getInfo();
if (indexOf(info, "(RGB)") >1) {
        run("RGB Split");
        run("Convert Images to Stack");
        exit("Draw your ROI and rerun the macro");}

stack = getImageID(); selectImage(stack); slices = nSlices();
results = newArray(pow(2, slices));
```

```
Greyscales = 255; if (indexOf(info, "pixel: 16")>1) {Greyscales = 65535;}

//run("Measure");


setBackgroundColor(0,0,0);

for (i =0; i<slices; i++) {
```

7.3 Raw data from mice co-infected with *H. polygyrus* and prions

C57BL/6J female mice (90 days old) were orally infected with 200 L3 infective larvae by gavage. Then, on different days post *H. polygyrus* infection (days 0, 1, 8 and 14) groups of mice (8 mice/group) were subsequently orally infected with 50 μl of a 1% dilution of scrapie brain homogenate prepared from mice terminally-affected with ME7 scrapie prions containing approximately 3.3 log10 i.c. ID50 units. A parallel group of mice were orally infected with prions alone as a control.

For early prion detection Peyer's patches (PP), spleens (SPL) and mesenteric lymph nodes (MLN) were analysed at 5, 10 and 15 weeks post prion infection. Mice allowed to develop terminal stage of prion disease were clinically assessed weekly, from day 210 post prion infection, for the development of clinical signs of prion disease (Section 2.3) to terminal stage of the disease (Figure 4.7). Data obtained from the analysed tissues are presented. Incubation period, clinical sign period, and survival time are presented in days. Blank spaces correspond to animals that do no present clinical signs of prion disease; grey lines mark mice with different causes of dead (not prion disease related); positive (+) and negative (-) scores for each tissue (SPL, PP and brain) and its respective analysis. For spleen and PP, CD 21/35, PrP^{d}, PrP^{Sc}. For brain PrP^{d}, vacuolation, PrP^{d} type (C, coarse; FP, fine punctate; PC, pericellular), GFAP and Iba1 are showed. Scores for each brain region are scored as mention in section 2.7.

7.3.1 Early prion detection in Peyer's patches

Group	Weeks post ME7	Mouse	CD21/35^{+} follicles/ PP	PrP^{Sc+} follicles	% of PrP^{Sc+} follicles	mean %/group
Scrapie alone	5	85039	7	5	71.4286	35.35714
		85040	10	2	20	
		85041	5	0	0	
		85042	2	1	50	
	10	85043				33.33333
		85044	5	2	40	
		85045	5	3	60	
		85047	1	0	0	
	15	85046	7	3	42.8571	56.13095
		85048	4	3	75	
		85049	6	4	66.6667	
		85050	10	4	40	
Day 0	5	85059	4	1	25	17.5
		85060	4	1	25	
		85061	2	0	0	
		85062	5	1	20	
	10	85063	5	1	20	24.82143
		85064	5	2	40	
		85065	4	1	25	
		85066	7	1	14.2857	
	15	85067	3	0	0	6.25
		85068	1	0	0	
		85069	12	3	25	
		85070	3	0	0	
Day -1	5	85099	11	5	45.4545	19.69697
		85100	3	1	33.3333	
		85101	8	0	0	
		85102	4	0	0	
	10	85103	2	1	50	22.22222
		85104				
		85105	6	1	16.6667	
		85106	3	0	0	
	15	85107	5	2	40	41.78571
		85108	10	2	20	
		85109	7	4	57.1429	
		85110	4	2	50	

Day -8	5	85119	7	2	28.5714	34.64286
		85120	4	2	50	
		85121	5	1	20	
		85122	5	2	40	
	10	85123	6	0	0	15.55556
		85124	6	0	0	
		85125	9	2	22.2222	
		85126	5	2	40	
	15	85127	7	4	57.1429	36.99405
		85128	6	2	33.3333	
		85129	10	2	20	
		85130	8	3	37.5	
Day -14	5	85139	3	1	33.3333	22.22222
		85140	3	1	33.3333	
		85141	5	0	0	
	10	85142	3	0	0	33.33333
		85143	5	2	40	
		85144	5	3	60	
		85145	9	3	33.3333	
	15	85146	3	1	33.3333	52.08333
		85147	2	2	100	
		85148	4	3	75	
		85149	5	0	0	

7.3.2 Early prion detection in mesenteric lymph nodes

Group	Weeks post ME7	Mouse	CD21/35^{+} follicles/ PP	PrP^{Sc+} follicles	% of PrP^{Sc+} follicles	mean %/group
Scrapie alone	5	85039	10	1	10	5.625
		85040	8	1	12.5	
		85041	7	0	0	
		85042	11	0	0	
	10	85043	10	0	0	0
		85044				
		85045	8	0	0	
		85047	8	0	0	
	15	85046	13	6	46.1538	65.3846
		85048	6	3	50	
		85049	12	12	100	
		85050				
Day 0	5	85059				0
		85060				
		85061	16	0	0	
		85062	3	0	0	
	10	85063	9	0	0	6.25
		85064	4	0	0	
		85065	4	1	25	
		85066	11	0	0	
	15	85067	3	0	0	0
		85068	7	0	0	
		85069	10	0	0	
		85070				
Day -1	5	85099				8.33333
		85100	7	0	0	
		85101	3	0	0	
		85102	4	1	25	
	10	85103	8	0	0	5.35714
		85104	14	3	21.4286	
		85105	3	0	0	
		85106	4	0	0	
	15	85107	4	0	0	0
		85108				
		85109	5	0	0	
		85110	8	0	0	

Day -8	5	85119	10	0	0	0
		85120	7	0	0	
		85121	13	0	0	
		85122	10	0	0	
	10	85123	9	1	11.1111	15.2778
		85124	12	1	8.33333	
		85125	6	1	16.6667	
		85126	4	1	25	
	15	85127	2	0	0	10
		85128	5	2	40	
		85129	3	0	0	
		85130	2	0	0	
Day -14	5	85139	12	1	8.33333	2.77778
		85140	20	0	0	
		85141	8	0	0	
	10	85142	26	0	0	0
		85143		0		
		85144	9	0	0	
		85145	10	0	0	
	15	85146	15	3	20	12.2222
		85147	30	5	16.6667	
		85148	7	0	0	
		85149				

7.3.3 Early prion detection in spleens

Group	Weeks post ME7	Mouse	CD21/35^{+} follicles/ PP	PrP^{Sc+} follicles	% of PrP^{Sc+} follicles	mean %/group
Scrapie alone	5	85039	53	0	0	0
		85040	36	0	0	
		85041	50	0	0	
		85042		0	0	
	10	85043	53	0	0	0
		85044	66	0	0	
		85045	385	0	0	
		85047	77	0	0	
	15	85046	61	0	0	0
		85048		0	0	
		85049		0	0	
		85050		0	0	
Day 0	5	85059		0	0	0.96154
		85060		0	0	
		85061		0	0	
		85062	26	1	3.8462	
	10	85063		0	0	3.59907
		85064		0	0	
		85065	68	8	11.765	
		85066	38	1	2.6316	
	15	85067		0	0	0
		85068		0	0	
		85069				
		85070				
Day -1	5	85099		0	0	0
		85100		0	0	
		85101		0	0	
		85102		0	0	
	10	85103	46	9	19.565	4.8913
		85104		0	0	
		85105		0	0	
		85106		0	0	
	15	85107	46	4	8.6957	3.58901
		85108	53	3	5.6604	
		85109		0	0	
		85110		0	0	

Day -8	5	85119		0	0	0
		85120		0	0	
		85121		0	0	
		85122		0	0	
	10	85123		0	0	3.57143
		85124		0	0	
		85125		0	0	
		85126	35	5	14.286	
	15	85127		0	0	0
		85128		0	0	
		85129		0	0	
		85130		0	0	
Day -14	5	85139		0	0	0
		85140		0	0	
		85141		0	0	
	10	85142	36	3	8.3333	7.08333
		85143		0	0	
		85144	60	12	20	
		85145		0	0	
	15	85146	38	2	5.2632	4.1567
		85147		0	0	
		85148		0	0	
		85149	44	5	11.364	

7.3.4 Incubation period, clinical signs period and survival time in days

Group	Mouse	Incubation period	Clinical signs period	Survival time
Scrapie	1	384	17	401
	2			504
	3			504
	4	391	10	401
	5	391	10	401
	6			504
	7			504
	8	370	3	373
Day 0	9	391	24	415
	10	217	272	489
	11			504
	12			504
	13			504
	14	342	10	352
	15	363	17	380
	16	378	2	380
Day 1	17	384	17	401
	18			260
	19			504
	20	391	10	401
	21	378	16	394
	22	391	10	401
	23	421	15	436
	24	363	10	373
Day 8	25	398	25	423
	26			394
	27			283
	28	391	45	436
	29	428	36	464
	30	217	287	504
	31	217	279	496
	32			504
Day 14	33	351	1	352
	34			139
	35	351	15	366
	36	351	36	387
	37			186
	38	370	17	387
	39	370	17	387
	40			504

7.3.5 Positive and negative scores for CD 21/35, PrP^{d}, PrP^{Sc} staining in spleen and PP; in brain, vacuolation and PrP^{d}

Group	Mouse	SPL			PP			Brain	
		CD21/35	PrP^{d}	PrP^{Sc}	CD21/35	PrP^{d}	PrP^{Sc}	Vacuolation	PrP^{d}
Scrapie	1	+	+	+	+	+	+	+	+
	2	+	-	-	+	+	-	-	-
	3	-	-	-	+	-	-	-	-
	4	+	+	+	+	+	+	+	+
	5	+	+	+	+	+	+	+	+
	6	+	-	-	+	-	-	-	-
	7	+	-	-	+	-	-	-	-
	8	+	+	+	+	+	+	+	+
Day 0	9	-	-	NT	+	+	+	+	+
	10	+	-	-	+	-	-	+	-
	11	+	-	-	+	-	-	-	NT
	12	+	-	-	+	-	-	-	-
	13	+	-	-	+	-	-	-	-
	14	+	+	NT	+	+	+	+	+
	15	+	+	+	+	+	+	+	+
	16	+	+	+	+	+	-	+	+
Day 1	17	+	+	+	+	+	+	+	+
	18	+	-	-	+	-	-	-	-
	19	+	-	-	+	-	-	-	-
	20	+	+	+	+	+	+	+	+
	21	+	+	+	+	+	+	+	+
	22	+	+	+	+	+	+	+	+
	23	+	+	+	NT	NT	NT	+	+
	24	+	+	+	+	+	NT	+	+
Day 8	25	+	+	+	NT	NT	NT	+	+
	26	+	-	-	+	-	-	-	-
	27	NT	NT	NT	NT	NT	NT	-	-
	28	+	+	+	+	+	+	+	+
	29	+	+	NT	+	+	+	+	+
	30	+	-	-	+	-	-	-	-
	31	+	-	-	+	-	-	-	-
	32	-	-	-	+	-	-	-	-
Day 14	33	+	+	+	+	+	+	+	+
	34	-	-	-	+	+	+	-	-
	35	+	-	+	+	+	-	+	+
	36	+	+	+	+	+	+	+	+
	37	NT	NT	NT	NT	NT	NT	-	-
	38	+	+	+	+	+	+	+	+
	39	+	+	+	+	+	+	+	+
	40	+	-	-	+	-	-	-	-

7.3.6 PrP^{d} scores and PrP types in different brain areas

Group	Mouse	PrP^{d}							PrP Type						
		Cortex	Hippocampus	Thalamus	Hypothalamus	Cerebellum	Septum	Cingulate	Cortex	Hippocampus	Thalamus	Hypothalamus	Cerebellum	Septum	Cingulate
Scrapie	1	1	2	2	1	1	1	1	C/FP	C	FP	FP	C	FP	FP
	2	0	0	0	0	0	0	0	0	0	0	0	0	0	0
	3	0	0	0	0	0	0	0	0	0	0	0	0	0	0
	4	1	2	1	1	0	2	1	C	C	C/FP	C/FP	0	C/FP	C/FP
	5	1	2	2	1	1	1	1	C	C	C	FP	PC	C	FP
	6	0	0	0	0	0	0	0	0	0	0	0	0	0	0
	7	0	0	0	0	0	0	0	0	0	0	0	0	0	0
	8	1	2	1	1	0	1	1	C	C	C	FP	0	FP	C/FP
Day 0	9	1	1	1	1	0	1	1	C	C	FP	FP	0	C	C
	10	0	0	0	0	0	NT	NT	0	0	0	0	0	NT	NT
	11	NT	NT	NT	0	0	NT	NT	NT	NT	NT	0	0	NT	NT
	12	0	0	0	0	0	0	0	0	0	0	0	0	0	0
	13	0	0	0	0	0	0	0	0	0	0	0	0	0	0
	14	1	1	1	1	0	1	1	C	C	FP	FP	0	FP	C
	15	1	1	1	1	0	1	1	C	C	FP	FP	0	C	C
	16	1	2	2	1	0	1	1	C	C	C	FP	0	C	C
Day 1	17	1	1	2	1	0	1	1	C	C	C/FP	FP	0	C/FP	C
	18	0	0	0	0	0	0	0	0	0	0	0	0	0	0
	19	0	0	0	0	0	NT	NT	0	0	0	0	0	NT	NT
	20	1	2	1	1	0	1	1	C/FP	C	C/FP	FP	0	FP	C
	21	1	1	2	2	0	1	1	C	C	C/FP	FP	0	FP	C/FP
	22	1	2	2	1	0	1	1	C/FP	C	FP	FP	0	FP	C
	23	1	1	2	1	0	1	1	C/FP	C	FP	FP	0	FP	C/FP
	24	1	2	1	1	0	2	1	C	C	C/FP	FP	0	C	C

C=coarse
FP=fine punctate
NT= no tissue available for analysis

Day 8	25	1	2	2	1	1	1	0	FP	C	C	FP	C	C	0
	26	0	0	0	0	0	0	0	0	0	0	0	0	0	0
	27	0	0	0	0	0	0	0	0	0	0	0	0	0	0
	28	1	2	2	1	1	2	2	C	C	C	FP	FP	C	C
	29	1	1	1	1	1	1	1	FP	C	FP	FP	C	C/FP	C/FP
	30	0	0	0	0	0	0	0	0	0	0	0	0	0	0
	31	0	0	0	0	0	0	0	0	0	0	0	0	0	0
	32	0	0	0	0	0	0	0	0	0	0	0	0	0	0
Day 14	33	1	2	1	0	0	1	1	C	C	C	0	0	C	1
	34	0	0	0	0	0	0	0	0	0	0	0	0	0	0
	35	1	2	1	1	0	1	1	C	C	FP	FP	0	C	1
	36	1	1	1	0	0	1	1	C	C	FP	0	0	C/FP	1
	37	0	0	0	0	0	0	0	0	0	0	0	0	0	0
	38	1	2	2	1	0	1	1	C/FP	C	C	FP	0	C/FP	1
	39	1	2	1	1	0	1	1	C	C	C	FP	0	C/FP	1
	40	0	0	0	0	0	0	0	0	0	0	0	0	0	0

7.3.7 GFAP and Iba1 scores in different brain areas

Group	Mouse	GFAP						Iba-1						
		Cortex	Hippocampus	Thalamus	Hypothalamus	Septum	Cingulate	Cortex	Hippocampus	Thalamus	Hypothalamus	Cerebellum	Septum	Cingulate
Scrapie	1	3	3	3	2	3	2	1	1	2	1	1	1	1
	2	1	1	1	2	1	1	1	1	1	1	1	1	1
	3	1	1	1	1	NT	NT	NT	NT	1	1	1	1	1
	4	3	2	3	2	2	1	2	2	3	2	1	1	1
	5	3	2	3	2	2	3	3	2	3	2	2	2	2
	6	1	1	2	1	1	3	NT	NT	NT	NT	1	NT	NT
	7	1	1	2	1	NT	NT	1	2	1	1	1	1	1
	8	3	2	2	1	2	3	2	2	3	1	2	1	1
Day 0	9	3	3	3	2	3	2	2	3	3	1	1	2	2
	10	1	1	2	2	NT	NT	1	1	1	NT	NT	NT	NT
	11	NT	NT	NT	NT	NT	NT	NT	NT	NT	NT	NT	NT	NT
	12	1	1	1	1	1	1	1	1	1	1	1	1	1
	13	1	1	2	1	3	1	NT	NT	NT	NT	NT	NT	NT
	14	2	2	2	2	3	3	2	3	2	1	1	2	2
	15	2	1	2	1	2	2	2	1	2	1	1	1	2
	16	3	3	3	2	3	2	2	2	3	1	2	2	2
Day 1	17	3	2	3	2	3	2	2	2	3	2	2	1	1
	18	1	1	1	1	1	1	1	1	1	1	1	1	1
	19	1	1	1	1	1	1	1	1	1	1	1	1	1
	20	3	2	2	1	3	3	2	3	3	1	1	3	2
	21	2	2	3	2	3	3	2	2	3	1	2	2	2
	22	3	2	2	1	3	3	1	2	2	1	1	2	1
	23	3	1	2	2	2	2	2	1	3	1	1	1	1
	24	3	3	2	1	2	3	2	2	1	1	1	1	1

Day 8	25	3	3	2	1	2	1	2	2	3	1	NT	2	1
	26	1	1	1	1	NT	NT	1	1	1	1	1	1	1
	27	1	1	1	1	2	1	1	1	1	1	1	NT	NT
	28	3	2	3	3	3	2	2	2	3	2	2	2	2
	29	3	2	2	1	2	2	1	1	2	1	1	1	1
	30	1	1	1	1	1	1	1	1	1	1	1	NT	NT
	31	1	1	1	2	1	1	1	1	1	1	1	1	1
	32	1	1	2	1	2	1	1	1	1	1	1	1	1
Day 14	33	3	3	2	3	2	2	NT	NT	3	3	2	2	1
	34	1	1	1	2	2	1	1	1	1	1	1	1	1
	35	2	2	3	1	3	3	2	3	3	1	2	2	2
	36	3	3	2	1	2	3	2	2	3	1	1	NT	1
	37	1	1	1	1	1	1	1	1	1	1	1	1	1
	38	3	3	2	3	3	2	2	2	3	1	2	1	1
	39	NT	NT	NT	NT	NT	NT	2	2	3	NT	2	NT	NT
	40	1	1	1	1	2	1	1	1	2	1	1	1	1